Metal Ion-Promoted Leaving Group Assistance in the Solvolysis of Phosphate Esters, Amides, and Thioamides

By

Mark A. R. Raycroft

A thesis submitted to the Department of Chemistry

in conformity with the requirements for

the degree of Doctor of Philosophy

Queen's University

Kingston, Ontario, Canada

April, 2016

Abstract

Toward the efficient solvolysis of phosphate esters and amides under mild conditions, many small-molecule metal-containing catalysts have been designed to activate the substrate toward metal-mediated nucleophilic addition. However, very few systems have been designed to also employ a metal ion to activate the leaving group (LG) toward departure. To this end, the following studies were undertaken to ascertain the magnitude and mechanism of metal ion-promoted leaving group assistance.

The solvolysis of a specially-designed set of phosphate mono-, di-, and triesters, having a Cu(II)-complexed 2-phenanthrolyl group at the *ortho*-position of a departing phenoxide, was studied in water and ethanol under pH-controlled conditions at 25 °C. A combination of pH/rate profiles, solvent deuterium kinetic isotope effect (DKIE) values, and activation parameters were collected and compared to the results in methanol. While a detailed comparison of the activation parameters reveals complex trends due to changes in the reaction medium, the rate-accelerating effects of the Cu(II)-promoted leaving group assistance in all three solvents are substantial, ranging from 10^5 to 10^{15} relative to their background reactions.

The methanolysis of the Cu(II) complexes of a series of substituted *N*,*N*-bis(2-picolyl)benzamides was studied under $^{s}_{s}$pH-controlled conditions at 25 °C. Hammett reaction constants, solvent DKIE values, activation parameters, and computational results

describe a mechanism where the metal ion, coordinated to the *N*,*N*-bis(2-picolyl)amide unit, delivers a Cu(II)-coordinated methoxide to the carbonyl group in the rate-limiting transition state of the reaction. The metal ion appears to activate the substrate through coordination to the amide nitrogen, activate and deliver the nucleophile, and subsequently assist LG departure. Expanding upon this work revealed a common mechanism for the methanolysis and ethanolysis of the Ni(II), Zn(II), and Cu(II) complexes of *N*,*N*-bis(2-picolyl)-*p*-nitrobenzamide and *N*,*N*-bis((1*H*-benzimidazol-2-yl)methyl)-*p*-nitrobenzamide. Comparing the rate constants for the attack of alkoxide on the M(II)-complexed 4-nitro-substituted benzamides to those for the uncomplexed forms reveals accelerations ranging from 10^{14} to 10^{19}.

Finally, the palladacycle-promoted methanolysis of a series of thiobenzanilides with different LGs was studied under $^{s}_{s}$pH-controlled conditions at 25 °C. The kinetic data indicate that two mechanisms are operative wherein either one or two catalysts effect cleavage depending on the nature of the LG.

Co-Authorship

The work described within this thesis has been collaborative in nature; the contributions of the authors are described below.

With minor formatting changes and the addition of Supporting Information 2-1, Chapter 2 is presented largely as it is published in *Inorganic Chemistry* (Raycroft, M. A. R.; Liu, C. T.; Brown, R. S. *Inorg. Chem.* **2012**, *51*, 3846). The kinetic experiments were performed by Mark Raycroft and the syntheses were performed by Dr. C. Tony Liu and Mark Raycroft. The manuscript was written by Mark Raycroft and Dr. R. Stan Brown. The published article is copyrighted by the American Chemical Society.

With minor formatting changes, Chapter 3 is presented largely as it is published in *Inorganic Chemistry* (Raycroft, M. A. R.; Maxwell, C. I.; Oldham, R. A. A.; Saffouri Andrea, A.; Neverov, A. A.; Brown, R. S. *Inorg. Chem.* **2012**, *51*, 10325). The corresponding Supporting Information is represented in part by Supporting Information 3-1 and can be found in its complete form via the Internet at http://pubs.acs.org. The kinetic experiments were performed by Mark Raycroft and Ms. Robyn Oldham, the syntheses were performed by Ms. Areen Saffouri Andrea, and the computations were performed by Dr. Christopher I. Maxwell. The manuscript was written by Mark Raycroft and Dr. R. Stan Brown with contributions from Dr. Christopher I. Maxwell. The published article is copyrighted by the American Chemical Society.

With minor formatting changes, Chapter 4 is presented largely as it is published in *Inorganic Chemistry* (Raycroft, M. A. R.; Cimpean, L.; Neverov, A. A.; Brown, R. S. *Inorg. Chem.* **2014**, *53*, 2211). The corresponding Supporting Information is represented in part by Supporting Information 4-1 to 4-3 and can be found in its complete form via the Internet at http://pubs.acs.org. The kinetic experiments were performed by Mark Raycroft and Ms. Luana Cimpean and the syntheses were performed by Mark Raycroft. The manuscript was written by Mark Raycroft and Dr. R. Stan Brown. The published article is copyrighted by the American Chemical Society.

Chapter 5 includes kinetic experiments and spectrophotometric titrations performed by Mark Raycroft as well as syntheses performed by Mark Raycroft, Ms. Stephanie Pipe, and Dr. C. Tony Liu.

Acknowledgements

First and foremost, I would like to thank Dr. R. Stan Brown for his meticulous supervision, unwavering support, and constant encouragement throughout my graduate studies. Dr. Brown continually fostered my passion for and skill development in research and teaching; his wisdom and example will always serve as guiding principles.

For their thorough and timely feedback on my research, their provision of teaching opportunities, their assistance with the completion of my thesis, and their ongoing support, I sincerely thank Dr. Anne Petitjean and Dr. Donal Macartney.

I would like to thank Dr. David Zechel who taught me the basic principles underlying physical organic chemistry as part of my undergraduate experience and who played an impactful role in my development as a researcher and teacher during my graduate studies.

I am grateful to the Brown research group for their warm welcome, thorough training, and continued support and friendship.

I would like to acknowledge the generous financial assistance of the Natural Sciences and Engineering Research Council of Canada (CGS-D3), the Ontario Government (QEII-GSST), and the Department of Chemistry at Queen's University.

Lastly, I am thankful for the ongoing and unconditional support of family and friends.

Statement of Originality

I hereby certify that all of the work described within this thesis is the original work of the author. Any published (or unpublished) ideas and/or techniques from the work of others are fully acknowledged in accordance with the standard referencing practices.

Mark A. R. Raycroft

April, 2016

Table of Contents

List of Figures

List of Tables

List of Schemes

List of Symbols and Abbreviations

Å	angstrom
α	Leffler coefficient
β_{eq}	Brønsted equilibrium coefficient
β_{lg}	Brønsted leaving group coefficient
β_{nuc}	Brønsted nucleophile coefficient
°C	degrees Celsius
δ	chemical shift
Δ	change in
ε	molar extinction coefficient
ε_0	permittivity of a vacuum
ε_r	dielectric constant (relative permittivity)
λ	wavelength
μ	ionic strength
ρ	Hammett reaction constant
σ	Hammett substituent constant
χ_N	Winkler-Dunitz parameter
Ω	ohm(s)

12N3	1,5,9-triazacyclododecane
Abs	absorbance
amu	atomic mass unit(s)
A_N	association
AP	alkaline phosphatase
ApAP	aminopeptidase from *Aeromonas proteolytica*
Ar	aryl
Asp	aspartic acid
B	base
B3LYP	Becke three parameter, Lee-Yang-Par
cal	calorie(s)
cm	centimeter(s)
CM	carboxymethyl
C=O	acyl = carbonyl = carbon double-bonded to oxygen
C=S	thioacyl = thiocarbonyl = carbon double-bonded to sulfur
d	doublet
Da	Dalton(s)
DFT	density functional theory
DI	de-ionized
DKIE	deuterium kinetic isotope effect
DMSO	dimethyl sulfoxide
D_N	dissociation
DNA	deoxyribonucleic acid

DPA	di(2-picolyl)amine
e	proton charge
E_a	activation energy
EI	electron impact
ESI	electrospray ionization
Et	ethyl
e.u.	entropy unit(s)
G	Gibbs free energy
$G^{‡}$	Gibbs free energy of activation
Glu	glutamic acid
GS	ground state
h	Planck constant or hour(s)
H	enthalpy
$H^{‡}$	enthalpy of activation
HA	acid
H-bond	hydrogen-bond
His	histidine
HRMS	high resolution mass spectrometry
Hz	hertz
Int	intermediate
IR	infrared
k	rate constant
k_B	Boltzmann constant

k_{cat}	rate constant for catalyzed reaction
k_{cat}^{max}	maximum rate constant for catalyzed reaction
k_D	rate constant determined in deuterated solvent
K_d	dissociation constant
k_{ex}	rate constant for exchange
k_h	rate constant for hydrolysis
k_H	rate constant determined in protic solvent
k_{max}	maximum rate constant
k_{obs}	observed rate constant
k_{obs}^{max}	maximum observed rate constant
K	equilibrium constant or Kelvin
K_a	acid dissociation constant (determined in water)
${}^{s}_{s}K_a$	acid dissociation constant (determined in alcohol)
K_a^H	acid dissociation constant of the conjugate acid
K_{auto}	autoprotolysis constant
K_b	binding constant
K_d	dissociation constant
KIE	kinetic isotope effect
LFER	linear free energy relationship
LG, lg	leaving group
LGA	leaving group assistance
Lys	lysine
m	meta or multiplet

M	molar
M^{x+}	metal ion with charge of x+
M(II)	metal ion with charge of 2+
Me	methyl
MHz	megahertz
mol	mole(s)
MS	mass spectrometry
N_{amide}	amide nitrogen
NLLSQ	nonlinear least squares
nm	nanometer(s)
NMR	nuclear magnetic resonance
Nu	nucleophile
o	ortho
OAr	aryloxy group
OTf	triflate = trifluoromethanesulfonate
p	para
pD	$-\log[D_3O^+]$
${}^{s}_{s}pD$	$-\log[ROD_2^+]$
PE	potential energy
pH	$-\log[H_3O^+]$
${}^{s}_{s}pH$	$-\log[ROH_2^+]$
pK_a	$-\log(K_a)$
${}^{s}_{s}pK_a$	$-\log({}^{s}_{s}K_a)$

pK_a^H	$-\log(K_a^H)$
PLC	phospholipase C
P=O	phosphoryl = phosphorus double-bonded to oxygen
P=S	thiophosphoryl = phosphorus double-bonded to sulfur
PS	product state
Py	pyridine
r	distance
R	gas constant or alkyl
RNA	ribonucleic acid
RT	room temperature
s	singlet or second(s)
S	entropy
$S^{\ddagger}$	entropy of activation
Ser	serine
SKIE	solvent kinetic isotope effect
t	triplet or tertiary
T	temperature
T_O-	tetrahedral intermediate bearing an oxyanion
T_S-	tetrahedral intermediate bearing a thiolate
T_{S-O}-	tetrahedral intermediate bearing a thiolate and an oxyanion
td	triplet of doublets
THF	tetrahydrofuran
TMPP	2,2,6,6-tetramethylpiperidine

TOF	time of flight
Trp	tryptophan
TS	transition state
UV	ultraviolet
v	reaction velocity = reaction rate
vis	visible
wt	weight
z	charge

Chapter 1 – Introduction

1.1 – Acyl and phosphoryl transfer reactions

Nature chose acyl and phosphoryl units to construct and protect the most important biomolecules, making acyl- and phosphoryl-transfer reactions central to life. In particular, phosphate monoesters are essential to protein function, energy regulation, metabolism, signal transduction, and several other vital cellular processes.[1] Phosphate diesters compose the stable backbone of DNA and RNA.[2] Phosphate triesters, while not naturally-occurring, have been synthesized by humans for use as acetylcholinesterase inhibitors.[3]

Nature found phosphate mono- and diesters well-suited in these roles for several reasons, one of which is their ability to act as a robust structural link while retaining their ability to ionize at physiological pH.[4] Anionic character retains it within a lipid membrane and importantly, protects the structure from hydrolysis through the repulsion of anionic nucleophiles. Under physiological conditions, the half-time for nonenzymatic hydrolytic cleavage of monoester dianions[5] has been estimated at 10^{12} years and at 110 years (RNA) and $10^{8\text{-}10}$ years (DNA) for diesters.[6] To overcome these kinetic barriers on a viable timescale, Nature developed enzymes capable of manipulating such barriers to accelerate the rates of these hydrolytic pathways to bring their half-times into the range of seconds.

Amides form the backbone of proteins and peptides and play roles in intra- and intermolecular association and recognition.[7] Not unlike phosphate esters, part of amide

suitability as linkages in biomolecules is due to its resistance to hydrolysis. The half-time for hydrolysis of a peptide linkage is close to 500 years at neutral pH and 25 °C.[8]

Inspired by the efficiency exhibited by enzymes, scientists have set out to understand the critical components of Nature's design in order to produce effective small-molecule catalysts. Given that many of the enzymes responsible for phosphate ester and amide cleavages contain one or more metal ions in their solvent-excluded active site, two of the critical steps toward harnessing enzyme efficiency have been to identify the roles played by the metal ions in the mechanism as well as characterizing the environment in which the reactions take place.

The employment of several modes of metallo-activation observed in enzymatic reactions in combination with a reduced dielectric medium (relative to water) characteristic of an enzyme active site produces significant rate enhancements in acyl- and phosphoryl-transfer reactions.[9] Given the structural complexity of enzymes, small-molecule systems are seldom able to accommodate all modes employed by enzymes. A key mode that has received relatively little attention in the literature despite its importance in the enzymatic cleavage of natural (nonactivated) substrates is metal ion-promoted leaving group assistance (LGA). Mechanistic insights thus far hint at its potential as a general means to accelerate cleavage reactions. The rates and mechanisms of the solvolyses of phosphate esters and amides in the absence of metal ions serve as a reference point to which the metal ion-promoted reactions may be compared and understood.

1.2 – Mechanistic details for phosphate ester solvolysis reactions

1.2.1 – Mechanistic possibilities for phosphoryl transfer

Substitution at phosphorus may occur by three limiting mechanisms: dissociative (D_N+A_N), associative (A_N+D_N), or concerted (A_ND_N).[1,10]

Dissociative mechanism

The dissociative mechanism is a two-step substitution where the leaving group dissociates, forming a tricoordinate metaphosphate ion (PO_3^-) that is subsequently attacked by a nucleophile (Scheme 1-1).

Scheme 1-1. Dissociative (D_N+A_N) mechanism for phosphoryl transfer.

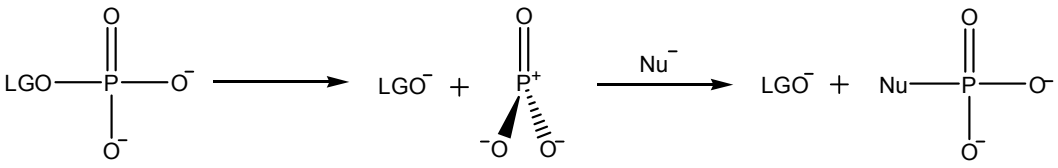

Associative mechanism

The associative mechanism follows an addition-elimination pathway where the nucleophile adds to the phosphate ester, forming a pentacoordinate phosphorane intermediate from which the leaving group departs in a subsequent step (Scheme 1-2).

Scheme 1-2. Associative (A_N+D_N) mechanism for phosphoryl transfer.

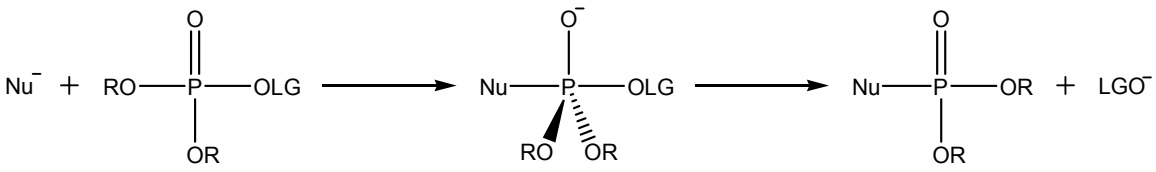

Concerted mechanism

The concerted mechanism is a one-step substitution involving simultaneous nucleophile-phosphorus bond formation and phosphorus-leaving group bond fission (Scheme 1-3). A spectrum of transition states exists in relation to the synchronicity between nucleophilic attack and leaving group departure.

Scheme 1-3. Concerted (A_ND_N) mechanism for phosphoryl transfer.

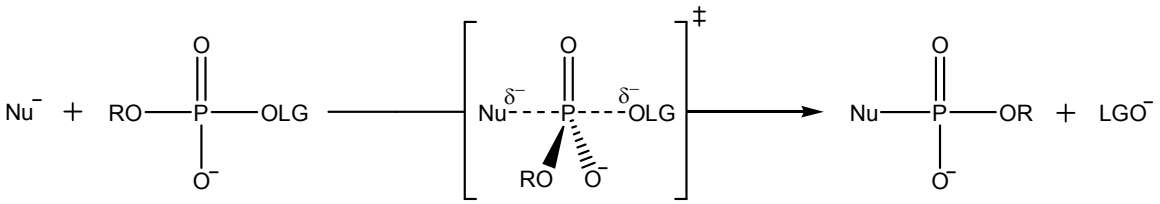

Intermediate and TS geometries

Upon departure of the LG (D_N), the ensuing metaphosphate ion takes on a trigonal-planar geometry. Upon addition of a nucleophile to a tetrahedral ester (A_N), the intermediate or TS structure assumes a trigonal-bipyramidal geometry where the nucleophile adds to, and the leaving group departs from, the apical positions (steric constraints permitting).

Mechanistic spectrum: More O'Ferrall-Jencks diagram

In light of a More O'Ferrall-Jencks plot (Figure 1-1), these three limiting mechanisms can be viewed in the context of a continuum that is characterized by the synchronicity between Nu–P bond formation and P–OLG bond fission. The mechanisms by which phosphate esters react depend on their state of *O*-alkylation or *O*-arylation. Monoesters react by either a dissociative mechanism or a concerted mechanism with a loose TS. Diesters and triesters react through concerted mechanisms (activated leaving groups) with progressively tighter TSs to the limit of an associative mechanism involving a phosphorane intermediate (unactivated leaving groups).

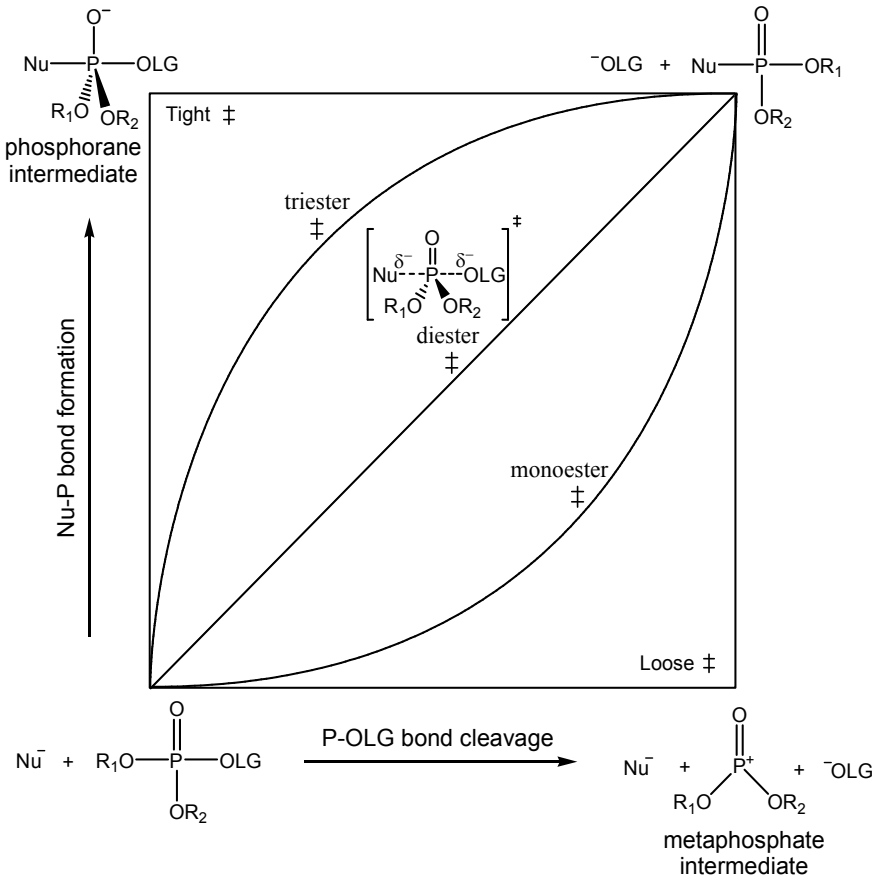

Figure 1-1. More O'Ferrall-Jencks diagram illustrating the 2D free energy surface and reaction pathways for phosphoryl transfer from phosphate mono-, di-, and triesters.[10]

1.2.2 – Phosphoryl-transfer from phosphate monoesters

Phosphate monoesters may exist in three possible ionization states: neutral, monoanionic, and dianionic. The first pK_a of an alkyl phosphate monoester is ~2.0 and the second is ~6.8.[10] Dianionic phosphoryl groups undergo phosphoryl transfer through a concerted A_ND_N mechanism with a loose TS. This is evidenced by near-zero entropies of activation, small dependences on nucleophile basicity (low Brønsted β_{nuc} values), large sensitivities to leaving group basicity (large β_{lg} values),[11] substantial P–O(LG) bond cleavage (large ^{18}O kinetic isotope effect values for the scissile bond),[12] and complete inversion of configuration for the solvolysis of a chiral (^{16}O, ^{17}O, ^{18}O-labelled) phosphate monoester.[13] While hydrolysis of the alkyl phosphate dianion is thermodynamically favourable, a significant barrier to attack is imposed by electrostatic repulsion between the anionic phosphate and the anionic nucleophile, leading to a half-time for hydrolysis of 1.1×10^{12} years ($k_{obs} = 2 \times 10^{-20}$ s^{-1}) at 25 °C.[5] Although loose TSs along a concerted pathway are inferred from experimental data, only in the case of the weakly-nucleophilic solvent *tert*-butanol has evidence been consistent with the formation of a metaphosphate intermediate (formation of racemic *t*-butyl phosphate, large positive entropy of activation).[14]

In the absence of catalysts, the monoanionic form of the monoester also reacts through a concerted process with a loose TS and tends to be more reactive than the corresponding dianion (when pK_a of HOLG > 5.5).[15] Due to the small sensitivity of the rate to the basicity of the leaving group ($\beta_{lg} = -0.27$), it has been proposed that the leaving group is protonated in the TS for cleavage.[11] Proton transfer may occur during leaving group

departure (less basic leaving groups) or prior to rate-limiting cleavage (more basic leaving groups).

1.2.3 – Phosphoryl-transfer from phosphate diesters

Large sensitivities of rate to the basicity of both the nucleophile and the leaving group indicate the cleavage of phosphate diesters is concerted.[16] Further evidence is provided by ^{18}O kinetic isotope effects, revealing Nu–P bond formation and P–O(LG) bond fission occur simultaneously in the rate-limiting TS.[17] Together, the LFER and KIE data suggest that the TSs for phosphate diester cleavage lie toward the central area of the More O'Ferrall-Jencks diagram (Figure 1-1). The half-time for hydrolysis of dialkyl phosphate anions (25 °C, pH = 6.5–13) has been estimated to be 3.1×10^7 years.[18]

1.2.4 – Phosphoryl-transfer from phosphate triesters

Without an ionizable P–OH group to hinder the approach of anionic nucleophiles, triesters are the most reactive of the three types of phosphate esters. In the case of 6-membered cyclic phosphate triesters, sufficient LFER,[16b] stereochemical,[19] and SKIE[20] data have been accrued to suggest that a mechanistic continuum exists from concerted with a loose TS to associative accompanied by the formation of a phosphorane intermediate. In the case of acyclic (aryl diphenyl and aryl diethyl) phosphate triesters, concerted mechanisms predominate but with TSs that vary depending on the LG as well as other structural features.[21] In particular, a loose TS is attributed to the attack of phenolate ions on 2,4-dinitrophenyl diphenyl phosphate, a more synchronous mechanism

is observed for triphenyl phosphate, and evidence suggesting a tight TS exists for phenyl diethyl phosphate.

1.3 – Mechanistic details for amide solvolysis reactions

1.3.1 – Amide hydrolysis reactions

Intermediates and products

Amide hydrolysis under basic conditions produces the parent carboxylate and the corresponding amine. The generally-accepted mechanism (Scheme 1-4) is a two-step one where attack of hydroxide leads to a tetrahedral intermediate (T_O-) followed by expulsion of the amide anion leaving group in the form of an amine. Depending on structural features as well as reaction conditions, leaving group departure may occur through several possible transition states.[22]

Scheme 1-4. Simplified mechanism for the alkaline hydrolysis of amides; R_1, R_2, R_3 = alkyl or aryl.[22]

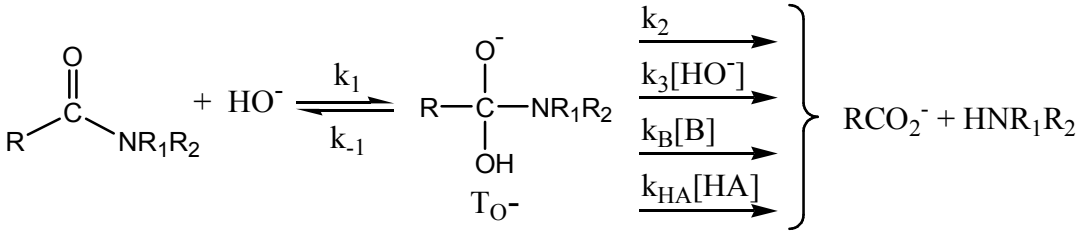

Structural features contributing to kinetic stability

Two intrinsic features make amides highly resistant to hydrolysis. Delocalization of π-electrons from the amide nitrogen into the adjacent π*(C=O) orbital imparts considerable ground state stabilization, diminishing the inherent electrophilicity of the carbonyl group and increasing the barrier for attack relative to a comparable process such

as ester hydrolysis. The high pK_a of the conjugate acid of the leaving group increases the barrier of the second step, namely leaving group departure. Under neutral conditions, it follows that amides are essentially inert to hydrolysis unless highly activated.[22]

Activation of amides toward hydrolysis

Activation can be built into the amide structure (intrinsic activation) or can come from external sources (extrinsic activation). A common method for extrinsic activation is to employ base (or acid) in the medium to promote hydrolysis. Provision of a more powerful nucleophile than water assists in overcoming the barrier to nucleophilic attack while hydrogen-bond donation has the potential to assist in overcoming both barriers through activation of the substrate toward attack (and/or stabilization of intermediate formation) and activation of the LG toward departure (and/or stabilization of LG departure). The simplified rate law for alkaline hydrolysis of an amide is shown in equation 1-1.[23]

$$v = k_2[amide][HO^-] \qquad (1\text{-}1)$$

Mechanistic studies of base-promoted amide hydrolysis

The current mechanistic picture of base-promoted amide hydrolysis reactions can be understood in light of three sets of complementary experimental data:[22]

1. Rate dependence of hydrolysis on [HO^-].
2. Kinetics of carbonyl ^{18}O-exchange.
3. Solvent kinetic isotope effects (SKIEs) on hydrolysis and exchange.

Stoichiometry

The dependence of rate on [HO^-] reveals information about the stoichiometry of the rate-limiting transition state (TS) for hydrolysis. Aliphatic amides, benzamides, and toluamides exhibit rates of hydrolysis that are first order in [HO^-]. That the rates of hydrolysis of acetanilides[24] and formanilides[25] are both first and second order in [HO^-] shows the requirement of a second hydroxide to effect breakdown of the corresponding tetrahedral intermediates to products. At high enough [HO^-], these intermediates become trapped such that reversal essentially halts and the rate-limiting step becomes k_1.[22]

^{18}O Exchange

Concurrent oxygen exchange between the carbonyl group and water during alkaline hydrolysis of benzamides (combined with buffer catalysis) provides evidence for the existence of a tetrahedral intermediate along the hydrolytic pathway. Under the assumptions that proton transfer is rapid between oxygen atoms in the intermediate, that only half of the reversal from the tetrahedral intermediate results in ^{18}O exchange, and that the intermediates leading to hydrolysis and exchange are on the same pathway, the rate constants for exchange (k_{ex}) and hydrolysis (k_h) are related to k_{-1} and k_2 as shown in equation 1-2.

$$\frac{k_{ex}}{k_h} = \frac{k_{-1}}{2k_2} \qquad (1\text{-}2)$$

The observation that ^{18}O-exchange is faster than hydrolysis implies that decomposition of the intermediate is at least partially rate-limiting in alkaline hydrolysis. This is the case for both benzamide and *N*-methylbenzamide; however, in the case of

N,*N*-dimethylbenzamide, k_{ex}/k_h = 0.05,[26] signifying little ^{18}O-exchange. The amount of ^{18}O-exchange for benzamides and toluamides follows the order primary > secondary >> tertiary.[23] It was eventually demonstrated that the leaving abilities of the amines (secondary amine > primary amine > NH_3) from the tetrahedral intermediate can account for the observed differences in ^{18}O-exchange in the corresponding amides.[27] It follows that the transition from significant to negligible exchange is attributable to a sufficient change in nucleofugality such that a change in rate-limiting step occurs from breakdown to attack.

Solvent kinetic isotope effects (SKIEs)

SKIE data for hydrolysis and exchange provide information about the relative effects of H and D on their respective rate-limiting TSs and whether proton transfer is involved. Three scenarios have been observed:[22]

1. A near-unit (or slightly normal) SKIE is observed when a proton is fully installed on the departing N prior to rate-limiting C–N cleavage. The SKIE value arises from a compensatory effect of the desolvation of the attacking hydroxide by the resolvation of the developing alkoxide in the intermediate.
2. The observation of an inverse SKIE for hydrolysis concurrent with ^{18}O-exchange reveals the mechanism involves rate-limiting expulsion of the amide anion from the tetrahedral intermediate.
3. A large normal SKIE is observed when the mechanism is second order in hydroxide where the second hydroxide is responsible for deprotonating the anionic tetrahedral intermediate concurrent with C–N cleavage.

1.3.2 – Amide alcoholysis reactions

Intermediates and products

Alkoxide-induced amide alcoholysis produces the corresponding alkyl ester and amine. The generally-accepted mechanism for amide methanolysis (Scheme 1-5) is a two-step one where attack of methoxide leads to a tetrahedral intermediate followed by expulsion of the amide anion leaving group in the form of an amine. Departure of the LG may be assisted through specific or general acid catalysis; the timing of proton transfer depends heavily on the structure of the LG.[28]

Scheme 1-5. Simplified mechanism for alkaline methanolysis of amides; R = CH_3; R_1, R_2, R_3 = alkyl, aryl.[22]

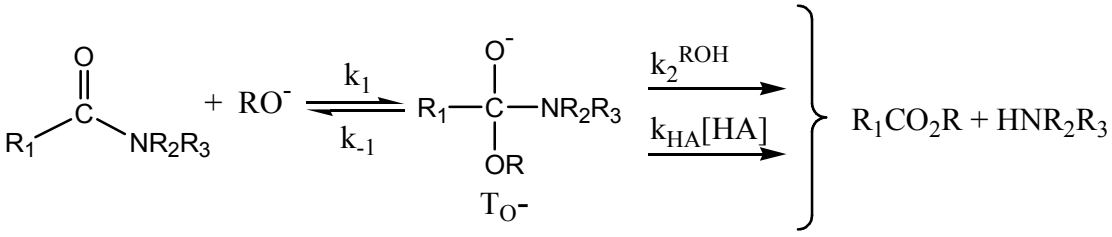

Anilides: Stoichiometry and linear free energy relationships (LFERs)

Alkaline methanolysis of acet- and benzanilides (**1.1**) is first order in both methoxide ion and anilide and tends to proceed by rate-limiting solvent-assisted departure of the LG ($\rho \approx 3$).[28,29,30] Exemplified by the Hammett data in Table 1-1, the mechanism appears consistent among members of the group (where the substituent on the ring, X, varies) as well as among anilide groups (where R_1 or R_2 varies). Exclusively in the case of *N*-methyl-4-nitroacetanilide ($R_1 = CH_3$; $R_2 = CH_3$; X = 4-nitro), addition of methoxide to the C=O unit (k_1) is rate-limiting ($\rho \approx 1.3$).[30] An alternative mechanism also becomes apparent in the case of *N*-methyl-2,2,2-trifluoroacetanilides bearing electron-donating

groups on the aniline which involves rate-limiting proton transfer with no concurrent C–N cleavage ($\rho \approx 0$).[29]

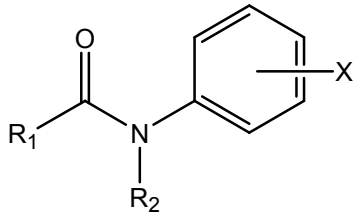

1.1

Table 1-1. Summary of Hammett data for the alkaline methanolysis of anilides (100 °C).[30]

Anilide	ρ
N-methylacetanilides	+3.4
N-methylbenzanilides	+2.8
Benzanilides	+2.9
Acetanilides	+3.1

Trifluoroacetanilides: Stoichiometry and SKIE data

The base-catalyzed methanolysis of *N*-methyl-2,2,2-trifluoroacetanilides[29] (Scheme 1-5; $R_1 = CF_3$; $R_2 = CH_3$; $R_3 = Ar$) is first order in both methoxide ion and amide and exhibits general base catalysis. Simple general base catalysis is observed as a consequence of general acid catalysis in the decomposition of the intermediate and the methoxide dependence of its formation. Normal SKIE data provide evidence that breakdown of the tetrahedral intermediate is rate-limiting as this step could involve some degree of proton transfer or H-bonding (electrophilic assistance by solvent). Conversely, an inverse SKIE

value would point to rate-limiting attack (since methoxide is a better nucleophile in CH_3OD than it is in CH_3OH), as is the case for the alkaline methanolysis of aryl acetates.[31]

Trifluoroacetanilides: LFERs and SKIEs

Base-catalyzed methanolysis of substituted *N*-methyl-2,2,2-trifluoroacetanilides yields a curved Hammett plot exhibiting small sensitivity to electron-donating substituents ($\rho = 0$) and large sensitivity to electron-withdrawing substituents ($\rho = 2.9$). Such upward curvature is indicative of a change in mechanism from one with rate-limiting proton transfer (Mechanism 1; electron-donating groups; $\sigma < 0$) to one with rate-limiting heavy-atom reorganization (Mechanism 2; electron-withdrawing groups; $\sigma > 0$). Mechanism 1 gives rise to a normal SKIE of 4.6 while Mechanism 2 gives rise to a smaller normal SKIE of 2. These values support mechanisms involving proton transfer with no C–N cleavage (proton transfer catalysis) and strong hydrogen-bond formation during C–N cleavage (solvation catalysis) in their rate-limiting TSs, respectively.[32]

Table 1-2. Summary of kinetic data for the base-catalyzed methanolysis of substituted *N*-methyl-2,2,2-trifluoroacetanilides.[28]

Mechanism	ρ	SKIE	TS Structure
1	0	4.6	**1.2**
2	+2.9	2	**1.3**

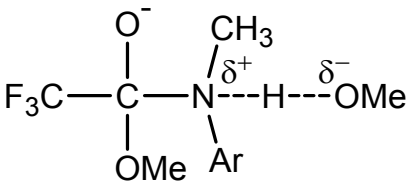

1.2

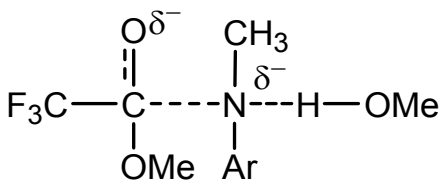

1.3

Benzanilides: Stoichiometry and LFERs

The base-catalyzed methanolysis of *N*-methylbenzanilides[28] is first order in both methoxide ion and amide. A study of the base-catalyzed methanolysis of the diaryl-substituted *N*-methylbenzanilides (**1.4**) revealed linear Hammett plots where ρ_X = 1.76 (100 °C) and ρ_Y = 2.5 (100 °C).[28] In contrast to the mechanistic variation as a consequence of the anilide substituent in the *N*-methyl-2,2,2-trifluoroacetanilides, the *N*-methylbenzanilides do not exhibit a change in mechanism or rate-limiting step within the substrate scope of this study. The results are consistent with a mechanism involving rate-limiting solvent-assisted C–N bond cleavage during the breakdown of the tetrahedral intermediate. The observation of linear Hammett plots in the case of *N*-methylbenzanilides compared with nonlinear plots for *N*-methylacetanilides can be accounted for by the facilitation of leaving group departure via conjugation of the acid ring with the developing carbonyl bond, rendering prior protonation of poor anilide leaving groups an unnecessary component.

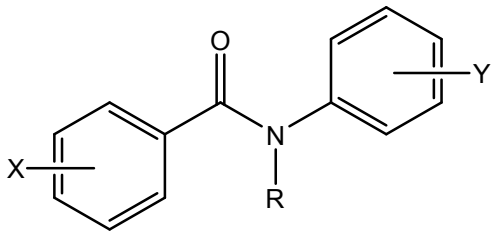

1.4

1.4 – Mechanistic details for thioamide solvolysis reactions

1.4.1 – Thioamide hydrolysis reactions

Intermediates, products, and stoichiometry

Thioamide hydrolysis produces some combination of the corresponding thionacid, amine, carboxamide, and hydrogen sulfide.[33] The thionacid may undergo subsequent hydrolysis to form the corresponding carboxylic acid and hydrogen sulfide as could the carboxamide to form the carboxylic acid and amine.

Scheme 1-6. Overall reaction pathways for hydrolysis of thioacetamides; R = alkyl.[36]

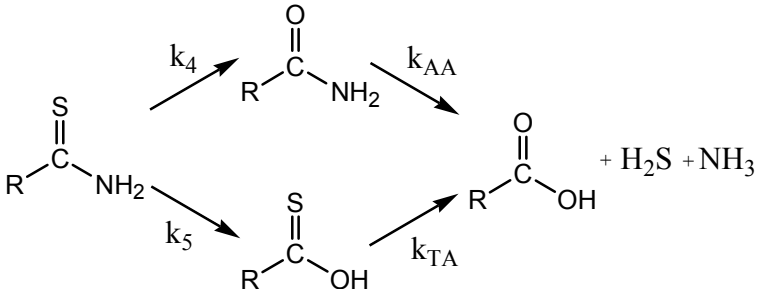

Both acids[34,35] and bases[36] catalyze hydrolysis and added salts (NaCl) enhance acid-catalyzed, but not base-catalyzed, hydrolysis.[37] Alkaline hydrolysis of thioacetamide is first order with respect to hydroxide ion activity and the amino-group hydrolysis is the prevailing pathway. Approximately 11% proceeds via thioxo hydrolysis while 79% proceeds via amino hydrolysis (10% discrepancy is attributed to sulfide oxidation or uncertainty in molar absorption coefficient of thioacetic acid). The rate was not affected by changes in salt concentrations, both pathways are first order in [HO^-] and they have the same E_a (20 kcal·mol^{-1}). Together, these data indicate ionic strength, pH, and temperature have no significant effect on the relative importance of the parallel pathways.

The ratio of intermediates shows 80% of hydrolyzed thioacetamide reacts via dipolar ion T_{S}-$_{O}$- (Scheme 1-7). Given that HS^{-} is a better LG than HNR_2R_3, the fact that the route via T_{S}-$_{O}$- predominates must be a consequence of the favourable equilibrium position between T_{S}- and T_{S}-$_{O}$-.[36] Alternatively, this result would have to arise from k_5 being much larger than k_4. From these results, it was concluded that the proton transfer between the tetrahedral intermediates may be rate-limiting.

Scheme 1-7. Simplified mechanism for the alkaline hydrolysis of thioacetamides; R_1 = alkyl; R_2, R_3 = H, alkyl.[36]

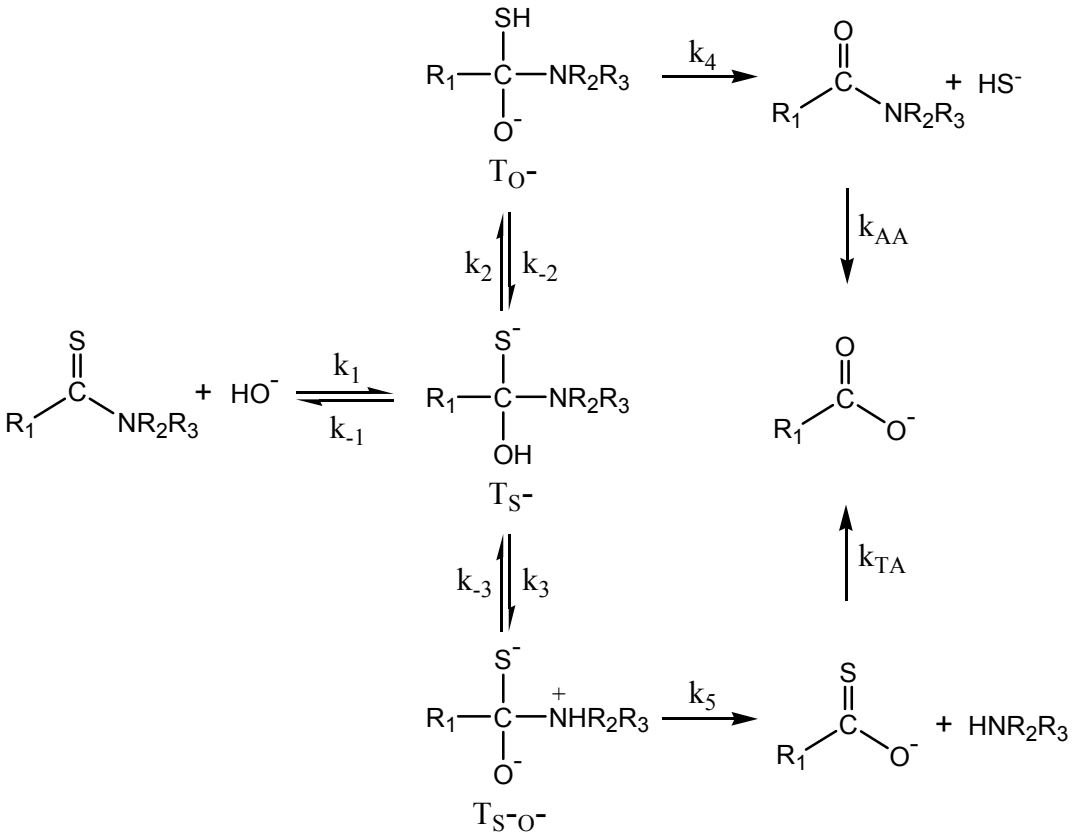

1.4.2 – Thioamide alcoholysis reactions

In the basic alcoholysis of *N*-aryl-*N*-methylthiobenzamides,[38] formation of the tetrahedral intermediate or its breakdown can be rate-limiting.

Scheme 1-8. Simplified mechanism for the alkaline methanolysis of thiobenzanilides; R = Me; R_1 = Ph; R_2 = Me; R_3 = aryl.

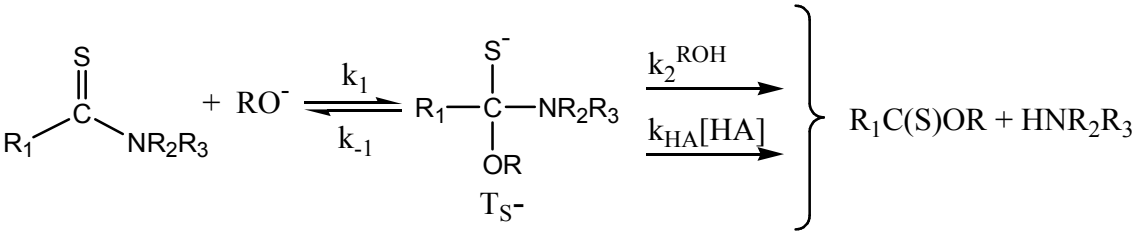

The identity of R_1, R_2, R_3, and the solvent have been shown to influence the mechanistic details. In the case of *N*-aryl-*N*-methylthiobenzamides (**1.5**), all substrates save for Y = 4-nitro exhibit rate-limiting solvent-assisted breakdown of the tetrahedral intermediate while the 4-nitro analogue undergoes rate-limiting attack.

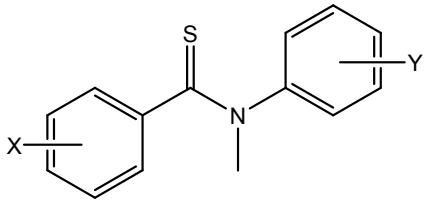

1.5

LFER data

The linear free energy relationships reveal similar ρ values to those obtained for C=O analogues. Series A (varying substituent X) exhibits a ρ_X value of 1.46 using sigma. Series B (varying substituent Y) exhibits a ρ_Y value of 2.16 using sigma-minus. The C=S series is less sensitive to substituent effects compared to its C=O analogues (ρ_X = 1.73 and ρ_Y = 2.83).[38]

Table 1-3. Summary of LFER data for the basic methanolysis of *N*-aryl-*N*-methylbenzamides and and *N*-aryl-*N*-methylthiobenzamides.[38]

C=X	Series	ρ
C=O	A	1.73
	B	2.83
C=S	A	1.46
	B	2.16

Relative rates and activation parameters

In cases where attack (k_1) is rate-limiting, such as alkaline ester hydrolysis, sulfur compounds tend to be more reactive (within a factor of two).[39] In this study,[38] the C=S substrates solvolyzed at slower rates than the C=O substrates, providing evidence for rate-limiting breakdown of the tetrahedral intermediate. The change from C=O to C=S does not alter the nature of the rate-limting step save for compounds containing Y = 4-nitro. Broxton and Deady propose that the sulfur atom affects the partitioning of the intermediate to make k_{-1} (loss of methoxide) faster than k_2 (loss of *N*-methyl-4-nitroaniline). This is supported by a study of thionester aminolysis[40] where it was shown that the relative leaving abilities of amines and oxyanions from the tetrahedral intermediate favour the amine more in the oxyester as compared with the thionester. Activation parameters also support this mechanistic shift since thiobenzanilides exhibit higher activation energies and more favourable entropies (rate-limiting breakdown).

1.5 – How enzymes conduct acyl and phosphoryl transfer

1.5.1 – Phosphate ester-cleaving enzymes

Monoesterase

Alkaline phosphatase (AP) is found in bacteria, mammals, and plants and is responsible for hydrolyzing phosphate monoesters to form inorganic phosphate. Given structural and functional similarities between the active sites for eukaryotic and prokaryotic AP enzymes, AP from *E. coli* has been studied extensively to probe the hydrolysis mechanism.[41] This enzyme is a homodimer that consists of two Zn(II) ions and one Mg(II) ion in the active site of each 47-kDa subunit. The mechanism can be generally understood by the following steps:[42]

1. Substrate binding.
2. Delivery of a Zn(II)-bound Ser102 to the phosphorus.
3. Formation of a pentacoordinate phosphorane intermediate.
4. Zn(II)-promoted departure of the alkoxide LG.
5. Delivery of a Zn(II)-bound hydroxide to the phosphorus.
6. Formation of a pentacoordinate phosphorane intermediate.
7. Zn(II)-promoted departure of Ser102.

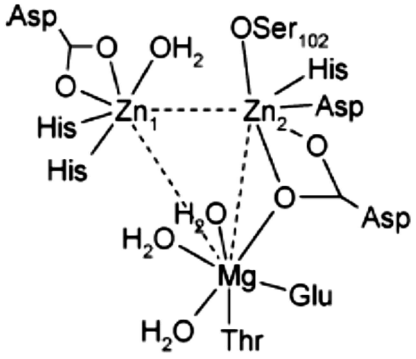

Figure 1-2. Schematic representation of the alkaline phosphatase active site.[41]

Isolation of a phosphoseryl enzyme-substrate intermediate[43] and the observation of retention of configuration in the product[44] provide evidence for a mechanism involving consecutive nucleophilic attacks by Ser102 and solvent. Under conditions where pH > 7, release of inorganic phosphate is rate-limiting; hydrolysis of the phosphoserine intermediate is rate-limiting below pH 7.[45] When chemistry is rate-limiting, LFER data (β_{lg} = -0.85 ± 0.1)[46] indicate extensive bond fission to the LG, hinting at a loose TS (direct evidence for the degree of nucleophile bond formation has not yet been obtained). The roles of the metal ions are several-fold. The two Zn(II) ions are required for phosphatase activity while the Mg(II) strictly acts to enhance activity. The following modes of catalysis are attributed to the two Zn(II) ions throughout the double-displacement mechanism:[47]

Direct, inner-sphere:[6]

1. Substrate binding and activation.
2. Nucleophile activation and delivery.
3. Intermediate stabilization.
4. Leaving group stabilization and release.

Indirect, outer sphere activation:

1. Metal-bound water or hydroxide acts as general acid or base, respectively.

Several characteristics contribute to the suitability of Zn(II) as a catalytic metal ion fulfilling the abovementioned roles including its unconstrained coordination geometry,

facile ligand exchange, lack of redox chemistry, borderline hard-soft properties, relatively high Lewis acidity, and high bioavailability.[2b] The role of Mg(II) has been debated and discussed in terms of binding hydroxide to act as a general base to deprotonate the Ser102 nucleophile,[48] induction of conformational changes to facilitate product release,[49] and/or electrostatic stabilization of charge in the TSs.

Diesterase

Phospholipase C (PLC) is a phosphodiesterase with an active site bearing semblance to that of AP (trimetal core with similar metal-metal distance and ligand orientation).[50] PLC can be isolated from *Bacillus cereus*[2c] and is responsible for hydrolyzing phosphodiesters in phospholipids toward the generation of secondary messengers.[2b] It contains three Zn(II) centres with trigonal bipyramidal geometries; each metal ion binds to a phosphate diester oxygen.[51] The mechanism of hydrolysis involves:

1. Substrate binding (concurrent with displacement of the bridging hydroxyl) and activation.
2. Nucleophilic attack concurrent with LG departure.
3. Product release.

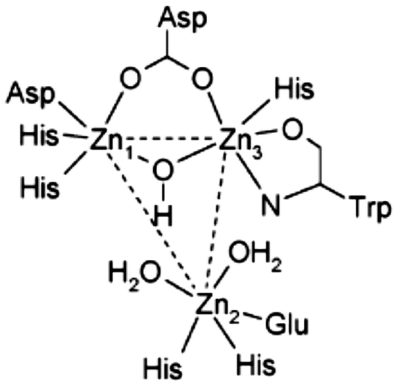

Figure 1-3. Schematic representation of the phospholipase C active site.[41]

The proposed mechanism is a concerted, in-line displacement where proton transfer from the nucleophile is rate-limiting.[52] The transition state structure is believed to be trigonal bipyramidal;[53] however, further stereochemical evidence is required. The primary role of the Zn(II) ions is to activate the substrate toward attack and stabilize charge in the TS; however, they have also been implicated in stabilizing the departing LG, either directly or through a general acid mechanism involving an activated water molecule.[2c,54] Activation of the nucleophile has been suggested to involve Zn(II) coordination[55] (the singly-displaced bridging hydroxide may act as a nucleophile or general base), but evidence suggests Asp55 is the general base responsible for activating an external water.[56]

Triesterase

The phosphotriesterase from *Pseudomonas diminuta*, like other phosphotriesterases,[57] possesses a di-Zn(II) catalytic core that catalyzes the hydrolysis of phosphate triesters, such as paraoxon.[58] It is capable of accelerating this reaction ~10^{12}-fold over the uncatalyzed reaction.

The mechanism of hydrolysis involves:

1. Substrate binding (concurrent with displacement of bridging hydroxyl) and activation.
2. Nucleophilic attack by Zn(II)-bound, His254/Asp301-activated[59] water, prior to or concurrent with LG departure.
3. Product release.

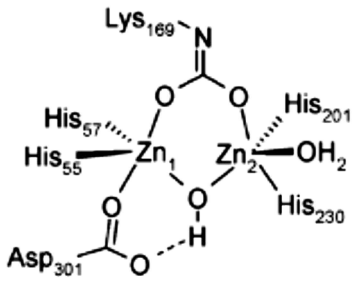

Figure 1-4. Schematic representation of the phosphotriesterase active site.[41]

The stereochemical outcome of this reaction is inversion of configuration at phosphorus, suggesting a single phosphoryl transfer event.[60] Through modeling studies, it was determined that, upon binding, the LG is oriented opposite the bridging hydroxide, pointing to its potential role as the active nucleophile.[61] The Zn(II) ions are implicated in activation of the substrate and nucleophile, however LFER data reveal they may not play a significant role in stabilizing LG departure. A break exists in the β_{lg} plot at $pK_a \approx 7$.[62] For good LGs ($pK_a < 7$), $\beta_{lg} \approx 0$ and proton transfer, subsequent to phosphoryl transfer, is the rate-limiting step. This is supported by a SKIE value of 2.0. For poor LGs ($pK_a > 7$), $\beta_{lg} \approx -1.8$, indicating rate-limiting phosphoryl transfer; in this domain, the SKIE value is 1.3.[1] The large gradient observed under conditions where phosphoryl transfer is rate-limiting indicates substantial charge accumulation on the LG heteroatom, signifying little to no participation by a metal ion in its stabilization in the rate-limiting TS.

1.5.2 – Amide-cleaving enzymes

Aminopeptidase

The metalloaminopeptidase from *A. proteolytica* is a 32-kDa enzyme that preferentially cleaves large hydrophobic *N*-terminal amino acids, such as Leucine.[63] The active site contains two Zn(II) ions. The current understanding of the mechanism is as follows:

1. Substrate binding via interaction between *N*-terminal peptide and hydrophobic pocket[64] and interactions between the acyl oxygen and a Zn(II) displaces the bridging hydroxide to produce a terminal hydroxide.[65]
2. Delivery of Zn(II)-bound hydroxide to the acyl carbon forming a tetrahedral intermediate.
3. Leaving group departure is general acid-assisted by Glu151.

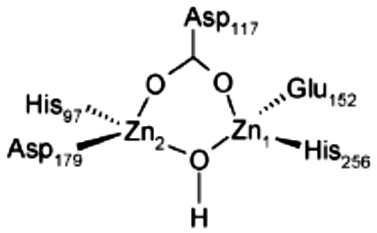

Figure 1-5. Schematic representation of the ApAP active site.[41]

A SKIE of 2.75[66] accompanies activation parameters $\Delta H^{\ddagger}$ = 8.1 kcal·mol^{-1} and $\Delta S^{\ddagger}$ = -22.5 cal·mol^{-1}·K^{-1}.[65] The enthalpy of activation may be a composite of conformational changes upon substrate binding involving bond formation and cleavage associated with nucleophilic addition to the carbonyl group[63] along with C–N cleavage; the negative entropy of activation may be a consequence of greater restrictions in the degrees of freedom due to binding events prior to cleavage and H-bond formation between the LG and Glu151 during the rate-limiting step. Together, these data point to departure of the LG concurrent with its protonation as the rate-limiting step.[65,67] The metal ions are implicated in activating and delivering the nucleophile, activating the substrate, and stabilizing TSs and intermediates on the pathway to cleavage.

1.6 – Catalytic roles of metal ions and importance of medium effects

1.6.1 – Metal ion-catalysis in solvolysis reactions

In metal ion-catalyzed solvolytic reactions of esters, amides, and phosphate esters, the metal ion may serve to:[9]

1. Activate the substrate toward nucleophilic attack through X=O--M^{x+} (X = C, P) coordination.
2. Decrease the pK_a of the metal-associated ROH (R = H, Me, Et) to form $M^{x+}(^{-}OR)$ near neutral pH.
3. Deliver the metal-bound nucleophile.
4. Stabilize intermediates and transition states along the reaction pathway.
5. Assist, if energetically required, the departure of the leaving group by stabilizing the development of charge on the departing heteroanion through coordination.

The latter, namely metal ion-promoted leaving group assistance, is a central focus of this work.

1.6.2 – Effect of solvent

Water as a reaction medium tends to heavily solvate ionic species, such as metal ions, nucleophiles, and substrates, thereby reducing their association and impeding catalysis. Importantly, the relatively large dielectric constant of water (ε_r = 78.5)[68] effectively weakens the interaction between a metal ion and its transforming substrate, a key component of metal ion catalysis. The Debye-Hückel theory for the association of spherical particles in solution predicts the potential energy of interaction between

oppositely charged ions is inversely proportional to the dielectric constant of the medium following Coulomb's law.

$$PE = \frac{1}{4\pi \cdot \varepsilon_0 \cdot \varepsilon_r} \cdot \frac{(z_+ e)(z_- e)}{r} \qquad (1\text{-}3)$$

In equation 1-3, ε_0 is the permittivity of a vacuum, ε_r is the dielectric constant (relative permittivity) of the medium, z_+e and z_-e are the charges in Coulombs (e = proton charge), and r is the distance between the centres of the ions.[69] It follows that media with lower dielectric constants than water, but that retain similar structural and H-bonding features, such as methanol (ε_r = 31.5)[68] and ethanol (ε_r = 24.3),[68] can enhance electrostatic ion-ion and ion-dipole interactions to promote catalysis.

Kinetic studies of metal ion-promoted hydrolytic reactions are plagued further by poor solubility of metal-hydroxo complexes which also play a critical role in the catalysis of solvolytic reactions. At pH values above the pK_a of a metal-aquo complex ($M^{x+}(H_2O)_n$), the metal-hydroxo complexes tend to form oligomers that precipitate out of solution. Circumvention of this issue typically involves complexation of the M^{x+} with ligands that are not necessarily ideal for controlling geometry or enhancing the reactivity of the complexes. In the context of specific solvent interactions, the use of light alcohols such as methanol and ethanol is advantageous due to the improved solubility of metal ion alkoxides enabling detailed mechanistic studies over a wide $^{s}_{s}$pH range.[70]

Additionally, given that enzyme active sites are inherently nonaqueous, it has been postulated that their effective dielectric constant is closer to that of organic solvents.[71] In the absence of metal ions, it has been shown that differential solvation effects between the ground and transition states translate into significant rate enhancements in the cleavage of phosphate esters.[72] Accelerations on the order of 10^6 (*p*-nitrophenylphosphate in 95% DMSO-5% H_2O and 95% hexamethylphosphoramide-5% H_2O),[73] 10^4 (aryl monoester dianions in *tert*-butyl and *tert*-amyl alcohols),[74] 10^5 (dineopentyl phosphate in wet acetone),[75] 10^9 (dineopentyl phosphate in wet cyclohexane),[75] and 10^{12} (neopentyl phosphate dianion in wet cyclohexane)[76] have been reported and attributed to entropic contributions associated with solvent effects on the GS compared with the TS. The use of lower-polarity protic solvents is therefore suitable as a medium in which to capitalize on the numerous acceleratory effects yielded by enzyme active sites.

Overall, moving from aqueous to alcohol media with lower dielectric constants than water offers:[9]

1. Enhanced ion pairing between metal ions and anionic or dipolar substrates.
2. Larger Lewis acid interactions between metal ions and substrates.
3. Improved metal-lyoxide solubility and activity.
4. More favourable differential solvation effects.
5. Better organic substrate solubility.

1.6.3 – Substrate activation, nucleophile activation/delivery, leaving group activation/departure

Three direct, inner-sphere modes of activation provided by a metal can be dissected as follows:

1. Substrate activation.

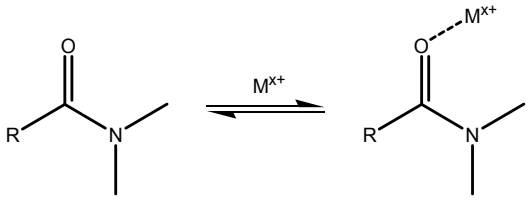

2. Nucleophile activation and delivery.

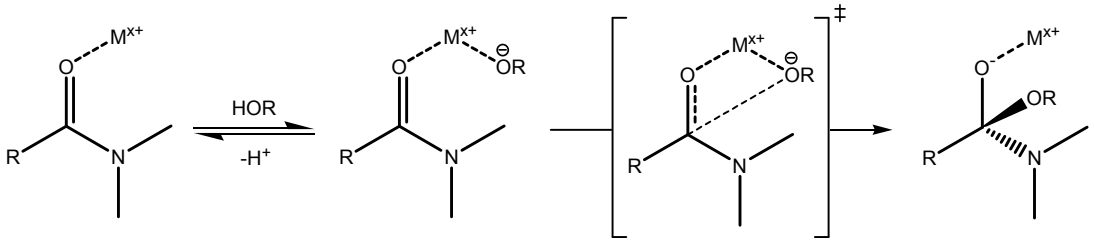

3. Leaving group activation and departure.

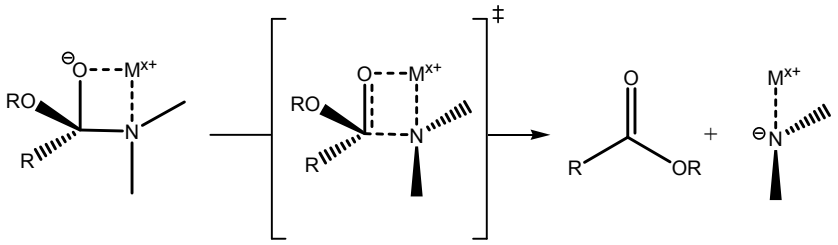

Substrate activation involves the metal ion acting as a Lewis acid to polarize the X=O (X = C, P) unit in order to enhance the electrophilicity at X. Nucleophile activation involves the metal ion acting as a Lewis acid to polarize the O–H bond of a solvent molecule, ROH (R = H, alkyl), acidifying the proton, and stabilizing formation of the conjugate base of the solvent. By virtue of a given metal ion binding and activating both the substrate and the nucleophile, the two are positioned in close proximity, permitting

facile intramolecular addition of the nucleophile to the X=O unit along the appropriate trajectory. The metal ion also acts to mitigate the electrostatic repulsion between electron-rich substrates and nucleophiles. Leaving group activation also involves the metal ion acting as a Lewis acid to polarize the X–LG bond and stabilizing the accumulation of negative charge on the departing heteroatom.

These three modes of activation have been quantitatively assessed in the context of phosphate ester hydrolysis.[6] Substrate activation is expected to yield 10^2-fold rate acceleration, intramolecular nucleophile activation is thought to contribute 10^8-fold rate acceleration, and leaving group activation is estimated to impart 10^6-fold rate acceleration (but theoretically could be as large as 10^{20}).[77] Additively, these effects can amount to upwards of 10^{16}-fold acceleration and in cases of substantial cooperativity, larger accelerations could be observed. Reactions taking place in lower-dielectric media such as methanol and ethanol may bring on further accelerations due to the enhanced interactions between the metal ion and the substrate/nucleophile/nucleofuge. Based on this analysis, it seems clear that leaving group activation plays a critical role in achieving the substantial accelerations brought on by particular enzymes and therefore has an enormous potential for integration into small-molecule catalysts.

1.7 – Metal ion-promoted LGA in small-molecule systems

1.7.1 – Metal ion-promoted leaving group assistance

Metal ion-promoted LGA has received much less attention in the literature than the other modes, likely due to the inherent challenge of positioning a metal ion in close proximity

to the LG heteroatom. In spite of this, its role in accelerating cleavage reactions should not be underestimated given that many natural substrates cleaved by enzymes contain nonactivated leaving groups. The use of metal ions by enzymes to stabilize leaving group departure from phosphate esters, for example, is crucial for achieving the rate accelerations required to sustain vital functions in living organisms.[78,79]

This mode of catalysis can take on at least two forms.[79] Firstly, acidification of a metal ion-coordinated solvent provides a general acid-promoted pathway. Second, direct coordination of the metal ion to the LG heteroatom, or possibly a distal site in electronic communication with the LG heteroatom, provides a Lewis acid-promoted pathway.

1.7.2 – Metal ion-promoted general acid assistance to LG departure

Alkaline earth metals have been shown to enhance the base-promoted ethanolysis of *N*-methyl-2,2,2-trifluoroacetanilide and its *m*-nitro analogue (Scheme 1-9).[80]

Scheme 1-9. Alkaline earth metal-promoted alkaline ethanolysis of *N*-methyl-2,2,2-trifluoroacetanilides; X = H, 3-NO_2; M = Ba, Sr.[80]

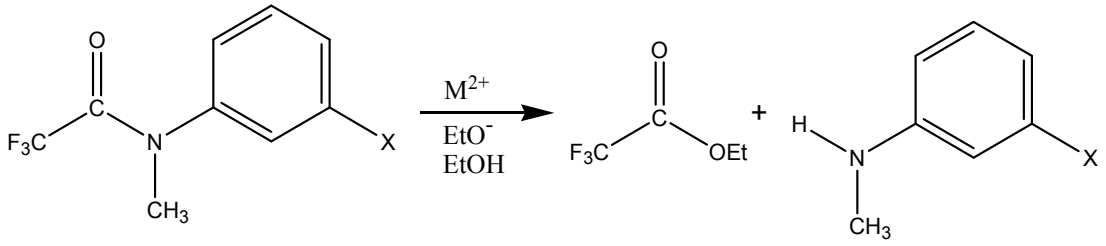

Rate enhancements of 15 and 19 times were observed in the presence of Ba^{2+} and Sr^{2+}, respectively, and were augmented to 55 and 150 times in the presence of 18-crown-6. The crown ether was proposed to reduce ion-pairing effects and the catalysis was

attributed to the general acid assistance to LG departure provided by a transiently-complexed metal ion-bound solvent as in **1.6**.

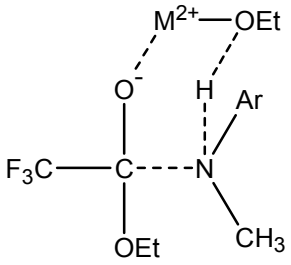

1.6

1.7.3 – Metal ion-promoted direct assistance to LG departure from carboxylate esters

One of the earliest accounts of the involvement of direct metal ion-promoted leaving group assistance in acyl-transfer reactions was described by Wasmuth and Freiser in 1962 when they postulated two modes by which a Cu(II) ion could accelerate hydrolysis of 8-acetoxyquinoline (**1.7**).[81]

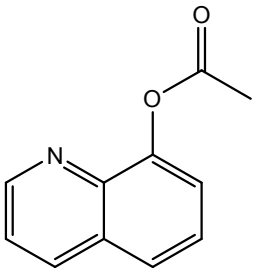

1.7

The Cu(II)-promoted reaction was found to be first order in the concentrations of ester, Cu(II), and hydroxide. The study was subsequently expanded to encompass a larger pH range as well a greater variety of di- and trivalent metal ions; the trends discovered were not straightforward, nor was quantifying the optimum acceleration, given that the

experiments were not carried out under saturating conditions for either metal ion or hydroxide (assuming the metal ion may activate the nucleophile directly or through a general base mechanism). It was proposed that the metal ion may play a dual role in activating the substrate through the carbonyl oxygen and subsequently rearranging to stabilize the departing phenoxy oxygen.[82] Alternatively, the metal ion may strictly bind in a bidentate fashion to the quinolyl N and aryl O in order to activate the substrate, mitigating the need for translocation in order to assist LG departure.

1.7.4 – Metal ion-promoted direct assistance to LG departure from carboxamides

Houghton and Puttner followed with the design of an amidic system, *N*,*N*-bis(2-picolyl)amide (**1.8**; R = *p*-$NO_2C_6H_4$, $(CH_3)_3C$, $CH_3CH{=}CH$), where the pyridine groups encourage binding of a Cu(II) ion to the amide nitrogen.[83]

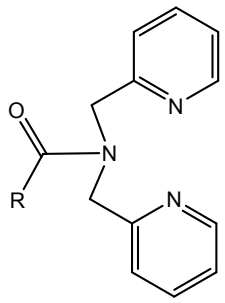

1.8

IR data suggest binding interactions exist between the Cu(II) and both pyridine nitrogens as well as the amide nitrogen. While solubility of the chloride complexes is poor in cold methanol, the authors noted that upon gentle heating, the reaction proceeds almost as quickly as the complex dissolves. The reaction also proceeds in hot water, however the Cu(II) complex is mostly dissociated, leading to a slower reaction.[83]

Lectka provided further spectroscopic as well as the first crystallographic evidence of a classical Werner-type complex involving coordination of a metal ion to a tertiary amide nitrogen.[84] The barrier to rotation was found to decrease (from 19.0 kcal·mol^{-1} in the free acetamide analogue to 16.3 kcal·mol^{-1} in the Cu(II) complex ($CDCl_3$, 20 °C)) concurrent with carbonyl bond strengthening (shift to 15–40 cm^{-1} higher frequency relative to the uncoordinated amide). Also of note, the crystal structure reveals clear Cu(II)-N_{amide} coordination through a Cu–N_{amide} bond distance of 2.49 Å. The geometry about Cu(II) is described as approximately trigonal-bipyramidal while the amide N is distinctly pyramidalized as a consequence of metal coordination.

Alsfasser and co-workers investigated several peptide analogues noting that while metal-coordination to the N_{amide} favours both cis-trans isomerization and bond cleavage, metal-promoted isomerization occurs on a millisecond timescale, whereas cleavage occurs at a considerably slower rate.[85] Studies on a family of similar peptidic compounds pointed to a structure-function relationship.[86] Firstly, a higher degree of N_{amide} pyramidalization (χ_N, Winkler-Dunitz parameter measuring pyramidalization of N_{amide}) was observed to correspond with a higher Lewis acidity of the coordinated metal. Pyramidalization was shown to either further augment or attenuate based on the electron-withdrawing or -donating nature of the coordinated ligands, respectively. Higher Lewis acidity of the complex also corresponds to a shorter Cu(II)–N_{amide} bond. Importantly, these structural features translate into higher rates of cis-trans isomerization as well as C–N bond cleavage.

More recently, the Brown group carried out a preliminary mechanistic investigation of the Cu(II)-promoted cleavage of *N*,*N*-bis(2-picolyl)acetamide (Scheme 1-10).[87] The kinetics for methanolytic decomposition of the Cu(II) complex were studied as a function of $^{s}_{s}$pH, revealing a kinetic $^{s}_{s}pK_a$ of 6.5 and a SKIE of 0.90 in the $^{s}_{s}$pH-independent plateau region. Together, these data are consistent with rate-limiting intramolecular delivery of a Cu(II)-bound methoxide to the C=O unit. Complementary computational data show binding of the Cu(II) involves coordination to the N_{amide} lone pair concomitant with delivery of a Cu(II)-bound methoxide to the C=O unit, forming a tetrahedral intermediate from which Cu(II) assists departure of the *N*,*N*-bis(2-picolyl)amide anion.

Scheme 1-10. Cu(II)-promoted methanolysis of *N*,*N*-bis(2-picolyl)acetamide.[87]

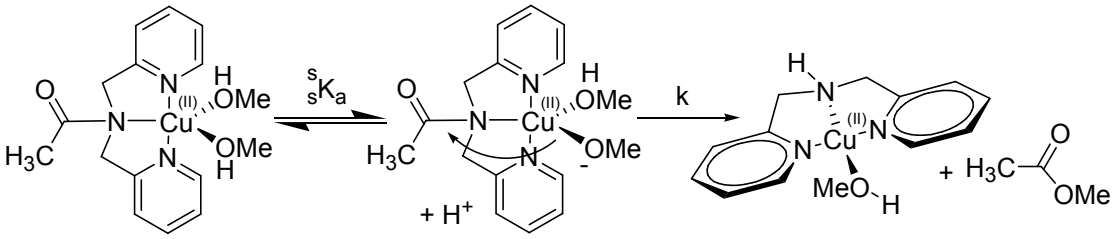

The modes of activation employed by the metal ion in this reaction are summarized below:

1. Activation of the substrate via association of Cu(II) with the N_{amide} lone pair, effectively decreasing amidic resonance.
2. Activation and delivery of the nucleophile through binding, acidification, and appropriate positioning of the metal-bound methoxide.
3. Stabilization of the TSs and tetrahedral intermediate through enhanced interactions between the metal and N_{amide} relative to those in the GS.

4. Stabilization of charge development on the N_{amide} through metal coordination, reducing the energy of the cleavage TS.

Of particular interest is the unique manner by which Cu(II) activates the substrate toward solvolysis – through binding the N_{amide} lone pair rather than conventional Lewis acid activation via the acyl oxygen. This form of activation nullifies the requirement to translocate the metal ion in order to carry out its multiple roles in escorting the substrate from reactant state to product state, making for highly efficient Lewis acid catalysis.

While direct coordination to the departing heteroatom of the LG leads to rate enhancements, binding of a distal heteroatom, which is in electronic communication with the departing atom, has also been shown to exert LGA. The second order rate constant for methoxide attack on the $(NH_3)_5Co(III)$ complex of acetyl imidazole (**1.10**) is 6000-fold larger than that on acetyl imidazole (**1.9**).[88] This degree of acceleration is afforded by a combination of substrate and LG activation by the coordination of $(NH_3)_5Co(III)$. Divalent transition metal ions such as Zn^{2+} and Co^{2+} catalyze the methanolysis of acetyl imidazole, but not its Co(III) complex, indicating these metal ions must act through transient binding to the distal N.

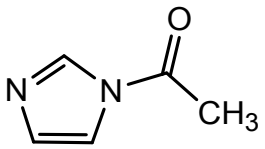

1.9

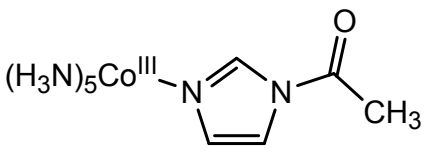

1.10

1.7.5 – Metal ion-promoted direct assistance to LG departure from phosphate esters

Early investigations into metal ion-promoted LGA in the context of phosphoryl-transfer reactions were conducted by Murakami in 1969.[89] Part of these accounts focused on the effect of divalent metal ions in promoting the hydrolysis of 2-, 3-, and 4-pyridylmethyl phosphates. The only notable acceleration was observed in the specific case of 2-pyridylmethyl phosphate (**1.11**) in the presence of Cu(II). The fact that Cu(II) did not enhance the cleavage to any significant extent for the other pyridylmethyl phosphates indicates the requirement for the metal ion to be in close proximity to the departing oxyanion in order to facilitate cleavage. Murakami delved further into the concept of metal ion-promoted LGA through a similar mechanistic study of 8-quinolyl phosphate (**1.12**).

Benkovic studied the hydrolysis of 2-(4(5)-imidazolyl)phenyl phosphate (**1.13**) in the presence of Cu(II) where it was observed that the imidazolyl nitrogen acts to position the metal ion in such a way as to enhance coordination to the phenoxy oxygen and subsequently stabilize the departing phenoxide oxyanion.[90] The pH/log(k) profile reveals the participation by Cu(II) increases upon conversion of the imidazolyl and phosphoryl moieties to their basic forms, but decreases upon ionization of a metal-coordinated water molecule. The acceleration obtained through metal ion participation is $>10^4$ compared to the uncatalyzed cleavage reaction.

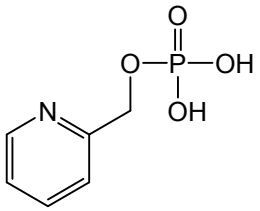

1.11

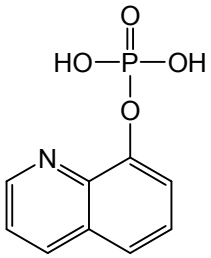

1.12

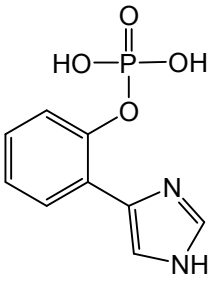

1.13

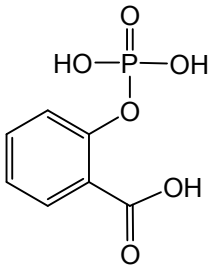

1.14

Inspired by the large rate accelerations for phosphate monoester cleavage brought on by Cu(II) reported by Benkovic[90] and those brought on by intramolecular general acid catalysis in the cleavage of salicyl phosphate reported by Kirby,[91] Hay reinvestigated two systems developed by Murakami[92] where relatively small accelerations were reported. Hay achieved rate accelerations on the order of 10^8 in the Cu(II)-promoted hydrolysis of salicyl phosphate (**1.14**).[93] Just as Benkovic had deduced from studying the Cu(II)-promoted cleavage of **1.13**, Hay proposed that the active species is the dianionic form of the phosphate monoester where the metal-coordinated water molecules remain protonated. Expanding his study to include 8-quinolyl phosphate revealed another system that anchors a Cu(II) in close proximity to the leaving group such that an estimated rate acceleration of $>10^6$ is achieved.[94]

Investigating the effect of La^{3+} on the hydrolysis of adenosine 3'-O(PO_2)–OCH_2R (R = 8-hydroxyquinol-2-yl and 8-(hydroxyquinolyl)-2-methylene) phosphate esters (**1.15**), Bruice proposed that the metal ion coordinates in such a way that it associates with the 8-quinolyloxy group to facilitate LG departure concurrent with nucleophilic attack. Along with Lewis acid activation, metal ion-promoted LGA by La^{3+} was shown to accelerate hydrolysis by 10^9.[95]

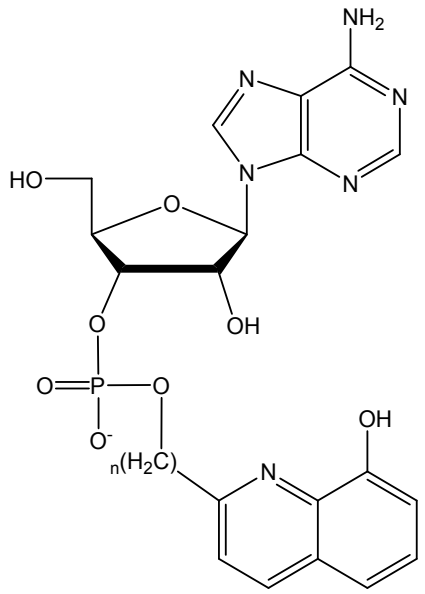

1.15

Other investigations into the ability of lanthanide metal ions to provide LGA in the methanolytic cleavage of *ortho*-methoxycarbonylphenyl phosphate di- and triesters revealed rate enhancements over the estimated background solvolytic reaction of 10^{12}- and 60-fold, respectively.[96,97] In the $Yb(OTf)_3$-promoted cleavage of phosphate diesters in methanol at low $^{s}_{s}$pH, rate accelerations on the order of 10^{12} were observed compared to the background reactions.

Scheme 1-11. $Yb(OTf)_3$-promoted cleavage of phosphate diesters in methanol; M = Yb.[96]

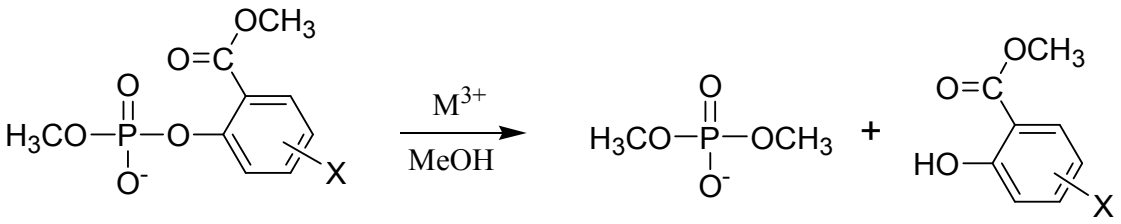

1.16

Given that methyl aryl phosphate diesters without the *ortho*-carboxymethyl (*o*-CM) substituent do not react under these conditions, this study is particularly instructive in the quantitation of the rate effect afforded by LGA as well as the degree of charge transfer from the LG to the metal ion. The study demonstrates that while the *ortho*-carboxymethyl-substituted phosphate diesters in the presence of $Yb(OTf)_3$ react by a rapid solvent-mediated process, the *para*-carboxymethyl (*p*-CM) analogue does not react under the same conditions within 24 hours. It follows that Yb^{3+} accelerates solvolysis by strong binding to the TS for leaving group departure. Given that the kinetically-determined binding constant for **1.16** (X = H) matches the one determined spectrophotometrically for the *p*-CM analogue, the GS binding appears to be dominated by the PO_2-portion of the substrate and the acceleratory effect originates from TS binding. Titration data of phenols with and without an *o*-CM substituent enabled a comparison that revealed a 3000-fold binding enhancement that translates into an added TS stabilization of ~4.7 kcal·mol^{-1}.[96]

Given the presence of two substituents on the LG, the Jaffé[98] extension was employed, determining that $\rho_{phosphate}$ and ρ_{CO_2Me} are +1.84 ± 0.11 and -0.85 ± 0.14, respectively. The positive $\rho_{phosphate}$ indicates electron-withdrawing substituents enhance reactivity by stabilizing the formation of negative charge on the phenolic oxygen. The negative ρ_{CO_2Me} reveals substituents capable of donating electron density toward the CM group enhance reactivity. It was also determined, through conversion of Jaffé relationships to Brønsted relationships and its employment in determining the Leffler coefficient, that $\alpha = 0.51$, indicating P–OAr is halfway between the GS and the PS. Analysis of charge map[99] data[96]

reveals effective charge values of +0.79 on the phenoxy oxygen in the GS, +0.31 in the TS, and -0.16 in the PS (compared to -1.0 in the PS in the absence of metal). The reduction in charge on the metal-bound LG accounts for more effective LGA in poorer LGs than better LGs relative to a comparison without LGA. The powerful effect of LGA is made clear by its reduction in the need for a strong nucleophile, such as the lyoxide of the solvent, to displace the LG. In this case, the weakest nucleophile in highest concentration, namely solvent, is sufficiently nucleophilic to carry out solvolysis. The reaction is thought to proceed through a concerted mechanism with minimal participation of the nucleophile in the activated complex. The solvent DKIE for **1.16** is $k_H/k_D = 1.10 \pm 0.15$ and activation parameters are $\Delta H^{\ddagger} = 16.1$ kcal·mol^{-1} and $\Delta S^{\ddagger} = -15$ cal·mol^{-1}·K^{-1}.[96] The small SKIE value is consistent with a loose TS and the $\Delta S^{\ddagger}$ is described as a composite of a loose TS with advanced P–OAr bond cleavage as well as order associated with the requirement for binding of the metal ion.

Charge map analysis was also applied to the $(La^{3+}(^{-}OCH_3))_2$-catalyzed cleavage of phosphate triesters without (**1.17**; R = Me, Et) and with (**1.18**) *o*-CM substituents on the LG, providing further insight into metal ion-promoted LGA and how it manifests in LFER data.[97]

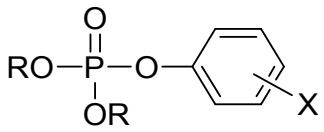

1.17

Scheme 1-12. $La(OTf)_3$-promoted cleavage of phosphate triesters in methanol; M = La.[97]

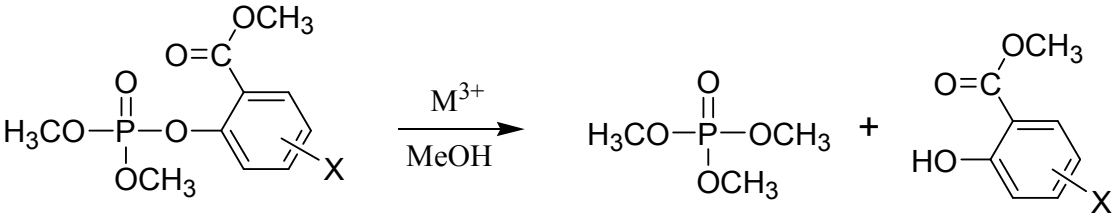

1.18

In this study, it was noted that although the magnitude of the β_{lg} value may decrease from a system lacking LGA (β_{lg} = -1.25) to one exhibiting LGA (β_{lg} = -0.82), that change is not necessarily a consequence of reduced scission of the bond to the LG, but rather due to a reduction in total charge development on the departing LG heteroatom rendered by charge transfer to the metal ion. It was shown that, in fact, the cleavage had progressed further, as assessed by the respective Leffler coefficients (α = 0.68 vs 0.88).[97]

In line with work performed by Murakami, Benkovic, and Hay, the Brown group conducted a detailed kinetic investigation into the Cu(II)-promoted cleavage of a homologous set of phosphate mono-, di-, and triesters bearing a 2′-(2-phenoxy)-1,10-phenanthroline leaving group (**1.19a**–**c**) that positions the metal ion within ~1.9 Å of the departing oxyanion (Scheme 1-13).[100]

Scheme 1-13. Cu(II)-promoted methanolysis of a homologous set of phosphate mono-, di-, and triesters bearing a 2′-(2-phenoxy)-1,10-phenanthroline leaving group.[100]

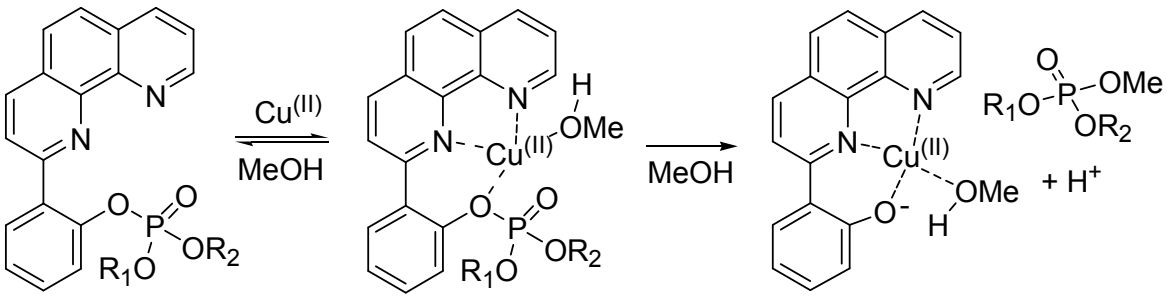

1.19a $OR_1 = OR_2 = O^-$
b $OR_1 = O^-$; OR_2 = OMe
c $OR_1 = OR_2$ = OMe

1.20

Substantial stabilization of the anionic form of the LG is demonstrated by the 15.6-unit reduction in the ${}^{s}_{s}pK_a$ of its conjugate acid relative to the uncomplexed form (Scheme 1-14); accompanying this is an increase of 10^{17} in the binding affinity of Cu(II) for the anionic species relative to the neutral form. It follows that some portion of this binding energy (23.3 kcal·mol^{-1}) must be realized in an analogous phosphoryl transfer process where **1.20** is formed.

Scheme 1-14. Thermodynamic cycle representing the acid dissociation constants ($^{s}_{s}pK_a$) for the Cu(II)-complexed and uncomplexed LG as well as the related dissociation constants (K_d) for Cu(II)-coordination to the protonated and ionized forms of the LG.[100]

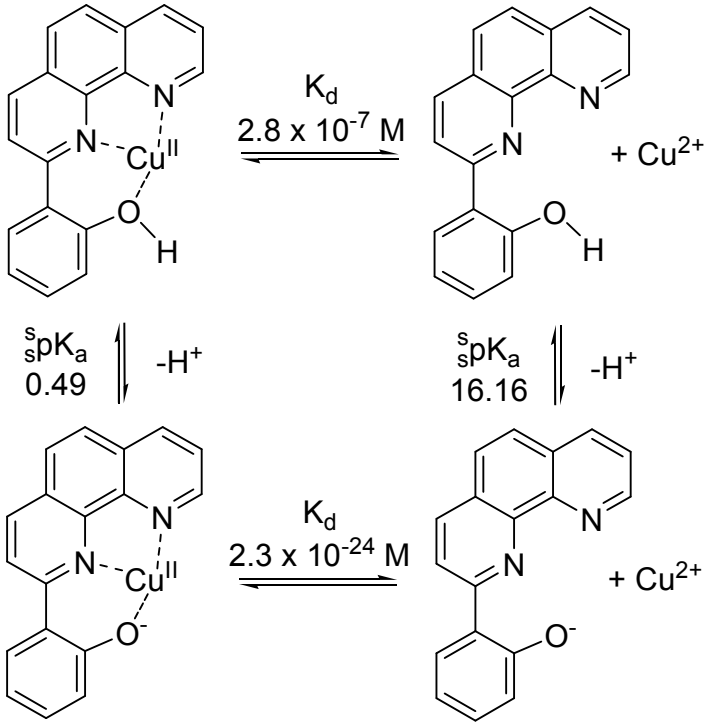

The rates of methanolytic cleavage of these complexes at their $^{s}_{s}pH$ maxima in the neutral $^{s}_{s}pH$ region indicate that Cu(II)-promoted LGA accelerates the cleavage of the phosphate mono-, di-, and triesters by 10^{14} to 10^{15}, 10^{14}, and 10^{5} (respectively) over the estimated rates of the background reactions. This study afforded further insight into the mechanistic implications of LGA as well as the energetic origins of its effects. In complement to observations from the $Yb(OTf)_3$-promoted cleavage of phosphate diesters in methanol,[96] the SKIE data indicate the active nucleophile is solvent in all three cases. Copper(II)-promoted solvolysis of the phosphate triester, whose TS requires the most involvement of the nucleophile and therefore sheds the most light on its identity, exhibits a SKIE of 2.2 ± 0.1 which points toward solvent acting as a general base to promote

nucleophilic attack of a second MeOH. Together, these studies suggest that sufficient extrinsic activation of the LG can reduce the requirement for nucleophilic participation to the point where the weakest nucleophile in greatest concentration is capable of ejecting the LG.

While all three reactions are expected to be concerted, the activation parameters shed light on the nature of the activated complexes. The enthalpies of activation for all three esters are the same within experimental error and so the differences in reactivity originate from the entropies of activation. The values can be interpreted in light of the tightness of the cleavage TS – the triester has a relatively tight and therefore restrictive TS ($\Delta S^{\ddagger}$ = -7.4 ± 1.7 cal·mol^{-1}·K^{-1}), the diester ($\Delta S^{\ddagger}$ = 2.3 ± 1.1 cal·mol^{-1}·K^{-1}) has a looser TS than the triester, but a tighter one than the monoester ($\Delta S^{\ddagger}$ = 18 ± 2 cal·mol^{-1}·K^{-1}).[100] The effect of Cu(II) on these TSs in the Hammond and anti-Hammond senses can be understood in light of a More O'Ferrall-Jencks diagram (Figure 1-6). By stabilizing the LG through Cu(II)-coordination, the cleavage TSs shift so as to reduce the requirement for nucleophilic participation in expelling the LG. Also contributing to these values is differential solvation where, depending on the change in charge from the GS to the TS, the restriction or release of solvent may augment or attenuate the abovementioned effects.

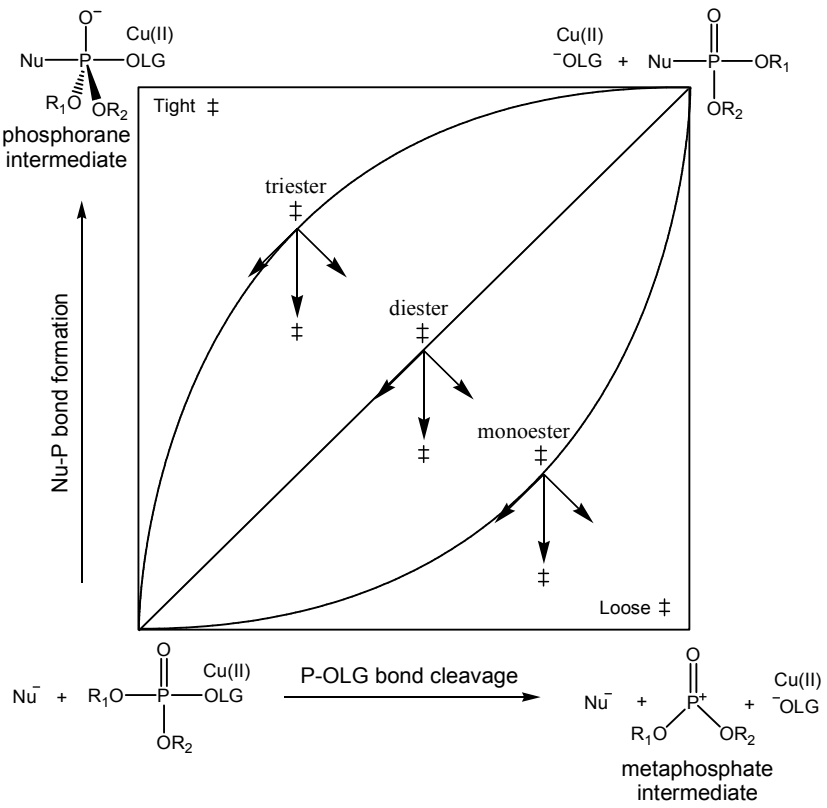

Figure 1-6. More O'Ferrall-Jencks diagram illustrating the effect of Cu(II)-coordination to the LG on the 2D free energy surface and reaction pathways for phosphoryl transfer from phosphate mono-, di-, and triesters.[100]

1.7.6 – Metal ion-promoted LGA in cases involving small-molecule catalysts

The vast majority of the abovementioned systems were designed to enforce a metal ion to interact with the LG. While such systems are instructive in assessing the magnitude and mechanism of metal ion-promoted LGA, they do not demonstrate whether this mode of catalysis is operative in small-molecule catalysts. The following examples typify systems in which there is physical evidence alongside thorough computational analyses that implicate LGA as a significant player in shaping the free energy surface on which the reactions proceed.

Phosphate ester cleavage

The dinuclear Zn(II)-containing catalyst (**1.21**) has been shown to provide enormous rate accelerations for the cleavage of phosphate diester models of DNA and RNA in methanol and ethanol.[101,102,103]

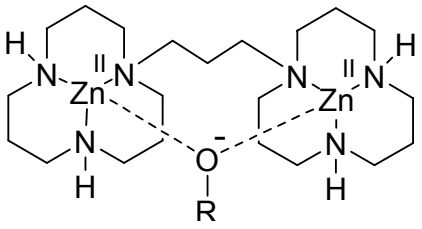

1.21

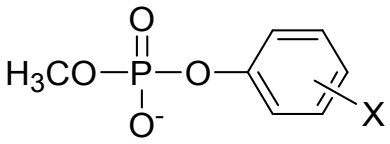

1.22

In the case of the methanolysis of a series of *O*-aryl *O*-methyl phosphate diesters (**1.22**),[102] the methoxide-promoted reaction exhibits a β_{lg} of -0.59, the di-Zn(II)-promoted reaction (excluding diesters containing *o*-NO_2 or *o*-CM substituents on their LG) exhibits a β_{lg} of -0.57, and the di-Zn(II)-promoted reaction of diesters containing *o*-NO_2 or *o*-CM substituents on their LG exhibits a β_{lg} of -0.34 (refer to Brønsted plots in Figure 1-7).

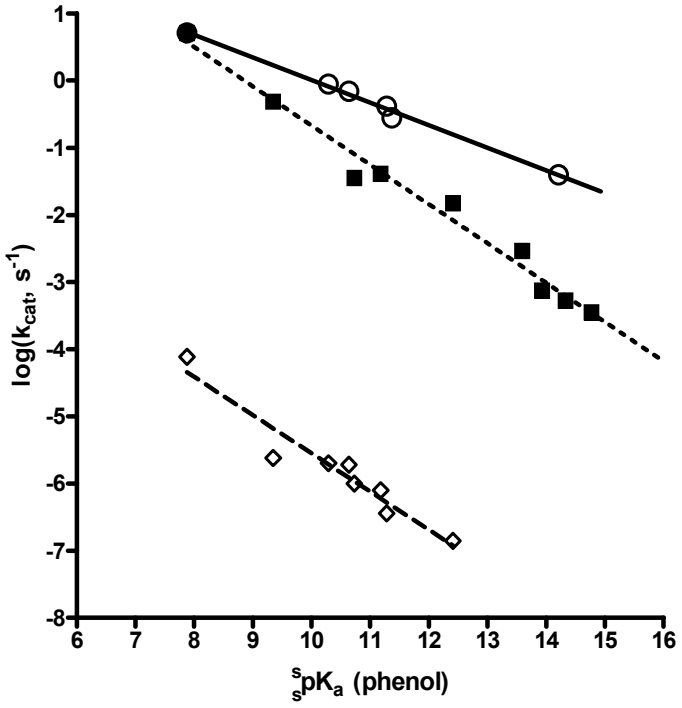

Figure 1-7. Brønsted plots: ◊-data represent log of the pseudo-first order rate constants for the methoxide-promoted methanolysis of **1.22** ($[CH_3O^-]$ = 1 mM) vs ${}^{S}_{S}pK_a^{HOAr}$; ■-data represent log of k_{cat} for the **1.21**-promoted methanolysis of **1.22** (excluding diesters containing *o*-NO_2 or *o*-CM substituents on their LG) vs ${}^{S}_{S}pK_a^{HOAr}$; ○-data represent log of k_{cat} for the **1.21**-promoted methanolysis of **1.22** which contain *o*-NO_2 or *o*-CM substituents on their LG.[102]

Given that the magnitude of such gradients reflects the amount of electron density accumulating on the LG in the rate-limiting TS, the smaller magnitude of β_{lg} in the cases where an *o*-NO_2 or *o*-CM substituent is available is a consequence of the interaction between the catalyst and departing phenoxide. Support is found in the stable complexes formed by the di-Zn(II) catalyst and the *o*-NO_2- or *o*-CM-substituted phenoxides in methanol[102] as well as detailed computational analyses.[104] The reaction was modelled starting with the substrate doubly-bound to the catalyst through the phosphoryl and

nonbridging oxygen atoms. Next, the bridging methoxide dissociates away from one Zn(II) to become terminal leading to four energetically feasible pathways.[104]

1. (Stepwise) Direct nucleophilic attack of a Zn_1(II)-bound methoxide at phosphorus leading to a phosphorane intermediate, followed by rate-limiting rearrangement of the LG in order for the departing oxygen to bind Zn_2(II) to provide LGA.
2. (Concerted) Direct nucleophilic attack of a Zn_1(II)-bound methoxide at phosphorus concurrent with Zn_2(II)-bound solvent-assisted LG departure.
3. (Enforced concerted) Attack of a methanol with assistance from a Zn_1(II)-bound methoxide concurrent with Zn_2(II)-assisted LG departure.
4. (Concerted) Attack of a methanol with assistance from a Zn_1(II)-bound methoxide concurrent with Zn_2(II)-bound solvent-assisted LG departure.

Mechanism 1 was considered the least feasible on the basis of a $\Delta G^{\ddagger}$ that is ~4.8 kcal·mol^{-1} higher than the others, which are close to one another and to the experimental value of 19.3 kcal·mol^{-1}.[104] The mechanistic diversity represented here was noted to be a consequence of conformational flexibility in the catalyst which can both escort the transforming substrate from GS to PS and accommodate a variety of substrates. Importantly, three of the four computed pathways involve some form of metal ion-promoted LGA despite the intrinsic assistance from a 4-nitro substituent. It is anticipated, based on the shallow gradient of pertinent Brønsted plots,[97] that such pathways would become even more important for poorer LGs, such as those employed by Nature.

Carboxylate ester cleavage

The mononuclear Zn(II)-containing catalyst **1.23** has been shown to provide substantial rate accelerations for the cleavage of carboxylate esters (**1.24**).[105]

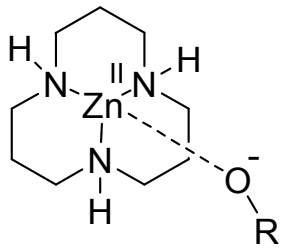

1.23

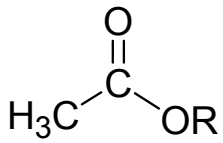

1.24

The Brønsted plot of the second-order rate constant for mono-Zn(II)-promoted methanolysis of esters **1.24** exhibits two domains which meet at a breakpoint of ${}^{s}_{s}pK_a^{HOLG} = 14.8$. In the lower ${}^{s}_{s}pK_a^{HOLG}$-domain, $\beta_{lg} \approx 0$; in the higher ${}^{s}_{s}pK_a^{HOLG}$-domain, $\beta_{lg} = -0.7$.[105] Such downward curvature may be indicative of a change in rate-limiting step where attack of the Zn(II)-coordinated methoxide is rate-limiting in the lower ${}^{s}_{s}pK_a^{HOLG}$-domain and breakdown of the tetrahedral intermediate is rate-limiting in the higher ${}^{s}_{s}pK_a^{HOLG}$-domain. Further insight into the mechanism was garnered through computational analysis of a subset of substrates as well as some additional esters which span a similar ${}^{s}_{s}pK_a^{HOLG}$ range.[106] The computed Brønsted plot reveals separate plots for aryl and alkyl acetates, clarifying the position of the seemingly-arbitrary breakpoint in the experimental data that is much lower than the symmetrical reaction of methyl acetate. In the lower-${}^{s}_{s}pK_a^{HOLG}$ domain (aryloxy LGs) where $\beta_{lg} = 0.07$, nucleophilic attack is rate-limiting; in the mid-${}^{s}_{s}pK_a^{HOLG}$ domain (alkoxy LGs) where $\beta_{lg} = -0.62$, nucleophilic attack is rate-limiting; in the higher-${}^{s}_{s}pK_a^{HOLG}$ domain (alkoxy LGs) where $\beta_{lg} = -2.04$, metal ion-promoted LGA is rate-limiting.[106] The break in the alkoxy-LG plot occurs at methyl

acetate, as expected on the basis of microscopic reversibility. In all cases, LGA appears to be operative. In addition, this study provides evidence that while in many cases two metal ions are implicated in mechanisms involving LGA, one metal ion may fulfill the various modes of metallo-catalysis so long as the steps for requisite rearrangements are sufficiently fast.

1.8 – Research outline

By combining several modes of metallo-activation with a reduced dielectric medium, significant rate enhancements are observed in acyl- and phosphoryl-transfer reactions.[9,70,79] One of the more elusive modes, namely metal ion-promoted LGA, has been studied only to a limited extent in terms of its magnitude and mechanism. The ongoing collection of linear free energy relationships, $^{s}_{s}$pH/log(k) profiles, activation parameters, and SKIE data in a variety of systems contributes to the developing mechanistic picture of LGA and hints at its potential as a general means to accelerate cleavage reactions. As part of this evolving program, three separate yet connected mechanistic studies are discussed.

1.8.1 – Metal ion-promoted LGA in the solvolysis of specially-designed phosphate esters in aqueous and alcohol solvents[107]

Chapter 2 compares the energetic origins of Cu(II)-promoted LGA in a homologous set of mono-, di-, and triesters in different hydroxylic solvents to evaluate medium effects on the mechanism and magnitude of LGA. This study builds on a previous one[100] that established the enormous potential for LGA to accelerate the methanolysis of these specially-designed complexes. Moving these systems into water and ethanol established

the general nature of these effects and enabled the quantitative assessment of how the medium influences this particular mode of catalysis.

1.8.2 – Metal ion-promoted LGA in the solvolysis of specially-designed tertiary benzamides in alcohol solvents[108]

Chapters 3 and 4 describe mechanistic studies of the Ni(II)-, Cu(II)-, and Zn(II)-promoted methanolysis and ethanolysis of substituted benzamides specially-designed to employ LGA (phenyl-substituted benzamides with either *N*,*N*-bis(2-picolyl) or *N*,*N*-bis((1*H*-benzimidazol-2-yl)methyl) binding groups). Building on a recent study,[87] as well as much earlier work,[83] and further motivated by its successful application as a synthetic methodology,[109] the mechanism of this elusive mode of catalysis was more completely elucidated using LFER, SKIE, Eyring, and computational data. The opportunity was also taken to assess the accelerations provided by LGA in combination with the other modes of metallo-catalysis relative to the background alkoxide-promoted reactions. The results of these studies form the basis on which more recent investigations have characterized similar effects in the solvolysis of specially-designed ureas[110] and carbamates.[111]

1.8.3 – Metal ion-promoted LGA in the solvolysis of a series of thiobenzanilides in methanol

Chapter 5 contributes more detail to the existing mechanistic picture[112] of the palladacycle-promoted methanolysis of a series of thiobenzanilides with leaving groups bearing different substituents. The kinetic data collected thus far appear to indicate two mechanisms are operating, depending on the nature of the leaving group, wherein either one or two catalysts employ the following modes of metallo-catalysis to promote

cleavage: substrate activation, nucleophile activation and delivery, and leaving group assistance. This study seems to demonstrate that as the nucleofugality of a LG worsens, Nature appears to recruit a second catalytic centre, seemingly to distribute the catalytic requirements of the mechanism over two metal centres rather than one.

The theme of this work is establishing a fundamental understanding of the origin, mechanism, and magnitude of the critical modes of catalysis employed by metal ions that enable the facile cleavage of kinetically-inert substrates. As this level of understanding improves, the capabilities of enzymes become ever more comprehensible and surpassing the magnitude of their catalysis becomes increasingly feasible.

1.9 – References and notes

[1] Hengge, A. C. *Adv. Phys. Org. Chem.* **2005**, *40*, 49.

[2] (a) Cowan, J. A. *Chem. Rev.* **1998**, *98*, 1067. (b) Lipscomb, W. N.; Straïter, N. *Chem. Rev.* **1996**, *96*, 2375. (c) Straïter, N.; Lipscomb, W. N.; Klabunde, T.; Krebs, B. *Angew. Chem., Int. Ed. Engl.* **1996**, *35*, 2024.

[3] (a) Main, R. A.; Iverson, F. *Biochem. J.* **1966**, *100*, 525. (b) Emsley, J.; Hall, D. *The Chemistry of Phosphorus*; Wiley: New York, 1976; p 494.

[4] Westheimer, F. H. *Science* **1987**, *235*, 1173.

[5] Lad, C.; Williams, N. H.; Wolfenden, R. *Proc. Natl. Acad. Sci. U.S.A.* **2003**, *100*, 5607.

[6] Williams, N. H; Takasaki, B.; Wall, M.; Chin, J. *Acc. Chem. Res.* **1999**, *32*, 485.

[7] Greenberg, A.; Breneman, C. M.; Liebman, J. F. *The Amide Linkage: Structural Significance in Chemistry, Biochemistry, and Materials Science.* Hoboken: John Wiley & Sons; 2003.

[8] Radzicka, A.; Wolfenden, R. *J. Am. Chem. Soc.* **1996**, *118*, 6105.

[9] Brown, R. S.; Neverov, A. A. *Adv. Phys. Org. Chem.* **2008**, *42*, 271.

[10] Cleland, W. W.; Hengge, A. C. *Chem. Rev.* **2006**, *106*, 3252.

[11] (a) Kirby, A. J.; Varvoglis, A. G. *J. Am. Chem. Soc.* **1967**, *89*, 415. (b) Kirby, A. J.; Jencks, W. P. *J. Am. Chem. Soc*. **1965**, *87*, 3209.

[12] (a) Hengge, A. C.; Edens, W. A.; Elsing, H. *J. Am. Chem. Soc*. **1994**, *116*, 5045. (b) Gorenstein, D. G.; Lee, Y.-G.; Kar, D. J. *J. Am. Chem. Soc.* **1977**, *99*, 2264.

[13] Buchwald, S. L.; Friedman, J. M.; Knowles, J. R. *J. Am. Chem. Soc.* **1984**, *106*, 4911.

[14] (a) Friedman, J. M.; Freeman, S.; Knowles, J. R. *J. Am. Chem. Soc.* **1987**, *110*, 1268. (b) Hoff, R. H.; Hengge, A. C. *J. Org. Chem.* **1998**, *63*, 6680.

[15] Di Sabato, G.; Jencks, W. P. *J. Am. Chem. Soc.* **1961**, *83*, 4400.

[16] (a) Kirby, A. J.; Younas, M. *J. Chem. Soc. B* **1970**, 1165. (b) Khan, S. A.; Kirby, A. J. *J. Chem. Soc. B* **1970**, 1172.

[17] Hengge, A. C. *Acc. Chem. Res.* **2002**, *35*, 105.

[18] Wolfenden, R. *Chem. Rev.* **2006**, *106*, 3379.

[19] Hall, C. R.; Inch, T. D. *Tetrahedron* **1980**, *36*, 2059.

[20] Rowell, R.; Gorenstein, D. G. *J. Am. Chem. Soc.* **1981**, *103*, 5894.

[21] (a) Ba-Saif, S. A.; Waring, M. A.; Williams, A. *J. Am. Chem. Soc.* **1990**, *112*, 8115. (b) Ba-Saif, S. A.; Waring, M. A.; Williams, A. *J. Chem. Soc. Perkin Trans. 2* **1991**, 1653.

[22] Brown, R. S.; Bennet, A. J.; Slebocka-Tilk, H. *Acc. Chem. Res.* **1992**, *25*, 481.

[23] Challis, B. C.; Challis, J. A. *The Chemistry of Amides: Reactions of the Carboxamide Group*, John Wiley & Sons Ltd.; New York, 1970; pp 731–857.

[24] Eriksson, S. O. *Acta Chem. Scand.* **1968**, *22*, 892.

[25] DeWolfe, R. H.; Newcomb, R. C. *J. Org. Chem.* **1971**, *36*, 3870.

[26] Bunton, C. A.; Nayak, B.; O'Connor, C. *J. Org. Chem.* **1968**, *33*, 572.

[27] Slebocka-Tilk, H.; Bennet, A. J.; Keillor, J. W.; Brown, R. S.; Guthrie, J. P.; Jodhan, A. *J. Am. Chem. Soc.* **1990**, *112*, 8507.

[28] Schowen, R. L.; Hopper, C. R.; Bazikian, C. M. *J. Am. Chem. Soc.* **1972**, *94*, 3095.

[29] Broxton, T. J.; Deady, L. W. *J. Org. Chem.* **1974**, *39*, 2767.

[30] Broxton, T. J.; Deady, L. W. *J. Org. Chem.*, **1975**, *40*, 2906.

[31] Mitton, C. G.; Gresser, M.; Schowen, R. L. *J. Am. Chem. Soc.* **1969**, *91*, 2045.

[32] Hopper, C. R.; Schowen, R. L.; Venkatasubban, K. S.; Jayaraman, H. *J. Am. Chem. Soc.* **1973**, 95, 3280.

[33] Swift, E. H.; Butler, E. A. *Division of Analytical Chemistry*. **1956**, *28*, 146.

[34] Peeters, O. M.; De Ranter, C. J. *J.C.S. Perkin II*, **1974**, 1832.

[35] Hall, A. J.; Satchell, D. P. N. *J.C.S. Perkin II*, **1974**, 1077.

[36] Peeters, O. M.; De Ranter, C. J. *J.C.S. Perkin II*, **1976**, 1062.

[37] Rosenthal, D.; Taylor, T. I. *J. Am. Chem. Soc.* **1957**, *79*, 2684.

[38] Broxton, T. J.; Deady, L. W.; Rowe, J. E. *Aust. J. Chem.* **1978**, *31*, 1731.

[39] Smith, S. G.; O'Leary, M. *J. Org. Chem.* **1963**, *28*, 2825.

[40] Campbell, P.; Lapinskas, B. A. *J. Am. Chem. Soc.* **1977**, *99*, 5378.

[41] Weston, J. *Chem. Rev.* **2005**, *105*, 2151.

[42] Parkin, G. *Chem*. *Rev*. **2004**, *104*, 699.

[43] Schwartz, J.; Crestfield, A.; Lipmann, F. *Proc. Natl. Acad. Sci. U.S.A.* **1963**, *49*, 722.

[44] Jones, S. R.; Kindman, L. A.; Knowles, J. R. *Nature* **1978**, *275*, 564.

[45] (a) Bale, J.; Huang, C.; Chock, P. *J. Biol. Chem.* **1980**, *255*, 8431. (b) Block, W.; Schlesinger, M. J. *J. Biol. Chem.* **1973**, *248*, 5794.

[46] O'Brien, P. J.; Herschlag, D. *Biochemistry* **2002**, *41,* 3207.

[47] (a) Freemont, P. S.; Friedman, J. M.; Beese, L. S.; Sanderson, M. R.; Steitz, T. A. *Proc. Natl. Acad. Sci. U.S.A.* **1988**, *85*, 8924. (b) Beese, L. S.; Steitz, T. A. *EMBO J.* **1991**, *10*, 25.

[48] Stec, B.; Holtz, K. M.; Kantrowitz, E. R. *J. Mol. Biol.* **2000**, *299*, 1303.

[49] Orhanović, S.; Pavela-Vrancic, M.; Flogel-Mrsić, M. *Acta. Pharm.* **1994**, *44*, 87.

[50] Rawlings, J.; Cleland, W.; Hengge, A. C., *J. Am. Chem. Soc.* **2006**, *128*, 17120.

[51] (a) Little, C.; Otnaess, A. *Biochim. Biophys. Acta* **1975**, *391*, 326. (b) Little, C. *Acta Chem. Scand. B* **1981**, *35*, 39. (c) Hough, E.; Hansen, L. K.; Birkness, B.; Jynge, K.; Hansen, S.; Hordvik, A.; Little, C.; Dodson, E.; Derwenda, Z. *Nature* **1989**, *338*, 355.

[52] Martin, S. F.; Follows, B. C.; Hergenrother, P. J.; Trotter, B. K. *Biochemistry* **2000**, *39*, 3410.

[53] Thrige, D. G.; Buur, J. R.; Jorgensen, F. S. *Biopolymers* **1997**, *42*, 319.

[54] Martin, S. F.; Hergenrother, P. J. *Biochemistry* **1999**, *38*, 4403.

[55] Wilcox, D. E. *Chem. Rev.* **1996**, *96*, 2435.

[56] Antikainen, N. M.; Monzingo, A. F.; Franklin, C. L.; Robertus, J. D.; Martin, S. F. *Arch*. *Biochem*. *Biophys*. **2003**, *417*, 81.

[57] (a) Mulbry, W. W.; Karns, J. S.; Kearney, P. C.; Nelson, J. O.; McDaniel, C. S.; Wild, J. R. *Appl. Environ. Microbiol*. **1986**, *51*, 926. (b) Horne, I.; Sutherland, T. D.; Harcourt, R. L.; Russell, R. J.; Oakeshott, J. G. *Appl. Environ. Microbiol.* **2002**, *68*, 3371.

[58] (a) Donarski, W. J.; Dumas, D. P.; Heitmeyer, D. P.; Lewis, V. E.; Raushel, F. M. *Biochemistry* **1989**, *28,* 4650. (b) Dumas, D. P.; Caldwell, S. R.; Wild, J. R.; Raushel, F. M. *J. Biol. Chem.* **1989**, *264*, 19659.

[59] Aubert, S. D.; Li, Y.; Raushel, F. M. *Biochemistry* **2004**, *43,* 5707.

[60] Lewis, V. E.; Donarski, W. J.; Wild, J. R.; Raushel, F. M. *Biochemistry* **1988**, *27,* 1591.

[61] Vanhooke, J. L.; Benning, M. M.; Raushel, F. M.; Holden, H. M. *Biochemistry* **1996**, *35,* 6020.

[62] Caldwell, S. R.; Newcomb, J. R.; Schlecht, K. A.; Raushel, F. M. *Biochemistry* **1991**, *30,* 7438.

[63] Holz, R. C. *Coord. Chem. Rev.* **2002**, *232*, 5.

[64] Ustynyuk, L.; Bennett, B.; Edwards, T.; Holz, R. C. *Biochemistry* **1999**, *38*, 11433.

[65] Chen, G.; Edwards, T.; D'souza, V.M.; Holz, R. C. *Biochemistry* **1997**, *36*, 4278.

[66] (a) Bienvenue, D. L.; Mathew, R. S.; Ringe, D.; Holz, R. C. *J. Biol. Inorg. Chem.* **2002**, *7*, 129. (b) Elrod, J. P.; Hogg, J. L.; Quinn, D. M.; Venkatasubban, K. S.; Schowen, R. L. *J. Am. Chem. Soc.* **1980**, *102*, 3917.

[67] Cleland, W. W. *Crit. Rev. Biochem.* **1982**, *13*, 385.

[68] Harned, H. S.; Owen, B. B. *The Physical Chemistry of Electrolytic Solutions*, 3rd ed.; ACS Monograph Series 137; Reinhold Publishing: New York, 1957; p 161.

[69] Levine, I. N. *Physical Chemistry*, 4th ed.; McGraw-Hill, Inc.; U.S.A., 1978; pp 276–281.

[70] Brown, R. S. *Prog. Inorg. Chem.* **2012**, *57*, 55.

[71] Cleland, W. W.; Frey, P. A.; Gerlt, J. A. *J. Biol. Chem.* **1998**, *273*, 25529. (b) Simonson, T.; Carlsson, F.; Case, D. A. *J. Am. Chem. Soc*. **2004**, *126*, 4167.

[72] Forconi, M. *Adv. Phys. Org. Chem.* **2015**, *49*, 57.

[73] Abell, K. W. Y.; Kirby, A. J. *Tetrahedron Lett.* **1986**, *27*, 1085.

[74] Hoff, R. H.; Hengge, A. C. *J. Org. Chem.* **1998**, *63*, 6680.

[75] Stockbridge, R. B.; Wolfenden, R. *Chem. Commun.* **2010**, *46*, 4306.

[76] Stockbridge, R. B.; Wolfenden, R. *J. Am. Chem. Soc.* **2009**, *131*, 18248.

[77] Lassila, J. K.; Zalatan, J. G.; Herschlag, D. *Annu. Rev. Biochem.* **2011**, *80*, 669.

[78] Cleland, W. W.; Hengge, A. C. *Chem. Rev.* **2006**, *106*, 3252.

[79] Brown, R. S. *Adv. Phys. Org. Chem.* **2015**, *49*, 1.

[80] Cacciapaglia, R.; Di Steano, S.; Kelderman, E.; Mandolini, L.; Spadola, F. *J. Org. Chem.* **1998**, *63*, 6476.

[81] Wasmuth, C. R.; Freiser, H. *Talanta* **1962**, *9*, 1061.

[82] Barca, R. H.; Freiser, H. *J. Am. Chem. Soc.* **1966**, *88*, 3744.

[83] Houghton, R. P.; Puttner, R. R. *Chem. Commun.* **1970**, 1270.

[84] Cox, C.; Ferraris, D.; Murthy, N. N.; Lectka, T. *J. Am. Chem. Soc.* **1996**, *118*, 5332.

[85] Niklas, N.; Hampel, F.; Liehr, G.; Zahl, A.; Alsfasser, R. *Chem. Eur. J.* **2001**, *7*, 5135.

[86] Niklas, N.; Heinemann, F. W.; Hampel, F.; Alsfasser, R. *Angew. Chem., Int. Ed.* **2002**, *41*, 3386.

[87] Barrera, I. F.; Maxwell, C. I.; Neverov, A. A.; Brown, R. S. *J. Org. Chem.* **2012**, *77*, 4156.

[88] (a) Neverov, A. A.; Brown, R. S. *Can. J. Chem.* **2000**, *78*, 1247. (b) Neverov, A. A.; Montoya-Pelaez, P. J.; Brown, R. S. *J. Am. Chem. Soc.* **2001**, *123*, 210.

[89] (a) Murakami, Y.; Makoto, T. *J. Am. Chem. Soc.* **1969**, *91*, 5130. (b) Murakami, Y.; Takagi, M. *Bull. Chem. Soc. Jpn.* **1969**, *42*, 3478.

[90] Benkovic, S. J.; Dunikoski, L. K., Jr. *J. Am. Chem. Soc.* **1971**, *93*, 1526.

[91] Bromilow, R. H.; Kirby, A. J. *J. Chem. Soc. Perkin Trans. 2* **1972**, 149.

[92] (a) Hofstetter, R.; Murakami, Y.; Mont, G.; Martell, A. E. *J. Am. Chem. Soc.* **1962**, *84*, 3041. (b) Murakami, Y.; Sunamoto, J.; Sadamori, H. *Chem. Commun.* **1969**, 983.

[93] Hay, R. W.; Basak, A. K.; Pujari, M. P.; Perotti, A. *J. Chem. Soc., Dalton Trans.* **1986**, 2029.

[94] Hay, R. W.; Basak, A. K.; Pujari, M. P. *J. Coord. Chem.* **1991**, *23*, 43.

[95] Bruice, T. C.; Tsubouchi, A.; Dempcy, R. O.; Olson, L. P. *J. Am. Chem. Soc.* **1996**, *118*, 9867.

[96] Edwards, D. R.; Neverov, A. A.; Brown, R. S. *J. Am. Chem. Soc.* **2009**, *131*, 368.

[97] Edwards, D. R.; Liu, C. T.; Garrett, G. E.; Neverov, A. A.; Brown, R. S. *J. Am. Chem. Soc.* **2009**, *131*, 13738.

[98] (a) Jaffé, H. H. *J. Am. Chem. Soc.* **1954**, 76, 4261. (b) Greig, I. R.; Kirby, A. J. *J. Phys. Org. Chem.* **2004**, *17*, 498.

[99] Williams, A. *Concerted Organic and Bio-organic Mechanisms*. Boca Raton, FL: CRC Press; 1999.

[100] Liu, C. T.; Neverov, A. A.; Maxwell, C. I.; Brown, R. S. *J. Am. Chem. Soc.* **2010**, *132*, 3561.

[101] Bunn, S. E.; Liu, C. T.; Lu, Z.-L.; Neverov, A. A.; Brown, R. S. *J. Am. Chem. Soc.* **2007**, *129*, 16238.

[102] Neverov, A. A.; Liu, C. T.; Bunn, S. E.; Edwards, D.; White, C. J.; Melnychuk, S. A.; Brown, R. S. *J. Am. Chem. Soc.* **2008**, *130*, 6639.

[103] Liu, C. T.; Neverov, A. A.; Brown, R. S. *J. Am. Chem. Soc.* **2008**, *130*, 16711.

[104] Maxwell, C. I.; Mosey, N. J.; Brown, R. S. *J. Am. Chem. Soc.* **2013**, *135*, 17209.

[105] Neverov, A. A.; Sunderland, N. E.; Brown, R. S. *Org. Biomol. Chem.* **2005**, *3*, 65.

[106] Maxwell, C. I.; Neverov, A. A.; Mosey, N. J.; Brown, R. S. *J. Phys. Org. Chem.* **2014**, *27*, 419.

[107] Raycroft, M. A. R.; Liu, C. T.; Brown, R. S. *Inorg. Chem.* **2012**, *51*, 3846.

[108] (a) Raycroft, M. A. R.; Maxwell, C. I.; Oldham, R. A. A.; Saffouri Andrea, A.; Neverov, A. A.; Brown, R. S. *Inorg. Chem.* **2012**, *51*, 10325. (b) Raycroft, M. A. R.; Cimpean, L.; Neverov, A. A.; Brown, R. S. *Inorg. Chem.* **2014**, *53*, 2211.

[109] (a) Bröhmer, M. C.; Mundinger, S.; Bräse, S.; Bannwarth, W. *Angew. Chem., Int. Ed.* **2011**, *50*, 6125. (b) Mundinger, S.; Jakob, U.; Bichovski, P.; Bannwarth, W. J. *Org. Chem.* **2012**, *77*, 8968.

[110] Belzile, M.-N.; Neverov, A. A.; Brown, R. S. *Inorg. Chem.* **2014**, *53*, 7916.

[111] Neverov, A. A.; Cimpean, L.; Chiykowski, V.; Vance, T; Brown, R. S. *J. Org. Chem.* **2015**, *80*, 1357.

[112] Liu, C. T.; Maxwell, C. I.; Pipe, S. G.; Neverov, A. A.; Mosey, N. J.; Brown, R. S. *J. Am. Chem. Soc.* **2011**, *133*, 20068.

Chapter 2 – Comparison of Cu(II)-promoted leaving group stabilization of the cleavage of a homologous set of phosphate mono-, di-, and tri-esters in water, methanol and ethanol

2.1 – Preface

With minor formatting changes and the addition of Supporting Information 2-1, this chapter is presented largely as it is published in *Inorganic Chemistry* (Raycroft, M. A. R.; Liu, C. T.; Brown, R. S. *Inorg. Chem.* **2012**, *51*, 3846). The kinetic experiments were performed by Mark Raycroft and the syntheses were performed by Dr. C. Tony Liu and Mark Raycroft. The manuscript was written by Mark Raycroft and Dr. R. Stan Brown.

2.2 – Introduction

The monoesters and diesters of phosphoric acid participate in a variety of biologically important phosphoryl transfer and hydrolysis reactions involving proteins, DNA, and RNA. The ionization of mono- and diester derivatives of these under physiological conditions is central to their suitability as biomolecules since it serves to prevent them from crossing biological membranes as well as to resist hydrolytic cleavage by simple nucleophilic means.[1] Triesters have no natural biological function, but man-made versions are used commercially as acetylcholinesterase inhibitors.[2] Phosphatase enzymes, some containing dinuclear active sites, have evolved to catalyze the cleavage of both naturally-occurring and man-made phosphate esters with very large rate enhancements over the uncatalyzed solvolysis reactions.[3] Various modes of metallo-catalysis[4] have been discussed, such as: (1) Lewis acid activation of the substrate via M^{x+}---O=P binding;

(2) delivery of a metal-bound hydroxide or alkoxide that serves as a nucleophile or a base; (3) electrostatic stabilization of the anionic substrate and nucleophile/base through binding to the (+)-charged active site and subsequent lowering of the transition state energy of the reaction;[5] and (4) stabilization of the leaving group through metal ion coordination. As important as the latter effect is believed to be, studies of systems incorporating metal ions that provide leaving group assistance (LGA) in the reactions of small-molecules is documented in only a few cases.[6,7,8,9,10,11,12,13,14]

In the absence of catalysts, the mechanisms by which phosphate esters react depend on their state of *O*-alkylation (R) or arylation (Ar).[15] Monoesters react either by a dissociative mechanism (D_N+A_N) or a concerted mechanism (A_ND_N) with a loose transition state. Diesters and triesters tend to react through concerted A_ND_N mechanisms (when containing an activated LG) with progressively tighter transition states to the limit of an associative mechanism involving a phosphorane intermediate when substituted with a poor LG. We have compared the rates and properties of the methanolysis reactions of molecules **2.1**–**2.3** in the presence of Cu(II) (Scheme 2-1) showing there is strong assistance of the LG departure by a closely situated *ortho*-phenanthroline-bound Cu(II).[16] The methanolyses are greatly accelerated (10^{14} to 10^{15} for monoester, 10^{14} for diester, and 10^5 for triester) over the background reactions in methanol. In all these cases, the Cu(II)-promoted LGA changes the reaction mechanism relative to the non-LGA process, with solvent methanol, rather than methoxide, as the active nucleophile in transition states that are more dissociative than are found for related processes in the absence of catalysts.

Herein we report on an expanded study where the reaction medium changes from methanol to both ethanol and water, and how these solvents affect the reaction mechanisms and the acceleration provided by LGA.

Scheme 2-1. Cu(II)-promoted methanolysis of phosphate esters **2.1–2.3**.

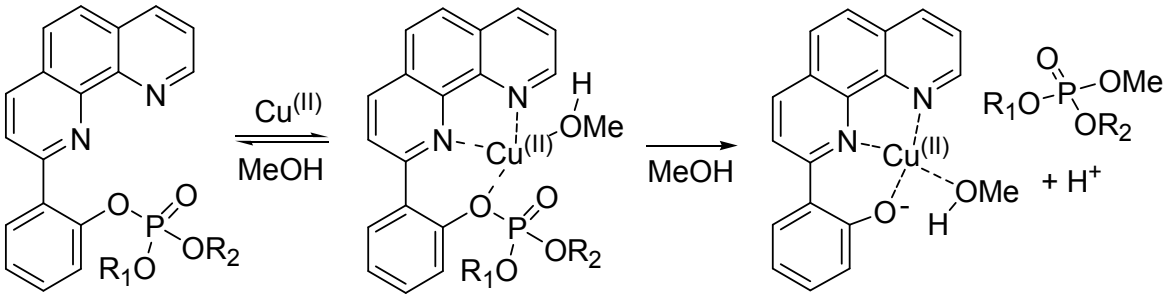

2.1 $OR_1 = OR_2 = O^-$
2.2 $OR_1 = O^-$; $OR_2 = OMe$
2.3 $OR_1 = OR_2 = OMe$

2.4

2.3 – Experimental

2.3.1 – Materials

Ethanol-OD (99 atom % D), trifluoromethanesulfonic acid (≥99%), $Cu(CF_3SO_3)_2$ (98%), 2-picoline (98%), 2,6-lutidine (99+%), 2,4,6-collidine (99%), 4-ethylmorpholine (99%), 1-methylpiperidine (≥98%), 1-ethylpiperidine (99%), triethylamine (99%), 2,2,6,6-tetramethylpiperidine (99+%), were used as supplied from Aldrich. Tetrabutylammonium ethoxide (40% in ethanol, titrated against N/2 certified standard aqueous HCl solution and found to be 1.13 M) was purchased from Fluka. Absolute ethanol (anhydrous, degassed and stored under argon, freshly dispensed between kinetic experiments) and deuterium oxide (D, 99.9%) were purchase from Fisher and CIL, respectively. Reverse-Osmosis (RO) purified water was further deionized to 18.2 MΩ•cm using a Millipore

filtration apparatus. The following phosphate esters *O*-(2-[2′-phenanthrolyl]phenyl) phosphate (**2.1**), *O*-(2-[2′-phenanthrolyl]phenyl) *O*-methyl phosphate (**2.2**), and *O*-(2-[2′-phenanthrolyl]phenyl) *O,O*-dimethyl phosphate (**2.3**) were synthesized and characterized as previously reported.[16]

2.3.2 – General methods

Concentrations of H_3O^+ and $CH_3CH_2OH_2^+$ were determined potentiometrically using a combination glass Fisher Scientific Accumet electrode calibrated with certified standard aqueous buffers (pH 4.00 and 10.00) as described previously.[17a] The pH was determined as $-\log[ROH_2^+]$. The autoprotolysis constant for ethanol was taken to be $10^{-19.1}$ M^2 and the ${}^{s}_{s}pH$ values[17b] in ethanol were determined by subtracting a correction constant of -2.54 from the electrode readings.[17a] The ${}^{s}_{w}pH$ values for the kinetic experiments were measured at the end of the reactions in order to avoid any effects associated with KCl leaching from the electrode.

2.3.3 – General UV-vis kinetics

The Cu(II)-catalyzed hydrolyses and ethanolyses of **2.1**, **2.2**, and **2.3** were followed at 390 and 415 nm respectively to determine the rate of appearance of Cu(II)-bound phenoxide **2.4** using a UV-vis spectrophotometer with the cell thermostatted at 25.0 ± 0.1 °C. Reactions were conducted in the presence of buffers composed of various ratios of amines (2-picoline, 2,6-lutidine, 2,4,6-collidine, *N*-isopropylmorpholine, 1-methyl-piperidine, 1-ethylpiperidine, triethylamine, 2,2,6,6-tetramethylpiperidine) and HOTf. For reactions at pH 3 or lower, an appropriate amount of HOTf was added to achieve the

required [ROH_2^+] in solution. Typical kinetic experiments involved preparing a solution of buffer (0.4–1.2 mM) followed by addition of the phosphate substrate (0.02 mM) in a 1-cm path length UV cuvette. To this was added an aliquot of Cu(II) stock solution to obtain a final concentration of 0.02 mM to initiate the reaction. In the case of reasonably fast reactions (slower than stopped-flow time-scale) duplicate kinetic experiments were carried out and the resulting Abs vs time traces were fitted to a standard first-order exponential equation to obtain the observed first order rate constants (k_{obs}). For very slow reactions, such as the Cu(II)-promoted hydrolysis or ethanolysis of **2.2**, initial rates of the reactions were obtained by fitting the first 5–10% of the Abs vs time traces to a linear regression. To obtain the k_{obs} values, the initial rates were then divided by the expected absorbance change (ΔAbs) if the reaction were to reach 100% completion. Separate pH/rate profiles were constructed for the Cu(II)-catalyzed cleavages of **2.1**–**2.3** in the presence of 20-fold excess buffer in water and ethanol. A typical solvent kinetic isotope experiment involved the addition of 1 mM $Cu(OTf)_2$ and 5 mM HOTf stock solutions in ROD to UV cells containing either ROH or ROD so that the final concentrations of $Cu(OTf)_2$, phosphate ester, and buffer were 0.02, 0.02, and 0.4 mM, respectively. The kinetic competition experiments were carried out in duplicate and the pH and pD values were measured after the reactions were complete. (The pD values measured at the end of the reactions were recorded as the pH meter readings (+2.54 in the case of the ethanolysis reactions) and are not corrected for the effect of the deuterated solvent on the reading or on the pK_a of the buffer. The actual pD value is less important since the experiments are carried out in the extensive plateau regions of the pH/rate profiles.)

2.3.4 – Stopped-flow kinetics

The Cu(II)-promoted cleavage of **2.1** was monitored at 390 nm in water and 415 nm in ethanol, obtaining the rate of appearance of product using a stopped-flow apparatus thermostatted at 25.0 ± 0.1 °C. One syringe of the stopped-flow instrument was loaded with a 0.8 mM solution of the desired buffer in water or ethanol containing 0.04 mM **2.1**. The second syringe was loaded with 0.04 mM $Cu(OTf)_2$ in water or ethanol. When mixed, the final concentrations of $Cu(OTf)_2$, **2.1**, and buffer were 0.02, 0.02, and 0.4 mM, respectively. At least five kinetic experiments were conducted at each pH and the obtained Abs vs time traces were fitted to a standard first-order exponential equation to give the k_{obs} values: these were averaged to give the reported values in the tables. Solvent kinetic isotope experiments were performed in same way as those previously described and the pH and pD values were measured after the reaction.

2.3.5 – Activation parameters

Kinetic experiments with Cu(II):**2.1** were performed at different temperatures using a thermostattable stopped-flow analyzer, while those for substrates Cu(II):**2.2** and Cu(II):**2.3** were determined using a UV-vis spectrophotometer. The solution temperatures were determined with a thermometer inserted into the cell at the end of the reaction. First order rate constants were measured in at least duplicate at a minimum of six different temperatures ranging from 15 to 40 °C for the Cu(II)-promoted hydrolysis or ethanolysis of **2.1** (both at 0.02 mM) in the presence of 0.4 mM 2,6-lutidine buffer, pH 6.9 ± 0.2, or 2,2,6,6-tetramethylpiperidine buffer, $^{s}_{s}$pH 11.4 ± 0.2. Eyring plots of ln(k/T) vs 1/T provided the $\Delta H^{\ddagger}$ and $\Delta S^{\ddagger}$ values given in Table 2-1. The activation parameters given in

Table 2-2 for substrate **2.2** were determined using solutions containing 0.02 mM $Cu(OTf)_2$, 0.02 mM **2.2**, and 1.0 mM HOTf in water (pH 3.0 ± 0.2) and ethanol ($^{s}_{s}$pH 3.0 ± 0.2) at seven temperatures ranging from 15 to 45 °C. The activation parameters given in Table 2-3 for substrate **2.3** were determined with solutions containing 0.02 mM $Cu(OTf)_2$, 0.02 mM **2.3**, and 1.0 mM HOTf in water (pH 3.0 ± 0.2) and ethanol ($^{s}_{s}$pH 3.0 ± 0.2) at six temperatures ranging from 15 to 68 °C. The Eyring plots from which the activation parameters were determined can be found in Figure 2-8 to Figure 2-13 of Supporting Information 2-1.

2.4 – Results

2.4.1 – Cu(II)-promoted hydrolysis and ethanolysis of 2.1

The pH/rate profile for hydrolysis of Cu(II):**2.1** in Figure 2-1 can be fitted by nonlinear least-squares (NLLSQ) methods to equation 2-1, derived for the model given in Scheme 2-2 having two ionizable groups with pK_a values of 4.33 and 9.17. Based on the $^{s}_{s}$pH/rate profile of Cu(II):**2.1** observed earlier in methanol,[16] in the lower pH regions [Cu(II):**2.1a**]$^{+}$ (or a kinetically equivalent form where the non-bridging phosphate O^{-} binds to Cu(II) displacing solvent) undergoes possible microscopic ionizations in water to form two formally neutral forms, [Cu(II):**2.1b**]^{0} and [Cu(II):**2.1c**]^{0} which differ by coordination of a non-bridging O^{-} to Cu(II) with displacement of solvent. The relative proportion of these may be influenced by solvent polarity and thus different in the three media. However, due to the availability of both non-bridging oxyanions to assist in the departure of the LG in [Cu(II):**2.1b**]^{0}, this is likely the more active of the two species. Further ionization leads to a less active (or possibly inactive) species, [Cu(II):**2.1d**]$^{-}$.

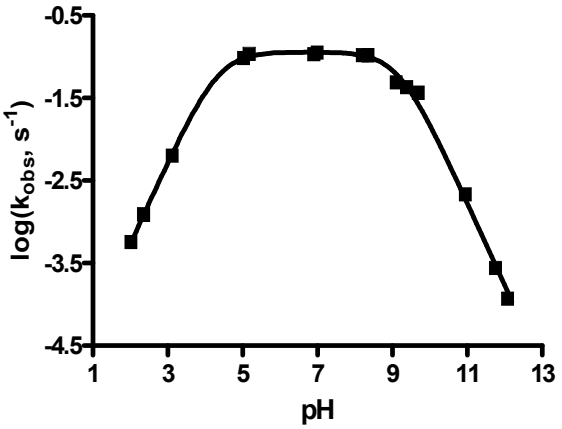

Figure 2-1. The pH/rate profile for cleavage of Cu(II):**2.1** (0.02 mM each of Cu(II) and **2.1**) under aqueous buffered conditions (0.4 mM amine, 0.2 mM HOTf) at 25 °C. The data are fitted by NLLSQ methods to equation 2-1 to give two macroscopic pK_a^2 and pK_a^3 values of 4.33 ± 0.05 and 9.17 ± 0.04 and a maximum rate constant (k_{cat}^{max}) of 0.115 ± 0.007 s^{-1}; $r^2 = 0.9972$.

$$k_{obs} = k_{cat}^{\max}\left(\frac{K_a^{\,2}}{K_a^{\,2}+[H^+]}\right)\left(\frac{[H^+]}{K_a^{\,3}+[H^+]}\right) \qquad (2\text{-}1)$$

Scheme 2-2. Microscopic ionizations for hydrolysis of [Cu(II):**2.1**].

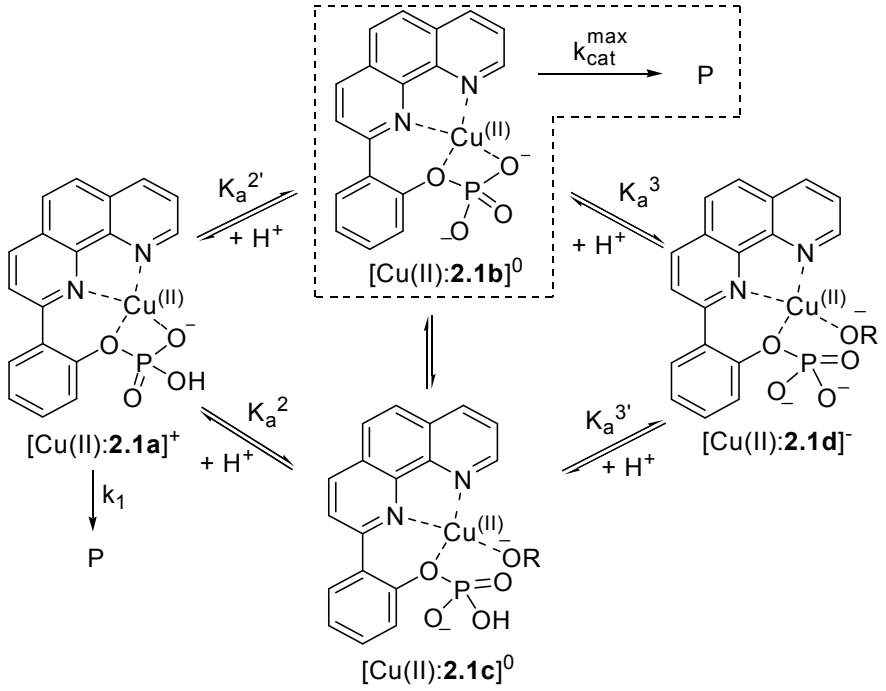

The solvent DKIE was determined to be $k_H/k_D = 0.91 \pm 0.01$ in the center of the pH 5–8 plateau region, at a measured pD = 6.8 ± 0.2 (0.4 mM 2,6-lutidine buffer).

The ${}^{s}_{s}$pH/rate profile data in Figure 2-2 for ethanolysis of Cu(II):**2.1** can be fitted to equation 2-2 derived for the model represented schematically in Scheme 2-3 where [Cu(II):**2.1**]$^{2+}$ undergoes two sequential acid dissociations having macroscopic ${}^{s}_{s}pK_a^{1}$ and ${}^{s}_{s}pK_a^{2}$ values of 2.1 and 7.7. The [Cu(II):**2.1a**]$^{+}$ formed at lower ${}^{s}_{s}$pH may undergo two possible microscopic ionizations to produce [Cu(II):**2.1b**]^{0} and [Cu(II):**2.1c**]^{0}. For similar reasoning as was described above for water, [Cu(II):**2.1b**]^{0} probably represents the more active species. In the less polar ethanol, further ionization of this to form [Cu(II):**2.1d**]$^{-}$ (see Scheme 2-2) is not observed up to at least ${}^{s}_{s}$pH 12.

The solvent DKIE of $k_H/k_D = 0.83 \pm 0.06$ was determined in the plateau region at an estimated ${}^{s}_{s}$pD value of 11.4 ± 0.2, uncorrected for D in the solvent (0.4 mM 2,2,6,6-tetramethylpiperidine buffer).

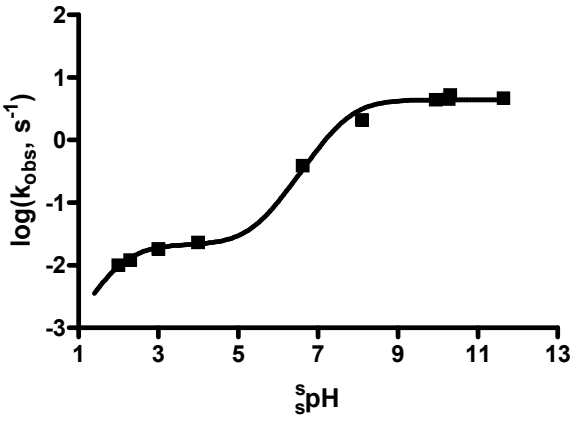

Figure 2-2. The $^{s}_{s}$pH/rate profile for cleavage of Cu(II):**2.1** (0.02 mM each of Cu(II) and **2.1**) in anhydrous ethanol under buffered conditions (0.4 mM amine, 0.2 mM HOTf) at 25 °C. The data are fitted by NLLSQ methods to equation 2-2 to give two macroscopic $^{s}_{s}$pK_a values of 2.1 ± 0.2 leading to a k_1 = (2.1 ± 0.2) × 10^{-2} s^{-1} and 7.7 ± 0.2 leading to a maximum rate constant (k_{cat}^{max}) of 4.4 ± 0.6 s^{-1}; r^2 = 0.9971.

$$k_{obs} = k_1\left(\frac{{}^{s}_{s}K^{1}_{a}}{{}^{s}_{s}K^{1}_{a} + [H^+]}\right) + k_{cat}^{max}\left(\frac{{}^{s}_{s}K^{2}_{a}}{{}^{s}_{s}K^{2}_{a} + [H^+]}\right) \qquad (2\text{-}2)$$

Scheme 2-3. Microscopic ionizations for ethanolysis of [Cu(II):**2.1**].

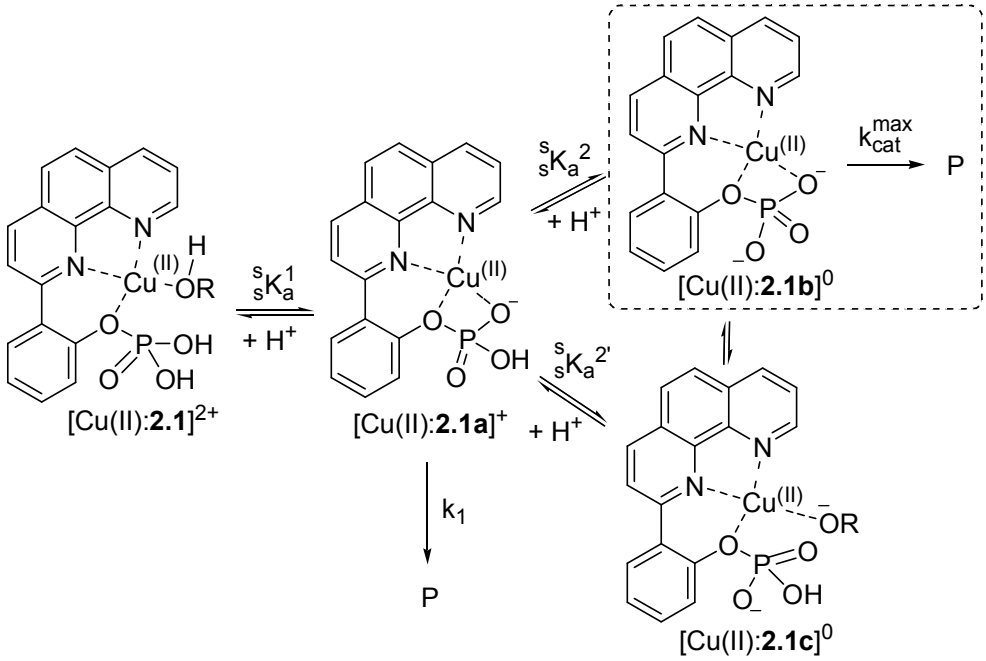

2.4.2 – Cu(II)-promoted hydrolysis and ethanolysis of 2.2

In Figure 2-3, the pH/rate profile for hydrolysis of Cu(II):**2.2** is shown. At low pH, [Cu(II):**2.2a**]$^{2+}$ (Scheme 2-4) ionizes (not observed) to form the reactive species [Cu(II):**2.2b**]$^{+}$ (or a chemically equivalent species where the non-bridging O^{-} is displaced from the Cu(II) by solvent) with an extended pH-independent region followed by its ionization (pK_a 7.94) to some inactive form, suggested to be the dimer of [Cu(II)**2.2c**]^{0}. That the descending portion of the profile at higher pH has a gradient of -2 may indicate involvement of two lyoxide molecules leading to a dimeric species with lower activity such as was proposed previously.[16] The solvent DKIE in the plateau region is $k_H/k_D = 1.22 \pm 0.01$ at a measured pD value of 3.0 ± 0.2 (1 mM DOTf).

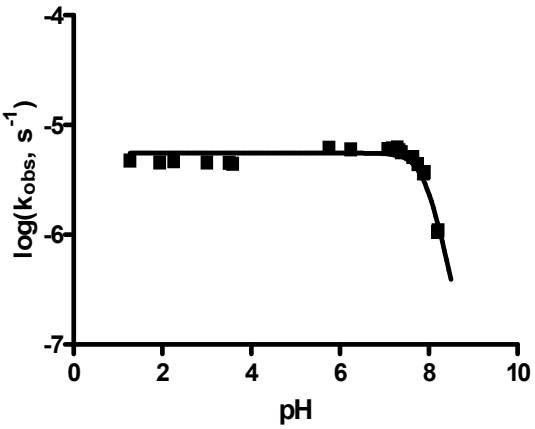

Figure 2-3. The pH/rate profile for cleavage of Cu(II):**2.2** (0.02 mM of Cu(II) and **2.2**) under aqueous buffered conditions (0.4 mM amine, 0.2 mM HOTf) at 25 °C. The data are fitted by NLLSQ methods to equation 2-3 to give one macroscopic pK_a value of 7.94 ± 0.03 and a maximum rate constant (k_{cat}^{max}) of (5.6 ± 0.2) × 10^{-6} s^{-1}; $r^2 = 0.9009$.

$$k_{obs} = k_{cat}^{\max}\left(\frac{[H^+]^2}{K_a^2/K_{\dim} + [H^+]^2}\right) \qquad (2\text{-}3)$$

Scheme 2-4. Microscopic ionizations for hydrolysis and ethanolysis of [Cu(II):**2.2**].

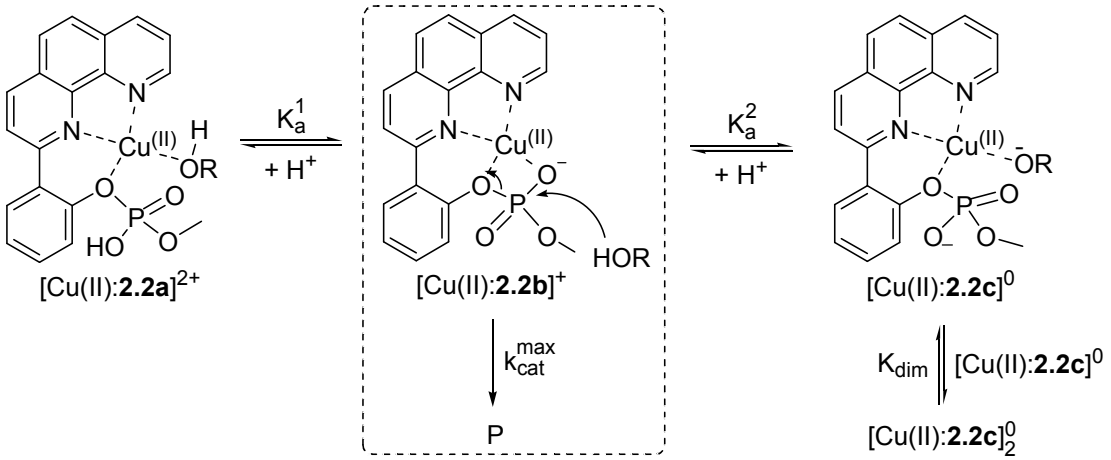

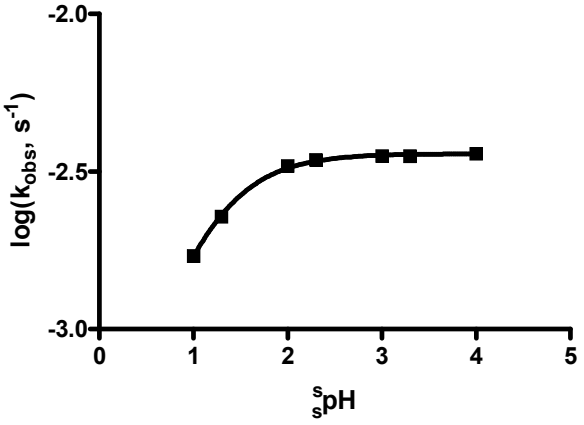

Figure 2-4. The $^{s}_{s}$pH/rate profile for cleavage of Cu(II):**2.2** (0.02 mM of Cu(II) and **2.2**) in anhydrous ethanol under buffered conditions (0.4 mM amine, 0.2 mM HOTf) at 25 °C. The data are fitted by NLLSQ methods to equation 2-4 to give one macroscopic $^{s}_{s}pK_a$ value of 1.05 ± 0.01 and a maximum rate constant (k_{cat}^{max}) of (3.60 ± 0.02) × 10^{-3} s^{-1}; r^2 = 0.9984.

$$k_{obs} = k_{cat}^{\max}\left(\frac{{}^{s}_{s}K_a^1}{{}^{s}_{s}K_a^1 + [H^+]}\right) \qquad (2\text{-}4)$$

The ionization process and plateau region indicated by the $^{s}_{s}$pH/rate profile for ethanolysis of Cu(II):**2.2** (Figure 2-4) are represented mechanistically in Scheme 2-4. At low $^{s}_{s}$pH, [Cu(II):**2.2a**]$^{2+}$ ionizes to produce [Cu(II):**2.2b**]$^{+}$ (or its similarly charged chemical equivalent with a solvent incorporated on the Cu(II)) which then reacts over a pH-independent region. The solvent DKIE in the plateau region is $k_H/k_D = 1.29 \pm 0.03$ at a measured $^{s}_{s}$pD value of 3.0, uncorrected for effect of D in solvent (1 mM DOTf).

2.4.3 – Cu(II)-promoted hydrolysis and ethanolysis of 2.3

The important species in the pH/rate profile for hydrolysis of Cu(II):**2.3** (Figure 2-5) are presented in Scheme 2-5. A broad pH-insensitive region exists between pH 2.5 and 7 where [Cu(II):**2.3a**]$^{2+}$ is likely the most active species. The solvent DKIE is $k_H/k_D = 1.94 \pm 0.01$ at an estimated pD value of 3.0 ± 0.2 in the plateau region (1 mM DOTf).

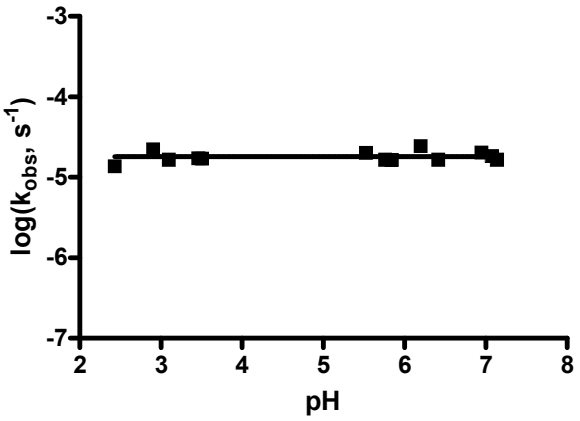

Figure 2-5. The pH/rate profile for cleavage of Cu(II):**2.3** (0.02 mM each of Cu(II) and **2.3**) under aqueous[18] buffered conditions (0.4 mM amine, 0.2 mM HOTf) at 25 °C. The data in the pH range 2.4–7.1 are averaged to give a rate constant of $k_{obs} = 1.7 \times 10^{-5}$ s^{-1}.

Scheme 2-5. Microscopic ionizations for hydrolysis and ethanolysis of [Cu(II):**2.3**].

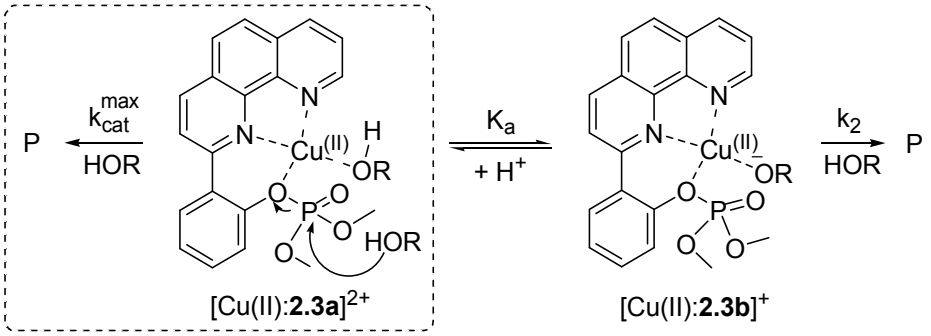

Figure 2-6 shows the ${}^{s}_{s}$pH/rate profile for the ethanolysis of Cu(II):**2.3** where a broad ${}^{s}_{s}$pH-insensitive region exists between ${}^{s}_{s}$pH 2.5 and 9.5 followed by an ionization to produce [Cu(II):**2.3b**]$^{+}$ (Scheme 2-5) which reacts with lower activity in the ${}^{s}_{s}$pH-insensitive region. The solvent DKIE was determined in the plateau region to be $k_H/k_D = 1.96 \pm 0.05$ at an estimated ${}^{s}_{s}$pD value of 3.0, uncorrected for the effect of D (1 mM DOTf).

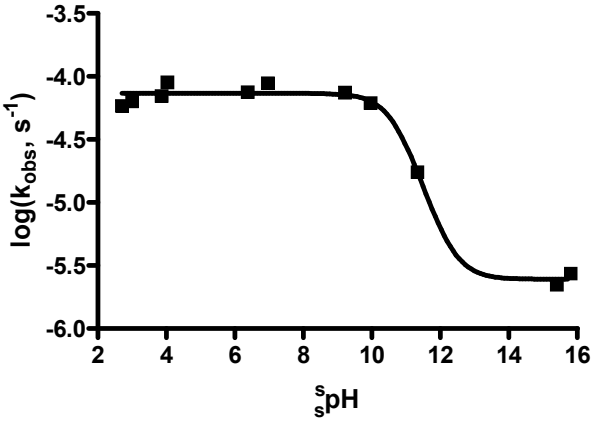

Figure 2-6. The ${}^{s}_{s}$pH/rate profile for the cleavage of Cu(II):**2.3** (0.02 mM of Cu(II) and **2.3**) in anhydrous ethanol under buffered conditions (0.4 mM amine, 0.2mM HOTf) at 25 °C. The data are fitted by NLLSQ methods to equation 2-5 to give one macroscopic ${}^{s}_{s}pK_a$ value of 10.8 ± 0.1 and a maximum rate constant (k_{cat}^{max}) of (7.3 ± 0.4) × 10^{-5} s^{-1} and k_2 = (2.5 ± 0.3) × 10^{-6} s^{-1}; $r^2 = 0.9907$.

$$k_{obs} = k_{cat}^{\max}\left(\frac{[H^+]}{{}^{s}_{s}K_a + [H^+]}\right) + k_2\left(\frac{{}^{s}_{s}K_a}{{}^{s}_{s}K_a + [H^+]}\right) \qquad (2\text{-}5)$$

2.4.4 – Activation parameters

Temperature dependent studies at the pH optima for the Cu(II)-promoted solvolyses of **2.1**–**2.3** in water, methanol,[16] and ethanol afforded the activation parameters that appear in Table 2-1 to Table 2-3.

Table 2-1. Activation parameters, rate constants, and SKIE values for cleavage of Cu(II):**2.1** in water, methanol,[16] and ethanol (ε_r = 78, 31.5, 24.3 respectively) at their pH optima in the plateau region where the reactive form is the formally neutral complex [Cu(II):**2.1b**]^0 and/or [Cu(II):**2.1c**]^0.[a]

Phosphate Complex	Solvent	k_{cat}^{max} (s^{-1})	$\Delta H^{‡}$ (kcal·mol^{-1})	$\Delta S^{‡}$ (cal·mol^{-1}·K^{-1})	$\Delta G^{‡}$ (25°C) (kcal·mol^{-1})	k_H/k_D
[Cu(II):**2.1b/c**]	H_2O	0.11	22.9 ± 0.2	13.6 ± 0.7	18.8 ± 0.3	0.91 ± 0.01
[Cu(II):**2.1b/c**]	MeOH	14.7	21.4 ± 0.7	18 ± 2	16.0 ± 0.9	0.95 ± 0.05
[Cu(II):**2.1b/c**]	EtOH	4.4	18.4 ± 0.1	5.8 ± 0.5	16.7 ± 0.2	0.83 ± 0.06

a. Data in methanol from reference 16.

Table 2-2. Activation parameters, rate constants, and SKIE values for cleavage of Cu(II):**2.2** in water, methanol,[16] and ethanol (ε_r = 78, 31.5, 24.3 respectively) at their pH optima in the plateau region where the reactive form is the formally positively charged complex [Cu(II):**2.2b**]$^{+}$.[a]

Phosphate Complex	Solvent	k_{cat}^{max} (s^{-1})	$\Delta H^{‡}$ ($kcal \cdot mol^{-1}$)	$\Delta S^{‡}$ ($cal \cdot mol^{-1} \cdot K^{-1}$)	$\Delta G^{‡}$ (25°C) ($kcal \cdot mol^{-1}$)	k_H/k_D
[Cu(II):**2.2b**]$^{+}$	H_2O	5.6×10^{-6}	23.0 ± 0.2	-5.8 ± 0.5	24.7 ± 0.2	1.22 ± 0.01
[Cu(II):**2.2b**]$^{+}$	MeOH	2.5×10^{-3}	21.6 ± 0.4	2.3 ± 1.1	20.9 ± 0.5	1.01 ± 0.04
[Cu(II):**2.2b**]$^{+}$	EtOH	3.5×10^{-3}	18.3 ± 0.2	-8.5 ± 0.6	20.8 ± 0.3	1.29 ± 0.03

a. Data in methanol from reference 16.

Table 2-3. Activation parameters, rate constants, and SKIE values for cleavage of Cu(II):**2.3** in water, methanol,[16] and ethanol (ε_r = 78, 31.5, 24.3 respectively) at their pH optima in the plateau region where the reactive form is the formally doubly positive charged complex [Cu(II):**2.3a**]$^{2+}$.[a]

Phosphate Complex	Solvent	k_{cat}^{max} (s^{-1})	$\Delta H^{‡}$ ($kcal \cdot mol^{-1}$)	$\Delta S^{‡}$ ($cal \cdot mol^{-1} \cdot K^{-1}$)	$\Delta G^{‡}$ (25°C) ($kcal \cdot mol^{-1}$)	k_H/k_D
[Cu(II):**2.3a**]$^{2+}$	H_2O	1.7×10^{-5}	19.1 ± 0.1	-16.4 ± 0.3	24.0 ± 0.1	1.94 ± 0.01
[Cu(II):**2.3a**]$^{2+}$	MeOH	2.0×10^{-5}	21.6 ± 0.5	-7.4 ± 1.7	23.8 ± 0.7	2.2 ± 0.1
[Cu(II):**2.3a**]$^{2+}$	EtOH	7.3×10^{-5}	18.4 ± 0.3	-16.0 ± 0.9	23.2 ± 0.4	1.96 ± 0.05

a. Data in methanol from reference 16.

2.5 – Discussion

There are postulates that the effective dielectric constants inside the enzyme active site resemble those of organic solvents rather than water.[19] Organic solvents like methanol and ethanol, with dielectric constants of 31.5 and 24.3 and properties and structures closest to water,[20] might be considered appropriate models for the media extant in the active sites of some enzymes,[19] although this ignores specific solvation effects such as the solvents' H-bond and electron accepting and donating properties. The large rate accelerations[12,13,16,21] that we see for the transesterifications of phosphate di- and triesters in methanol and ethanol are anomalous when compared with what is generally seen in water,[22] but, as will be seen, there are very large accelerations for the cleavages of [Cu(II):**2.1**,**2.2**,**2.3**] in water as well.

According to X-ray diffraction studies of a close model for the metal-bound leaving group ([Cu(II):**2.4**$^{-}$], Scheme 2-1), namely [(Cu(II)$_2$:**2.4**$^{-}$)$_2$:(μ-MeCO$_2^{-}$)][PF$_6^{-}$],[23] the departing phenoxy oxygen is positioned within ~1.9 Å of the Cu(II) ion. This is expected to be the situation in all solvents investigated. The proposed driving force for the cleavage of the phosphates in methanol[16] stems from progressively enhancing the metal cation's and departing phenoxy anion's interactions during the transformation of [Cu(II):**2.1**,**2.2**,**2.3**] into Cu(II):**2.4**$^{-}$. Thus, the endothermicity of the P–O(LG) bond cleavage process is offset by an exothermic binding of the transition state attributable to the progressively enhanced Cu(II):$^{-}$O(LG) electrostatic interaction. The activation parameters and rate constants in Table 2-1 to Table 2-3 refer to the reactions in the plateau regions of the pH/rate profiles where the effective nucleophile is solvent, (either

external or metal ion-coordinated in the case of attack on [Cu(II):**2.1b**]^{0}, [Cu(II):**2.2b**]$^{+}$, and [Cu(II):**2.3a**]$^{2+}$) and the charges of the active forms of the three Cu(II) complexes vary by one unit each in passing from [Cu(II):**2.1b**]^{0} to [Cu(II):**2.2b**]$^{+}$ and [Cu(II):**2.3a**]$^{2+}$.

2.5.1 – pH and $^{s}_{s}$pH/rate profiles for the cleavage of [Cu(II):2.1,2.2,2.3] in water, methanol, and ethanol

General: The rate constants for the solvolysis of the three complexes were determined under conditions similar to what was used previously for the study in methanol.[16] The kinetics were determined using 1:1 mixtures of Cu(II)(triflate)$_2$ and substrate under the assumption that the Cu(II):substrate binding is essentially complete. This assumption is warranted since the rate constants obtained for this study are independent of increasing total concentration of Cu(II) + substrate, when these are introduced to the solution in a 1:1 mixture. In addition, Cu(II) binding to phenanthroline systems is known to be very strong. For example, the binding constant of phenanthroline and Cu(II) in water[24] is 1.6×10^{9} M^{-1} and we have previously determined that the dissociation constant of Cu(II):**2.3** in methanol is 2.8×10^{-7} M.[16] While we have not determined the binding constants for the mono- and diesters, these are also expected to be stronger than that for Cu(II):**2.3** due to electrostatic interactions, particularly in ethanol. In all cases, the product of the solvolyses is the corresponding 2(2'-phenanthrolyl)phenoxide:Cu(II) complex which is verified by the characteristic UV-vis spectrum as derived from authentic material. Finally, as in the case in methanol, there is no effect of buffer as can be judged from the pH/rate profiles which show no evidence of breaks between different buffers.

2.5.1.1 – [Cu(II):**2.1**]

The general pH-dependent species of [Cu(II):**2.1**,**2.2**,**2.3**] and processes for the decomposition of each ester are expected to be similar in the three solvents, although the pH range over which each of their microscopic states of ionization exist is expected to be different. The pH/rate profile from 2–12 for the hydrolysis of Cu(II):**2.1** shown in Figure 2-1 is bell-shaped with a k_{cat}^{max} of 0.12 s^{-1} and two acid dissociation constants of ${}^{s}_{s}pK_a^2$ = 4.33 and ${}^{s}_{s}pK_a^3$ = 9.17 corresponding to the transition from [Cu(II):**2.1a**]$^+$ to two possible neutral forms [Cu(II):**2.1b/c**]^0, and transformation of [Cu(II):**2.1b/c**]^0 into [Cu(II):**2.1d**]$^-$ as in Scheme 2-2. In methanol, from ${}^{s}_{s}$pH 2.5–12.5, the profile is also bell-shaped with two ${}^{s}_{s}pK_a^2$ and ${}^{s}_{s}pK_a^3$ values of 7.83 and 11.8, with plateaus from ${}^{s}_{s}$pH 2.4–4, $k_1 = 6.3 \times 10^{-4}$ s^{-1}, and from ${}^{s}_{s}$pH 8–11, k_{cat}^{max} = 14.7 s^{-1}.[16] However, in the lowest polarity solvent ethanol, the ${}^{s}_{s}$pH/rate profile (Figure 2-2) is sigmoidal with the hint of a ${}^{s}_{s}pK_a^1$ at 2.4, a plateau from ${}^{s}_{s}$pH 3–5 ($k_1 = 2.1 \times 10^{-2}$ s^{-1}), a ${}^{s}_{s}pK_a^2$ of 7.70 followed by a long plateau with k_{cat}^{max} = 4.4 s^{-1}. There is no evidence of a ${}^{s}_{s}pK_a^3$ value for ionization of [Cu(II):**2.1**] in ethanol up to ${}^{s}_{s}$pH 12. The difference in observed ${}^{s}_{s}pK_a^3$ and ${}^{s}_{s}pK_a^2$ values from water to methanol and ethanol media might be a consequence of the poorer ability of the alcohol to stabilize anion formation (as in [Cu(II):**2.1d**]$^-$), and/or a change in the relative amounts of [Cu(II):**2.1b/c**]^0 in the three solvents. The autoprotolysis constants of the three solvents increase (pK_{auto} = 14, 16.77, and 19.1 respectively)[17] so that neutrality is at pH 7, ${}^{s}_{s}$pH 8.4 and 9.55, respectively. Thus, in passing from methanol to ethanol, ${}^{s}_{s}pK_a^2$ ionization occurs at substantially less than neutrality which is consistent with the lower polarity solvent favoring the formation of the charge neutral species [Cu(II):**2.1b/c**]^0.

The rate constants for decomposition of [Cu(II):**2.1a**]$^{+}$ can be compared only in methanol and ethanol, since the $^{s}_{s}$pH/rate profiles in these solvents exhibit plateaus in the low $^{s}_{s}$pH domain. The k_1 value in ethanol is about 30 times greater than in methanol (2.1×10^{-2} s^{-1}/6.4×10^{-4} s^{-1}), suggesting that ethanol favors a transition state where charge is being dispersed relative to the mono-cationic ground state of the complex. The k_{cat}^{max} rate constants for the decomposition of the formally neutral complex [Cu(II):**2.1b/c**]^{0} varies by a factor of about 100 in the three solvents from 0.12 s^{-1} in water to 14.7 s^{-1} and 4.4 s^{-1} in methanol and ethanol. There is not a simple rationalization for this apparently inverted order as a function of solvent polarity; perhaps this is consistent with the proportions of [Cu(II):**2.1b/c**]^{0} being different in the two alcohol solvents and/or greater stability of the ground state of the neutral species in water than in either alcohol since pK_a^2 in water is less than $^{s}_{s}pK_a^2$ in either methanol or ethanol, even accounting for the differences in the autoprotolysis constants. Nevertheless, considerable ambiguity exists due to trade-offs in dielectric constant effects and specific solvent interactions with the ground and transition states, making any rationale highly speculative.

2.5.1.2 – [Cu(II):**2.2**,**2.3**]

With [Cu(II):**2.2**] in water, no pK_a^1 value is observed down to pH 1 but there is a second apparent pK_a^2 value for ionization of [Cu(II):**2.2b**]$^{+}$ of 7.94 which is tied to a following dimerization of [Cu(II):**2.2**]^{0}. The latter value shifts to an apparent $^{s}_{s}pK_a^2$ value of 10.25 in methanol. The only observed ionization of [Cu(II):**2.2**] in ethanol is $^{s}_{s}pK_a^1$ = 1.05 forming [Cu(II):**2.2b**]$^{+}$. The rate constants for decomposition of [Cu(II):**2.2b**]$^{+}$ vary by about 2000

in the three solvents, with the lowest in water being 5.6×10^{-6} s^{-1}, while those in methanol and ethanol are 2.5×10^{-3} and 3.5×10^{-3} s^{-1}.

With [Cu(II):**2.3]** there is no possible acid dissociation of the phosphate, so the only pH-dependent change in charge on the complex results from formation of Cu(II) hydroxides or alkoxides. No process corresponding to the conversion of [Cu(II):**2.3a**]$^{2+}$ to the Cu(II):hydroxide form [Cu(II):**2.3b**]$^{+}$ is observed from pH 1–7 in water. In methanol, the ${}^{s}_{s}pK_a{}^{1}$ value is 6.05 and shifts to a value of 10.75 in ethanol. The observed rate constants for decomposition of [Cu(II):**2.3a**]$^{2+}$ in the three solvents are very similar, being 1.7×10^{-5} s^{-1} in water and 2.0×10^{-5} s^{-1} in methanol and 7.3×10^{-5} s^{-1} in ethanol. As will be shown, this stems from a compensation of change in both the activation enthalpies and entropies in the three solvents.

2.5.2 – Trends in enthalpies and entropies of activation for decomposition of Cu(II)-bound phosphate esters

The rates of solvolytic cleavage of complex molecules depend on the relative energy levels of the ground and rate-limiting transition states. Thus, a change in reaction rate brought on by a change in solvent relates to how the medium alters these relative energies.[25] The relevant free energies for the processes and their transfer from one solvent to another are shown in Scheme 2-6, where S1 and S2 are the two solvents in question and $\Delta G^{o}_{(S1\rightarrow S2)_{GS}}$ and $\Delta G^{\ddagger}_{(S1\rightarrow S2)}$ represent the free energies of transfer of the ground and transition states between the two solvents. The latter values are determined[26] by

interactions of the solvent molecules with: (1) the ground state; (2) the transition state; and (3) other solvent molecules.

Scheme 2-6. A scheme depicting the free energies for dissolution and reaction transition state of [Cu(II):**2.1**,**2.2**,**2.3**] and the change in free energies induced by changing the solvent.

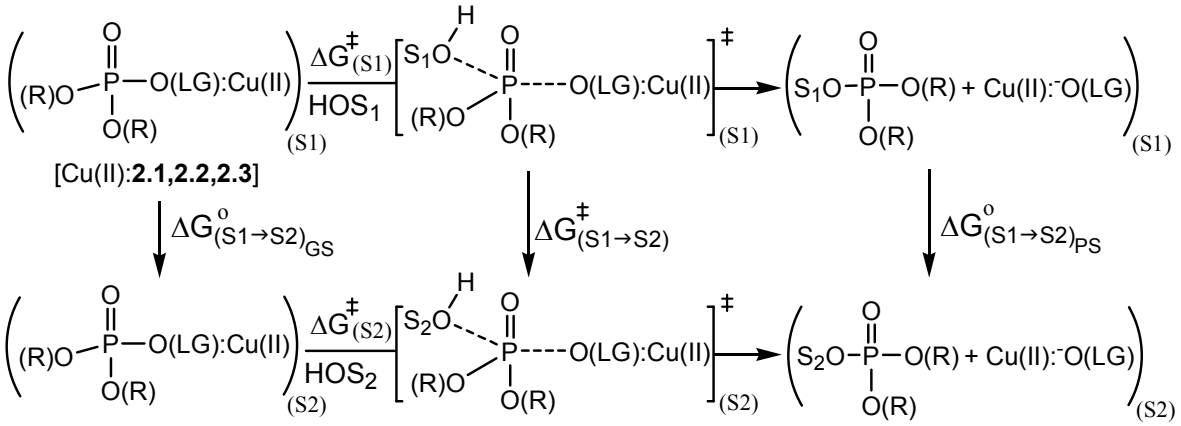

Equation 2-6 gives an expression for the $\Delta\Delta G^{‡}$ resulting from a solvent change on the free energies of the transition and ground states, which is further broken into the effects on $\Delta\Delta H^{‡}$ and $\Delta\Delta S^{‡}$ as in equations 2-7 and 2-8.

$$\Delta\Delta G^{‡} = \Delta G^{‡}_{(S1\rightarrow S2)} - \Delta G^{o}_{(S1\rightarrow S2)_{GS}} \qquad (2\text{-}6)$$

$$\Delta\Delta H^{‡} = \Delta H^{‡}_{(S1\rightarrow S2)} - \Delta H^{o}_{(S1\rightarrow S2)_{GS}} \qquad (2\text{-}7)$$

$$\Delta\Delta S^{‡} = \Delta S^{‡}_{(S1\rightarrow S2)} - \Delta S^{o}_{(S1\rightarrow S2)_{GS}} \qquad (2\text{-}8)$$

For the three complexes in question, the change in free energies computed on the basis of the changes in the activation parameters for the decomposition of [Cu(II):**2.1b/c**]^{0}, [Cu(II):**2.2b**]$^{+}$, and [Cu(II):**2.3a**]$^{2+}$ in passing from water to methanol and methanol to

ethanol at 25 °C are given in Table 2-4. This can be more clearly seen in Figure 2-7 where $-T\Delta S^{\ddagger}$ is plotted vs $\Delta H^{\ddagger}$ for the decomposition of [Cu(II):**2.1**,**2.2**,**2.3**] in water, methanol, and ethanol. The figure can be referred to using a compass, where moving along the diagonal southeast (SE) in Figure 2-7 increases the activation $\Delta H^{\ddagger}$ but reduces the $-T\Delta S^{\ddagger}$ contribution to $\Delta G^{\ddagger}$, resulting in little effect on the reaction rate. Moving NE increases both the enthalpy and entropy contribution, slowing the reaction considerably. In the case of cleavage of [Cu(II):**2.3a**]$^{2+}$, moving NW from MeOH to water leads to a decrease in $\Delta H^{\ddagger}$ and more positive $-T\Delta S^{\ddagger}$, compensating each other to an extent that the reaction rate does not change appreciably.

Table 2-4. Listing of changes in activation parameters for the decomposition of [Cu(II):**2.1**,**2.2**,**2.3**] accompanying changes in solvent from methanol to water, and from methanol to ethanol.

	$CH_3OH \rightarrow H_2O$				$CH_3OH \rightarrow CH_3CH_2OH$			
Complex	$\Delta\Delta H^{\ddagger a}$	$\Delta\Delta S^{\ddagger}$ (e.u.)[b]	$-T\Delta\Delta S^{\ddagger a}$ (25 °C)	$\Delta\Delta G^{\ddagger a}$ (25 °C)	$\Delta\Delta H^{\ddagger a}$	$\Delta\Delta S^{\ddagger}$ (e.u.)[b]	$-T\Delta\Delta S^{\ddagger a}$ (25 °C)	$\Delta\Delta G^{\ddagger a}$ (25 °C)
[Cu(II):**2.1b/c**]^{0}	1.5	-4.4	1.3	2.8	-3.0	-12.2	3.6	0.6
[Cu(II):**2.2b**]$^{+}$	1.4	-8.1	2.4	3.8	-3.3	-10.8	3.2	-0.1
[Cu(II):**2.3a**]$^{2+}$	-2.5	-9.0	2.7	0.2	-3.2	-8.6	2.6	-0.6

a. In units of $kcal \cdot mol^{-1}$.
b. In units of $cal \cdot mol^{-1} \cdot K^{-1}$.

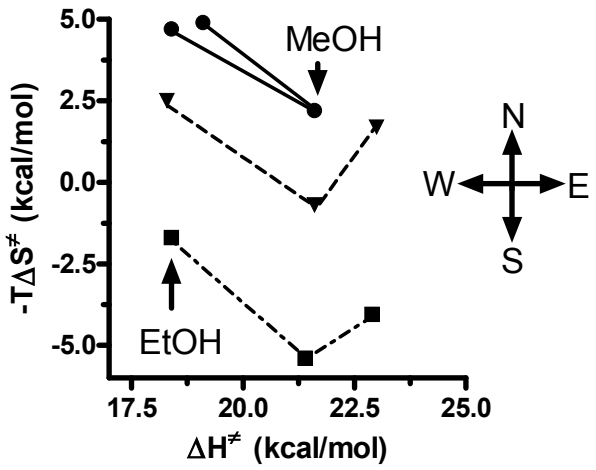

Figure 2-7. A plot of $-T\Delta S^{\ddagger}$ vs $\Delta H^{\ddagger}$ for the decomposition of [Cu(II):**2.1**,**2.2**,**2.3**] (■, ▼, ● respectively) in ethanol (leftmost vertical points), methanol (center vertical points) and water (unmarked points) at 25 °C in the plateau regions where the active forms are [Cu(II):**2.1b/c**]^{0}, [Cu(II):**2.2b**]$^{+}$, and [Cu(II):**2.3a**]$^{2+}$. The various lines connecting the three species are not fits, but aids for visualization.

Pertinent to Figure 2-7 are Leffler's and Lumry and Rajender's treatises discussing the enthalpy-entropy relationship for various solvolytic and other reactions where emphasis was put on the possible linear relationships between the two activation parameters.[27,28] These refer to related reactions or equilibria involving modest changes in substrate or solvent, where it is often found that the ΔH and ΔS parameters vary in a dependent way. The Figure 2-7 data indicate that, for the decomposition of [Cu(II):**2.1b/c**]^{0}, [Cu(II):**2.2b**]$^{+}$, and [Cu(II):**2.3a**]$^{2+}$, moving from methanol (center vertical points) to ethanol (leftmost vertical points), there is a decrease in the $\Delta H^{\ddagger}$ of each reaction of roughly 3.0–3.3 kcal·mol^{-1}, which is offset by a net increase in the $-T\Delta S^{\ddagger}$ term of 2.6–3.6 kcal·mol^{-1}; thus the change in the overall free energy of reaction for all three substrates does not vary appreciably at 25 °C. However, passing from methanol to water causes wider variations of the activation parameters in the series, increasing both $\Delta H^{\ddagger}$ and

$-T\Delta S^{\ddagger}$ by moving NE in Figure 2-7 for [Cu(II):**2.1b/c**]^{0} and [Cu(II):**2.2b**]$^{+}$ such that the $\Delta G^{\ddagger}$ for these two reactions is raised by 2.8 and 3.8 kcal·mol^{-1}. This accounts for the 10^{2}–10^{3} drop in the rates of these reactions in passing from methanol to water. By contrast there is an approximate cancelation of these two terms for cleavage of [Cu(II):**2.3a**]$^{2+}$ in passing from methanol to water moving NW, leading to a reduction of 2.5 kcal·mol^{-1} in $\Delta H^{\ddagger}$ and an increase in $-T\Delta S^{\ddagger}$ of 2.7 kcal·mol^{-1} such that the net change in $\Delta G^{\ddagger}$ is only -0.2 kcal·mol^{-1}.

Moving from alcohol to water induces irregular perturbations on $\Delta H^{\ddagger}$ and $-T\Delta S^{\ddagger}$ in the series for reasons that are not obvious. Winstein and Fainberg[26] have pointed out how exceedingly difficult it is to evaluate the effect of solvent changes such as MeOH → H_2O and EtOH → H_2O even on an apparently simple process like the solvolysis of *tert*-butyl chloride. While not strictly comparable to the more complex situation of spontaneous solvolysis of the Cu(II) complexes here with their varying formal charges, it is clear that changes in the free energy of solvation of the ground state ($\Delta\Delta G^{o}_{s}$) are just as, or more, important as those in the transition state, $\Delta\Delta G^{\ddagger}_{s}$.[29] Given the difficulties in separating the effect of solvent changes on $\Delta\Delta G^{o}_{s}$ into the individual $\Delta\Delta H^{o}_{s}$ and $\Delta\Delta S^{o}_{s}$ terms, it is inappropriate to attempt further interpretations as to the origins of the solvent effect on the activation parameters other than to say that water seems to be the outlier.

2.5.3 – Mechanistic picture

Cleavage of phosphate esters in solution without catalysts

In water, the decomposition of phosphate monoester dianions containing aryloxy leaving groups proceeds by an apparent unimolecular route involving a significant positive entropy and unit solvent isotope effect that is consistent with a dissociative mechanism with little involvement of a nucleophilic role for solvent.[30] There is a significantly more positive entropy of activation for the solvolysis of *p*-nitrophenyl phosphate dianion in *tert*-butyl alcohol which supports a dissociative ($D_N + A_N$) mechanism confirming that racemization at phosphorus in this reaction is attributed to the direct formation of a metaphosphate anion, with no nucleophilic role for the solvent in the P–OAr cleavage.[31]

Kirby and Younas[32] reported that the aqueous cleavage of phosphate diesters is exceedingly slow and highly dependent on the LG basicity. The reaction is bimolecular with hydroxide being the active nucleophile down to pH 5 where a water-promoted reaction was observable with leaving groups as good as, or better than, 4-nitrophenoxy but not with poorer ones like phenoxy or 4-methoxyphenoxy. Methanolysis of aryl methyl phosphates involves methoxide attack on the monoanion, probably with a concerted departure of the leaving group via an A_ND_N mechanism.[33]

Hydrolyses of dialkyl aryl phosphate triesters[34] with good leaving groups in water is subject to HO^-, H_3O^+, and solvent promoted reactions. For the least reactive of the tested esters (such as the 4-nitrophenyl derivative), the base and acid wings account for the hydrolysis over almost all the investigated pH range except for a small deviation at

pH ≈ 4 that may result from a water reaction. The methanolysis of dimethyl aryl phosphates is methoxide promoted.[14,35] Recent computational studies indicate that both the hydroxide[36] and methoxide[37] reactions are enforced concerted with good aryloxy leaving groups having pK_a ($^{s}_{s}pK_a$) values < 8 (*m*-nitrophenol in water) or < 12.3 (3,5-dichlorophenol in methanol), but stepwise with rate-limiting formation of an anionic 5-coordinate phosphorane intermediate when the phosphate has poorer leaving groups.

*Decompositions of [Cu(II):**2.1**,**2.2**,**2.3**] promoted by leaving group assistance*

Rate data presented here and earlier[16] support the idea that positioning the Cu(II) ion close to the leaving group's developing oxyanion results in a loosening of the transition state for P–O(LG) cleavage for [Cu(II):**2.1**,**2.2**,**2.3**] by reducing the requirement for nucleophilic participation in expelling the leaving group. Using More O'Ferrall-Jencks diagrams, the effect of Cu(II) on the cleavage relative to the uncatalyzed methanolysis of mono-, di-, and triesters has been rationalized as moving the transition state earlier with respect to P–nucleophile interaction with little change in the extent of P–O(LG) cleavage,[16] and the same is likely true in ethanol and water. The leaving group acceleration provided by Cu(II) coordination comes from converting the poor leaving group, uncomplexed 2(2'-phenathrolyl)phenoxide, into a far better leaving group.[38] Extant data indicate that the β_{nuc} for the attack of oxyanion nucleophiles on phosphate triesters becomes smaller as the leaving group gets better,[34] and also that the k_{H2O} for water attack on both phosphate diester anions[32] and monoester dianions[30] increases as the leaving group gets better. It follows that, in the limit when the leaving group is very good, the effective nucleophile will be the one having the highest concentration in

solution, namely solvent. For all three phosphate complexes in this study, this is the case since the reactions in ethanol, methanol, or water involve only solvent attack on [Cu(II):**2.1b/c**]^{0}, [Cu(II):**2.2b**]$^{+}$, or [Cu(II):**2.3a**]$^{2+}$.

The data herein also indicate that there is a very large acceleration of P–O(LG) cleavage attributable to LGA relative to the background reactions in each solvent. While this is quantified in only methanol[16] as being 10^{14} to 10^{15} for the monoester, 10^{14} for the diester and 10^{5} for the triester, the fact that similar rate constants are observed in all solvents (changes ranging from little effect to no more than 500-fold rate reduction in the case of [Cu(II):**2.2b**]$^{+}$ in moving from methanol to water) suggests that the high degree of acceleration obtained from LGA is attainable in all three media.

The synthetic difficulties in making appropriate small molecule systems that position the metal ion optimally to assist in the departure of the leaving group impose serious limitations in achieving significant LGA. Nevertheless, the present results seem to suggest that in optimized cases, such as enzymes where the tertiary structure controls the placement of the metal ion relative to the departing leaving group, this mode of catalysis could provide a significant source of acceleration.

2.6 – Supporting Information

2.6.1 – Supporting Information 2-1: Eyring plots

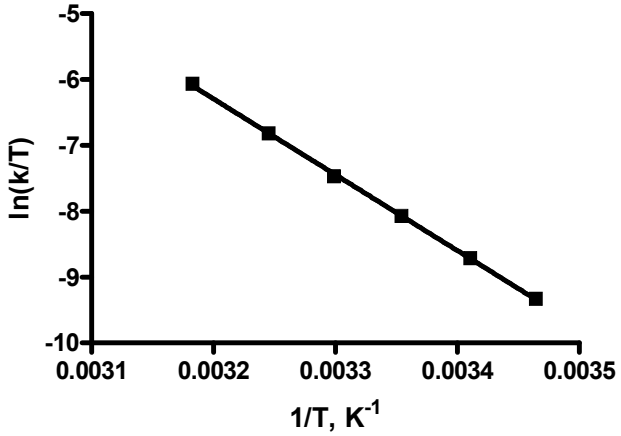

Figure 2-8. Eyring plot of ln(k/T) vs 1/T for the hydrolysis of Cu(II):**2.1** (0.02 mM of Cu(II) and **2.1**) determined at pH 6.9 under aqueous buffered conditions (0.4 mM 2,6-lutidine, 0.2 mM HOTf). The data are fitted by NLLSQ methods to the linear form of the Eyring equation[39] to give $\Delta H^{\ddagger}$ = 22.9 ± 0.2 kcal·mol^{-1} and $\Delta S^{\ddagger}$ = 13.6 ± 0.7 cal·mol^{-1}·K^{-1}; r^2 = 0.9997.

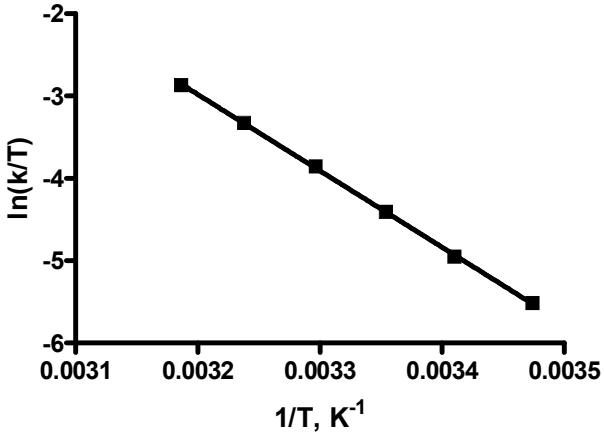

Figure 2-9. Eyring plot of ln(k/T) vs 1/T for the cleavage of Cu(II):**2.1** (0.02 mM of Cu(II) and **2.1**) determined at $^{s}_{s}$pH 11.4 in anhydrous ethanol under buffered conditions (0.4 mM 2,2,6,6-tetramethylpiperidine, 0.2 mM HOTf). The data are fitted by NLLSQ methods to the linear form of the Eyring equation[39] to give $\Delta H^{\ddagger}$ = 18.4 ± 0.1 kcal·mol^{-1} and $\Delta S^{\ddagger}$ = 5.8 ± 0.5 cal·mol^{-1}·K^{-1}; r^2 = 0.9997.

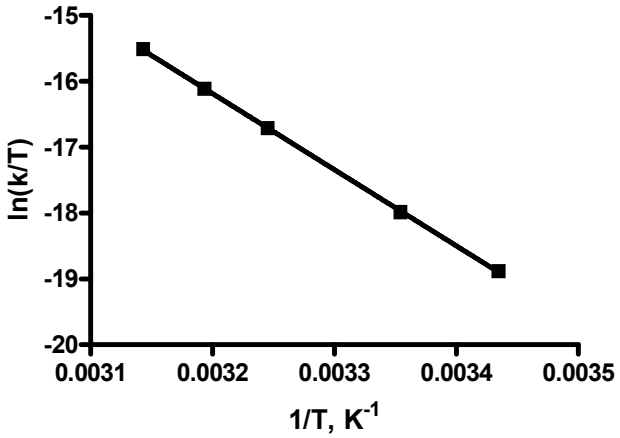

Figure 2-10. Eyring plot of ln(k/T) vs 1/T for the hydrolysis of Cu(II):**2.2** (0.02 mM of Cu(II) and **2.2**) determined at pH 3.0 (1.0 mM HOTf). The data are fitted by NLLSQ methods to the linear form of the Eyring equation[39] to give $\Delta H^{\ddagger}$ = 23.0 ± 0.2 kcal·mol^{-1} and $\Delta S^{\ddagger}$ = -5.8 ± 0.5 cal·mol^{-1}·K^{-1}; r^2 = 0.9999.

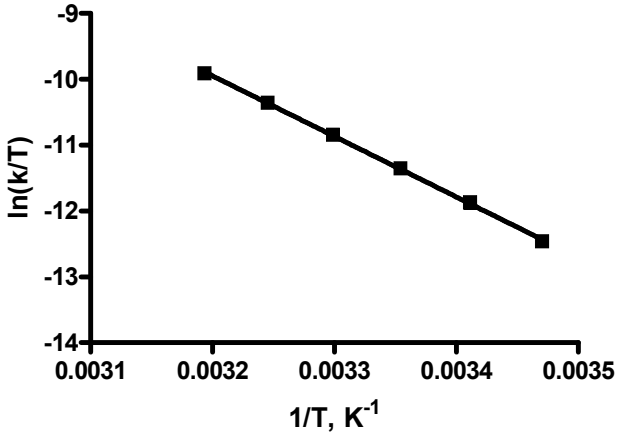

Figure 2-11. Eyring plot of ln(k/T) vs 1/T for the cleavage of Cu(II):**2.2** (0.02 mM of Cu(II) and **2.2**) determined at $^{s}_{s}$pH 3.0 (1.0 mM HOTf) in anhydrous ethanol. The data are fitted by NLLSQ methods to the linear form of the Eyring equation[39] to give $\Delta H^{\ddagger}$ = 18.3 ± 0.2 kcal·mol^{-1} and $\Delta S^{\ddagger}$ = -8.5 ± 0.6 cal·mol^{-1}·K^{-1}; r^2 = 0.9995.

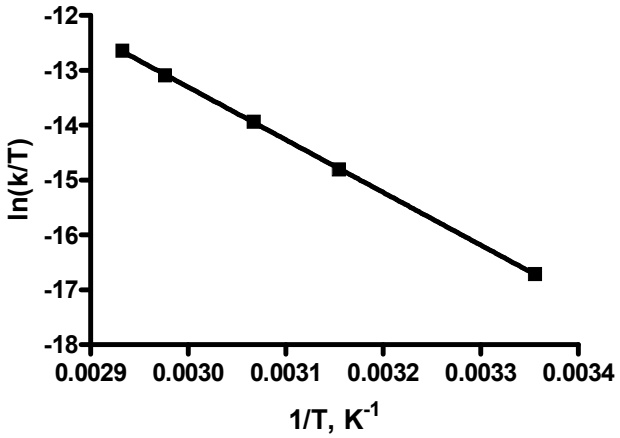

Figure 2-12. Eyring plot of ln(k/T) vs 1/T for the hydrolysis of Cu(II):**2.3** (0.02 mM of Cu(II) and **2.3**) determined at pH 3.0 (1.0 mM HOTf). The data are fitted by NLLSQ methods to the linear form of the Eyring equation[39] to give $\Delta H^{\ddagger}$ = 19.1 ± 0.1 kcal·mol^{-1} and $\Delta S^{\ddagger}$ = -16.4 ± 0.3 cal·mol^{-1}·K^{-1}; r^2 = 0.9999.

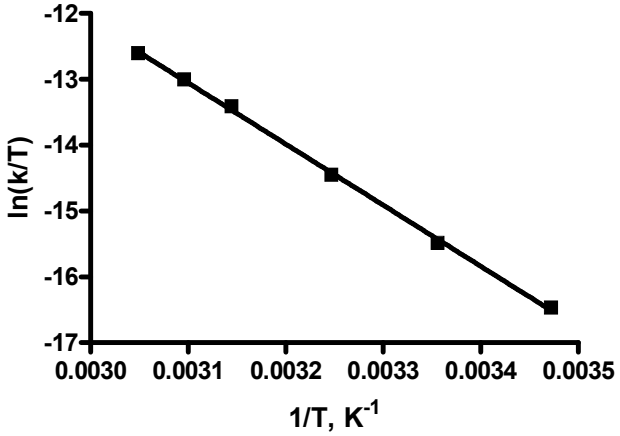

Figure 2-13. Eyring plot of ln(k/T) vs 1/T for the cleavage of Cu(II):**2.3** (0.02 mM of Cu(II) and **2.3**) determined at $^{s}_{s}$pH 3.0 (1.0 mM HOTf) in anhydrous ethanol. The data are fitted by NLLSQ methods to the linear form of the Eyring equation[39] to give $\Delta H^{\ddagger}$ = 18.4 ± 0.3 kcal·mol^{-1} and $\Delta S^{\ddagger}$ = -16.0 ± 0.9 cal·mol^{-1}·K^{-1}; r^2 = 0.9995.

2.7 – References and notes

[1] Westheimer, F. H. *Science* **1987**, *235*, 1173.

[2] Hengge, A. C. *Adv. Phys. Org. Chem.* **2005**, *40*, 49.

[3] (a) Zalatan, J. G.; Herschlag, D. *J. Am. Chem. Soc.* **2006**, *128*, 1293. (b) Weston, J. *Chem. Rev.* **2005***, 105*, 2151. (c) Mancin, F.; Tecilla, P. *New J. Chem.* **2007**, *31*, 800. (d) Aubert, S. D.; Li, Y.; Raushel, F. M. *Biochemistry* **2004**, *43*, 5707. (e) Morrow, J. R. *Comments Inorg. Chem.* **2008**, *29*, 169.

[4] (a) Brown, R. S.; Lu, Z.-L.; Liu, C. T.; Tsang, W. Y.; Edwards, D. R.; Neverov, A. A. *J. Phys. Org. Chem.* **2009**, *22*, 1. (b) Williams, N. H.; Takasaki, B.; Wall, M.; Chin, J. *Acc. Chem. Res.* **1999**, *32*, 485. (c) Morrow, J. *Comments Inorg. Chem.* **2008**, *29*, 169. (d) Mitić, N.; Smith, S. J.; Neves, A.; Guddat, L. W.; Gahan, L. R.; Schenk, G. *Chem. Rev.* **2006**, *106*, 3338.

[5] Fothergill, M.; Goodman, M. F.; Petruska, J.; Warshel, A. *J. Am. Chem. Soc.* **1995**, *117*, 11619.

[6] Zalatan, J. G.; Catrina, I.; Mitchell, R.; Grzyska, P. K.; O'Brien, P. J.; Herschlag, D.; Hengge, A. C. *J. Am. Chem. Soc.* **2007**, *129*, 9789.

[7] Benkovic, S. J.; Dunikoski, L. K., Jr. *J. Am. Chem. Soc*. **1971**, *93*, 1526.

[8] Hay, R. W.; Basak, A. K.; Pujari, M. P. *J. Coord. Chem*. **1991**, *23*, 43.

[9] Hay, R. W.; Basak, A. K.; Pujari, M. P.; Perotti, A. *J. Chem. Soc. Dalton Trans.* **1986**, 2029.

[10] Fife, T. H.; Pujari, M. P. *J. Am. Chem. Soc*. **1988**, *110*, 7790.

[11] Bruice, T. C.; Tsubouchi, A.; Dempcy, R. O.; Olson, L. P. *J. Am. Chem. Soc*. **1996**, *118*, 9867.

[12] Edwards, D. R.; Neverov, A. A. Brown, R. S. *J. Am. Chem. Soc*. **2009**, *121*, 368.

[13] Neverov, A. A.; Liu, C. T.; Bunn, S. E.; Edwards, D.; White, C. J.; Melnychuk, S. A.; Brown, R. S. *J. Am. Chem. Soc.* **2008**, *130*, 6639.

[14] Edwards, D. R.; Liu, C. T.; Garrett, G. E.; Neverov, A. A.; Brown, R. S. *J. Am. Chem. Soc.* **2009**, *131*, 13738.

[15] Hoff, R. H.; Hengge, A. C. *J. Org. Chem.* **1998**, *63*, 6680.

[16] Liu, C. T.; Neverov, A. A.; Brown, R. S. *J. Am. Chem. Soc.* **2010**, *132*, 3561.

[17] (a) Gibson, G. T. T.; Mohamed, M. F.; Neverov, A. A.; Brown, R. S. *Inorg. Chem.* **2006**, *45*, 7891. (b) For the designation of pH in non-aqueous solvents we use the nomenclature recommended by *IUPAC: Compendium of Analytical Nomenclature. Definitive Rules 1997*, 3rd ed.; Blackwell: Oxford, U.K., 1998. The pH meter reading for an aqueous solution determined with an electrode calibrated with aqueous buffers is designated as ${}^{w}_{w}$pH; if the electrode is calibrated in water and the "pH" of the neat buffered methanol solution is then measured, the term ${}^{s}_{w}$pH is used; and if the electrode is calibrated in the same solvent in which the "pH" reading is made, then the term ${}^{s}_{s}$pH is used. In ethanol, ${}^{s}_{w}$pH – (-2.54) = ${}^{s}_{s}$pH and since the autoprotolysis constant of ethanol is $10^{-19.1}$, the neutral ${}^{s}_{s}$pH is 9.6.

[18] Solvent composition = water-methanol (95-5 mol %).

[19] (a) Cleland, W. W.; Frey, P. A.; Gerlt, J. A. *J. Biol. Chem.* **1998**, *273*, 25529. (b) Simonson, T.; Carlsson, F.; Case, D. A. *J. Am. Chem. Soc.* **2004**, *126*, 4167 and references therein. (c) Richard, J. P.; Amyes, T. L. *Bioorg. Chem.* **2004**, *32*, 354.

[20] Harned, H. S.; Owen, B. B. *The Physical Chemistry of Electrolytic Solutions*, 3rd ed.; ACS Monograph Series 137; Reinhold Publishing: New York, 1957; p 161.

[21] (a) Neverov, A. A.; Lu, Z.-L.; Maxwell, C. I.; Mohamed, M. F.; White, C. J.; Tsang, J. S. W.; Brown, R. S. *J. Am. Chem. Soc.* **2006**, *128*, 16398. (b) Bunn, S. E.; Liu, C. T.; Lu, Z.-L.; Neverov, A. A.; Brown, R. S. *J. Am. Chem. Soc.* **2007**, *129*, 16238.

[22] (a) Brown, R. S. In *Progress in Inorganic Chemistry*; Karlin, K., Ed.; John Wiley and Sons: New York, NY, 2011; Vol. *57*, p 55. (b) Brown, R. S.; Neverov, A. A. *Advances in Physical Organic Chemistry*; Richard, J. P., Ed.; Elsevier: San Diego, CA, 2007, Vol. *42*, p 271.

[23] Holligan, B. M.; Jeffery, J. C.; Ward, M. D. *J. Chem. Soc. Dalton Trans.* **1992**, 3337.

[24] Sillén, L. G.; Martell, A. E. In *Stability Constants*; Special Publications-Chemical Society, 1964; pp 664–665; Supp. No. 1 1971, p 676.

[25] For a simplified introduction to the effects of solvent on reaction rates and parameters to measure certain properties of solvents see: Carroll, F. A. *Perspectives on Structure and Mechanism in Organic Chemistry*. 2nd ed.; John Wiley and Sons: Hoboken, NJ, 2010; pp 337–339 and references therein.

[26] Winstein, S.; Fainberg, A. H. *J. Am. Chem. Soc.* **1957**, *79*, 5937.

[27] Leffler, J. E. *J. Org. Chem.* **1955**, *20*, 1202.

[28] Lumry, R.; Rajender, S. *Biopolymers* **1970**, *9*, 1125.

[29] Hvidt, A. *Annu. Rev. Biophys. Bioeng.* **1983**, 12, 1.

[30] Kirby, A. J.; Varvoglis, A. G. *J. Am. Chem. Soc.* **1967**, *89*, 415.

[31] Hoff, R. H.; Hengge, A. C. *J. Org. Chem.* **1998**, *63*, 6680.

[32] Kirby, A. J.; Younas, M. *J. Chem. Soc. B* **1970**, 510.

[33] Liu, C. T.; Neverov, A. A.; Brown, R. S. *J. Am. Chem. Soc*. **2008**, *130*, 16711.

[34] Khan, S. A.; Kirby, A. J. *J. Chem. Soc. B* **1970**, 1172.

[35] Liu, T.; Neverov, A. A.; Tsang, J. S. W.; Brown, R. S. *Org. Biomol. Chem.* **2005**, *3*, 1525.

[36] Tarrat, N. *J. Mol. Struct. THEOCHEM* **2010**, *941*, 56.

[37] Maxwell, C. I.; Liu, C. T.; Neverov, A. A.; Mosey, N. J.; Brown, R. S. *J. Phys. Org. Chem.* **2012**, *25*, 437.

[38] The ${}^{s}_{s}pK_a$ of 2(2'-phenanthrolyl)phenol drops from 16.17 to 0.40 and methanol when coordinated to Cu(II).[16] While the equivalent pK_a values are not known in water or ethanol, it is certain that Cu(II) complexation will substantially acidify the phenol.

[39] $\ln\left(\frac{k}{T}\right) = \frac{-\Delta H^{\neq}}{R} \cdot \frac{1}{T} + \ln\left(\frac{k_B}{h}\right) + \frac{\Delta S^{\neq}}{R}$

Chapter 3 – Trifunctional metal ion-catalyzed solvolysis: Cu(II)-promoted methanolysis of *N,N*-bis(2-picolyl)benzamides involves unusual Lewis acid activation of substrate, delivery of coordinated nucleophile, and powerful assistance of the leaving group departure

3.1 – Preface

With minor formatting changes, this chapter is presented largely as it is published in *Inorganic Chemistry* (Raycroft, M. A. R.; Maxwell, C. I.; Oldham, R. A. A.; Saffouri Andrea, A.; Neverov, A. A.; Brown, R. S. *Inorg. Chem.* **2012**, *51*, 10325). The corresponding Supporting Information is represented in part by Supporting Information 3-1 and can be found in its complete form via the Internet at http://pubs.acs.org. The kinetic experiments were performed by Mark Raycroft and Ms. Robyn Oldham, the syntheses were performed by Ms. Areen Saffouri Andrea, and the computations were performed by Dr. Christopher I. Maxwell. The manuscript was written by Mark Raycroft and Dr. R. Stan Brown with contributions from Dr. Christopher I. Maxwell.

3.2 – Introduction

The usual ways that metal ions promote solvolytic reactions of carboxylate esters and amides, as well as neutral and anionic organophosphorus esters comprise: (1) electrophilic Lewis acid activation of the substrate through X=O or X=S coordination, where X = C or P; (2) intramolecular delivery of metal-coordinated lyoxide nucleophiles; (3) electrostatic stabilization of the transforming substrate-nucleophile species; and (4) electrophilic assistance of the departure of the leaving group.[1,2,3,4] The first three of these roles have been demonstrated with several types of substrates, and particularly for

the decomposition of poorly reactive anionic phosphate mono- and diesters or neutral phosphate triesters as well as carboxylate esters and amides. In most of these cases, metal binding ligands are attached to the substrate to position the metal ion close to the X=O or X=S unit to optimize Lewis acid activation. Metal ion catalysis for the decomposition of amides, particularly peptides in metallo-peptidase enzymatic systems, is also of general importance,[5] but less well-described are small molecule systems for the cleavage of carboxamides[6] where the leaving group is not activated. These are notoriously inert to solvolysis of the >N–C=O due to the inherent resonance stability which shields the substrate from nucleophilic attack, and also due to poor leaving group ability of the amide anion from the subsequently formed tetrahedral intermediates.[7] Because the interaction of neutral amides and positively charged metal ions or their complexes in solution, particularly water, is weak, catalyzed solvolysis is depressed further[6e] unless the substrate possesses some mode of attraction such as a pronounced soft-soft interaction,[8] a residue acting as an attractive site,[9] or attached ligands[6b] that position the metal ion close to the scissile bond. Even so, amides with normal amine leaving groups are generally not very active because of the reluctance of their departure from the tetrahedral intermediate unless they have a low pK_a (e.g. imidazole or anilide) or there is a physical effect such as release of strain (as in distorted amides[10] and lactams[11]).

Recently we communicated a mechanistic study[12] of an unusual methanolysis reaction of the Cu(II)-complex of *N,N*-bis(2-picolyl)acetamide, **3.1**, the products of which are methyl acetate and Cu(II):*N,N*-bis(2-picolyl)amine. This reaction was the subject of an early report by Houghton and Puttner[13] some 40 years ago describing the methanolysis of some

N-acyl derivatives of *N,N*-bis(2-picolyl)amine in the presence of Cu(II). Subsequent physical studies with such amides,[14,15,16] the demonstration of their synthetic utility[17] as well as the recent reports on the methanolysis of metal complexes of secondary amides[18] and demonstration of mild methanolytic cleavage of a special class of amides, **3.2**,[19] prompted us to expand a program[20] investigating the scope and importance of metal ion-promoted leaving group assistance (LGA) during the alcoholysis reactions.

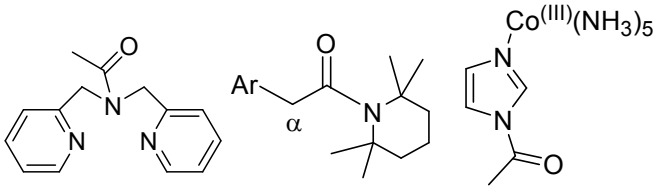

3.1 **3.2** **3.3**

3.4a X = 3,5-dinitro
3.4b X = 4-nitro
3.4c X = 3-nitro
3.4d X = 4-chloro
3.4e X = H
3.4f X = 4-methyl
3.4g X = 4-methoxy

Our initial observation[6e] of where this effect might be operative was during the methoxide reaction of the $(H_3N)_5Co(III)$-complex of acetyl imidazole (**3.3**); there the second order rate constant for methoxide attack (k_{MeO}- = 4.69 × 10^7 $M^{-1}\cdot s^{-1}$) was four orders of magnitude higher than that for acetyl imidazole itself (k_{MeO}- = 7.9 × 10^3 $M^{-1}\cdot s^{-1}$). The large acceleration was surmised to result in part from $(H_3N)_5Co(III)$-activation of the acyl group by reducing the imidazole's resonance donation, in part from a methanolic medium induced electrostatic enhancement of the reaction of oppositely charged substrate and nucleophile and partly from the reduction in pK_a of the conjugate acid of the leaving group (10 for H-Im-Co(III)$(NH_3)_5$ vs 14 for H-Im)[21] as a consequence of LGA. In the case of **3.1**:Cu(II), the metal ion enacted a trifunctional role[12] (which we term as trifunctional catalysis) to accelerate the methanolysis by: (1) positioning the metal ion close to the amide N, binding to its lone pair to reduce amidic resonance; (2) binding and intramolecularly delivering a coordinated methoxide to the C=O unit; and (3) electrophilically assisting the departure of the leaving group amide anion.

Herein we report experimental details of the Cu(II)-promoted cleavage of a series of *N,N*-bis(2-picolyl)benzamides **3.4a**–**g** under $^{s}_{s}$pH-controlled[22] conditions along with supporting DFT computations. This study complements and expands the communication of the methanolysis of **3.1**:Cu(II),[12] presenting additional details of the mechanism by providing the Hammett linear free energy relationship of $\log(k_x)$ vs σ_x for cleavage of various **3.4**:Cu(II), solvent kinetic isotope effect (SKIE) values, and activation parameters for the cleavage of representative examples **3.4b**:Cu(II) and **3.4g**:Cu(II), as well as a comparative DFT computational study for the cleavage of **3.4a**:Cu(II), **3.4b**:Cu(II), and **3.4g**:Cu(II).

3.3 – Experimental

3.3.1 – Materials

Methanol (99.8%, anhydrous) and acetonitrile (99.8%, anhydrous) were purchased from EMD Chemicals. Trifluoromethanesulfonic acid (HOTf, ≥99%), methanol-OD (99.5 atom % D), 2-pyridinecarboxaldehyde (99%), 2-aminomethylpyridine (98%), 4-nitrobenzoyl chloride (98%), benzoyl chloride (99%), 4-methoxybenzoyl chloride (99%), 3,5-dinitrobenzoyl chloride (98+%), 4-chlorobenzoyl chloride (99%), 4-toluoyl chloride (98%), 3-nitrobenzoyl chloride (98%), and triethylamine (99%) were obtained from Aldrich. Chloroform-*d* (99.8% D), methylene chloride-d_2 (99.9% D), and $Cu(OTf)_2$ (98%) were obtained from TCI America Laboratory Chemicals; 2,4,6-collidine (98%) was obtained from BDH Laboratory Reagents.

3.3.2 – General methods

All ^{1}H NMR spectra were determined at 400 MHz and ^{13}C NMR spectra at 100.58 MHz; all chemical shift values were referenced internally to the solvent. All high-resolution mass spectra were determined by EI-TOF. $CH_3OH_2^+$ concentrations were determined potentiometrically using a combination glass Fisher Scientific Accumet electrode model no. 13-620-292 calibrated with certified standard aqueous buffers (pH 4.00 and 10.00) as described previously.[23] The $^{s}_{s}$pH values in methanol were determined by subtracting a correction constant of -2.24 from the electrode readings and the autoprotolysis constant for methanol was taken to be $10^{-16.77}$ M^2.[22] The $^{s}_{s}$pH values for the kinetic experiments were measured at the end of the reactions to avoid the effect of KCl leaching from the electrode.

3.3.3 – Synthesis of materials

3.3.3.1 – *N*,*N*-Bis(2-picolyl)amine or dipicolylamine (DPA)

A modification of the literature procedure was used.[24] To a solution of 2-pyridinecarboxaldehyde (4.44 mL, 46 mmol) in dry MeOH (150 mL) was added 2-aminomethylpyridine (4.76 mL, 46 mmol) at RT after which the brown mixture was stirred for 5 h. Sodium borohydride (3.5 g, 92 mmol) was added in small portions with stirring, maintaining the reaction at 0 °C using an ice bath. The mixture changed colour from brown to yellow and was stirred for 15 h at room temperature. Concentrated HCl was added slowly to adjust the pH to 1 and the solution was stirred for 2 h. Next, a saturated solution of NaOH was added to adjust the pH to 11. The reaction mixture was filtered and the solvent was removed under vacuum. Water was added to the residue; the

aqueous mixture was extracted twice with CH_2Cl_2, and the combined extracts dried over anhydrous magnesium sulfate and filtered. The solvent was removed under vacuum. The product was obtained as a brown oil in 85% yield (7.78 g, 39.1 mmol).

^{1}H NMR (400 MHz, CD_2Cl_2, 25 °C): δ 8.51 (d, J = 4.9 Hz, 2H), 7.63 (td, J_t = 16.7 Hz, J_d = 7.7 Hz, 2H), 7.33 (d, J = 8.1 Hz, 2H), 7.13–7.16 (m, 2H), 3.91 (s, 4H), 2.37 (bs, 1H); ^{13}C NMR (100.58 MHz, CD_2Cl_2, 25 °C): δ 160.3, 149.5, 136.7, 122.5, 122.3, 55.0; HRMS (EI+ TOF): calculated for $C_{12}H_{13}N_3$ 199.1109 amu, found 199.1102 amu.

3.3.3.2 – 4-Nitro-*N*,*N*-bis(2-picolyl)benzamide (**3.4b**)

To a solution of dipicolylamine (1.5 g, 7.53 mmol) in CH_2Cl_2 was slowly added 4-nitrobenzoyl chloride (1.7 g, 9.16 mmol) and triethylamine (1.27 mL, 9.16 mmol). The mixture was refluxed for 3.5 hours then stirred for 2 hours at room temperature. The reaction mixture was washed with water (2×), saturated sodium carbonate solution (2×) and finally with water (2×), then dried over anhydrous $MgSO_4$. The CH_2Cl_2 was removed under vacuum and the crude product was purified by column chromatography on silica gel using CH_2Cl_2/MeOH (90:10) as the eluent. The solvent was removed under vacuum and the resulting solid was recrystallized in anhydrous ethyl ether and ethyl acetate. The product was obtained as fine pale yellow needles in 75% yield (1.97 g, 5.65 mmol).

^{1}H NMR (400 MHz, CD_2Cl_2, 25 °C): δ 8.60 (d, J = 4.7 Hz, 1H), 8.53 (d, J = 4.7 Hz, 1H), 8.19 (d, J = 9.0 Hz, 2H), 7.77 (d, J = 9.0 Hz, 2H), 7.64–7.72 (m, 2H), 7.36 (d, J = 7.8 Hz, 1H), 7.20–7.24 (m, 2H), 7.11 (d, J = 7.8 Hz, 1H), 4.80 (s, 2H), 4.59 (s, 2H); ^{13}C NMR (100.58 MHz, $CDCl_3$, 25 °C): δ 170.4, 156.5, 155.6, 150.0, 149.4, 142.3, 136.8, 128.3, 123.6, 122.82, 122.78, 122.5, 121.9, 54.1, 50.4; HRMS (EI+ TOF): calculated for

$C_{19}H_{16}N_4O_3$ 348.1222 amu, found 348.1231 amu; λ_{max} (CH_3OH): 260 nm (ε = 14940 ± 90 $M^{-1}\cdot cm^{-1}$); melting point: 95 °C.

3.3.3.3 – 3,5-Dinitro-*N*,*N*-bis(2-picolyl)benzamide (**3.4a**)

This compound was synthesized from dipicolylamine (1 g, 5.02 mmol), 3,5-dinitrobenzoyl chloride (1.38 g, 6.02 mmol) and triethylamine (0.84 mL, 6.02 mmol) using a procedure similar to that above for the preparation of 4-nitro-*N*,*N*-bis(2-picolyl)benzamide. The compound was obtained as pale yellow needles in 68% yield (1.34 g, 3.42 mmol).

^{1}H NMR (400 MHz, CD_2Cl_2, 25 °C): δ 9.02–9.04 (m, 3H), 8.70 (d, *J* = 3.9 Hz, 1H), 8.55 (d, *J* = 3.9 Hz, 1H), 7.67–7.73 (m, 2H), 7.38 (d, *J* = 7.8 Hz, 1H), 7.22–7.29 (m, 2H), 7.15 (d, *J* = 7.5 Hz, 1H), 4.78 (s, 2H), 4.61 (s, 2H); ^{13}C NMR (100.58 MHz, CD_2Cl_2, 25 °C): δ 168.1, 156.7, 155.5, 150.5, 149.8, 148.8, 140.3, 137.3, 137.2, 128.7, 123.6, 123.2, 123.1, 123.0, 119.8, 51.1; HRMS (EI+ TOF): calculated for $C_{19}H_{15}N_5O_5$ 393.1073 amu, found 393.1065 amu; λ_{max} (CH_3OH): 235 nm (ε = 20400 ± 700 $M^{-1}\cdot cm^{-1}$); melting point: 120 °C.

3.3.3.4 – 3-Nitro-*N*,*N*-bis(2-picolyl)benzamide (**3.4c**)

This compound was synthesized from dipicolylamine (1 g, 5.02 mmol), 3-nitrobenzoyl chloride (1.12 g, 6.02 mmol) and triethylamine (0.84 mL, 6.02 mmol) using a procedure similar to that above for the preparation of 4-nitro-*N*,*N*-bis(2-picolyl)benzamide. The compound was obtained as a brown oil in 80% yield (1.40 g, 4.02 mmol).

^{1}H NMR (400 MHz, CD_2Cl_2, 25 °C): δ 8.62 (d, J = 3.8 Hz, 1H), 8.54 (d, J = 4.0 Hz, 1H), 8.52 (t, 1H), 8.21–8.24 (m, 1H), 7.96 (td, J_t = 7.6 Hz, J_d = 1.6 Hz, 1H), 7.66–7.72 (m, 2H), 7.57 (t, 1H), 7.38 (d, J = 7.2 Hz, 1H), 7.21–7.25 (m, 2H), 7.13 (d, J = 7.5, 1H), 4.80 (s, 2H), 4.62 (s, 2H); ^{13}C NMR (100.58 MHz, CD_2Cl_2, 25 °C): δ 170.2, 157.2, 156.3, 150.3, 149.7, 148.4, 138.4, 137.13, 137.07, 133.7, 130.0, 124.6, 123.2, 122.9, 122.8, 122.4, 54.6, 50.9; HRMS (EI+ TOF): calculated for $C_{19}H_{16}N_4O_3$ 348.1222 amu, found 348.1231 amu; λ_{max} (CH_3OH): 260 nm (ε = 9200 ± 200 $M^{-1}\cdot cm^{-1}$).

3.3.3.5 – 4-Chloro-*N*,*N*-bis(2-picolyl)benzamide (**3.4d**)

This compound was synthesized from dipicolylamine (1 g, 5.02 mmol), 4-chlorobenzoyl chloride (1.05 g, 6.02 mmol) and triethylamine (0.84 mL, 6.02 mmol) using a procedure similar to that above for the preparation of 4-nitro-*N*,*N*-bis(2-picolyl)benzamide. The compound was obtained as pale yellow needles in 45% yield (0.76 g, 2.26 mmol).

^{1}H NMR (400 MHz, CD_2Cl_2, 25 °C): δ 8.58 (d, J = 2.7 Hz, 1H), 8.52 (d, J = 2.5 Hz, 1H), 7.68 (bs, 2H), 7.52 (d, J = 8.6 Hz, 2H), 7.37 (m, 1H), 7.33 (d, J = 8.6 Hz, 2H), 7.21 (bs, 2H), 7.14 (d, J = 7.5 Hz, 1H), 4.78 (s, 2H), 4.63 (s, 2H); ^{13}C NMR (100.58 MHz, CD_2Cl_2, 25 °C): δ 171.6, 157.5, 156.8, 150.2, 149.6, 137.0, 135.9, 135.2, 129.0, 128.9, 122.9, 122.7, 122.1, 54.8, 50.7; HRMS (EI+ TOF): calculated for $C_{19}H_{16}N_3OCl$ 337.0982 amu, found 337.0975 amu; λ_{max} (CH_3OH): 260 nm (ε = 13500 ± 200 $M^{-1}\cdot cm^{-1}$); melting point: 73 °C.

3.3.3.6 – *N*,*N*-Bis(2-picolyl)benzamide (**3.4e**)[14]

This was synthesized from dipicolylamine (1.42 g, 7.13 mmol), benzoyl chloride (1.20 g, 8.56 mmol) and triethylamine (1.20 ml, 8.56 mmol) using a procedure similar to that above for the preparation of 4-nitro-*N*,*N*-bis(picolyl)benzamide. The crude product was purified by column chromatography on silica gel using EtOAc/MeOH (95:5) as the eluent. The compound was obtained as a pale yellow solid in 65% yield (1.40 g, 4.63 mmol).

^{1}H NMR (400 MHz, CD_2Cl_2, 25 °C): δ 8.56 (d, 1H), 8.52 (d, 1H), 7.64–7.69 (m, 2H), 7.51–7.54 (m, 2H), 7.33–7.40 (m, 4H), 7.15–7.21 (m, 3H), 4.80 (s, 2H), 4.65 (s, 2H); ^{13}C NMR (100.58 MHz, CD_2Cl_2, 25 °C): δ 172.6, 157.7, 157.2, 150.2, 149.7, 137.0, 136.8, 129.9, 128.7, 127.3, 122.8, 122.6, 122.0, 54.9, 50.7; HRMS (EI+ TOF): calculated for $C_{19}H_{17}N_3O$ 303.1372 amu, found 303.1359 amu; λ_{max} (CH_3OH): 260 nm (ε = 8300 ± 100 $M^{-1}\cdot cm^{-1}$); melting point: 66 °C.

3.3.3.7 – 4-methyl-*N*,*N*-bis(2-picolyl)benzamide (**3.4f**)

This compound was synthesized from dipicolylamine (1 g, 5.02 mmol), *p*-toluoyl chloride (0.93 g, 6.02 mmol) and triethylamine (0.84 mL, 6.02 mmol) using a procedure similar to that above for the preparation of 4-nitro-*N*,*N*-bis(2-picolyl)benzamide. The crude product was purified by column chromatography on silica gel using EtOAc/MeOH (95:5) as the eluent. The compound was obtained as fine white needles in 76% yield (1.21 g, 3.82 mmol).

^{1}H NMR (400 MHz, CD_2Cl_2, 25 °C): δ 8.56 (d, 1H), 8.52 (d, 1H), 7.68 (m, 2H), 7.41 (d, J = 8.1 Hz, 2H), 7.37 (d, J = 6.7 Hz, 1H), 7.16–7.21 (m, 5H), 4.79 (s, 2H), 4.67 (s, 2H),

2.34 (s, 3H); ^{13}C NMR (100.58 MHz, CD_2Cl_2, 25 °C): δ 172.7, 150.1, 149.6, 140.3, 137.0, 133.7, 129.3, 127.3, 122.8, 122.5, 121.8, 54.9, 50.7, 21.5; HRMS (EI+ TOF): calculated for $C_{20}H_{19}N_3O$ 317.1528 amu, found 317.1519 amu; λ_{max} (CH_3OH): 255 nm ($\varepsilon = 8900 \pm 40\ M^{-1}\cdot cm^{-1}$); melting point: 103 °C.

3.3.3.8 – 4-Methoxy-*N*,*N*-bis(2-picolyl)benzamide (**3.4g**)

This compound was synthesized from dipicolylamine (1.52 g, 7.63 mmol), 4-methoxybenzoyl chloride (1.56 g, 9.15 mmol) and triethylamine (1.27 ml, 9.15 mmol) using a procedure similar to that above for the preparation of 4-nitro-*N*,*N*-bis(picolyl)benzamide. The crude product was purified by column chromatography on silica gel using EtOAc/MeOH (90:10) as the eluent. The compound was obtained as fine white needles in 55% yield (1.4 g, 4.20 mmol).

^{1}H NMR (400 MHz, CD_2Cl_2, 25 °C): δ 8.55 (bs, 2H), 7.68 (m, 2H), 7.51 (d, J = 8.8 Hz, 2H), 7.36 (bs, 1H), 7.20 (m, 3H), 6.86 (d, J = 8.8 Hz, 2H), 4.75 (bs, 4H), 3.80 (s, 3H); ^{13}C NMR (100.58 MHz, CD_2Cl_2, 25 °C): δ 172.7, 161.2, 137.0, 129.3, 128.7, 122.6, 113.9, 55.7; HRMS (EI+ TOF): calculated for $C_{20}H_{19}N_3O_2$ 333.1477 amu, found 333.1471 amu; λ_{max} (CH_3OH): 255 nm ($\varepsilon = 15200 \pm 600\ M^{-1}\cdot cm^{-1}$); melting point: 83 °C.

3.3.4 – General UV-vis kinetics

The Cu(II)-catalyzed methanolyses of the Cu(II):($^-OCH_3$)($HOCH_3$) complexes of **3.4a–g** were followed at 360 nm for the disappearance of the **3.4**:Cu(II):($^-OCH_3$)($HOCH_3$) complex using a UV-vis spectrophotometer with the cell compartment thermostatted at 25.0 ± 0.1 °C. The reactions were conducted in the presence of buffers composed of

various ratios of 2,4,6-collidine and HOTf ($^{s}_{s}$pH 7.2, 7.6, and 7.9) to maintain the $^{s}_{s}$pH in methanol. A typical kinetic experiment involved preparing a methanol solution containing buffer (10–20 mM) and Cu(II) (1.0–2.0 mM) in a 1-cm path length quartz cuvette. Initiation of the reaction involved addition of an aliquot of the pre-formed **3.4**:Cu(II) complex (0.5 mM) in acetonitrile to the buffered methanol solution to achieve the desired concentrations of the reaction components in a final volume of 2.5 mL. The absorbance vs time traces were fitted to a standard first order exponential equation to obtain the observed first order rate constants (k_{obs}). The rate constants for the methanolysis of **3.4**:Cu(II):($^{-}OCH_3$) in the presence of excess Cu(II), required to ensure complete binding, exhibited small buffer and Cu(II) concentration effects. The observed k_{obs} values were extrapolated to zero buffer concentration for each [$Cu(OTf)_2$] using three buffer concentrations (10 mM, 15 mM, 20 mM). These extrapolated values were then extrapolated to zero excess Cu(II) using two or three excess Cu(II) concentrations (1.0 mM, 1.5 mM, 2.0 mM) to provide corrected rate constants for a given $^{s}_{s}$pH. Averages of the three rate constants for a given substrate (k_x) are presented in Table 3-1.

3.3.5 – Product analysis

The methanolysis of **3.4b**:Cu(II):($^{-}OCH_3$)($HOCH_3$) and **3.4g**:Cu(II):($^{-}OCH_3$)($HOCH_3$) were conducted at higher concentration in CH_3OH (10 mM 2,4,6-collidine buffer, 4 mM Cu(II), 3 mM **3.4b**,**g**). After completion of the reaction (assessed by UV-vis spectroscopy), the solvent was evaporated using a rotary evaporator, redissolved in $CDCl_3$, and the ^{1}H NMR spectrum at 400 MHz was collected. The only observable product in each case was the corresponding methyl benzoate. The Cu(II) complex of

N,*N*-bis(2-picolyl)amine was not observed by ^{1}H NMR due to Cu(II)-induced paramagnetic broadening.

3.3.6 – Solvent kinetic isotope effect (SKIE) experiments

The SKIE experiments for Cu(II)-assisted cleavage of **3.4b**:Cu(II):($^{-}$OCH$_3$)(HOCH$_3$) and **3.4b**:Cu(II):($^{-}$OCH$_3$)(HOCH$_3$) involved the addition of 2,4,6-collidine buffer, Cu(II), and **3.4b**,**g**:Cu(II) to UV cells containing either CH$_3$OH or CH$_3$OD so that the final concentrations of buffer, Cu(II), and substrate were 10 mM, 1.5 mM, and 0.5 mM, respectively. Triplicate competition experiments were done and the $^{s}_{s}$pH and $^{s}_{s}$pD values were measured at the end of the reactions (**3.4b**:Cu(II) – $^{s}_{s}$pH = 7.1 ± 0.2, $^{s}_{s}$pD = 7.2 ± 0.2; **3.4g**:Cu(II) – $^{s}_{s}$pH = 7.4 ± 0.2, $^{s}_{s}$pD = 7.4 ± 0.2). (The $^{s}_{s}$pD values measured at the end of the reactions are not corrected for the effect of the deuterated solvent on the reading or on the $^{s}_{s}$pK_a of the buffer. The actual $^{s}_{s}$pD value is less important since the experiments are carried out in the extensive plateau regions of the $^{s}_{s}$pH/rate profiles.)

3.3.7 – Activation parameters

Kinetic experiments with **3.4b**:Cu(II):($^{-}$OCH$_3$)(HOCH$_3$) and **3.4g**:Cu(II):($^{-}$OCH$_3$)(HOCH$_3$) were conducted at five different temperatures from 15.0 to 55.1 °C using a UV-vis spectrophotometer with a thermostatted cell holder. Solution temperatures were determined using a dummy cell adjacent to the reaction cell into which a thermometer was inserted before and after the reaction. First order rate constants were determined in triplicate for 0.5 mM **3.4b**:Cu(II):($^{-}$OCH$_3$)(HOCH$_3$) and **3.4g**:Cu(II):($^{-}$OCH$_3$)(HOCH$_3$) along with 1.0 mM excess Cu(II) in the presence of 10 mM collidine buffer, $^{s}_{s}$pH 7.0 ±

0.2. Eyring plots of ln(k/T) vs 1/T shown in Figure 3-3 and Figure 3-4 of Supporting Information 3-1 provided the $\Delta H^{\ddagger}$ and $\Delta S^{\ddagger}$ values given in Table 3-2.

3.4 – Results

3.4.1 – Kinetics

The Cu(II)-promoted methanolysis of coordinated *N*,*N*-bis(2-picolyl) acetamide (**3.1**) exhibits a kinetic ${}^{s}_{s}pK_a$ of 6.5 leading to a broad ${}^{s}_{s}pH$-insensitive region from 7 to 10 where the complex is in its basic active form, **3.1**:Cu(II):($^{-}OCH_3$)($HOCH_3$).[12] With the expectation that the reactivity of **3.4**:Cu(II) has a similar sensitivity to ${}^{s}_{s}pH$ as **3.1**:Cu(II), their methanolyses were studied at three ${}^{s}_{s}pH$ values in the 7–8 plateau region of the ${}^{s}_{s}pH/\log(k_x)$ profile under buffered conditions (excess 2,4,6-collidine buffer) in the presence of excess Cu(II) (three concentrations of 1.0, 1.5, and 2.0 mM) to ensure that **3.4** is completely bound to Cu(II) during the reaction. The three rate constants (k_{obs}) for unimolecular decomposition of each complex, corrected for buffer and excess Cu(II) effects were averaged to obtain k_x values. According to the mechanism depicted in Scheme 3-1, ionization of **3.4**:Cu(II):$(HOCH_3)_2$ generates the active form **3.4**:Cu(II):($^{-}OCH_3$)($HOCH_3$) which spontaneously decomposes. Given in Table 3-1 are the various k_x rate constants for the decomposition of **3.4a**–**g**:Cu(II):($^{-}OCH_3$)($HOCH_3$) in the ${}^{s}_{s}pH/\log(k_x)$ plateau region from which a linear free energy relationship was constructed, correlating $\log(k_x)$ with the Hammett substituent constants, σ_x, as shown in Figure 3-1.

Scheme 3-1. Simplified scheme for the $^{s}_{s}$pH-dependent decomposition of **3.4**:Cu(II):($^{-}$OCH$_3$)(HOCH$_3$) to form Cu(II):*N*,*N*-bis(2-picolyl)amine (Cu(II):DPA, **P**) and the corresponding methyl benzoate (**MB**).

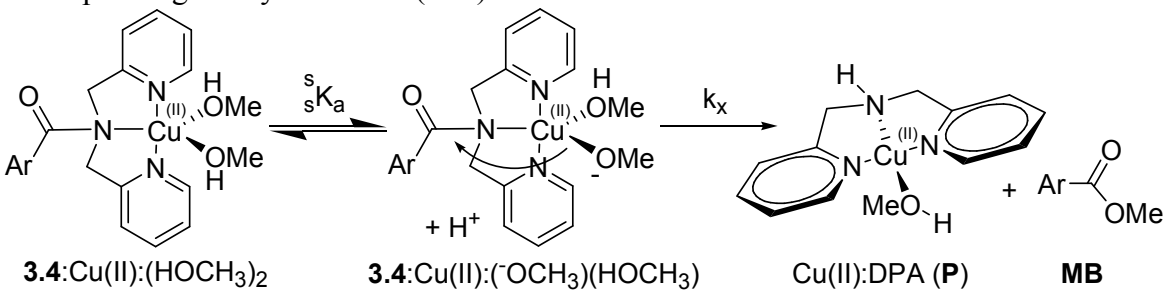

Table 3-1. σ_x and average rate constants (k_x) for the decomposition of **3.4a–g**:Cu(II):($^{-}$OCH$_3$)(HOCH$_3$) at 25 °C, determined from data at three $^{s}_{s}$pH values between 7 and 8.

Substrate	σ_x	10^4 k_x (s^{-1}) [a]
3.4a	1.42	193 ± 40
3.4b	0.78	53 ± 2
3.4c	0.71	58 ± 6
3.4d	0.23	24.8 ± 0.7
3.4e	0.0	11 ± 1
3.4f	-0.17	11 ± 2
3.4g	-0.27	8.3 ± 0.5

a. Determined as the average of three corrected rate constants (k_{obs}) for decomposition of **3.4a–g**:Cu(II):($^{-}$OCH$_3$)(HOCH$_3$) in the plateau in the $^{s}_{s}$pH/log(k_x) profile between 7 and 8.

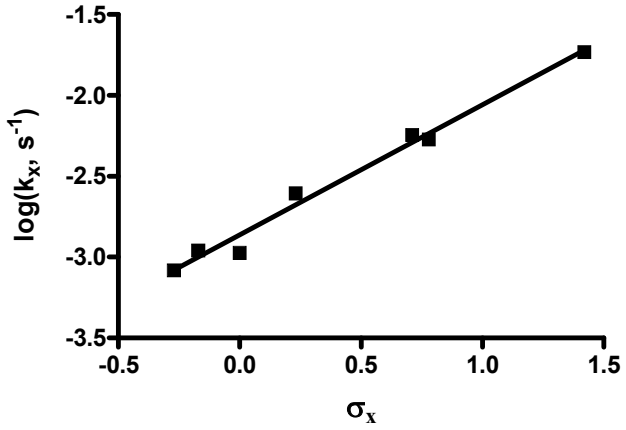

Figure 3-1. Hammett plot of $\log(k_x)$ vs σ_x for the Cu(II)-promoted cleavage of **3.4a–g** (5×10^{-4} M) in methanol at 25 °C in the plateau region (7–8) of the ${}^{s}_{s}\text{pH}/\log(k_x)$ profile. The line through the data is generated from a linear regression to provide $\rho = 0.80 \pm 0.05$; $r^2 = 0.9844$.

3.4.2 – Activation parameters and solvent kinetic isotope effects

Experiments were carried out at five different temperatures in the plateau region of the ${}^{s}_{s}\text{pH}/\log(k_x)$ profile for substrates **3.4b**:Cu(II):($^{-}OCH_3$)($HOCH_3$) and **3.4g**:Cu(II):($^{-}OCH_3$)($HOCH_3$). The respective Eyring plots at ${}^{s}_{s}\text{pH}$ 7.0 ± 0.2 and 7.1 ± 0.2 are shown in Figure 3-3 and Figure 3-4 (Supporting Information 3-1), while the corresponding activation parameters are given in Table 3-2. Also included in Table 3-2 are solvent deuterium kinetic isotope effect (SKIE) values determined in triplicate for cleavage of **3.4b**:Cu(II):($^{-}OCH_3$)($LOCH_3$) and **3.4g**:Cu(II):($^{-}OCH_3$)($LOCH_3$) in CH_3OL (L = H, D) buffered with 2,4,6-collidine, **3.4b**:Cu(II):($^{-}OCH_3$)($LOCH_3$) ${}^{s}_{s}\text{pH} = 7.1 \pm 0.2$, ${}^{s}_{s}\text{pD} = 7.2 \pm 0.2$; **3.4g**:Cu(II):($^{-}OCH_3$)($LOCH_3$) ${}^{s}_{s}\text{pH} = 7.4 \pm 0.2$, ${}^{s}_{s}\text{pD} = 7.4 \pm 0.2$). The ${}^{s}_{s}\text{pD}$ values were measured at the end of the reactions in the same fashion as for ${}^{s}_{s}\text{pH}$; these are not corrected for the effect of the deuterated solvent on the ${}^{s}_{s}\text{pK}_a$ of the buffer or on the electrode readings. Since we are dealing with an extended plateau region of

the ${}^{s}_{s}$pH/log(k_x) profiles, the actual ${}^{s}_{s}$pD values are less important since the rate constants in deuterated and proteated solvents are determined in the plateau region.

Table 3-2. Activation parameters, rate constants, and SKIE values for cleavage of [**3.4b**:Cu(II):($^{-}$OCH$_3$)(HOCH$_3$)]$^{+}$ and [**3.4g**:Cu(II):($^{-}$OCH$_3$)(HOCH$_3$)]$^{+}$ in methanol at ${}^{s}_{s}$pH 7.0 ± 0.2 and 7.1 ± 0.2 respectively, determined in the plateau region of their ${}^{s}_{s}$pH/log(k_x) profiles.

Substrate	k_x (s^{-1})	$\Delta H^{\ddagger}$ (kcal·mol^{-1})	$\Delta S^{\ddagger}$ (cal·mol^{-1}·K^{-1})	$\Delta G^{\ddagger}$ (25 °C) (kcal·mol^{-1})	k_H/k_D
[**3.4b**:Cu(II):($^{-}$OCH$_3$)]$^{+}$	3.9×10^{-3}	19.1 ± 0.2	-5.4 ± 0.6	20.7 ± 0.3	1.12 ± 0.01
[**3.4g**:Cu(II):($^{-}$OCH$_3$)]$^{+}$	5.7×10^{-4}	21.3 ± 0.3	-2 ± 1	21.8 ± 0.4	1.20 ± 0.02

3.4.3 – DFT computations

The cleavage reactions of the Cu(II):($^{-}$OCH$_3$)(HOCH$_3$) complexes of **3.4a**,**b**,**g** were modeled using DFT to ascertain detailed mechanistic information and to correlate the computed energies of the transition states with their kinetic data. The starting ground state for each of the calculated pathways was the 5-coordinate monocationic complex [**3.4**:Cu(II):($^{-}$OCH$_3$)(HOCH$_3$)]$^{+}$. The primary goal of the calculations was to determine differences in relative free energies of the various transition states for each of the three substrates and their intermediates along the reaction pathway. Although the absolute values of the free energies of activation will be affected by the omission of explicit molecules of solvation, these were not included under the assumption that solvation should be similar for each substrate, and thus not important in determining the *differences*

in energies between the same states of the three substrates. Geometry optimizations and energetic determinations for all intermediates and transition states were performed using the unrestricted B3LYP[25] functional employing the IEFPCM[26] continuum solvation model as implemented in the Gaussian 09 program.[27] The 6-31G(d,p) basis set was used for C and H; the 6-31++G(d,p) basis set was used for O and N; and the LANL2DZ[28] pseudopotential was used for Cu(II). Frequency calculations were conducted on optimized structures to determine free energy values at 298 K as well as to characterize intermediates and transition states. The lowest energy pathway for each amide is shown in Figure 3-2 and relevant structural data and activation parameters are shown in Table 3-3 and Table 3-4.

Table 3-3. Structural data for DFT-calculated structures for the Cu(II):($^{-}OCH_3$)($HOCH_3$) complexes of **3.4a**,**b**,**g**.[a]

Cu(II):($^{-}OCH_3$) ($HOCH_3$) complex of **3.4a**,**b**,**g**		(Py)N–Cu(II)–N(Py)	χ_N[b]	Cu(II)–N_{trig} (Å)	Cu(II)–OCH_3 (Å)	CH_3O–C(=O) (Å)	N_{trig}–C(=O) (Å)
GS	**3.4a**	105.0°	150.1°	2.73	1.84	3.43	1.38
	3.4b	105.8°	149.6°	2.76	1.84	3.52	1.38
	3.4g	104.5°	154.1°	2.73	1.84	3.40	1.39
	3.1:Cu(II)	105.5°	152.6°	2.67	1.84	3.26	1.38
TS_{Nu}	**3.4a**	108.1°	132.9°	2.05	1.98	1.80	1.54
	3.4b	108.1°	132.9°	2.05	1.99	1.78	1.56
	3.4g	107.7°	132.6°	2.03	2.00	1.73	1.59
	3.1:Cu(II)	110.2°	136.5°	2.03	1.99	1.69	1.57
INT	**3.4a**	116.4°	133.1°	2.02	2.15	1.53	1.64
	3.4b	116.7°	132.7°	2.01	2.12	1.54	1.66
	3.4g	114.4°	132.6°	2.01	2.10	1.55	1.68
TS_{Clv}	**3.4a**	129.0°	129.2°	1.99	2.27	1.45	1.91
	3.4b	125.3°	130.1°	1.99	2.23	1.47	1.88
	3.4g	120.9°	130.7°	1.99	2.16	1.50	1.83
	3.1:Cu(II)	158.7°	131.8°	2.01	2.38	1.47	1.82
P^+		161.6°		1.97			
MB	**3.4a**					1.33	
	3.4b					1.34	
	3.4g					1.35	

a. Structural information for **3.1**:Cu(II):($^{-}OCH_3$)($HOCH_3$) taken from reference 12.
b. χ_N corresponds to the C–C–N–C(O) dihedral and is a measure of the trigonal nitrogen's pyramidalization that varies from 180° (sp^2 hybridization) to 120° (sp^3 hybridization). (Winkler, F. K.; Dunitz, J. D. *J. Mol. Biol.* **1971**, *59*, 169.)

Table 3-4. DFT-calculated activation parameters for the cleavage of the Cu(II): ($^{-}OCH_3$)($HOCH_3$) complexes of **3.4a**,**b**,**g** (298 K, 1 atm). All energies are relative to the respective ***GS*** structure.

Structure		$\Delta G^{‡}$ (kcal·mol^{-1})	$\Delta H^{‡}$ (kcal·mol^{-1})	$\Delta S^{‡}$ (cal·mol^{-1}·K^{-1})
TS_{Nu}	**3.4a**	14.7	11.8	-9.8
	3.4b	15.8	12.5	-11.1
	3.4g	16.7	13.2	-11.9
INT	**3.4a**	13.5	11.2	-7.8
	3.4b	15.6	12.2	-11.3
	3.4g	16.0	13.4	-8.7
TS_{Clv}	**3.4a**	13.8	11.2	-9.1
	3.4b	15.7	11.8	-13.0
	3.4g	16.0	13.5	-8.2

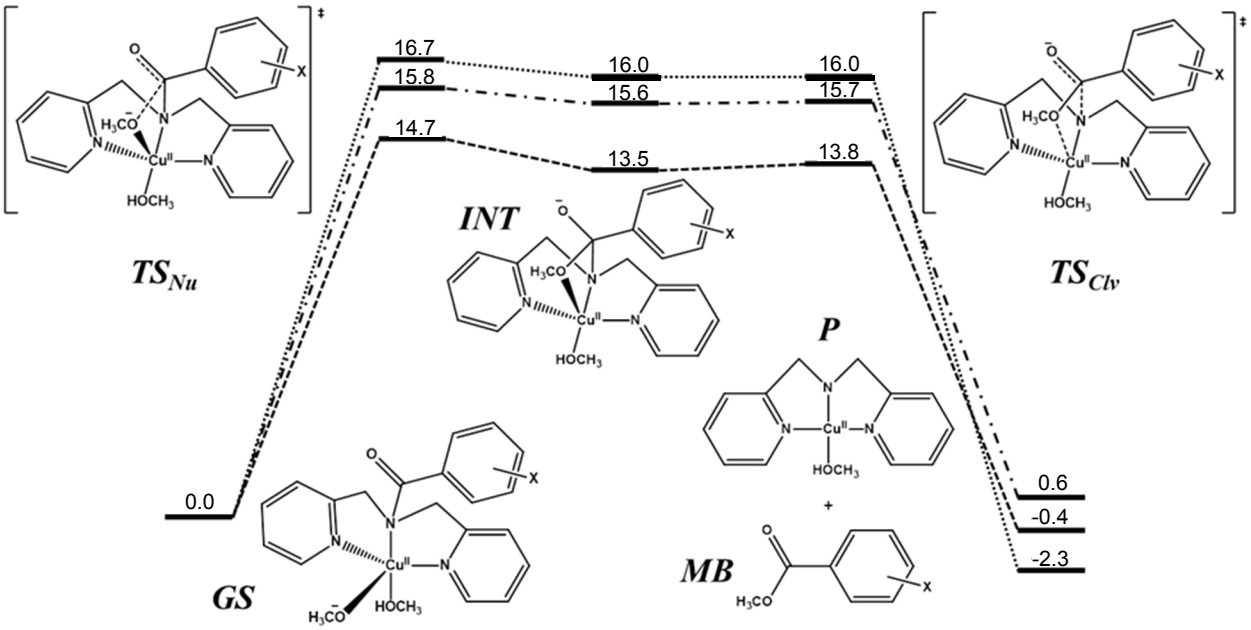

Figure 3-2. DFT-computed reaction pathway for the cleavage of the Cu(II): ($^{-}OCH_3$)($HOCH_3$) complexes of **3.4a** (– – – –); **3.4b** (– ▪ – ▪ –); and **3.4g** (▪ ▪ ▪ ▪) in methanol. All free energy values are to scale and are reported in kcal·mol^{-1} at 298 K relative to the ***GS*** structure.

3.5 – Discussion

3.5.1 – Lyoxide-promoted kinetics of acyl transfer

We first consider what is known about base-promoted acyl transfer from amides to solvent in the absence of metal-ion catalysts. The kinetics for alkaline hydrolysis of benzamides and toluamides[7,29] and those for anilides[30] as well as the basic methanolysis of anilides and benzamides[31] have received attention. In Scheme 3-2[32] is the general picture where there are two primary steps for acyl transfer involving nucleophilic attack to form an anionic tetrahedral intermediate (T_O-), followed by its breakdown to form the corresponding amine and carboxylate (if hydrolysis) or ester (if alcoholysis where R' = alkyl or aryl). The latter step poses most of the interesting kinetic behaviour since the departure of the leaving group often requires assistance from specific or general acids and

bases. Schowen[33] reports that the kinetic rate law for basic hydrolysis of anilides has first and second order terms in [$^{-}$OH], and the rate-determining step changes with base concentration. Some simplification of the kinetics is seen in the methanolysis of anilides where the attacking CH_3O^{-} group precludes lyoxide deprotonation of T_O- (R' = CH_3) so the kinetics are simply first order in [$^{-}$$OCH_3$]. SKIE data for methanolysis indicate general acid assistance by the solvent for departure of the leaving group and, in certain cases, added buffers such as substituted phenols can also exert general assistance of the departure of the poor leaving group. Substituent effects exerted by Y-groups on the departing anilide (NRArY) show an increase in the amount of negative charge on the leaving group in the transition state for its departure as the substituents become more electron withdrawing ($\rho_y \approx 0$ for electron donors like *p*-OCH_3 in the anilide ring, but ρ_y = 2.9 for withdrawers such as *m*-NO_2 or *p*-NO_2).

Scheme 3-2. Generalized mechanism for the base-promoted acyl transfer of amides.

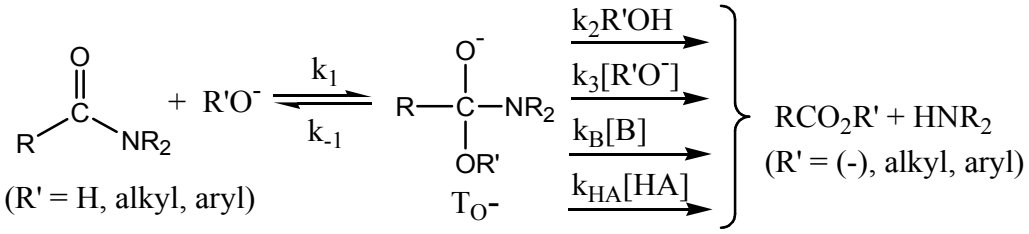

As we deal here with the cleavage of benzamides, it is relevant that Meloche and Laidler[29c] reported a Hammett ρ = 0.7 for hydroxide attack on some substituted benzamides at 100 °C in water. However, later ^{18}O=C exchange studies[29e] indicated that the $^{-}$OH-promoted hydrolyses of benzamide, and to a lesser extent, *N*-methyl benzamide,

but apparently not the tertiary *N,N*-dimethyl benzamide, suffer reversible formation of T_O^- (Scheme 3-2). Thus, Meloche's and Laidler's Hammett ρ–value, and related activation parameters, do not refer to a discrete kinetic step, but a complex term derived from Scheme 3-2 where $k_x = k_1[^-OH]k_2/(k_{-1} + k_2)$. Particularly relevant to the present work are the reports of Broxton and Deady on the basic methanolysis of *N*-methylbenzanilides[31f] and *N*-phenylbenzanilides[31c] (**3.5**). Rate constants for the methanolysis of compounds substituted in the benzoyl ring (i.e. X; Y = H) correlate well with σ_x (ρ_x = 1.76 (**3.5a**), 1.95 (**3.5b**)), indicative of a mechanism common to tertiary benzamides in methanol where the rate-limiting step is a solvent-assisted departure of the leaving group. This is generally confirmed by the Hammett plot of the rate constants for compounds **3.5** substituted on the anilide ring (i.e. Y; X = H) which correlates well with σ_y (ρ_y = 2.5 (**3.5a**), 2.82 (**3.5b**)) in methanol, the large value of ρ_y being indicative of rate-limiting solvent-assisted departure of the LG (k_2(MeOH) in Scheme 3-2) where negative charge is building up on the anilide. Additional data from Broxton, Deady and Rowe[31c] indicate that, as the amine leaving group gets better, k_2 increases and the rate-limiting step becomes nucleophilic attack.

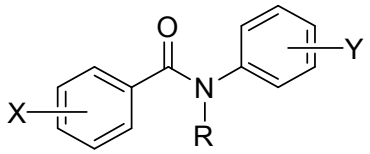

3.5a R = Me
3.5b R = Ph

3.5.2 – Kinetics of decomposition of 3.4:Cu(II):($^{-}OCH_3$)($HOCH_3$)

The k_x data in Table 3-1 for the reaction of **3.4a**–**g** in the presence of Cu(II) ion, refer to the unimolecular decomposition of **3.4**:Cu(II):($^{-}OCH_3$)($HOCH_3$). The experimental activation parameters for the *p*-nitro and *p*-methoxy derivatives, [**3.4b**:Cu(II):($^{-}OCH_3$):($HOCH_3$)]$^{+}$ and [**3.4g**:Cu(II):($^{-}OCH_3$)($HOCH_3$)]$^{+}$ are, respectively, $\Delta H^{\ddagger}$ = 19.1 and 21.3 kcal·mol^{-1}, and $\Delta S^{\ddagger}$ = -5.4 and -2 cal·mol^{-1}·K^{-1}. The reactions proceed readily at 25 °C, $t_{1/2}$ = ~2 minutes and 19 minutes respectively, indicating that the Cu(II) has a profound effect. A simple calculation indicates that the apparent second order rate constant for the reaction of CH_3O^{-} with **3.4b**:Cu(II):$(HOCH_3)_2$ is 1 × 10^{8} M^{-1}·s^{-1}. This value is at least 2.0 × 10^{16} larger than the k_{MeO}- for attack of methoxide on **3.4b** in the absence of the Cu(II).[34]

As was the case for the previously reported reaction of **3.1**:Cu(II):($^{-}OCH_3$)($HOCH_3$),[12] the activation parameters and SKIE data (k_x^H/k_x^D = 1.1–1.2) observed here for decomposition of [**3.4b**:Cu(II):($^{-}OCH_3$) ($HOCH_3$)]$^{+}$ and [**3.4g**:Cu(II):($^{-}OCH_3$)($HOCH_3$)]$^{+}$ support a process involving rate-limiting intramolecular nucleophilic attack of a Cu(II)-coordinated methoxide on the N-bound >N–C=O(Ar) unit. The Hammett ρ_x of 0.80 suggests a transition state where some negative charge is building up on the aromatic ring, but not as much as in the case of the methoxide-promoted methanolysis of the tertiary benzanilides, **3.5**. The fact that the plot in Figure 3-1 is linear, with no sign of an upward or downward break, suggests that there is no change in mechanism or rate-limiting step in passing through the members of series **3.4a**–**g**. The Hammett value can be compared to the ρ_x for attack of hydroxide on substituted methyl benzoate esters (2.2),[35a]

hydroxide on benzamides (0.7),[29b] and methoxide on methyl aryl carbamates (2.15, 1.7)[35b] or benzanilides (1.76, 1.95),[31f,31c] all of which show development of negative charge on the benzoyl group in the transition states. However, in addition to the solvent, nucleophile and substrate differences, none of the mechanisms operative in those systems is directly comparable to the mechanism for the decomposition of **3.4**:Cu(II):($^{-}OCH_3$)($HOCH_3$). This is made clearer by the additional information for the decomposition of the Cu(II) complexes derived from the computational data presented below.

3.5.3 – DFT computational studies

The lowest energy pathways computed for the cleavage reactions of **3.4a**,**b**,**g**:Cu(II):($^{-}OCH_3$)($HOCH_3$) are shown in Figure 3-2 with the relevant structural data and activation parameters given in Table 3-3 and Table 3-4. Several possible ground state structures were calculated, and the lowest energy complex found was the trigonal bipyramidal Cu(II):($^{-}OCH_3$)-containing structure labeled as ***GS*** having the pyridine moieties and methoxide occupying equatorial positions. In ***GS***, the aryl ring is coplanar with the adjacent C=O bond. All free energy values are reported relative to the free energy of this structure. The amide nitrogen geometry in this structure suggests a degree of Cu(II)–N_{amidic} interaction, however to a lesser extent than is shown with the corresponding acyl structure, **3.1**:Cu(II):($^{-}OCH_3$)($HOCH_3$), as judged from the Cu(II)–N_{amidic} distance[12] (2.73–2.76 Å vs 2.67 Å).

Nucleophilic attack proceeds via closure of the amidic O=C---($^{-}$OCH$_3$):Cu(II) bond distance in ***TS$_{Nu}$***, and is associated with free energies of 14.7 kcal·mol^{-1} (**3.4a**), 15.8 kcal·mol^{-1} (**3.4b**) and 16.7 kcal·mol^{-1} (**3.4g**). The O=C---($^{-}$OCH$_3$) interatomic distances given in Table 3-3 for ***TS$_{Nu}$*** vary from 1.80 Å (**3.4a**) to 1.73 Å (**3.4g**), indicating tighter transition states and higher transition state energies with more electron-donating aryl substituents. For each **3.4** tested, there is a larger degree of Cu(II)–N$_{amidic}$ interaction during nucleophilic attack, as indicated by a shortening of that bond (from 2.73–2.76 Å to 2.03–2.05 Å) and an increase in nitrogen pyramidalization (χ_N decreases from ~150–154° to 132.6–132.9°; Table 3-3). The ***TS$_{Nu}$*** structure leads to a single tetrahedral intermediate structure ***INT***, which occupies a shallow minimum on the free energy surface. This can be contrasted with the previously reported[12] DFT-calculated mechanism for the breakdown of the acetyl derivative **3.1**:Cu(II):($^{-}$OCH$_3$)(HOCH$_3$) which was found to involve two sequential tetrahedral intermediates separated by a transition state that largely involved the rearrangement of the ligands about the Cu(II). Such a rearrangement of the ligands around the Cu(II) in **3.4** does not appear to be operative, as there is a single ***INT*** that rapidly progresses to product through ***TS$_{clv}$*** where the latter involves departure of the amide anion coordinated to Cu(II). The ***INT*** breakdown is virtually barrierless, involving a shortening of the Cu(II)-trigonal N bond distance by 0.02–0.03 Å to 1.99 Å for **3.4b**,**g** and **3.4a** with concurrent planarization of the Cu(II) (opening of the (Py)N–Cu(II)–N(Py) angle). The trigonal N–C(=O) interatomic distance lengthens in ***TS$_{clv}$***, varying from 1.91 Å (**3.4a**) to 1.83 Å (**3.4g**), indicative of later transition states for benzamides containing more electron withdrawing groups. The square planar product structure (***P***) follows this transition state; the (Py–CH$_2$)$_2$N^{-}---Cu(II) departs without

N-protonation, but having departed, is assumed to be rapidly protonated under the reaction conditions.

3.5.4 – Computed Hammett plot

The computed mechanisms for all substrates reveal that the rate-determining process is the intramolecular nucleophilic attack of the Cu(II)-coordinated methoxide on the C=O unit. Where a direct comparison can be made for [**3.4b**:Cu(II):($^{-}$OCH$_3$)(HOCH$_3$)]$^+$ and [**3.4g**:Cu(II):($^{-}$OCH$_3$)(HOCH$_3$)]$^+$, the computed free energies (Table 3-4) are less than those determined experimentally by 3.4 and 4.6 kcal·mol^{-1}. The differences are likely due to the absence of explicit solvent-solute interactions in the calculated process, specifically in desolvating the nucleophilic methoxide and resolvating the developing C–O$^-$ in ***TS$_{Nu}$***. Since all the substrates should experience similar desolvation/resolvation, or ones that change regularly with the electron withdrawing nature of the substituent on Ar, we assume these can be omitted, leaving the differences in free energy of activation of the three computed species as being more representative of the process at hand. Indeed, the DFT calculated free energies for the structures are used to construct a Hammett Plot with $\rho = 0.84 \pm 0.16$, which is the same as the experimental value of 0.80 ± 0.05.

3.6 – Conclusions

Together, the present and earlier studies[12,13-17] indicate that poorly reactive amides having O=C–N(Lig)$_2$ units that bind metal ions such as Cu^{2+} become unusually reactive toward methanolysis of their metal-complexes at room temperature and neutral $^{s}_{s}$pH. The close positioning of Cu(II) to the amidic N of a N–C=O unit permits several catalytic roles for

the metal ion. Some of these are common to metal ion-catalyzed solvolytic cleavage of other systems, such as: (1) positioning a nucleophilic lyoxide and a bound substrate to a metal ion closely enough for reaction; (2) reduction of the pK_a of a metal-bound solvent molecule so that it becomes the preferred nucleophile; and (3) electrostatic stabilization by the metal ion of a developing anionic $\boldsymbol{TS_{Nu}}$. The present system exhibits unusual modes of the Cu(II) interaction with the $\boldsymbol{TS_{Nu}}$ that are rarely observed in metal ion-catalyzed solvolyses, possibly due to the difficulty in positioning the metal ion, in small molecule examples, to enable coordination with the amidic N. With substrates such as **3.1** and **3.4** there is an enforced Cu(II) interaction with the amidic N-lone pair that decouples its conjugation with the adjacent C=O. This is an alternative to the usual Lewis acid M(II)---O=C interaction; the present work shows that both types can activate the amide toward nucleophilic attack. A referee[36] has offered that this mode of binding of the Cu(II) to the amidic N activates the substrate for the initial steps of the reaction because it renders the system more like an acylammonium[37] than a regular amide. Because the binding of the metal ion to amides **3.4** and **3.1** is relatively strong, the reduction of amidic resonance stabilization (as measured by the decrease in the barrier to rotation[38] or effects on solvolytic reactivity) is brought about by utilizing the binding energy of the Cu(II) to the two 2-picolyl groups. However, according to the DFT-computed rotational barriers for **3.4b** and **3.4b**:Cu(II):($^-$OMe)(HOMe) as well as **3.1** and **3.1**:Cu(II):($^-$OMe)(HOMe), there is only a 3.4 and 4.9 kcal·mol^{-1} reduction of the rotational barrier in the Cu(II) complexes.[39] This is consistent with the experimental results for Lectka et al.[38] and suggests that the Cu(II) binding to substrate does not reduce the amidic resonance nearly as much as would be anticipated by an acylammonium analogue. Nevertheless, the very

large acceleration of the methanolytic reaction provides a small-molecule example supporting the hypothesis that, for enzyme-catalyzed acyl transfer reactions of peptides, a portion of the exothermicity of substrate binding is utilized in a productive way by the enzyme to destabilize and thereby activate the scissile substrate bond as the transition state for the acyl transfer reaction is approached.[40]

A subsequent important role of the metal ion in this system is to assist, through Lewis acid coordination to the developing amide anion, the departure of the leaving group, lowering the transition state energy for the cleavage of the tetrahedral intermediate. This is a fundamentally important aspect for a two-step, metal ion-catalyzed process where the metal ion must promote both the addition and breakdown steps, fulfilling a trifunctional role. This sort of interaction is likely to be an important phenomenon in enzyme-catalyzed hydrolytic or alcoholytic cleavage of substrates with poor leaving groups where electrophilic assistance must be provided to enhance both nucleophilic attack and LG departure.

According to the principles of enzyme catalysis first enunciated by Pauling,[41] "the enzyme has a configuration complementary to the activated complex, and accordingly has the strongest power of attraction for the activated complex." Extending this leads to the widely held notion that good catalysts bind transition states stronger than they bind ground states. Furthermore, for any catalyst promoting a multi-step reaction, each of the steps must be lowered in energy to achieve the overall high rates for the catalytic reaction. Zhang and Houk have recently analyzed a large number of enzymatic systems,

concluding that the very best catalytic systems have a transition state binding energy well in excess of what can be achieved by non-covalent interactions.[42] That proficiency arises from additional covalent effects such as heavy atom- and H-bond formation, and strong interactions of co-factors such as metal ions with transforming substrates that develop between the enzyme (catalyst) and transition state, altering the mechanism from what is seen in the absence of catalyst. It is an interesting observation that this sort of covalent bonding is manifested in the way the Cu(II) binds the transition states for the two-step solvolysis reaction described herein, and in other systems we have reported for efficient alcoholysis of phosphorothioates[43] and thioamides[44] promoted by a simple palladacycle. These types of interactions should be manifested in other systems where ligands are bound to departing groups so that a metal ion can facilitate the solvolytic cleavage of amides, esters, carbamates, phosphates, phosphoramidates and sulfates in such a way that they may prove more generally useful in synthetic applications.

3.7 – Supporting Information

3.7.1 – Supporting Information 3-1: Eyring plots

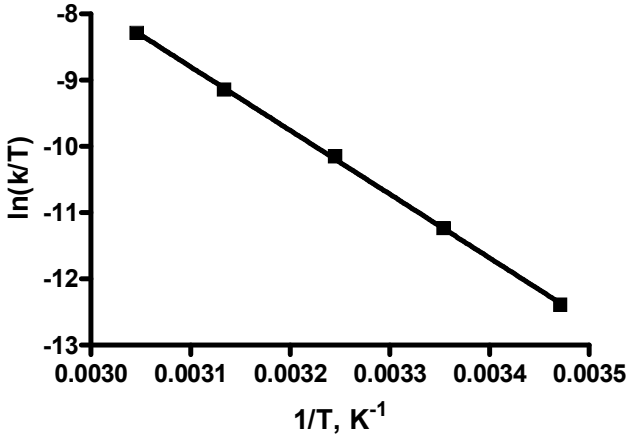

Figure 3-3. Eyring plot of ln(k/T) vs 1/T for the Cu(II)-promoted methanolysis of **3.4b**:Cu(II):($^{-}OCH_3$). In methanol, 1.5 mM Cu(II), 0.5 mM **3.4b** and 10 mM 2,4,6-collidine buffer ($^{s}_{s}$pH 7.0 ± 0.2). Activation parameters determined from the fits of the data to the Eyring equation[45] are presented in Table 3-2.

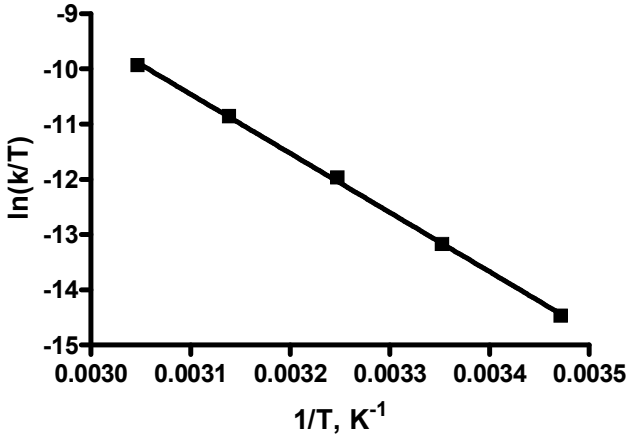

Figure 3-4. Eyring plot of ln(k/T) vs 1/T for the Cu(II)-promoted methanolysis of **3.4g**:Cu(II):($^{-}OCH_3$). In methanol, 1.5 mM Cu(II), 0.5 mM **3.4g** and 10 mM 2,4,6-collidine buffer ($^{s}_{s}$pH 7.1 ± 0.2). Activation parameters determined from the fits of the data to the Eyring equation[45] are presented in Table 3-2.

3.8 – References and notes

[1] (a) Brown, R. S.; Neverov, A. A. *J. Chem. Soc. Perkin 2* **2002**, 1039. (b) Brown, R. S.; Neverov, A. A.; Tsang, J. S. W.; Gibson, G. T. T.; Montoya-Pelaez, P. J. *Can. J. Chem.* **2004**, *82*, 1791. (c) Brown, R. S.; Neverov, A. A. *Adv. Phys. Org. Chem*. **2008**, *42*, 271. (d) Brown, R. S.; Lu, Z.-L.; Liu, C. T.; Tsang, W. Y.; Edwards, D. R.; Neverov, A. A. *J. Phys. Org. Chem.* **2009**, *23*, 1 and references therein.

[2] Brown, R. S. In *Progress in Inorganic Chemistry*; Karlin, K., Ed.; John Wiley and Sons: New York, 2011; Vol. *57*, p 55 and references therein.

[3] (a) Williams, N. H.; Takasaki, B.; Wall, M.; Chin, J. *Acc. Chem. Res.* **1999**, *32*, 485. (b) Morrow, J. *Comments Inorg. Chem.* **2008**, *29*, 169. (c) Fothergill, M.; Goodman, M. F.; Petruska, J.; Warshel, A. *J. Am. Chem. Soc.* **1995**, *117*, 11619. (d) Richard, J. P.; Amyes, T. L. *Bioorg. Chem.* **2004**, *32*, 354.

[4] Liu, C. T.; Neverov, A. A.; Maxwell, C. I.; Brown, R. S. *J. Am. Chem. Soc.* **2010**, *132*, 3561.

[5] Rawlings, N. D.; Barrett, A. J. Introduction: Metallopeptidases and their Clans. In *Handbook of Proteolytic Enzymes*, 2nd ed.; Barrett, A. J.; Rawlings, N. D.; Woessner, J. F., Eds.; Academic: Oxford, U.K., 2004, Vol. *1*, p 231.

[6] (a) Polzin, G. M.; Burstyn, J. N. *Metal Ions Biol. Syst.* **2001**, *38*, 103. (b) Fife, T. H.; Bembi, R. *J. Am. Chem. Soc.* **1994**, *115*, 11358. (c) Schepartz, A.; Breslow, R. *J. Am. Chem. Soc.* **1987**, *109*, 1814. (d) Suh, J.; Moon, S.-J. *Inorg. Chem.* **2001**, *40*, 4890. (e) Neverov, A. A.; Montoya-Pelaez, P. J.; Brown, R. S. *J. Am. Chem. Soc.* **2001**, *123*, 210. (f) Neverov, A. A.; Brown, R. S. *Can. J. Chem.* **2000**, *78*, 1247 and references therein.

[7] Brown, R. S.; Bennet, A. J.; Slebocka-Tilk, H. *Acc. Chem. Res.* **1992**, *25*, 481.

[8] Stoffregen, S. A.; Griffin, A. K. K.; Kostic, N. M. *Inorg. Chem.* **2005**, *44*, 8899 and references therein.

[9] Milovic, N. M.; Badjic, J. D.; Kostic, N. M. *J. Am. Chem. Soc.* **2004**, *126*, 696.

[10] (a) Somayaji, V.; Brown, R. S. *J. Org. Chem.* **1986**, *5*1, 2676. (b) Wang, Q.-P.; Bennet, A. J.; Brown R. S.; Santarsiero, B. D. *Can. J. Chem*. **1990**, *68*, 1732. (c) Wang, Q.-P.; Bennet, A. J.; Brown, R. S.; Santarsiero, B. D. *J. Am. Chem. Soc.* **1991**, *113*, 5757. (d) Slebocka-Tilk, H.; Brown, R. S. *J. Org. Chem*. **1987**, *52*, 805.

[11] Montoya-Pelaez, P.; Gibson, G. T. T.; Neverov, A. A.; Brown, R. S. *Inorg. Chem.* **2004**, *42*, 8624.

[12] Barrera, I. F.; Maxwell, C. I.; Neverov, A. A.; Brown, R. S. *J. Org. Chem.* **2012**, *77*, 4156.

[13] Houghton, R. P.; Puttner, R. R. *Chem. Commun.* **1970**, 1270.

[14] Niklas, N.; Heinemann, F. W.; Hampel, F.; Clark T.; Alsfasser, R. *Inorg. Chem.* **2004**, *43*, 4663 and references therein.

[15] Niklas, N.; Alsfasser, R. *Dalton Trans*. **2006**, 3188.

[16] Bröhmer, M. C.; Bannwarth, W. *Eur. J. Org. Chem.* **2008**, 4412.

[17] Bröhmer, M. C.; Mundinger, S.; Bräse, S.; Bannwarth, W. *Angew. Chem., Int. Ed.* **2011**, *50*, 6125.

[18] (a) Szajna-Fuller, E.; Ingle, G. K.; Watkins, R. W.; Arif, A. M.; Berreau, L. M. *Inorg. Chem.* **2007***, 46*, 2353. (b) Ingle, G. K; Watkins, R. W.; Arif, A. M.; Berreau, L. M. *J. Coord. Chem.* **2008**, *61*, 61.

[19] Hutchby, M.; Houlden, C. E.; Haddow, M. F.; Tyler, S. N. G.; Lloyd-Jones, G. C.; Booker-Milburn, K. I. *Angew. Chem., Int. Ed.* **2012**, *51*, 548.

[20] (a) Edwards, D. R.; Garrett, G. E.; Neverov, A. A.; Brown, R. S. *J. Am. Chem. Soc.* **2009**, *131*, 13738. (b) Liu, C. T.; Neverov, A. A.; Maxwell, C. I.; Brown, R. S. *J. Am. Chem. Soc.* **2010**, *132*, 35. (c) Raycroft, M. A. R.; Liu, C. T.; Brown, R. S. *Inorg. Chem.* **2012**, *51*, 3846.

[21] Sundberg, R. J.; Martin, R. B. *Chem. Rev.* **1974**, *74*, 471.

[22] For the designation of pH in non-aqueous solvents we use the nomenclature recommended by the IUPAC, *Compendium of Analytical Nomenclature. Definitive Rules 1997*, 3rd ed.; Blackwell: Oxford, U.K., 1998. The pH meter reading for an aqueous solution determined with an electrode calibrated with aqueous buffers is designated as ${}^{w}_{w}$pH; if the electrode is calibrated in water and the 'pH' of the neat buffered methanol solution then measured, the term ${}^{s}_{w}$pH is used; and if the electrode is calibrated in the same solvent and the 'pH' reading is made, then the term ${}^{s}_{s}$pH is used. In methanol, ${}^{s}_{w}$pH – (-2.24) = ${}^{s}_{s}$pH and since the autoprotolysis constant of methanol is $10^{-16.77}$, neutral ${}^{s}_{s}$pH is 8.4. ${}^{s}_{s}$pK_a refers to the negative log of the acid dissociation constant for the process **3.4**:Cu(II):($HOCH_3$) + $HOCH_3$ $\rightleftharpoons$ **3.4**:Cu(II):($^{-}OCH_3$) + $H_2O^{+}CH_3$ measured in, and referenced to, solvent methanol.

[23] Gibson, G.; Neverov, A. A.; Brown, R. S. *Can. J. Chem.* **2004**, *81*, 495.

[24] Carvalho, N. M. F.; Horn, A., Jr.; Bortoluzzi, A. J.; Drago, V.; Antunes, O. A. C. *Inorg. Chim. Acta* **2006**, *359*, 90.

[25] (a) Becke, A. D. *Phys. Rev. A* **1988**, *38,* 3098. (b) Lee, C.; Yang, W.; Parr, R. G. *Phys. Rev. B* **1988**, *37*, 785.

[26] (a) Tomasi, J.; Mennuccia, B.; Cancés, E. *THEOCHEM* **1999**, *464*, 211. (b) Tomasi, J.; Mennuccia, B.; Cammi, R. *Chem. Rev.* **2005**, *105*, 2999.

[27] Frisch, M. J.; *et al. Gaussian 09,* Revision C.01; Gaussian, Inc.: Wallingford, CT, 2009.

[28] (a) Hay, P. J.; Wadt, W. R. *J. Chem. Phys.* **1985**, *82*, 270. (b) Wadt, W. R.; Hay, P. J. *J. Chem. Phys.* **1985**, *82*, 284.

[29] (a) Meresaar, U.; Bratt, L. *Acta Chem. Scand. A*. **1974**, *28*, 715. (b) Bunton, C. A.; Nayak, B. O'Connor, C. *J. Org. Chem.* **1968**, *33*, 572. (c) Meloche, I.; Laidler, K. J. *J. Am. Chem. Soc.* **1951**, *73*, 1712. (d) Broxton, T. J.; Deady, L. W.; Pang, Y.-T, *J. Am. Chem. Soc.* **1977**, *99*, 2268. (e) Slebocka-Tilk, H.; Bennet, A. J.; Keillor, J. W.; Brown, R. S.; Guthrie, J. P.; Jodhan, A. *J. Am. Chem. Soc.* **1990**, *112,* 8507. (f) Slebocka-Tilk, H.; Bennet, A. J.; Hogg, H. J.; Brown, R. S. *J. Am. Chem. Soc*. **1991**, *113,* 1288.

[30] (a) De Wolfe, R. H.; Newcomb, R. S. *J. Org. Chem.* **1971**, *36*, 3870. (b) Bender, M. L.; Thomas, R. J. *J. Am. Chem. Soc.* **1961**, *83*, 4183. (c) Kotch, A.; Krol, L. H.; Verkade, P. E.; Wepster, B. M. *Rec. Trav. Chim. Pays-Ba*s **1952**, *71*, 108. (d) Biekart, H. J. B.; Dessens, H. B.; Verkade, P. E.; Wepster, B. M. *Rec. Trav. Chim. Pays-Ba*s **1952**, *71*, 1246.

[31] (a) Schowen. R. L.; Hopper, C. R.; Bazikian, C. M. *J. Am. Chem. Soc.* **1972**, *94*, 3095. (b) Broxton, T. J.; Deady, L. W. *J. Org. Chem.* **1967**, *31*, 2767. (c) Broxton, T. J.; Deady, L. W.; Rowe, J. E. *J. Org. Chem.* **1980**, *45*, 2404. (d) Broxton, T. J.; Duddy, N.

W. *Aust. J. Chem.* **1980**, *33*, 903. (e) Venkatasubban, K. S.; Schowen, R. L. *J. Org. Chem.* **1984**, *49*, 653. (f) Broxton, T. J.; Deady, L. W.; Rowe, J. E. *J. Org. Chem.* **1974**, *39*, 2767.

[32] Bennet, A. J.; Brown, R. S. Physical Organic Chemistry of Acyl Transfer Reactions. In *Comprehensive Biological Catalysis: A Mechanistic Reference*; Sinnott, M., Ed.; Academic Press: New York, 1997; Vol. *1*, pp 293–326.

[33] (a) Kershner, L. D.; Schowen, R. L. *J. Am. Chem. Soc.* **1971**, *93,* 2014. (b) Drake, D.; Schowen, R. L.; Jayaraman, H. *J. Am. Chem. Soc.* **1973**, *95*, 454.

[34] The methoxide-promoted reaction of 0.15 M **3.4b** in 0.3 M $KOCH_3$ shows no indication of product formation after 52.5 days. Assuming we could detect 1 mM of the product, an upper limit for the second order rate constant is $k_{MeO^-} = 4.9 \times 10^{-9}\ M^{-1}\cdot s^{-1}$. By comparison, the rate constant for attack of methoxide on the Cu(II) complex of **3.4b** is given as $k_{obs}^{\mathbf{3.4b}} = k_x^{\mathbf{3.4b}}\cdot({}^{s}_{s}K_a/({}^{s}_{s}K_a + [H^+]))$[12]. Under conditions where $[H^+] > {}^{s}_{s}K_a$ (or ${}^{s}_{s}pH < {}^{s}_{s}pK_a$) the reaction is first order in $[^-OCH_3]$. Given a ${}^{s}_{s}pK_a$ of 6.5[12] for formation of **3.4b**:Cu(II):$(^-OCH_3)(HOCH_3)$, and an autoprotolysis constant for methanol of $K_{auto} = 10^{-16.77}\ M^2$, one computes that $k_{obs}^{\mathbf{3.4b}} = k_x^{\mathbf{3.4b}}\cdot({}^{s}_{s}K_a/(K_{auto}))[^-OCH_3]$. The apparent second order rate constant for the reaction of methoxide with **3.4b**:Cu(II):$(HOCH_3)_2$ is $5.3 \times 10^{-3}\ s^{-1}\cdot 10^{10.27}\ M^{-1} = 10^8\ M^{-1}\cdot s^{-1}$. This value is 2.0×10^{16} larger than the k_{MeO^-} for attack of methoxide on **3.4b** in the absence of the Cu(II). Note: Chapter 4 reports on an extended timeframe where no product formation is observed in the methoxide-promoted reaction under the aforementioned conditions after 250 days.

[35] (a) Tommila, E.; Hinshelwood, C. N. *J. Chem. Soc.* **1948**, 1801. (b) Jaffé, H. H. *Chem. Rev.* **1954**, *53*, 192.

[36] It is a valid comment that "… a (partial) positive charge should be present on this N and the conjugation of the electron pair with the C=O should be less important than in a regular amide. Compared to a "normal" amide bond this one is … higher in energy and, consequently, closer in energy to the transition state for methanolysis." We thank the referee for the opportunity to discuss this point within the context of destabilization of a substrate through binding to a catalyst.

[37] For a discussion of the hydrolysis and reactivity of acylammonium species in water see: Williams, A. *J. Am. Chem. Soc.* **1976**, *98*, 5645.

[38] For a discussion of the decrease of the rotational barrier of amides **3.1** and **3.4** in the presence of Cu(II) and other metals see: (a) Cox, C.; Ferraris, D.; Murthy, N. N.; Lectka, T. *J. Am. Chem. Soc.* **1996**, *118*, 5332. (b) Cox, C.; Lectka, T. *Acc. Chem. Res.* **2000**, *33*, 849.

[39] The DFT-computed transition state free energies for interconverting the planar and orthogonal forms of the amides by rotation about the amidic N–C=O(R) bond in a methanol continuum are 22.1 and 20.8 kcal·mol^{-1} for **3.4b** and **3.1** respectively, and 18.7 and 15.9 kcal·mol^{-1} for their respective Cu(II):($^{-}$OMe)(HOMe) complexes. See Supporting Information.

[40] (a) Jencks, W. P. *Adv. Enzymol.* **1975**, *43*, 219. (b) Jencks, W. P. *Adv. Enzymol.* **1980**, *51*, 75. (c) Bruice, T. C. *The Enzymes*; Boyer, P. D., Ed.; Academic Press: New York, 1970; Vol. *11*, pp 217–279. (d) Fersht, A. *Enzyme Structure and Mechanism*;

2nd ed.; W. H. Freeman: San Francisco, 1985; pp 311–346. (e) Jencks, W. P. *Catalysis in Chemistry and Enzymology*; McGraw-Hill: New York, 1969. (f) Wolfenden, R. *Acc. Chem. Res.* **1972**, *5*, 10. (g) Haldane, J. B. S. *Enzymes*; Longmans, Green and Co.: London, U.K., 1930. (h) Lumry, R. *The Enzymes*; Boyer, P. D., Ed.; Academic: New York, 1959; Vol. *1*, pp 157–258.

[41] (a) Pauling, L. *Nature* **1948**, *161*, 707. (b) Pauling, L. *Am. Sci*. **1948**, *36*, 51.

[42] Zhang, X.; Houk, K. N. *Acc. Chem. Res.* **2005**, *38*, 379.

[43] (a) Liu, C. T.; Maxwell, C. I.; Edwards, D. R.; Neverov, A. A.; Mosey, N. J.; Brown, R. S. *J. Am. Chem. Soc.* **2010**, *132*, 16599. (b) Liu, C. T.; Neverov, A. A.; Brown, R. S. *Inorg. Chem.* **2011**, *50*, 7852.

[44] Liu, C. T.; Maxwell, C. I.; Pipe, S. G.; Neverov, A. A.; Mosey N. J.; Brown, R. S. *J. Am. Chem. Soc.* **2011**, *133*, 20068.

[45] $\ln\left(\frac{k}{T}\right) = \frac{-\Delta H^{\neq}}{R} \cdot \frac{1}{T} + \ln\left(\frac{k_B}{h}\right) + \frac{\Delta S^{\neq}}{R}$

Chapter 4 – Rapid Ni, Zn, and Cu ion-promoted alcoholysis of *N,N*-bis(2-picolyl)- and *N,N*-bis((1*H*-benzimidazol-2-yl)methyl)-*p*-nitrobenzamides in methanol and ethanol

4.1 – Preface

With minor formatting changes, this chapter is presented largely as it is published in *Inorganic Chemistry* (Raycroft, M. A. R.; Cimpean, L.; Neverov, A. A.; Brown, R. S. *Inorg. Chem.* **2014**, *53*, 2211). The corresponding Supporting Information is represented in part by Supporting Information 4-1 to 4-3 and can be found in its complete form via the Internet at http://pubs.acs.org. The kinetic experiments were performed by Mark Raycroft and Ms. Luana Cimpean and the syntheses were performed by Mark Raycroft. The manuscript was written by Mark Raycroft and Dr. R. Stan Brown. The published article is copyrighted by the American Chemical Society.

4.2 – Introduction

The ways by which metal ions promote acyl and phosphoryl transfer reactions include: (1) Lewis acid activation of the substrate; (2) intramolecular delivery of a metal-coordinated lyoxide nucleophile to an activated C=X or P=X unit, where X = O or S; (3) electrostatic stabilization of the transforming activated complex; and (4) electrophilic assistance of the departure of the leaving group (leaving group assistance, LGA).[1,2,3] The latter role is particularly important for substrates having poor leaving groups with high pK_a values for their conjugate acids such as amides and phosphate or carboxylate esters with scissile alkoxy groups. The catalytic cleavage of amides promoted by small molecules presents a stringent challenge due to the amide's inherent resonance stability

which retards nucleophilic addition to the C=O unit, and to poor leaving group ability of the amide anion which hinders the breakdown of the tetrahedral addition intermediates.[4] The latter case typifies departure of a poor leaving group that is facilitated by protonation or coordination to a metal ion prior to, or concurrent with, its departure.

The catalytic mechanisms of several peptidase enzymes that employ transition metal ions in their active sites have been discussed in the above terms.[5,6] Nature uses Ni(II) ions in the enzyme urease to cleave amide bonds in urea[7] and Zn(II) ions in metallopeptidases like thermolysin and carboxypeptidase[8] to cleave amide bonds in peptides. Considering how effective the metal ions in these metallo-enzymes are, it is surprising that there are only a few small molecule systems capable of cleaving carboxamides[9,10,11] unless the amide leaving group is activated in some way. Such modes of activation include the release of strain or internal stabilization of the departing amide via resonance which facilitates departure from the tetrahedral addition intermediates, thus obviating the need for stabilization through LGA.

Metal ion-promoted LGA seems to be an extremely effective, but not-often-observed phenomenon in small molecule examples unless there is some special structural character that renders metal ion coordination to the amidic N possible. An interesting example first described by Houghton and Puttner,[12] and subsequently by the groups of Alsfasser[13,14] and Bannwarth,[15] concerned the Cu(II)-promoted methanolysis of *N*-acyl derivatives of *N*,*N*-bis(2-picolyl)amine. We have reported detailed kinetic studies of the latter process[16,17] with $^{s}_{s}$pH control in methanol,[18] and show that the reaction elicits a

trifunctional role for the Cu(II) that involves its pre-equilibrium coordination to, or close to, the amidic N, subsequent intramolecular attack of a Cu(II)-coordinated methoxide on the C=O, and Cu(II)-assisted C–N cleavage. The catalytically active form of the Cu(II):bis(2-picolyl)amide complexes involves a substrate-coordinated Cu(II):($^{-}OCH_3$) formed by acid dissociation of the Cu(II):($HOCH_3$) which has a $^{s}_{s}pK_a$ of ≤ 6.5 in methanol. The catalytic effect of the Cu(II) ion in this solvolysis is quantified to be at least 10^{16} times faster than the rate constant for methoxide attack on *N*,*N*-bis(2-picolyl)-*p*-nitrobenzamide (**4.1**).[17] This suggests that, under optimized conditions, man-made catalysts employing metal ion-promoted LGA alongside other modes of metallo-catalysis might rival the rates for peptide (amide) cleavage achievable by enzymes.

The previous studies on the metal ion-promoted methanolysis of *N*,*N*-bis(2-picolyl)-carboxamides[12-15] were performed mostly with Cu(II) salts, but a recent report[15b] discloses that other metal salts including $FeCl_3$, $NiCl_2$, $Fe(OTf)_3$, AgOTf, and $Zn(OTf)_2$ facilitate the cleavage of *N*,*N*-bis(2-picolyl)amides in methanol. These experiments were not $^{s}_{s}$pH-controlled, making it difficult to ascertain the relative reactivity of each metal ion under conditions where their speciation was unknown. The importance of the M(II)- or M(III)-methoxides for catalytic efficacy in these metal ion-promoted cleavage reactions prompted us to undertake a more detailed kinetic study of the solvolytic cleavage of *N*,*N*-bis(2-picolyl)-*p*-nitrobenzamide (**4.1**) in methanol and ethanol promoted by Ni(II), Zn(II), and Cu(II) under $^{s}_{s}$pH-controlled conditions. In addition, we have completed an analogous study of the metal ion-promoted cleavage of *N*,*N*-bis((1*H*-benzimidazol-2-

yl)methyl)-*p*-nitrobenzamide (**4.2**) where the amine ligand is readily available from an easily scalable, one-step reaction.[19]

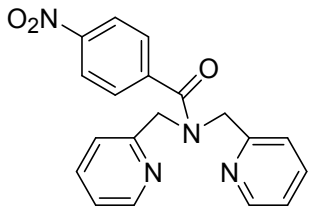

4.1

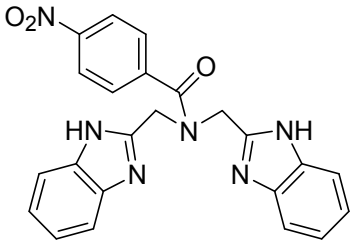

4.2

4.3 – Experimental

4.3.1 – Materials

Methanol (99.8%, anhydrous) and acetonitrile (99.8%, anhydrous) were purchased from EMD Chemicals. Absolute ethanol (anhydrous, degassed, stored under argon, and freshly dispensed for kinetic experiments) was purchased from Commercial Alcohols (GreenField Ethanol Inc.). Acetone (99.5%) was purchased from ACP Chemicals. Trifluoromethanesulfonic acid (HOTf, ≥99%), 1,2-phenylenediamine (99.5%), *p*-nitrobenzoyl chloride (98%), 2-bromo-6-methylpyridine (98%), 2-picoline (98%), 2,6-lutidine (≥99%), *N*-ethylmorpholine (99%), *N*-methylpiperidine (99%), zinc trifluoromethanesulfonate (98%), and sodium ethoxide (21 wt % in denatured ethanol) were purchased from Aldrich and 2-methoxy-6-methylpyridine (98%) from AK Scientific. 2,4,6-Collidine (98%) was purchased from BDH Laboratory Reagents. Iminodiacetic acid (98%) was purchased from Alfa Aesar. Potassium carbonate (99%), ethylene glycol (≥99%), and sodium methoxide (0.5 M solution in methanol) were purchased from Sigma-Aldrich. Copper(II) trifluoromethanesulfonate (98%) was

obtained from TCI America Laboratory Chemicals. Nickel(II) perchlorate hexahydrate (reagent grade) was purchased from GFS Chemicals.

4.3.2 – General methods

^{1}H NMR spectra were determined at 400 MHz and ^{13}C NMR spectra at 100.58 MHz; all chemical shift values were referenced internally to the solvent. High-resolution mass spectra were determined by EI-TOF. All $CH_3OH_2^+$ and $CH_3CH_2OH_2^+$ concentrations were determined potentiometrically using a combination glass Fisher Scientific Accumet electrode (model no. 13-620-292) calibrated with certified standard aqueous buffers (pH 4.00 and 10.00) as described previously.[20] The $^{s}_{s}$pH values in methanol were determined by subtracting a correction constant of -2.24 from the electrode readings and the autoprotolysis constant for methanol was taken to be $10^{-16.77}$ M^2.[18] The $^{s}_{s}$pH values in ethanol were determined by subtracting a correction constant of -2.54 from the electrode readings and the autoprotolysis constant for ethanol was taken to be $10^{-19.1}$ M^2.[18] The $^{s}_{s}$pH values for the kinetic experiments were measured at the end of the reactions to avoid the effect of KCl leaching from the electrode.

4.3.3 – Synthesis of materials

N,*N*-Bis(2-picolyl)-*p*-nitrobenzamide (**4.1**) was synthesized and characterized as previously reported.[17]

N,*N*-Bis((1*H*-benzimidazol-2-yl)methyl)-*p*-nitrobenzamide (**4.2**) was prepared by acylation with *p*-nitrobenzoyl chloride, modelled on that for the acylation by acetyl chloride.[21] In a 50-mL round-bottom flask, *N*,*N*-bis((1*H*-benzimidazol-2-yl)methyl)amine

(573.3 mg, 2.067 mmol) was dissolved in acetone (15 mL) by stirring for 10 minutes. Excess potassium carbonate was added and the mixture was stirred for an additional 10 minutes at RT, and then placed in an ice-water bath. In a separate vial, *p*-nitrobenzoyl chloride (728.3 mg, 3.924 mmol) was dissolved in acetone (5 mL), cooled in an ice-water bath, and then added drop-wise to the reaction mixture. The solution was left to stir and warm to RT overnight. The resulting orange solid was vacuum-filtered and dried under vacuum. Column chromatographic separation was carried out using a MPLC apparatus (silica stationary phase, EtOAc/MeOH mobile phase). The product was obtained as a yellow solid in 65.8% yield (580.0 mg, 1.360 mmol).

^{1}H NMR (400 MHz, CD_3OD, 25 °C) δ 7.98 (m, 2H; A^{phenyl}), 7.63 (m, 2H; B^{phenyl}), 7.52 (m, 4H; $A^{benzimidazolyl}$), 7.18 (bm, 4H; $B^{benzimidazolyl}$), 5.06 (bs, 2H), 4.85 (bs, 2H). ^{13}C NMR (100.58 MHz, CD_3OD, 25 °C) δ 172.5, [152.0, 151.7], 150.0, 142.2, 139.6 (br), 129.3, 124.8, [124.0, 123.9], 116.0 (br), [49.5 (br), 46.0 (br)] (square brackets are used to designate pairs of ^{13}C signals that are related by rotation). Both ^{1}H and ^{13}C NMR spectra can be found in Supporting Information 4-2 (Figure 4-10 to Figure 4-14). HRMS (EI+ TOF): calculated for $C_{23}H_{18}N_6O_3$ 426.1440 amu, found 426.1457 amu; λ_{max} (CH_3OH): 274 nm (ε = 26300 ± 300 $M^{-1}\cdot cm^{-1}$), 281 nm (ε = 24700 ± 300 $M^{-1}\cdot cm^{-1}$); melting point: 202.8 °C (decomp.).

4.3.4 – General UV-vis kinetics

All kinetic experiments were conducted using a UV-vis spectrophotometer with the cell compartment thermostatted at 25.0 ± 0.1°C. The reactions were conducted in the presence of buffers composed of various ratios of amine and HOTf to maintain the $^{s}_{s}$pH in

methanol or ethanol (2-methoxy-6-methylpyridine ${}^{s}_{s}pH^{MeOH}$ = 5.0, ${}^{s}_{s}pH^{EtOH}$ = 4.2–4.5; 2-picoline ${}^{s}_{s}pH^{MeOH}$ = 5.3–6.6, ${}^{s}_{s}pH^{EtOH}$ = 5.0–6.5; 2,6-lutidine ${}^{s}_{s}pH^{EtOH}$ = 5.9–6.8; 2,4,6-collidine ${}^{s}_{s}pH^{MeOH}$ = 7.0–8.0, ${}^{s}_{s}pH^{EtOH}$ = 7.0–7.9, *N*-ethylmorpholine ${}^{s}_{s}pH^{MeOH}$ = 8.5–9.2; *N*-methylpiperidine ${}^{s}_{s}pH^{MeOH}$ = 9.8–10.5). The upper limits on ${}^{s}_{s}pH$ were determined by the ${}^{s}_{s}pK_a$ values for the acid dissociation of the alcohol solvates of Ni(II), Zn(II), and Cu(II) in methanol and ethanol (from their potentiometric titration profiles)[22] in order to avoid oligomerization of metal ion alkoxides. A typical kinetic experiment for the alcoholysis of **4.1** involved preparation of an alcohol solution containing buffer (10 mM), **4.1** (0.05 mM or 0.5 mM), and M^{2+} (0.1–4.0 mM as the perchlorate or triflate) in a 1-cm path length quartz cuvette. The reaction was initiated by the addition of an aliquot of the M^{2+} stock solution to the buffered solution containing **4.1** to achieve the desired concentrations of the reaction components at a final volume of 2.5 mL. A typical kinetic experiment for the alcoholysis of **4.2** involved preparation of an alcohol solution containing buffer (2 mM), **4.2** (0.02 mM), and M^{2+} (0.02–0.2 mM as the perchlorate or triflate) in a 1-cm path length quartz cuvette. The reaction was initiated by the addition of an aliquot of the M^{2+} stock solution to the buffered solution containing **4.2** to achieve the desired concentrations of the reaction components at a final volume of 2.5 mL. Experiments were performed in duplicate and the Abs vs time traces for the disappearance of the starting complex were fitted with a standard first-order exponential equation to a minimum of 5 half-life times to obtain the k_{obs} values.

The analogous Ni^{2+}, Cu^{2+}, and Zn^{2+} promoted methanolyses and ethanolyses of **4.1** or **4.2** were conducted under ${}^{s}_{s}pH$-controlled conditions using various buffers, and were

monitored by observing, with UV-vis spectrophotometry at 25 °C, the rate of loss of complex or formation of M(II)-coordinated amine at various wavelengths. The details for each metal ion and complex are described in Supporting Information 4-1.

4.3.5 – Product analyses

The methanolysis and ethanolysis of M(II):**4.1** and M(II):**4.2** (M(II) = Ni(II), Zn(II), Cu(II)) were conducted at higher concentration in ROH (R = CH_3, CH_3CH_2) where [M^{2+}] = 4 mM, [**4.1** or **4.2**] = 2 mM, [NaOR] = 2 mM. After completion of the reaction (assessed by UV-vis spectroscopy), the solvent was rotary-evaporated and the residue was dissolved in CD_3OD after which the ^{1}H NMR spectrum (400 MHz) was collected. In the cases of Ni(II) and Cu(II), the only observable product was the corresponding methyl or ethyl benzoate. The Ni(II) or Cu(II) complex of *N*,*N*-bis(2-picolyl)amine or *N*,*N*-bis((1*H*-benzimidazol-2-yl)methyl)amine was not observed by ^{1}H NMR due to Ni(II)- or Cu(II)-induced paramagnetic broadening. In the case of Zn(II), sharp signals corresponding to the methyl or ethyl benzoate were observed as well as broadened signals corresponding to the Zn(II) complex of *N*,*N*-bis(2-picolyl)amine or *N*,*N*-bis((1*H*-benzimidazol-2-yl)methyl)amine.

4.4 – Results

4.4.1 – M(II)-promoted methanolysis of 4.1

4.4.1.1 – Kinetics of the Ni(II)-promoted methanolysis of **4.1**

The Ni(II)-promoted methanolysis of 5 × 10^{-5} M **4.1** was studied in the range of 7.2 ≤ $^{s}_{s}$pH ≤ 10.5 under buffered conditions in the presence of variable, but excess

$[Ni(ClO_4)_2]$. The effect of buffer inhibition was assessed at each ${}^{s}_{s}pH$ by monitoring the $[M^{2+}]$-dependence at two concentrations (10 mM and 20 mM) of buffer; in all cases the two $[M^{2+}]$-dependent second order rate constants were either very close to or within experimental error. As the effect of [buffer] was found to be insignificant, only the data at 10 mM buffer are reported. The upper limit on the ${}^{s}_{s}pH$ range was limited by the ${}^{s}_{s}pK_a$ ($(Ni(II)_s{:}(HOCH_3) + HOCH_3 \rightleftharpoons Ni(II)_s{:}(^{-}OCH_3) + H_2O^{+}CH_3$ (${}^{s}_{s}pK_a = 11.24$)[22]) for the acid dissociation of the solvated metal in methanol to maintain the speciation of Ni(II) reasonably constant in its neutral solvated form. Saturation binding of Ni(II) with **4.1** was not observed as evidenced by linear dependences of the k_{obs} values on $[Ni^{2+}]$ at each ${}^{s}_{s}pH$ over the range $0 < [Ni(ClO_4)_2] \leq 4.0$ mM; a representative example is shown in Figure 4-1.

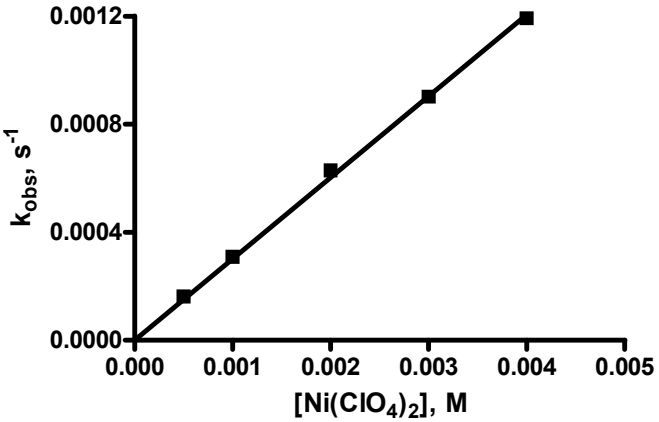

Figure 4-1. Plot of k_{obs} for the cleavage of 5×10^{-5} M **4.1** vs $[Ni(ClO_4)_2]$ buffered at ${}^{s}_{s}pH$ 8.5 (10 mM *N*-ethylmorpholine, 5 mM HOTf) in anhydrous methanol at 25 °C. The data are fitted to a linear regression computing $k_2 = (0.301 \pm 0.003)\ M^{-1}{\cdot}s^{-1}$.

The lack of saturation kinetics for the decomposition of **4.1** with increasing $[Ni^{2+}]$ signifies that the metal ion is far from being completely bound under the experimental conditions, a conclusion supported by ^1H NMR experiments where the addition of

1 equivalent of $Ni(ClO_4)_2$ resulted in only a small perturbation of the ^1H NMR spectrum of **4.1**. The second order rate constants (k_2) for the metal ion-promoted reactions are given as the gradients of the k_{obs} vs $[Ni(ClO_4)_2]$ plots at each ^s_spH. Shown in Figure 4-15 (Supporting Information 4-3) is a plot of $\log(k_2)$ vs ^s_spH, which is linear with a slope of 0.89 ± 0.03 which is considered as experimental support that one methoxide is involved in the TS for the reaction, probably by way of its being coordinated to the Ni(II).

4.4.1.2 – Kinetics of the Zn(II)-promoted methanolysis of **4.1**

The Zn(II)-promoted methanolysis of **4.1** was studied in the range of $8.5 \leq {}^s_spH \leq 10.0$ under buffered conditions in the presence of excess $Zn(OTf)_2$. Buffer concentration dependence studies were conducted as described above for Ni(II) and the effect of [buffer] was found to be insignificant. As is the case of Ni(II)-promoted cleavage of **4.1**, the k_{obs} values depend linearly on metal ion concentration, this time over a narrower concentration range 0–2 mM of $Zn(OTf)_2$. As has been confirmed by experiments with varying concentrations of **4.1** at the higher ^s_spH values, an observed downward curvature of the concentration/rate profile at $[Zn(OTf)_2] > 2$ mM is not due to saturation binding with **4.1**, but rather due to dimerization or oligomerization of the Zn(II):($^-OCH_3$) species. Given in Figure 4-16 (Supporting Information 4-3) is a plot of $\log(k_2)$ vs ^s_spH, which is linear with a slope of 0.97 ± 0.05.

4.4.1.3 – Kinetics of the Cu(II)-promoted methanolysis of **4.1**

Our previous study[17] of the Cu(II)-promoted methanolysis of **4.1** was expanded to encompass a broader ^s_spH range of 5.0–8.0 under buffered conditions in the presence of

excess $Cu(OTf)_2$ (to ensure complete binding to **4.1**). All k_{obs} values were corrected for inhibitory effects of buffer and excess $Cu(OTf)_2$, and a plot of the log of the corrected rate constants ($\log(k_{obs}^{corr})$) vs ${}^{s}_{s}pH$ is given in Figure 4-2. NLLSQ fitting of the data to equation 4-1 yielded a kinetic ${}^{s}_{s}pK_a$ value of 5.79 ± 0.07 and a maximum rate constant (k_{max}) of $(5.7 \pm 0.4) \times 10^{-3}$ s^{-1}.

$$k_{obs} = k_{\max}\left(\frac{{}^{s}_{s}K_a}{{}^{s}_{s}K_a + [H^+]}\right) \qquad (4\text{-}1)$$

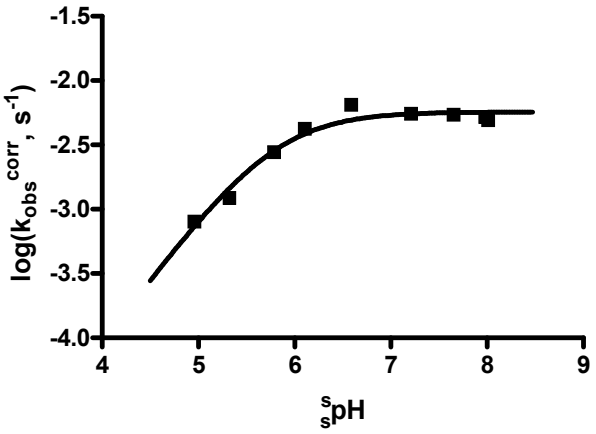

Figure 4-2. Plot of $\log(k_{obs}^{corr})$ for the cleavage of **4.1**:Cu(II):($^{-}OCH_3$)($HOCH_3$) (0.5 mM each of Cu(II) and **4.1** and corrected for buffer and excess $Cu(OTf)_2$ effects) vs ${}^{s}_{s}pH$ in anhydrous methanol under buffered conditions at 25 °C. The data are fitted to equation 4-1 computing one macroscopic ${}^{s}_{s}pK_a$ of 5.79 ± 0.07 and a maximum rate constant (k_{max}) of $(5.7 \pm 0.4) \times 10^{-3}$ s^{-1}; $r^2 = 0.9666$.

4.4.2 – M(II)-promoted ethanolysis of 4.1

4.4.2.1 – Kinetics of the Ni(II)-promoted ethanolysis of **4.1**

Although saturation kinetics are not observed with Ni^{2+} or Zn^{2+} in methanol, the favored process for the reaction of other divalent metal ion complexes should proceed via

formation of the essential intermediate, **4.1**:M(II):($^{-}OCH_3$), with the metal ion bound to the two pyridines and an alkoxide as in Scheme 4-1. Earlier studies[23] have shown that a change in medium to one with a lower dielectric constant, such as from methanol to ethanol (ε_r = 31.5 to 24.3),[24] greatly increases the binding of anionic substrates and metal ion complexes and a similar phenomenon should exist with the binding of M^{2+} and **4.1**.

Scheme 4-1. Proposed reaction scheme for the M(II)-promoted solvolysis of **4.1** (R = Me, Et).

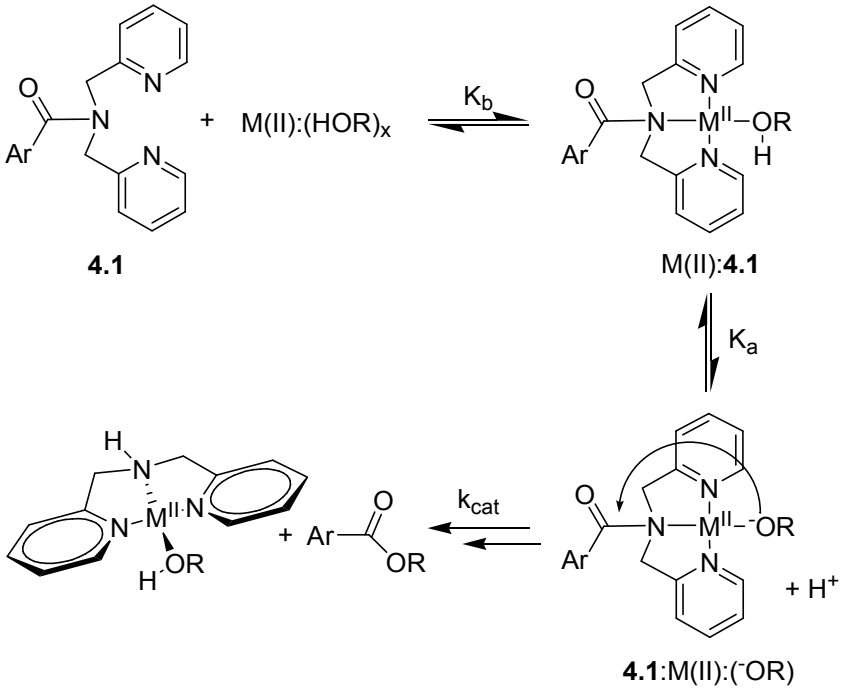

The Ni(II)-promoted ethanolysis of 5×10^{-5} M **4.1** was studied in the range of $5.9 \leq {}^{s}_{s}pH \leq 7.9$ under buffered conditions in the presence of excess $Ni(ClO_4)_2$.[25] At all ${}^{s}_{s}pH$ values in this range, the plots of k_{obs} vs $[Ni(ClO_4)_2]$ exhibit a downward curvature consistent with a saturation binding process; a representative example is shown in Figure 4-3.

NLLSQ fitting of the data to a standard one-site binding model gives the metal binding constant (K_b) and maximal observed rate constant (k_{obs}^{max}) at each $^{s}_{s}$pH. Additional kinetic experiments using increasing concentrations of tetrabutylammonium perchlorate (0–20 mM) demonstrated that there is no significant effect of additional perchlorate anions on the rate of the reaction. The linear plot of $\log(k_{obs}^{max})$ vs $^{s}_{s}$pH shown in Figure 4-4 has a slope of 0.89 ± 0.06.

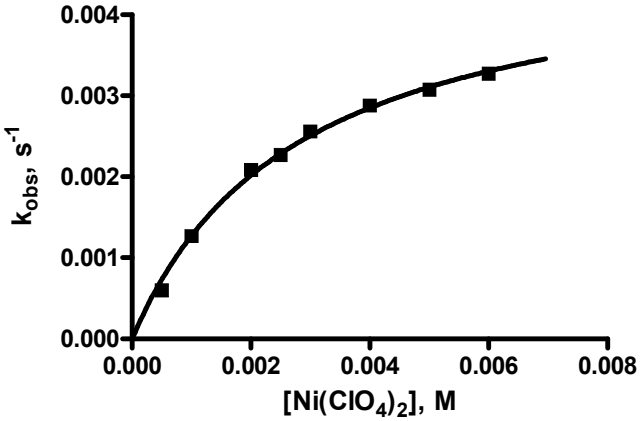

Figure 4-3. Plot of k_{obs} for the cleavage of 5×10^{-5} M **4.1** vs [$Ni(ClO_4)_2$] buffered at $^{s}_{s}$pH 6.7 (10 mM 2,6-lutidine, 5 mM HOTf) in anhydrous ethanol at 25 °C. The data were fitted to a standard one site binding model to give $K_b = (360 \pm 30)$ M^{-1} and $k_{obs}^{max} = (4.8 \pm 0.2) \times 10^{-3}$ s^{-1}; $r^2 = 0.9953$.

Considering the error limits and the fact that k_{obs}^{max} and K_b are heavily correlated, second order rate constants for the metal ion-catalyzed reaction at each $^{s}_{s}$pH (k_2) were calculated as the product of the k_{obs}^{max} and K_b values. Figure 4-4 also presents a plot of $\log(k_2)$ vs $^{s}_{s}$pH that exhibits a linear dependence on [$^{-}OCH_3$] with a gradient of 0.93 ± 0.09.

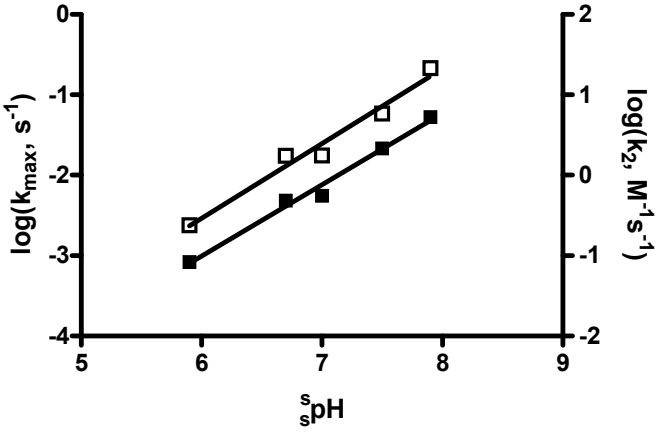

Figure 4-4. Plots of $\log(k_{obs}^{max})$ (■) and $\log(k_2)$ (□) for the Ni(II)-promoted cleavage of **4.1** vs ${}^{s}_{s}$pH in anhydrous ethanol under buffered conditions (10 mM amine, various concentrations of HOTf) at 25 °C. The lines through the data are generated from linear regressions to provide slopes of 0.89 ± 0.06 (r^2 = 0.9864) and 0.93 ± 0.09 (r^2 = 0.9731), respectively.

4.4.2.2 – Kinetics of the Zn(II)-promoted ethanolysis of **4.1**

The Zn(II)-promoted ethanolysis of 5 × 10^{-5} M **4.1** was studied in the range of 6.2 ≤ ${}^{s}_{s}$pH ≤ 7.2 under buffered conditions in the presence of excess $Zn(OTf)_2$. Over this range, the plots of k_{obs} vs $[Zn(OTf)_2]$ exhibit a slight downward curvature indicative of a weak, yet quantifiable, binding between Zn(II) and **4.1**. Fits of the k_{obs} vs $[Zn^{2+}]$ data to a standard 1:1 binding expression gave the binding constants (K_b) and maximum rate constants (k_{obs}^{max}) for the decomposition of the metal-bound complex at each ${}^{s}_{s}$pH. The plot of $\log(k_{obs}^{max})$ vs ${}^{s}_{s}$pH in Figure 4-5 has a slope of 1.19 ± 0.07. Second-order rate constants for the reaction of Zn(II)-promoted reaction of **4.1** at each ${}^{s}_{s}$pH were calculated as the product of the k_{obs}^{max} and K_b values. The plot of $\log(k_2)$ vs ${}^{s}_{s}$pH (Figure 4-5) gives a straight line with a gradient of 0.96 ± 0.07.

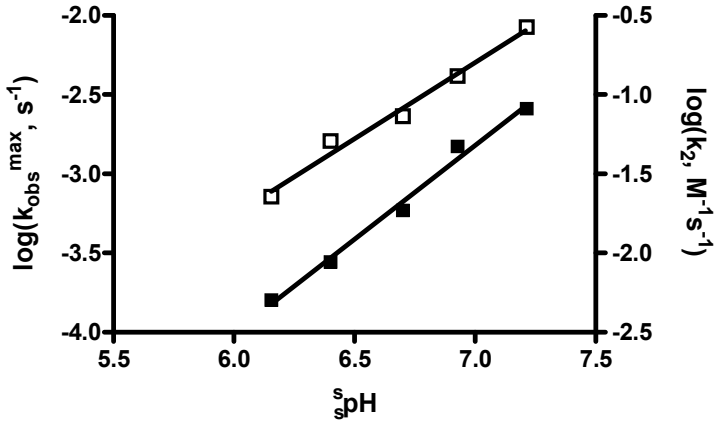

Figure 4-5. Plots of $\log(k_{obs}^{max})$ (■) and $\log(k_2)$ (□) for the Zn(II)-promoted cleavage of 5×10^{-5} M **4.1** vs ${}^{s}_{s}$pH in anhydrous ethanol under buffered conditions (10 mM amine, various concentrations of HOTf) at 25 °C. The lines through the data are generated from linear regressions to provide slopes of 1.19 ± 0.07 (r^2 = 0.9890) and 0.96 ± 0.07 (r^2 = 0.9833), respectively.

4.4.2.3 – Kinetics of the Cu(II)-promoted ethanolysis of **4.1**

The Cu(II)-promoted ethanolysis of 5×10^{-4} M **4.1** was studied in the range of $3.3 \leq {}^{s}_{s}\text{pH} \leq 7.6$ under buffered conditions in the presence of excess $Cu(OTf)_2$ (to ensure complete binding to **4.1**). All k_{obs} values were corrected for inhibitory buffer and excess $Cu(OTf)_2$ effects and the k_{obs}^{corr} was plotted in logarithmic form as a function of ${}^{s}_{s}$pH (Figure 4-22, Supporting Information 4-3). NLLSQ fits of these data to equation 4-1 yield a kinetic ${}^{s}_{s}pK_a$ of 5.4 ± 0.1 and a maximum rate constant (k_{max}) of $(9 \pm 1) \times 10^{-3}$ s^{-1}.

4.4.3 – M(II)-promoted methanolysis of 4.2

4.4.3.1 – Kinetics of the Ni(II)-promoted methanolysis of **4.2**

The Ni(II)-promoted methanolysis of 2×10^{-5} M **4.2** was studied in the range of $7.2 \leq {}^{s}_{s}\text{pH} \leq 10.2$ in the presence of variable concentrations of excess $Ni(ClO_4)_2$. Unlike the Ni(II)-catalyzed cleavage of **4.1** in methanol, a plot of the k_{obs} values vs $[Ni^{2+}]$ in

ethanol exhibits saturation metal binding which was analyzed to give K_b and k_{obs}^{max} values. The linear plot of $\log(k_{obs}^{max})$ vs ${}^{s}_{s}pH$ shown in Figure 4-23 (Supporting Information 4-3) has a slope of 0.94 ± 0.02. Second-order rate constants were calculated from the product of the k_{obs}^{max} and K_b values and plotted as $\log(k_2)$ vs ${}^{s}_{s}pH$ (Figure 4-24, Supporting Information 4-3), exhibiting a linear dependence with a gradient of 0.98 ± 0.05.

4.4.3.2 – Kinetics of the Zn(II)-promoted methanolysis of **4.2**

The Zn(II)-promoted methanolysis of 2×10^{-5} M **4.2** was studied in the range of $7.0 \leq {}^{s}_{s}pH \leq 9.2$ in the presence of variable concentrations of excess $Zn(OTf)_2$. The plots of the k_{obs} values for the cleavage of **4.2** vs $[Zn^{2+}]$ in ethanol exhibit saturation binding. NLLSQ fitting of the $\log(k_{obs}^{max})$ and ${}^{s}_{s}pH$ data (Figure 4-6) to equation 4-1 gives a kinetic ${}^{s}_{s}pK_a$ of 8.36 ± 0.07 and a maximum rate constant (k_{max}) of $(5.8 \pm 0.6) \times 10^{-4}$ s^{-1}. Second-order rate constants for the metal ion-catalyzed reaction were calculated from the product of the k_{obs}^{max} and K_b values and plotted in the form of $\log(k_2)$ as a function of ${}^{s}_{s}pH$ (Figure 4-6) exhibiting a linear dependence with a gradient of 0.97 ± 0.04. Of note in Figure 4-6 is the fact that the $\log(k_2)$ value is linear above the saturation ${}^{s}_{s}pH$ for the k_{obs}^{max} plot, suggesting that the binding of the metal ion is strongest when it has an attached methoxide.[26,27]

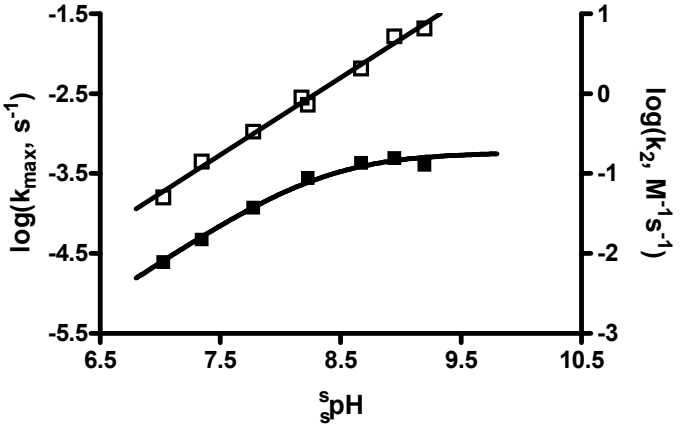

Figure 4-6. Plots of $\log(k_{obs}^{max})$ (■) and $\log(k_2)$ (□) for the Zn(II)-promoted cleavage of **4.2** vs ${}^{s}_{s}$pH in anhydrous methanol under buffered conditions (10 mM amine, various concentrations of HOTf) at 25 °C. The ■-data are fitted using NLLSQ methods to equation 4-1 to give a kinetic ${}^{s}_{s}pK_a$ of 8.36 ± 0.07 and a maximum rate constant for the decomposition of the **4.2**:Zn(II):($^{-}OCH_3$) complex (k_{max}) of (5.8 ± 0.6) × 10^{-4} s^{-1}; r^2 = 0.9903. The linear regression fit of the □-data has a slope of 0.97 ± 0.04; r^2 = 0.9912.

4.4.3.3 – Kinetics of the Cu(II)-promoted methanolysis of **4.2**

The Cu(II)-promoted methanolysis of 2 × 10^{-5} M **4.2** was studied in the range of $4 \leq {}^{s}_{s}pH \leq 8.5$ under buffered conditions. Cu(II) is completely bound to **4.2** as evidenced by a maximum in the k_{obs} vs $[Cu^{2+}]$ plot at a 1:1 ratio of metal ion to substrate, followed by a slight decrease in cleavage rate with increasing $[Cu(OTf)_2]$. Such a decrease in rate may be attributed to inhibition by triflate ions or minor changes in ionic strength. The ${}^{s}_{s}$pH-independent plateau region depicted in Figure 4-27 (Supporting Information 4-3) arises from the decomposition of the **4.2**:Cu(II):($^{-}$OMe) complex, the average of all k_{obs}^{max} values being (8.0 ± 0.8) × 10^{-4} s^{-1}.

4.4.4 – M(II)-promoted ethanolysis of 4.2

4.4.4.1 – Kinetics of the Ni(II)-promoted ethanolysis of **4.2**

The Ni(II)-promoted ethanolysis of 2×10^{-5} M **4.2** was studied in the range of $5.2 \leq {}^{s}_{s}pH \leq 8.7$ under buffered conditions and in the presence of variable concentrations of excess $Ni(ClO_4)_2$. The kinetics also indicate saturation binding with increasing $[Ni^{2+}]$ which is analyzed to give a k_{obs}^{max} value at each ${}^{s}_{s}pH$. The linear plot of $\log(k_{obs}^{max})$ vs ${}^{s}_{s}pH$ shown in Figure 4-7 has a slope of 1.11 ± 0.03. Second-order rate constants were calculated from the product of the k_{obs}^{max} and K_b values and plotted in the form of $\log(k_2)$ as a function of ${}^{s}_{s}pH$ (Figure 4-7) exhibiting a linear dependence with a gradient of 1.05 ± 0.09.[28]

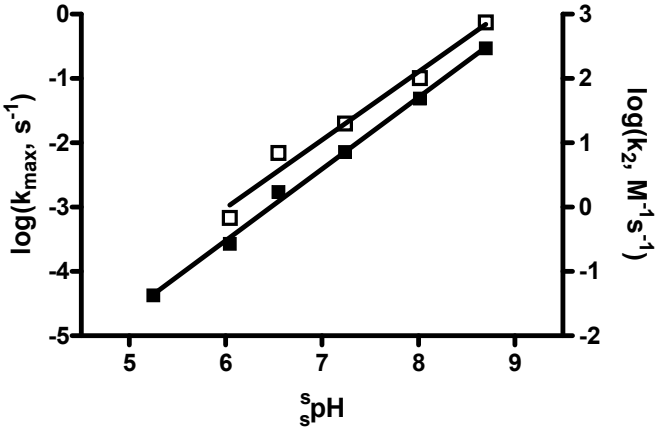

Figure 4-7. Plots of $\log(k_{obs}^{max})$ (■) and $\log(k_2)$ (□) for the Ni(II)-promoted cleavage of **4.2** vs ${}^{s}_{s}pH$ in anhydrous ethanol under buffered conditions (10 mM amine, various concentrations of HOTf) at 25 °C. The lines through the data are generated from linear regressions to provide slopes of 1.11 ± 0.03 ($r^2 = 0.9967$) and 1.05 ± 0.09 ($r^2 = 0.9787$), respectively.

4.4.4.2 – Kinetics of the Zn(II)-promoted ethanolysis of **4.2**

The Zn(II)-promoted ethanolysis of 2×10^{-5} M **4.2** was studied in the range of $5.9 \leq {}^{s}_{s}pH \leq 7.5$ in the presence of three concentrations of excess $Zn(OTf)_2$. The k_{obs}

values for the cleavage of **4.2** exhibit a saturation phenomenon with increasing [Zn^{2+}]. The linear plot of log(k_{obs}^{max}) vs $^{s}_{s}$pH shown in Figure 4-8 has a slope of 1.00 ± 0.04. The second-order rate constants (k_2^{Zn}) were not calculated due to the large uncertainties in the binding constants (K_b) which stem from strong interactions between the metal ion and the substrate.[29] The kinetically-determined K_b values are large, being in the range of 10^5–10^6 M^{-1}, which can only be determined kinetically with an appreciable error.

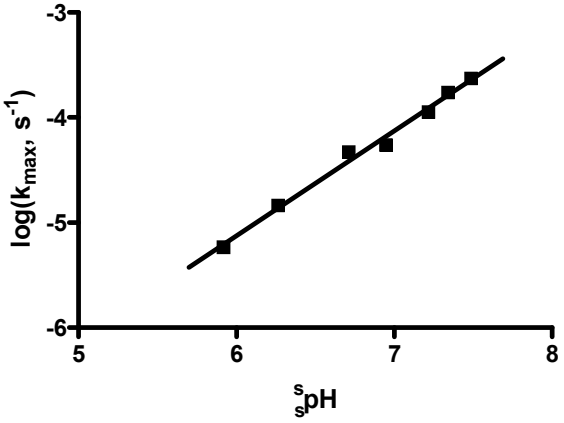

Figure 4-8. Plot of log(k_{obs}^{max}) for the Zn(II)-promoted cleavage of **4.2** vs $^{s}_{s}$pH in anhydrous ethanol under buffered conditions (2 mM amine, various concentrations of HOTf) at 25 °C. The line through the data is generated from a linear regression with a slope of 1.00 ± 0.04; $r^2 = 0.9914$.

4.4.4.3 – Kinetics of the Cu(II)-promoted ethanolysis of **4.2**

The Cu(II)-promoted ethanolysis of 2×10^{-5} M **4.2** was studied over a narrow range of $6.9 \leq {}^{s}_{s}\text{pH} \leq 7.7$ under buffered conditions where, at 1:1 concentrations, Cu(II) is expected to be completely bound to **4.2** for the same reasons described for the reaction in methanol. The plateau region depicted in Figure 4-31 (Supporting Information 4-3) represents the maximum rate constant (k_{max}) for the unimolecular decomposition **4.2**:Cu(II):($^{-}$OEt), the average value being $(3.8 \pm 0.2) \times 10^{-4}$ s^{-1}.

4.5 – Discussion

Previous studies examined the Cu(II)-promoted solvolytic cleavage of *N,N*-bis(2-picolyl)amides facilitated by its binding to the amidic nitrogen. These provided evidence for the mechanism shown in Scheme 4-1 in truncated form which involves metal ion complexation followed by formation of the metal-bound lyoxide, that then acts as the nucleophile toward the closely-positioned C=O. Importantly, in a subsequent step, the Cu(II) acts to assist the departure of the leaving amide group.[16,17] In those studies, the experimental and computational data with 3,5-dinitro-, 4-nitro-, and 4-methoxy-substituted benzoyl derivatives supported a mechanism where a Cu(II) ion is bound to the *N*,*N*-bis(2-picolyl) amide unit and positioned so that it permits delivery of a metal-coordinated methoxide nucleophile to the C=O in the rate-limiting TS of the reaction. This proceeds to a tetrahedral intermediate occupying a shallow minimum on the free energy surface with the Cu(II) coordinated to both the methoxide and amidic N. Breakdown of the latter is virtually barrierless, involving a Cu(II)-assisted departure of the bis(2-picolyl)amide anion and a loosening of the Cu(II)–OCH_3 bond. Given the shallowness of the potential surface subsequent to formation of the tetrahedral intermediate, the latter is considered to have an insufficient lifetime to exist, so the overall process is termed enforced-concerted.[30] While we have not performed the required computations with all metal ions, substrates, and solvents that form the subject matter in the present study, the overall mechanism is likely similar with rate-limiting nucleophilic attack of the metal-coordinated alkoxide, and subsequent fast, or barrierless, breakdown of an unstable intermediate.

Bannwarth and co-workers have reported a brief survey of the potential of some other metal ions in a study of what were termed "chelating carboxylic acid amides as robust relay protecting groups of carboxylic acids".[15b] The latter study compared the effectiveness of several metal ion salts on the cleavage of *N*,*N*-bis(2-picolyl)-*p*-iodobenzamide in methanol containing a set amount of metal ion for 16 hours at room temperature. Because this study was a comparative assessment of the utility of various metal ions under a common condition, there was no determination of the relative constants for metal binding to the substrates, nor was the ${}^{s}_{s}$pH measured and controlled. Given that the recent mechanistic work[16,17] indicates the lyoxide form of the bound metal complex is important for the Cu(II)-promoted cleavage, the speciation of other analogous metal ion complexes may also be important. In such cases, the complexes may only exhibit their maximal activities when fully bound with metal ion methoxide and these activities may well be far greater than what was reported to be the case at the set condition.[15b]

The observations in the present work indicate all the metal ions are active and suggest that their various behaviors fall into three subsets of a common mechanism encompassed by that shown in Scheme 4-1. These are controlled by the values of the substrate:M(II) binding constant, K_b, and the substrate:M(II):(HOR) acid dissociation constant, ${}^{s}_{s}K_a$, leading to formation of the essential substrate:M(II):($^{-}$OR) complex. In a given case one can observe: (1) saturation binding of substrate with metal ion, as well as a low ${}^{s}_{s}pK_a$ for formation of substrate:M(II):($^{-}$OR) complex; (2) saturation of metal ion binding, but a high enough ${}^{s}_{s}pK_a$ for proton dissociation from the substrate:M(II):(HOR) complex that

the reaction appears first order in ($^{-}$OR) throughout the $^{s}_{s}$pH range investigated; and (3) no saturation of metal binding to substrate, and an observed first order dependence on the reaction rate on both [M^{2+}] and [$^{-}$OR] over the $^{s}_{s}$pH range investigated.

4.5.1 – Ni(II)- and Zn(II)-promoted methanolysis of *N,N*-bis(2-picolyl)-*p*-nitro-benzamide (4.1)

Neither metal ion gives evidence of saturation binding to the substrate up to concentrations of 4 mM (Ni^{2+}) or 2 mM (Zn^{2+}). The near-unit value of the gradients of the log(k_2) vs $^{s}_{s}$pH plots in Figure 4-15 and Figure 4-16 (Supporting Information 4-3) is consistent with a first order dependence of the reaction rate on [$^{-}OCH_3$] as expected for the mechanism in Scheme 4-1. This is similar to what was previously proposed for the Cu(II)-promoted cleavage of **4.1**,[17] which involves strong coordination of Cu^{2+} followed by nucleophilic attack by the Cu(II)-coordinated methoxide and metal-assisted departure of the leaving group.[31] Strong binding of Cu^{2+} to **4.1** was evident from the observation of a downward curvature in the k_{obs} vs [Cu^{2+}] plots, and the plateau in its $^{s}_{s}$pH/log(k_{obs}^{max}) plot above $^{s}_{s}$pH 6 is consistent with the maximal activity being due to unimolecular decomposition of the **4.1**:Cu(II):($^{-}OCH_3$) form. The weaker binding of Ni(II) and Zn(II) relative to Cu(II) correlates well with their known binding constants with pyridine. For example, the dissociation constant for the complex Ni(II):Py_2 in water (1.48×10^{-3} M^2; μ = 0.5 M) is approximately 40 times larger than that for Cu(II):Py_2 (4.11×10^{-5} M^2; μ = 0.5 M),[32] while the stability constants of the mono-pyridine complexes of Ni(II) and Cu(II) are 87 and 398 M^{-1} respectively at μ = 0.5 M.[33] Weaker complexes are formed between Zn(II) and pyridine ligands relative to Ni(II). The dissociation constant for the complex

Zn(II):Py_2 in water is 7.8×10^{-2} M^2 (μ = 0.1 M) vs 1.48×10^{-3} M^2 (μ = 0.5 M) for Ni(II):Py_2[32] while the stability constants for the mono-pyridine complexes of Zn(II) and Ni(II) are 14 and 87 M^{-1} respectively.[33]

The strong effect that ${}^{s}_{s}$pH has on the rate of the Ni(II)-, Zn(II)- and other metal ion-catalyzed processes[12-15] gives a clear message that the activated complexes contain methoxide, probably bound to the ligand-complexed metal ion prior to the rate-limiting decomposition. In a given case, without confirmation of speciation and ${}^{s}_{s}$pH control, the overall catalytic effect of different metal ions with different substrates may be understated since the reactions may not have been investigated under conditions where the **4.1**:M(II):($^{-}OCH_3$) complex is fully formed. Due to the stronger binding of Cu(II), and its acidifying effect on coordinated solvent, the active form of **4.1**:Cu(II):($^{-}OCH_3$) is generated at a relatively low ${}^{s}_{s}$pH (${}^{s}_{s}pK_a \approx 6$ or lower as found here) thereby spontaneously forming an appreciable amount of the active form in methanol without adding additional base. In fact, Ni(II) is more catalytically active when fully present as **4.1**:Ni(II):($^{-}OCH_3$) than is **4.1**:Cu(II):($^{-}OCH_3$). At a ${}^{s}_{s}$pH of 10.5, well below the ${}^{s}_{s}pK_a$ for the ionization of the **4.1**:Ni(II)-coordinated methanol, the maximum observed rate constant for the Ni(II)-catalyzed cleavage of **4.1** ($k_{obs} \approx 0.07$ s^{-1} at 4 mM Ni(II), not saturating conditions) is 12 times larger than the Cu(II)-catalyzed process ($k_{obs} \approx 0.0057$ s^{-1} under saturation conditions). At higher ${}^{s}_{s}$pH, and with full binding of the metal ion-methoxide to **4.1**, the k_{max} for the Ni(II)-promoted reaction would be far greater.

4.5.2 – Ni(II)- and Zn(II)-promoted ethanolysis of 4.1

The mechanism given in Scheme 4-1 is also favored for the Ni(II)- and Zn(II)-promoted ethanolysis of **4.1**. Due to the lower polarity of the medium, their binding to **4.1** in ethanol is stronger than in methanol, leading to saturation of the k_{obs} vs $[M^{2+}]$ plots (see Figure 4-3). The binding constants for Ni(II) to **4.1** in ethanol are consistently larger than those for Zn(II) which correlates with the aforementioned trends in binding constants for metal ion-pyridine complexes in water. From the data in Figure 4-18 and Figure 4-20 in Supporting Information 4-3, one sees that that the k_{obs}^{max} values for the Ni(II) and Zn(II) complexes of **4.1** at respective ${}^{s}_{s}pH$ values of 7.9 and 7.2 are 0.05 s^{-1} and 2.6×10^{-3} s^{-1}. Because these ${}^{s}_{s}pH$ values are below the ${}^{s}_{s}pK_a$ for formation of their maximally active **4.1**:M(II):($^{-}$OEt) forms, both reactions would be faster at higher ${}^{s}_{s}pH$, and indeed faster than the reaction of **4.1**:Cu(II):($^{-}$OEt) in ethanol, $k_{max}^{Cu} = 9 \times 10^{-3}$ s^{-1}.

4.5.3 – Cu(II)-promoted methanolysis and ethanolysis of 4.1

The ${}^{s}_{s}pH/\log(k_{obs}^{corr})$ profile for the Cu(II)-promoted methanolysis of **4.1** from our previous study was extended in order to determine a kinetic ${}^{s}_{s}pK_a$ of 5.79. This is lower than the value of 6.5 observed for the analogous *N,N*-bis(2-picolyl)acetamide-copper(II) complex and may be attributed to a greater stabilization of the conjugate base originating from the more electron-withdrawing *p*-nitrobenzoyl group relative to the acetyl group. The kinetic studies were also carried out in ethanol where the cleavage reaction has a similar dependence on ${}^{s}_{s}pH$ as in methanol. The kinetic ${}^{s}_{s}pK_a$ in ethanol is 5.4, beyond which the k_{max}^{Cu} is 9×10^{-3} s^{-1} (1.5-fold larger than in methanol, 5 times less reactive than

the Ni(II) complex in ethanol at $^{s}_{s}$pH 7.9, and 3–4 times more reactive than the Zn(II) complex at $^{s}_{s}$pH 7.2 in ethanol).

4.5.4 – Ni(II)- and Zn(II)-promoted methanolysis of *N*,*N*-bis((1*H*-benzimidazol-2-yl)methyl)-*p*-nitrobenzamide (4.2)

The onset of saturation of k_{obs} with increasing $[M^{2+}]$ for the cleavage of **4.2** indicates that it binds Ni(II) and Zn(II) stronger than does **4.1** in methanol. The stability constants for the 1:1 complexes formed between Ni^{2+}or Zn^{2+} and benzimidazole in water at 25 °C and μ = 0.5 M ($NaNO_3$) are 100 M^{-1} and 41 M^{-1},[34] values larger than those found for the their mono-pyridine complexes which mirrors the larger binding constants observed for M(II) complexes of **4.2** relative to **4.1**. A somewhat contrasting trend is seen in the order of binding strength of **4.2** to Zn(II) being slightly stronger than Ni(II) when compared to the values reported for benzimidazole.[34] This discrepancy may be attributable to the differences in the preferred geometry of each metal ion on complexation with polydentate ligands. A distinct characteristic of the **4.2**:Zn(II) system is the $^{s}_{s}$pH independence of k_{obs}^{max} beyond its kinetic $^{s}_{s}pK_a$ of 8.36 representing a plateau region with a k_{max} of 5.8×10^{-4} s^{-1} (Figure 4-25, Supporting Information 4-3).

4.5.5 – Ni(II)- and Zn(II)-promoted ethanolysis of 4.2

The binding constants between Ni^{2+} or Zn^{2+} and **4.2** in ethanol are larger than those observed with **4.1** in ethanol. It is noteworthy that **4.2** appears to bind Zn^{2+} more tightly than Ni^{2+} in ethanol, the opposite of what is seen with **4.1**, but parallel to the trend observed in methanol. In each case, plots of $\log(k_{obs}^{max})$ vs $^{s}_{s}$pH do not show evidence of

complete formation of **4.2**:M(II):($^{-}$OEt), the highest values attained for the respective Ni(II) and Zn(II) complexes being 0.3 s^{-1} ($^{s}_{s}$pH 8.7) and 2.3 × 10^{-4} s^{-1} ($^{s}_{s}$pH 7.5) (see Figure 4-28 and Figure 4-30, Supporting Information 4-3).

4.5.6 – Cu(II)-promoted methanolysis and ethanolysis of 4.2

The k_{max} value for Cu(II) mediated cleavage of **4.2** in methanol is about twice that in ethanol ((3.8 ± 0.2) × 10^{-4} s^{-1}) , the opposite of what is observed in the case of **4.1**. These values are almost an order of magnitude smaller than those observed for **4.1** in the corresponding solvents suggesting a less desirable proximity, or more severe restriction of access of the metal-bound ethoxide in the transition state for attack on the C=O unit of the Cu(II)-complex of **4.2**.

4.5.7 – Comparison of relative activity

A convenient way to compare the relative activities of most of the systems considered here assesses the apparent second order rate constant for the attack of alkoxide (k_2^{-OR}) on the fully formed substrate:M(II) complex as defined in equation 4-2. These are shown in Table 4-1 along with other k_{max} values which have been determined in various ways. The binding of Cu^{2+} with **4.2** in methanol and ethanol is sufficiently strong that only a value of the maximum unimolecular rate constant k_{max}^{M} for decomposition of the substrate:Cu(II):($^{-}$OR) complex at three different $^{s}_{s}$pH values could be obtained. In theory, complete plots of the log(k_{max}^{obs}) values vs $^{s}_{s}$pH will show linear behavior with a gradient of unity at values below the $^{s}_{s}pK_a$ for formation of the substrate:M(II):($^{-}$OR) complex, and a plateau with a zero gradient at greater $^{s}_{s}$pH values. The latter behavior with respect to

increasing $^{s}_{s}$pH was only realized with Cu^{2+} and **4.1** in methanol and ethanol, and with Zn^{2+} and **4.2** in methanol. A complete analysis through NLLSQ fitting of the log(k_{max}^{obs}) vs $^{s}_{s}$pH values to equation 4-1 yields first order rate constants (k_{max}^{M}) for decomposition of the maximally active substrate:M(II):($^{-}$OR) form and their kinetic $^{s}_{s}pK_a$ values which are given in Table 4-1. Plots of k_{obs} vs [M^{2+}] show saturation for Cu^{2+}, Zn^{2+}, and Ni^{2+} with **4.1** in ethanol, Cu^{2+} with **4.1** in methanol, and Zn^{2+} and Ni^{2+} with **4.2** in methanol and ethanol which allow us to obtain the k_{obs}^{max} rate constant for reaction of the substrate:M(II) complex at each experimentally attainable $^{s}_{s}$pH. For these examples which do not show a saturation in the log(k_{obs}^{max}) vs $^{s}_{s}$pH plots (due to the fact that the experimentally accessible $^{s}_{s}$pH values are less than the $^{s}_{s}pK_a$) one can obtain the apparent k_2^{-OR} rate constant for $^{-}$OR attack on the substrate:M(II) complex by averaging the individual k_2^{-OR} values at each [$^{-}$OR].[35]

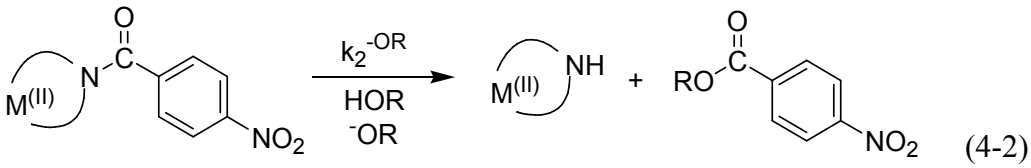

(4-2)

Table 4-1. Second-order rate constants for attack of alkoxide on the fully-formed substrate:M(II) complex under saturation conditions with respect to [M^{2+}], maximal rate constants for selected substrate:M(II):($^{-}$OR) complexes at 25 °C.

Sub	Solvent	Ni k_2^{-OR} ($M^{-1}\cdot s^{-1}$)	Zn k_2^{-OR} ($M^{-1}\cdot s^{-1}$)	k_{max}^{Zn} (s^{-1})	Cu k_2^{-OR} ($M^{-1}\cdot s^{-1}$)	k_{max}^{Cu} (s^{-1})
4.1	MeOH	[a] $k_3 = 4.4 \times 10^7$ $M^{-2}\cdot s^{-1}$ [b]	[a] $k_3 = 4.5 \times 10^6$ $M^{-2}\cdot s^{-1}$ [b]	a	5.4×10^8	5.7×10^{-3} [d]
	EtOH	1.0×10^{10}	1.7×10^9	a	4.5×10^{11}	9.0×10^{-3} [e]
4.2	MeOH	6.3×10^5	1.5×10^5	5.8×10^{-4} [c]	7.6×10^7	8.0×10^{-4} [f]
	EtOH	7.3×10^9	9.5×10^7	a	1.9×10^{10}	3.8×10^{-4} [f]

a. K_b constants are not available due to the fact that saturation is not observed in the k_{obs} vs [M^{2+}] plots or k_{obs}^{max} vs $^{s}_{s}$pH plots.
b. k_3 is a third order rate constant calculated for the hypothetical process involving substrate + M^{2+} + $^{-}$OR.
c. Kinetic $^{s}_{s}pK_a$ 8.36.
d. Kinetic $^{s}_{s}pK_a$ 5.79.
e. Kinetic $^{s}_{s}pK_a$ 5.4.
f. No observed kinetic $^{s}_{s}pK_a$.

The **M** k_2^{-OR} constants given in Table 4-1 are large for all complexes in both solvents, and in some cases approach, or even exceed, the diffusion limit in methanol (1–2 × 10^{10} $M^{-1}\cdot s^{-1}$),[36] and ethanol (2 × 10^{10} $M^{-1}\cdot s^{-1}$).[37] The fact that the k_2^{-OR} value for **4.1**:Cu(II) in ethanol (shaded in the Table 4-1 entry) is computed to exceed the diffusion limit in that solvent by ~20 times can be taken as confirmation that the true reaction does not involve the attack of external ethoxide on **4.1**:Cu(II), but rather decomposition of a **4.1**:Cu(II):($^{-}$OEt) complex. By extension, it seems reasonable to propose that all of these reactions occur through the metal-bound lyoxide form, as proposed previously.[16,17]

4.5.8 – Acceleration of amide cleavage provided by the presence of a metal ion

The acceleration of the alcoholysis of benzamides **4.1** and **4.2** provided by the metal ion can be conveniently measured in three ways. The first involves comparing the k_2^{-OR} rate constant for alkoxide attack on the substrate:M(II) complex with that for attack of alkoxide on the uncomplexed **4.1** or **4.2**. Previously, we experimentally determined that the methoxide-promoted reaction of 0.15 M **4.1** in 0.3 M $KOCH_3$ shows no indication of product formation after 52.5 days.[17] We have now extended the time to 250 days without observing product formation. Assuming we could detect 1 mM of the product, the upper limit for the second order rate constant is $k_{-OMe}^{\mathbf{4.1}} = 1 \times 10^{-9}\ M^{-1}\cdot s^{-1}$. While we do not have experimental data for the ethanolysis reaction of **4.1**, Phan and Mayr have reported that the k_{-OMe} values for nucleophilic addition of methoxide in methanol to trinitrotoluene or benzhydrilium ions is five times less than the nucleophilic addition of ethoxide in ethanol.[38] In another comparison, methoxide attack on *p*-nitrophenyl acetate in methanol is reported[39a] to be essentially the same as the attack of ethoxide in ethanol.[39b] If we are allowed to use these comparisons, then the approximate upper limit for the k_2^{-OEt} reaction with **4.1** would be $\sim 1 \times 10^{-9}\ M^{-1}\cdot s^{-1}$. Unfortunately experimental data corresponding to the alkoxide reactions of **4.2** are not obtainable due to technical problems of deprotonation of the benzimidazole N–H under strongly basic conditions.

The second methodology involves comparing the first order rate constant observed for decomposition of substrate:M(II):(HOR) at the ${}^{s}_{s}pK_a$ for its acid dissociation, with the pseudo-first order rate constant that would be observed for alkoxide attack on substrate at a ${}^{s}_{s}pH$ corresponding to that ${}^{s}_{s}pK_a$. Using the above comparisons, the accelerations in

methanol and ethanol for the various complexes of **4.1** compared with the background methoxide reactions are given in Table 4-2.

Table 4-2. Acceleration of amide **4.1** alcoholysis provided by the presence of a divalent metal ion at 25 °C.

Benzamide	Solvent	Ni(II)	Zn(II)	Cu(II)
4.1	MeOH	(1.3×10^{14}) [a]	(4.9×10^{13}) [b]	(3.5×10^{17}) [c] (3.0×10^{17}) [d]
	EtOH	(1.7×10^{18}) [e]	(2.5×10^{17}) [e]	(9.0×10^{18}) [f]

a. Computed from k_{obs} value for decomposition of **4.1**:Ni(II) at ${}^{s}_{s}$pH 10.5 (k_{obs} = 0.07 s^{-1} at 4 mM Ni(II), not saturating conditions). This provides a lower limit for the acceleration since the Ni(II) complex is not fully formed.
b. Computed from k_{obs} value for decomposition of **4.1**:Zn(II) at ${}^{s}_{s}$pH 9.6 (k_{obs} = 3.3 × 10^{-4} s^{-1} at 1 mM Zn(II), not saturating conditions). This provides a lower limit for the acceleration since the Zn(II) complex is not fully formed.
c. Computed from comparison of the k_2^{-OMe} value for attack of methoxide on **4.1**:Cu(II) given in Table 4-1 with the second order rate constant for attack of methoxide on **4.1**.
d. Computed from comparison of the first order rate constant for decomposition of **4.1**:Cu(II):($HOCH_3$) at ${}^{s}_{s}$pH 5.79, corresponding to the kinetic ${}^{s}_{s}pK_a$, with the pseudo first order rate constant for reaction of methoxide with **4.1** at that ${}^{s}_{s}$pH.
e. Computed from the k_2^{-OEt} values for the Ni(II) and Zn(II) complexes of **4.1** from Table 4-1 compared with the second order rate constant for attack of ethoxide on **4.1**.
f. Computed from comparison of the first order rate constant for decomposition of **4.1**:Cu(II):(HOEt) at ${}^{s}_{s}$pH 5.4, corresponding to the kinetic ${}^{s}_{s}pK_a$ in ethanol, with the pseudo first order rate constant for reaction of ethoxide with **4.1** at that ${}^{s}_{s}$pH.

A third and more informative method for judging the efficacy of the metal ion-promoted reaction compares the ΔG^{o} of binding of the metal ion to the transition state of the presumed lyoxide-promoted reaction, namely [**S**:M(II):($^{-}$OR)]‡ with that of the lyoxide

reaction, [**S**:($^-$OR)]‡.[40,41] The thermodynamic cycle is shown in Scheme 4-2 where M(II) is represented as **M** and the various free energies for the kinetic and equilibrium terms can be obtained from the rate constants for attack of alkoxide on the substrate or its metal-complexed form (k_2^{-OR} and $\mathbf{M}k_2^{-OR}$) and the metal binding constants (K_b).

Scheme 4-2. A thermodynamic cycle describing the free energies for various equilibrium and kinetic steps for alkoxide attack on substrate **S**, equilibrium binding of the metal ion to **S** and alkoxide attack on the **S:M** complex (metal ion charges omitted for clarity). Products include the dipicolyl or dibenzimidazol-2-ylmethyl amine ligand.

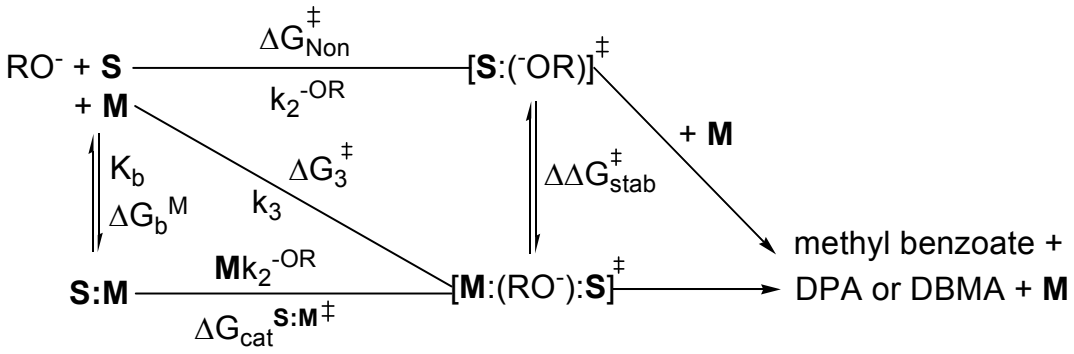

$\Delta\Delta G_{stab}^{‡}$ is computed from the expression given in equation 4-3 which is applicable for the situations where Ni, Zn, and Cu bind with saturation to the substrate in ethanol.

$$\Delta\Delta G_{stab}^{\neq} = (\Delta G_b^{\mathbf{M}} + \Delta G_{cat}^{\mathbf{S}:\mathbf{M}\neq}) - \Delta G_{Non}^{\neq} = -RT\ln\left[\frac{(k_2)(K_b)}{k_2^{-\mathrm{OR}}}\right] \qquad (4\text{-}3)$$

For the situation where no saturation binding of the metal ion to the substrate is observed, in the cases of Zn and Ni in methanol, the hypothetical third order rate constant (k_3) for reaction of substrate + M(II) + $^-$OR was computed,[42] and the $\Delta\Delta G_{stab}^{‡}$ is obtained from the expression given in equation 4-4.

$$\Delta\Delta G_{stab}^{\neq} = \Delta G_3^{\neq} - \Delta G_{Non}^{\neq} = -RT\ln\left[\frac{k_3}{k_2^{-\mathrm{OR}}}\right] \qquad (4\text{-}4)$$

The results at a standard state of 1 M and 298 K are shown graphically in Figure 4-9 using the value of 1×10^{-9} $M^{-1} \cdot s^{-1}$ as the upper limit for attack of methoxide or ethoxide on substrate **4.1** in methanol or ethanol in the absence of catalytic metal ion. On the right side of the diagram are included the numerical values obtained for the process in ethanol where metal binding to **4.1** is sufficiently strong to obtain K_b and a $\Delta G_b^{\mathbf{M}}$. It is of interest to note that the $\Delta G_{cat}^{\mathbf{4.1:M‡}}$ values obtained from the large $\mathbf{M}k_2^{\text{-OEt}}$ values in Table 4-1 nearly offset the $\Delta G_b^{\mathbf{M}}$ values such that the [**4.1**:⁻OEt:**M**]‡ transition states lie very close in energy to the free energy of the non-associated substrate, metal ion and alkoxide partners. This illustrates that, once the metal ion binds the ethoxide and substrate, their transition states for reaction are stabilized by 27.7 and 29.3 kcal·mol^{-1} for Zn and Ni, respectively. For these two metal ions in methanol, the transition state binding is not as large, being 21.3 and 22.7 kcal·mol^{-1} for Zn and Ni, respectively. That this is less than in ethanol is a consequence of the reduced affinity of the metal ion for the substrate and methoxide binding in the ground state, which is more largely manifested in binding the transition state, although less so than in ethanol. This sort of effect is reminiscent of a dinuclear Zn(II) catalyst that promotes the methanolytic and ethanolytic cleavage of phosphate diesters where extremely large binding of the catalyst to the [alkoxide:substrate] transition states leads to very large rate accelerations.[41d]

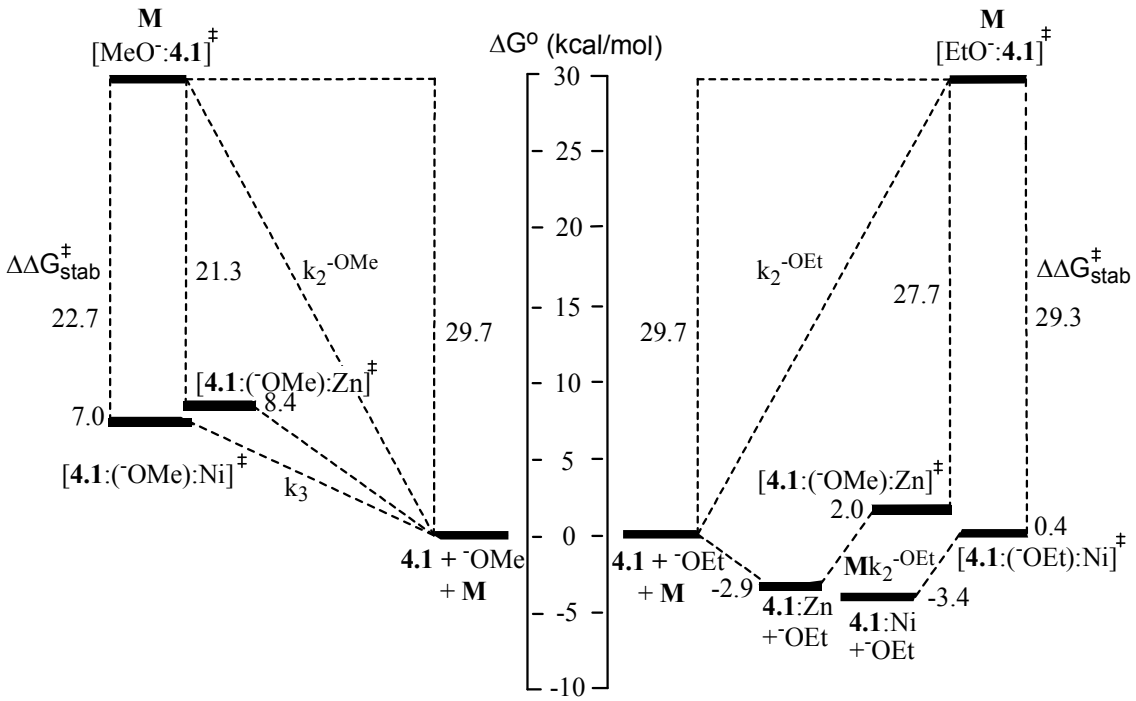

Figure 4-9. A free energy diagram obtained at a standard state of 1 M and 25 °C for the alcoholysis of **4.1** in the presence of methoxide in methanol (left side) and ethoxide in ethanol (right side), and in the presence of Zn and Ni in both solvents. The computed stabilizations of the [lyoxide:**4.1**]‡ by its binding to the metal ions, $\Delta\Delta G_{stab}^{‡}$, are given numerically on the extreme left and right sides of the diagram and are computed as described in the text.

4.6 – Conclusions

The results of this study in combination with related ones[12-17] have established that large accelerations for amide cleavage reactions over background base-promoted reactions can be achieved by the multifunctional role of a single metal ion that is appropriately positioned relative to the >N–C=O moiety. To fully realize these effects in small molecules requires a substrate design where the metal ion is forced into binding the lone pair of the amidic N, concurrently positioning a metal-bound nucleophile in a favourable trajectory for attack on the acyl group, with subsequent assistance of the departure of the LG anion. In an optimized system, the metal ion seems to enact several catalytic roles

such as was seen earlier in the methanolytic cleavage of a thiobenzanilide catalyzed by a simple palladacycle catalyst.[43] In that case, the Pd enhances the electrophilicity of the thioamide through favourable binding of the C=S unit, delivers the activated methoxide nucleophile to form a tetrahedral intermediate which subsequently rearranges to allow assisted leaving group departure through Pd–N-coordination. That this sort of tri-functional role for three other transition metal ions is seen to provide catalytic accelerations of 10^{14} to 10^{19} in the present systems dealing with alcoholysis of benzamides **4.1** and **4.2** may imply that metal ion assistance of leaving group departure plays a key role that may also be operative in metallo-enzyme promoted cleavage of peptides.

4.7 – Supporting Information

4.7.1 – Supporting Information 4-1: UV-vis kinetics

The Ni(II)-catalyzed methanolyses and ethanolyses of **4.1** (5×10^{-5} M) were monitored at 283 nm (with the exception of kinetic experiments using 2,4,6-collidine buffer, which were followed at 290 nm), to determine the rate of disappearance of Ni(II):**4.1**. The reactions were conducted in the presence of buffers composed of various ratios of 2-picoline, 2,6-lutidine, 2,4,6-collidine, *N*-ethylmorpholine, or *N*-methylpiperidine and HOTf to maintain the ${}^{s}_{s}$pH in methanol (7.2 to 10.5) and ethanol (5.9 to 7.9).

The Zn(II)-catalyzed methanolyses and ethanolyses of **4.1** (5×10^{-5} M) were monitored at 283 nm (with the exception of kinetic experiments using 2,4,6-collidine buffer, which were followed at 290 nm) to determine the disappearance of Zn(II):**4.1**. The reactions were conducted in the presence of buffers composed of various ratios of 2-picoline, 2,6-lutidine, 2,4,6-collidine, *N*-ethylmorpholine, or *N*-methylpiperidine and HOTf to maintain the ${}^{s}_{s}$pH in methanol (8.5 to 10.0) and ethanol (6.2 to 7.2).

The Cu(II)-catalyzed methanolyses and ethanolyses of **4.1** (5×10^{-4} M) were monitored at 360 nm for the disappearance of the **4.1**:Cu(II):($^{-}$OR)(HOR) complex. The reactions were conducted in the presence of buffers composed of various ratios of 2-bromo-6-methylpyridine, 2-methoxy-6-methylpyridine, 2-picoline, 2,6-lutidine, or 2,4,6-collidine and HOTf to maintain the ${}^{s}_{s}$pH in methanol and ethanol. The rate constants for the alcoholysis of **4.1**:Cu(II):($^{-}$OR)(HOR) in the presence of excess Cu(II) (required to ensure complete binding) exhibited small buffer and $Cu(OTf)_2$ concentration effects. Thus, the k_{obs} values were extrapolated to zero buffer concentration for each [$Cu(OTf)_2$] using three buffer concentrations (10 mM, 15 mM, 20 mM). These extrapolated values

were then extrapolated to zero excess $Cu(OTf)_2$ using at least two excess $Cu(OTf)_2$ concentrations (typically 1.0 mM, 2.0 mM, 3.0 mM) to provide corrected rate constants for a given $^{s}_{s}$pH.

The Ni(II)-catalyzed methanolyses and ethanolyses of **4.2** (2×10^{-5} M) were monitored at 281.0 nm and 282.5 nm, respectively, for the disappearance of Ni(II):**4.2**. The reactions were conducted in the presence of buffers composed of various ratios of 2-picoline, 2,4,6-collidine, *N*-ethylmorpholine, *N*-methylpiperidine and HOTf to maintain the $^{s}_{s}$pH.

The Zn(II)-catalyzed methanolyses and ethanolysis of **4.2** (2×10^{-5} M) were monitored at 281.5 nm and 281.0 nm or 290.0 nm, respectively, for the disappearance of Zn(II):**4.2**. The reactions were conducted in the presence of buffers composed of various ratios of 2,6-lutidine, 2,4,6-collidine, *N*-ethylmorpholine, or *N*-methylpiperidine and HOTf to maintain the $^{s}_{s}$pH.

The Cu(II)-catalyzed methanolyses and ethanolyses of **4.2** (2×10^{-5} M) were monitored at 280.5 nm for the disappearance of Cu(II):**4.2**. The reactions were conducted in the presence of buffers composed of various ratios of 2,4,6-collidine and HOTf to maintain the $^{s}_{s}$pH.

4.7.2 – Supporting Information 4-2: NMR characterization of 4.2

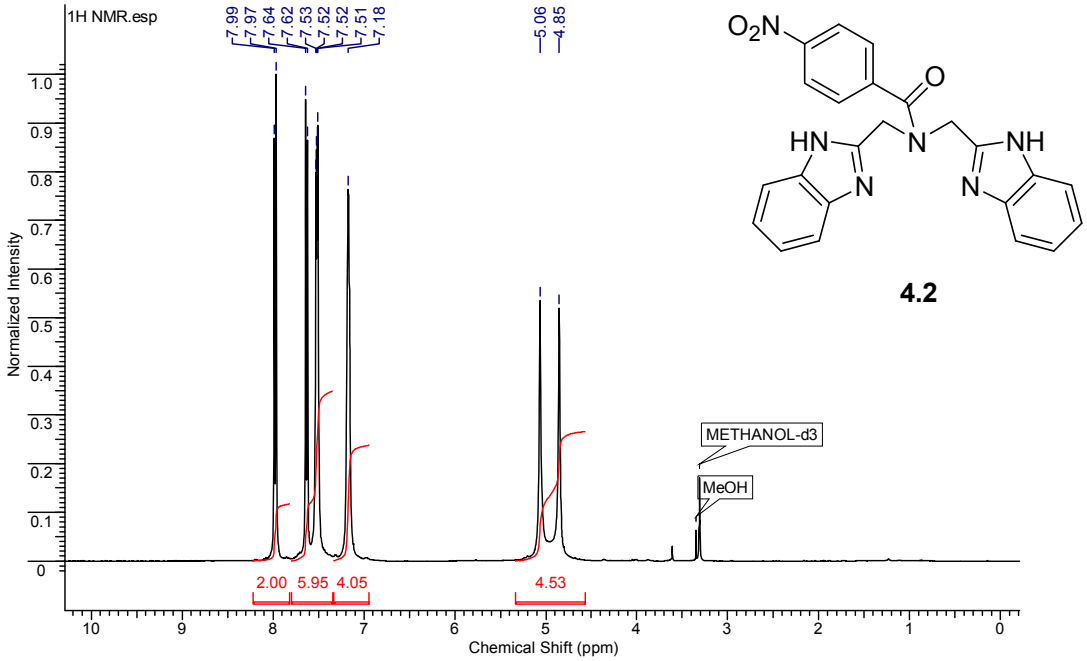

Figure 4-10. ^{1}H NMR spectrum of **4.2** (400 MHz, CD_3OD, 25 °C). Integration of the methylene protons at 5.06 and 4.85 ppm is obscured by the water/methanol OH signal.

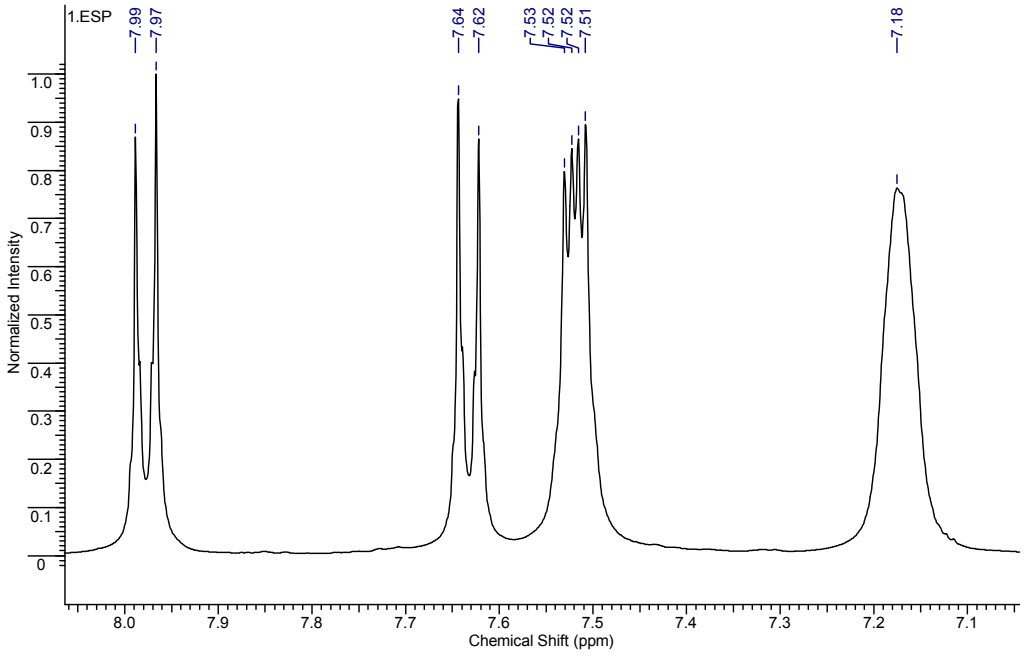

Figure 4-11. Portion of the ^{1}H NMR spectrum of **4.2** (400 MHz, CD_3OD, 25 °C) emphasizing additional splitting due to AA'BB' spin systems present in the phenyl and benzimidazole rings.

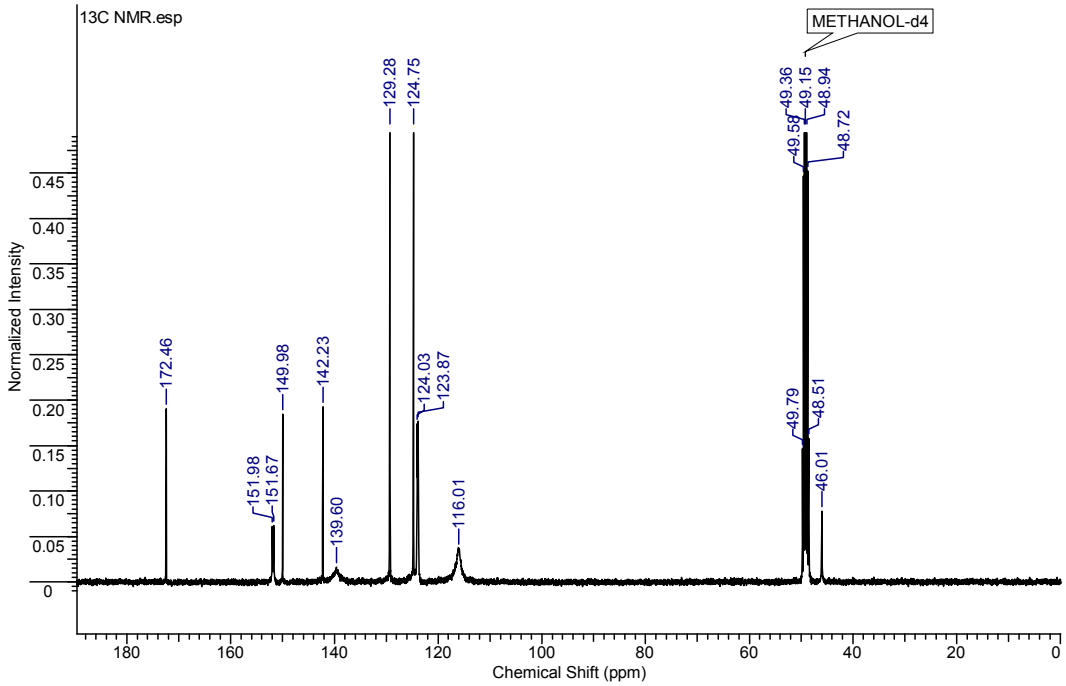

Figure 4-12. ^{13}C NMR spectrum of **4.2** (400 MHz, CD_3OD, 25 °C).

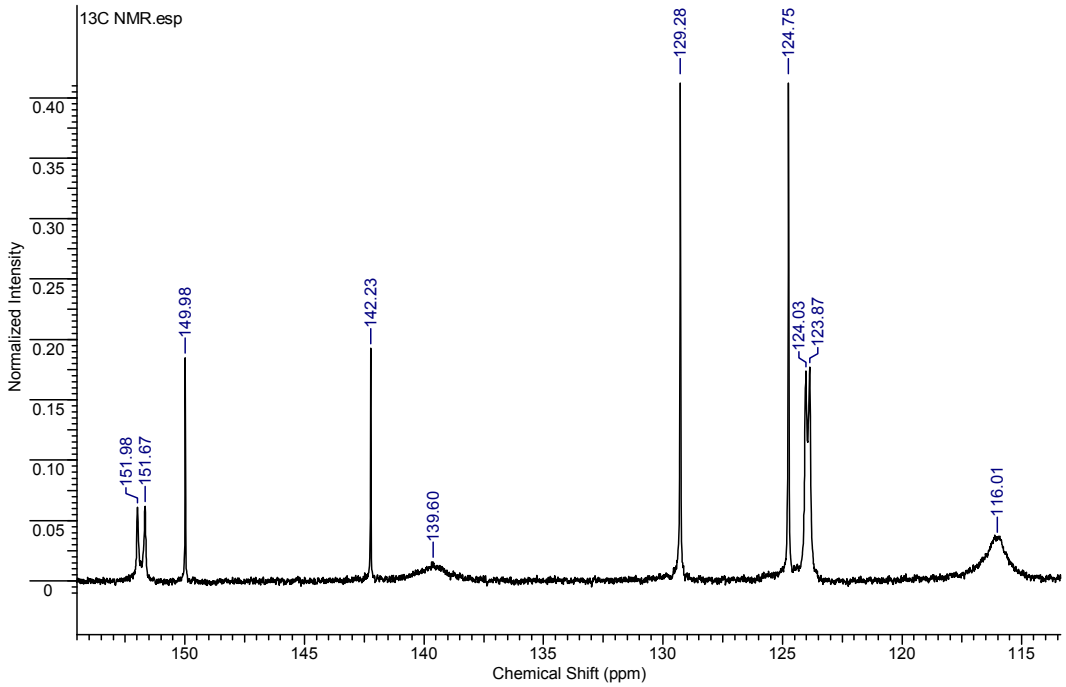

Figure 4-13. Portion of the ^{13}C NMR spectrum of **4.2** (400 MHz, CD_3OD, 25 °C).

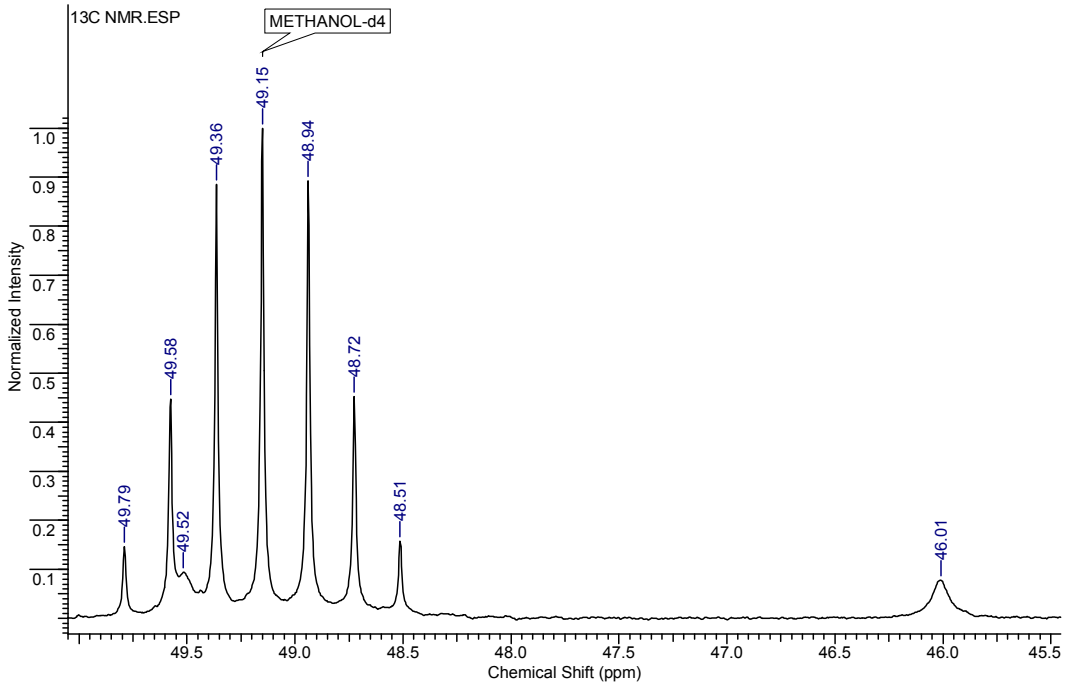

Figure 4-14. Portion of the ^{13}C NMR spectrum of **4.2** (400 MHz, CD_3OD, 25 °C). The signal at 49.52 ppm is related to the signal at 46.01 ppm via slow rotation about the amide bond.

4.7.3 – Supporting Information 4-3: Plots of log(k) vs $^{s}_{s}$pH

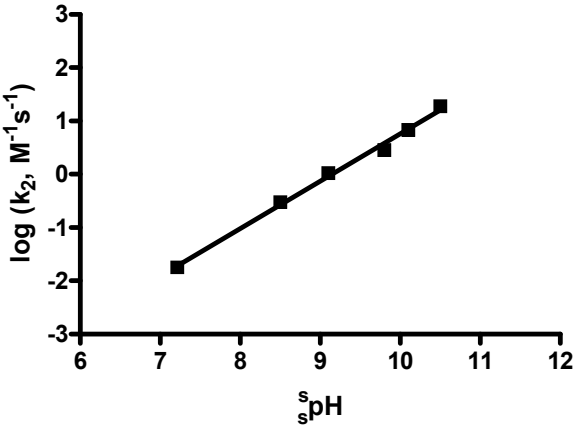

Figure 4-15. Plot of log(k_2) for the Ni(II)-promoted cleavage of **4.1** (5×10^{-5} M) vs $^{s}_{s}$pH in anhydrous methanol under buffered conditions (10 mM amine, various concentrations of HOTf) at 25 °C. The line through the data is generated from a linear regression to provide a slope of 0.89 ± 0.03; $r^2 = 0.9956$.

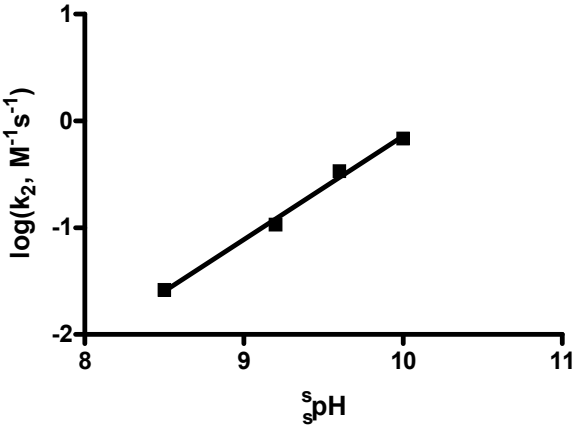

Figure 4-16. Plot of $\log(k_2)$ for the Zn(II)-promoted cleavage of **4.1** (5×10^{-5} M) vs ${}^{s}_{s}$pH in anhydrous methanol under buffered conditions (10 mM amine, various concentrations of HOTf) at 25 °C. The line through the data is generated from a linear regression to provide a slope of 0.97 ± 0.05; $r^2 = 0.9937$.

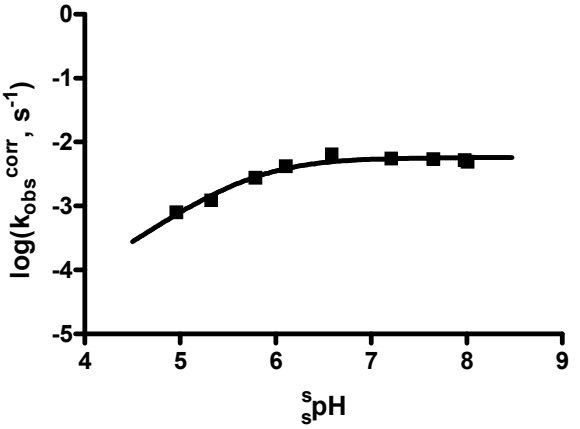

Figure 4-17. Plot of $\log(k_{obs}^{corr})$ for the cleavage of **4.1**:Cu(II):($^{-}$OMe)(HOMe) (0.5 mM each of Cu(II) and **4.1** and corrected for buffer and excess $Cu(OTf)_2$ effects) vs ${}^{s}_{s}$pH in anhydrous methanol under buffered conditions at 25 °C. The data are fitted to equation 4-1 computing one macroscopic ${}^{s}_{s}pK_a$ value of 5.79 ± 0.07 and a maximum rate constant (k_{max}) of $(5.7 \pm 0.4) \times 10^{-3}$ s^{-1}; $r^2 = 0.9666$.

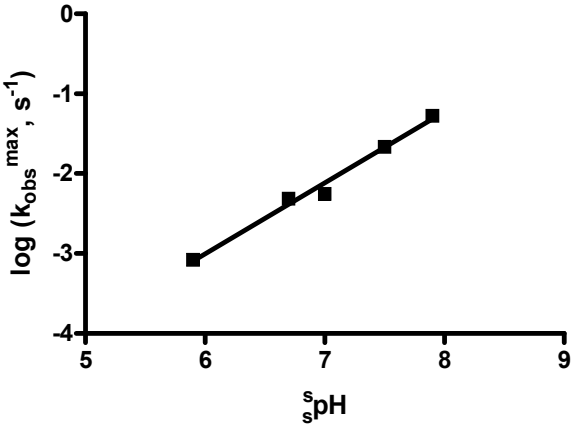

Figure 4-18. Plot of log(k_{obs}^{max}) for the Ni(II)-promoted cleavage of **4.1** (5×10^{-5} M) vs $^{s}_{s}$pH in anhydrous ethanol under buffered conditions (10 mM amine, various concentrations of HOTf) at 25 °C. The line through the data is generated from a linear regression to provide a slope of 0.89 ± 0.06; $r^2 = 0.9864$.

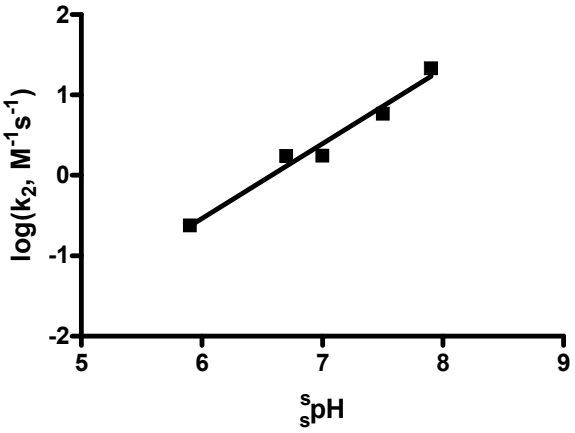

Figure 4-19. Plot of log(k_2) for the Ni(II)-promoted cleavage of **4.1** (5×10^{-5} M) vs $^{s}_{s}$pH in anhydrous ethanol under buffered conditions (10 mM amine, various concentrations of HOTf) at 25 °C. The line through the data is generated from a linear regression to provide a slope of 0.93 ± 0.09; $r^2 = 0.9731$.

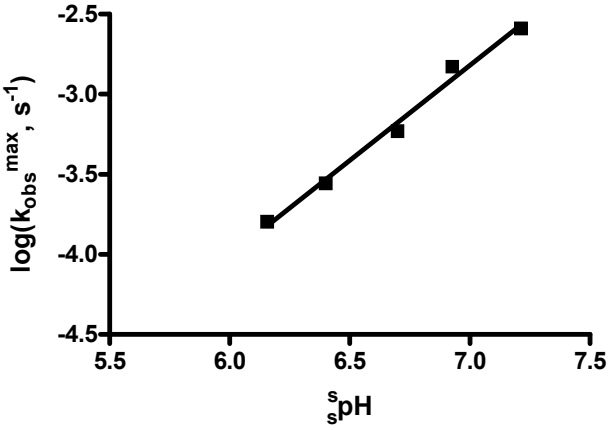

Figure 4-20. Plot of $\log(k_{obs}^{max})$ for the Zn(II)-promoted cleavage of **4.1** (5×10^{-5} M) vs ${}^{s}_{s}$pH in anhydrous ethanol under buffered conditions (10 mM amine, various concentrations of HOTf) at 25 °C. The line through the data is generated from a linear regression to provide a slope of 1.19 ± 0.07; $r^2 = 0.9890$.

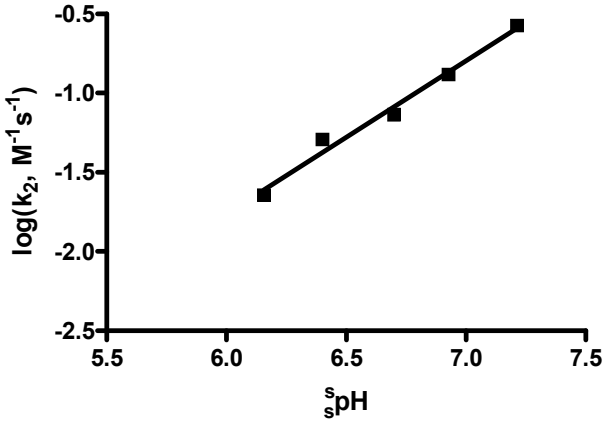

Figure 4-21. Plot of $\log(k_2)$ for the Zn(II)-promoted cleavage of **4.1** (5×10^{-5} M) vs ${}^{s}_{s}$pH in anhydrous ethanol under buffered conditions (10 mM amine, various concentrations of HOTf) at 25 °C. The line through the data is generated from a linear regression to provide a slope of 0.96 ± 0.07; $r^2 = 0.9833$.

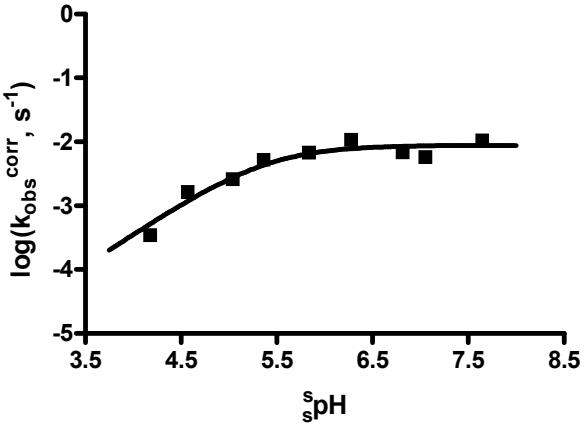

Figure 4-22. Plot of $\log(k_{obs}^{corr})$ for the cleavage of **4.1**:Cu(II):($^{-}$OEt)(HOEt) (0.5 mM each of Cu(II) and **4.1** and corrected for buffer and excess $Cu(OTf)_2$ effects) vs ${}^{s}_{s}pH$ in anhydrous ethanol under buffered conditions at 25 °C. The data are fitted to equation 4-1 computing one macroscopic ${}^{s}_{s}pK_a$ value of 5.4 ± 0.1 and a maximum rate constant (k_{max}) of (9 ± 1) × 10^{-3} s^{-1}; r^2 = 0.9306.

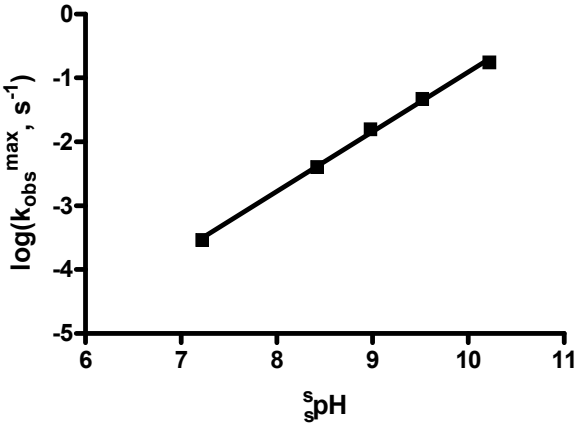

Figure 4-23. Plot of $\log(k_{obs}^{max})$ for the Ni(II)-promoted cleavage of **4.2** (2 × 10^{-5} M) vs ${}^{s}_{s}pH$ in anhydrous methanol under buffered conditions (2 mM amine, various concentrations of HOTf) at 25 °C. The line through the data is generated from a linear regression to provide a slope of 0.94 ± 0.02; r^2 = 0.9982.

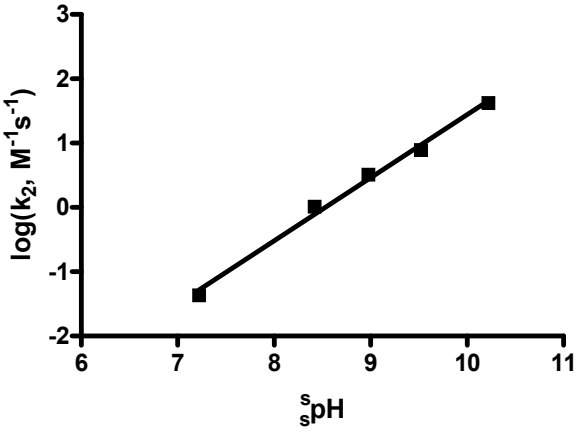

Figure 4-24. Plot of log(k_2) for the Ni(II)-promoted cleavage of **4.2** (2×10^{-5} M) vs $^{s}_{s}$pH in anhydrous methanol under buffered conditions (2 mM amine, various concentrations of HOTf) at 25 °C. The line through the data is generated from a linear regression to provide a slope of 0.98 ± 0.05; $r^2 = 0.9936$.

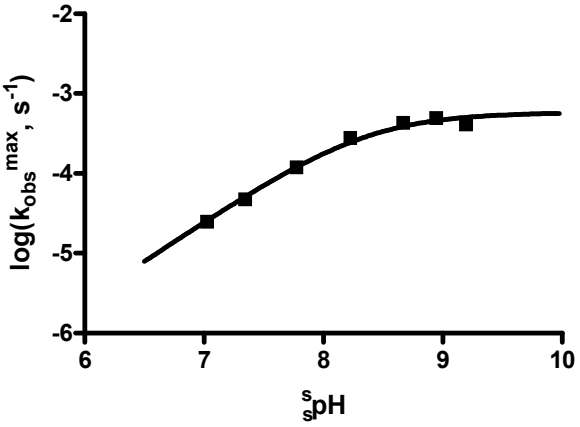

Figure 4-25. Plot of log(k_{obs}^{max}) for the Zn(II)-promoted cleavage of **4.2** (2×10^{-5} M) vs $^{s}_{s}$pH in anhydrous methanol under buffered conditions (2 mM amine, various concentrations of HOTf) at 25 °C. The data are fitted to equation 4-1 computing one macroscopic $^{s}_{s}pK_a$ value of 8.36 ± 0.07 and a maximum rate constant (k_{max}) of (5.8 ± 0.6) $\times 10^{-4}$ s^{-1}; $r^2 = 0.9903$.

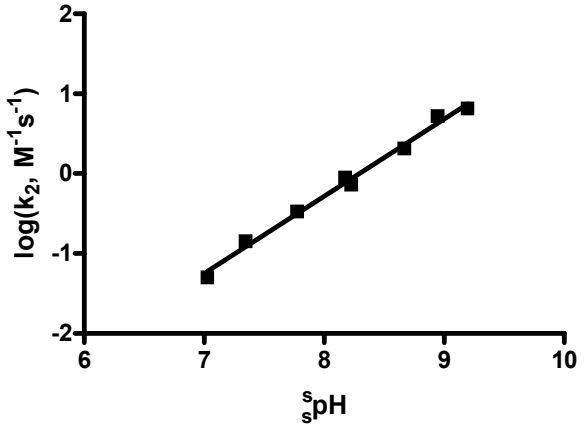

Figure 4-26. Plot of log(k_2) for the Zn(II)-promoted cleavage of **4.2** (2×10^{-5} M) vs $^{s}_{s}$pH in anhydrous methanol under buffered conditions (2 mM amine, various concentrations of HOTf) at 25 °C. The line through the data is generated from a linear regression to provide a slope of 0.97 ± 0.04; $r^2 = 0.9912$.

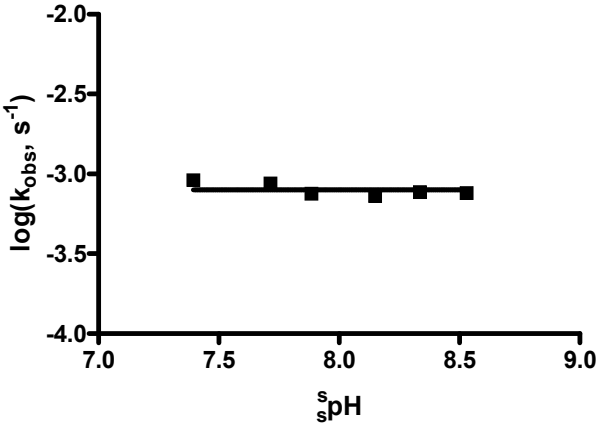

Figure 4-27. Plot of log(k_{obs}) for the cleavage of **4.2**:Cu(II):($^{-}$OMe)(HOMe) (0.02 mM each of Cu(II) and **4.2**) vs $^{s}_{s}$pH in anhydrous methanol under buffered conditions (2 mM amine, various concentrations of HOTf) at 25 °C. The averaged maximum rate constant (k_{max}) is $(8.0 \pm 0.8) \times 10^{-4}$ s^{-1}.

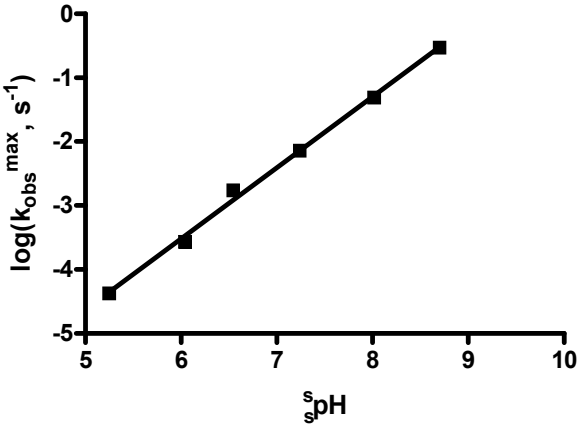

Figure 4-28. Plot of $\log(k_{obs}^{max})$ for the Ni(II)-promoted cleavage of **4.2** (2×10^{-5} M) vs ${}^{s}_{s}$pH in anhydrous ethanol under buffered conditions (2 mM amine, various concentrations of HOTf) at 25 °C. The line through the data is generated from a linear regression to provide a slope of 1.11 ± 0.03; $r^2 = 0.9967$.

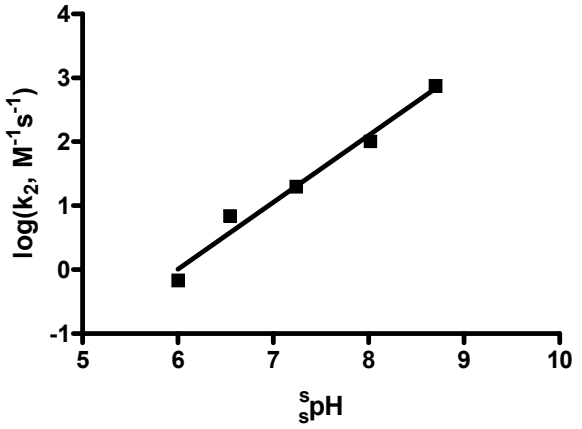

Figure 4-29. Plot of $\log(k_2)$ for the Ni(II)-promoted cleavage of **4.2** (2×10^{-5} M) vs ${}^{s}_{s}$pH in anhydrous ethanol under buffered conditions (2 mM amine, various concentrations of HOTf) at 25 °C. The line through the data is generated from a linear regression to provide a slope of 1.04 ± 0.08; $r^2 = 0.9802$.

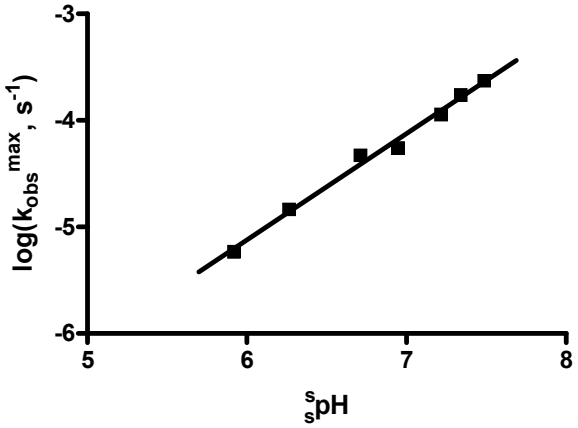

Figure 4-30. Plot of $\log(k_{obs}^{max})$ for the Zn(II)-promoted cleavage of **4.2** (2×10^{-5} M) vs ${}^{s}_{s}$pH in anhydrous ethanol under buffered conditions (2 mM amine, various concentrations of HOTf) at 25 °C. The line through the data is generated from a linear regression to provide a slope of 1.00 ± 0.04; $r^2 = 0.9914$.

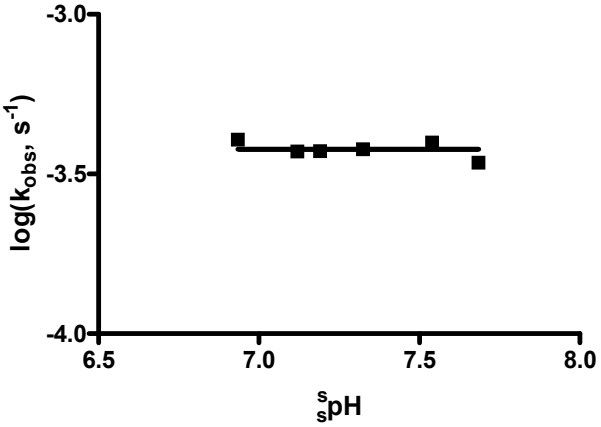

Figure 4-31. Plot of $\log(k_{obs})$ for the cleavage of **4.2**:Cu(II):($^{-}$OEt)(HOEt) (0.02 mM each of Cu(II) and **4.2**) vs ${}^{s}_{s}$pH in anhydrous ethanol under buffered conditions (2 mM amine, various concentrations of HOTf) at 25 °C. The data are averaged, indicating a maximum rate constant (k_{max}) of $(3.8 \pm 0.2) \times 10^{-4}$ s^{-1}.

4.8 – References and notes

[1] (a) Brown, R. S.; Neverov, A. A. *J. Chem. Soc. Perkin Trans. 2* **2002**, 1039. (b) Brown, R. S.; Neverov, A. A.; Tsang, J. S. W.; Gibson, G. T. T.; Montoya-Pelaez, P. J. *Can. J. Chem.* **2004**, *82*, 1791. (c) Brown, R. S.; Neverov, A. A. *Adv. Phys. Org. Chem*. **2008**, *42*, 271. (d) Brown, R. S.; Lu, Z.-L.; Liu, C. T.; Tsang, W. Y.; Edwards, D. R.; Neverov, A. A. *J. Phys. Org. Chem.* **2009**, *23*, 1 and references therein. (e) Brown, R. S. In *Progress in Inorganic Chemistry*; Karlin, K., Ed.; John Wiley and Sons: New York, 2011; Vol. *57*, p 55 and references therein.

[2] (a) Williams, N. H.; Takasaki, B.; Wall, M.; Chin, J. *Acc. Chem. Res.* **1999**, *32*, 485. (b) Morrow, J. *Comments Inorg. Chem.* **2008**, *29*, 169. (c) Fothergill, M.; Goodman, M. F.; Petruska, J.; Warshel, A. *J. Am. Chem. Soc.* **1995**, *117*, 11619. (d) Richard, J. P.; Amyes, T. L. *Bioorg. Chem.* **2004**, *32*, 354.

[3] (a) Liu, C. T.; Neverov, A. A.; Maxwell, C. I.; Brown, R. S. *J. Am. Chem. Soc.* **2010**, *132*, 3561. (b) Raycroft, M. A. R.; Liu, C. T.; Brown, R. S. *Inorg. Chem.* **2012**, *51*, 3846.

[4] Brown, R. S.; Bennet, A. J.; Slebocka-Tilk, H. *Acc. Chem. Res.* **1992**, *25*, 481.

[5] (a) Kester, W. R.; Matthews, B. W. *Biochemistry* **1977**, *16*, 2506. (b) Matthews, B. W. *Acc. Chem. Res.* **1988**, *21*, 333. (c) Pelmenschikov, V.; Blomberg, M. R. A.; Siegbahn, P. E. M. *J. Biol. Inorg. Chem.* **2002**, *7*, 284.

[6] Rawlings, N. D.; Barrett, A. J. Introduction: Metallopeptidases and their Clans. In *Handbook of Proteolytic Enzymes*, 2nd ed.; Barrett, A. J.; Rawlings, N. D.; Woessner, J. F., Eds.; Academic: Oxford, U.K., 2004, Vol. *1*, p 231.

[7] Balasubramanian A.; Ponnuraj K. *J. Mol. Biol.* **2010**, *400*, 274.

[8] Fukasawa, K. M.; Hata, T.; Ono, Y.; Hirose, J. *J. Amino Acids* **2011**, Article ID 574816, 7 pages.

[9] (a) Polzin, G. M.; Burstyn, J. N. *Met. Ions in Biol. Syst.* **2000**, *38*, 103. (b) Fife, T. H.; Bembi, R. *J. Am. Chem. Soc.* **1994**, *115*, 11358. (c) Schepartz, A.; Breslow, R. *J. Am. Chem. Soc.* **1987**, *109*, 1814. (d) Suh, J.; Moon, S.-J. *Inorg. Chem.* **2001**, *40*, 4890. (e) Neverov, A. A.; Montoya-Pelaez, P. J.; Brown, R. S. *J. Am. Chem. Soc.* **2001**, *123*, 210. (f) Neverov, A. A.; Brown, R. S. *Can. J. Chem.* **2000**, *78*, 1247 and references therein.

[10] Liu, C. T.; Maxwell, C. I.; Pipe, S. G.; Neverov, A. A.; Mosey, N. J.; Brown, R. S. *J. Am. Chem. Soc.* **2011**, *133*, 20068.

[11] Elton, E. S.; Zhang, T.; Prabhakar, R.; Arif, A. M.; Berreau, L. M. *Inorg. Chem.* **2013**, *52*, 11480 and references therein.

[12] Houghton, R. P.; Puttner, R. R. *Chem. Commun.* **1970**, 1270.

[13] Niklas, N.; Heinemann, F. W.; Hampel, F.; Clark T.; Alsfasser, R. *Inorg. Chem.* **2004**, *43*, 4663 and references therein.

[14] Niklas, N.; Alsfasser, R. *Dalton Trans.* **2006**, 3188.

[15] (a) Bröhmer, M. C.; Bannwarth, W. *Eur. J. Org. Chem.* **2008**, 4412. (b) Bröhmer, M. C.; Mundinger, S.; Bräse, S.; Bannwarth, W. *Angew. Chem., Int. Ed.* **2011**, *50*, 6125.

[16] Barrera, I. F.; Maxwell, C. I.; Neverov, A. A.; Brown, R. S. *J. Org. Chem.* **2012**, *77*, 4156.

[17] Raycroft, M. A. R.; Maxwell, C. I.; Oldham, R. A. A.; Saffouri Andrea, A.; Neverov, A. A.; Brown, R. S. *Inorg. Chem.* **2012**, *51*, 10325.

[18] For the designation of pH in non-aqueous solvents we use the nomenclature recommended by the IUPAC: *Compendium of Analytical Nomenclature. Definitive Rules 1997*, 3rd ed.; Blackwell: Oxford, U.K., 1998. The pH meter reading for an aqueous solution determined with an electrode calibrated with aqueous buffers is designated as ${}^{w}_{w}$pH; if the electrode is calibrated in water and the "pH" of the neat buffered alcohol solution is then measured, the term ${}^{s}_{w}$pH is used; and if the electrode is calibrated in the same solvent in which the "pH" reading is made, then the term ${}^{s}_{s}$pH is used. In methanol, ${}^{s}_{s}$pH = ${}^{s}_{w}$pH − (-2.24) and since the autoprotolysis constant of methanol is $10^{-16.77}$ M^2, neutral ${}^{s}_{s}$pH is 8.4. In ethanol, ${}^{s}_{s}$pH = ${}^{s}_{w}$pH − (-2.54) and since the autoprotolysis constant of ethanol is $10^{-19.1}$ M^2, the neutral ${}^{s}_{s}$pH is 9.6.

[19] Siddiqi, Z. A., Kumar, S., Khalid, M., Shahid, M. *Spectrochim. Acta, Part A* **2009**, *71*, 1845.

[20] (a) Gibson, G.; Neverov, A. A.; Brown, R. S. *Can. J. Chem.* **2003**, *81*, 495. (b) Gibson, G. T. T.; Mohamed, M. F.; Neverov, A. A.; Brown, R. S. *Inorg. Chem.* **2006**, *45*, 7891.

[21] Li, C.; Tian, H.; Duan, S.; Liu, X.; Xu, P.; Qiao, R.; Zhao, Y. *J. Phys. Chem. B* **2011**, *115*, 13350.

[22] Gibson, G. T. T. *Metal Ion Speciation in Methanol and Ethanol Determined by Potentiometric Titration and its Relevance to Metal Ion-Catalyzed Alcoholysis Reactions.* Ph.D. Dissertation, Queen's University, Kingston, Ontario, Canada, 2006.

[23] Liu, C. T.; Neverov, A. A.; Brown, R. S. *J. Am. Chem. Soc.* **2008**, *130*, 1671.

[24] Harned, H. S.; Owen, B. B. *The Physical Chemistry of Electrolytic Solution*; ACS Monograph Series 137, 3rd ed.; Reinhold Publishing: New York, NY, 1957, p 161.

[25] (a) ${}^{s}_{s}$pH values in ethanol were determined as discussed in references 18 and 20. (b) The first macroscopic ${}^{s}_{s}pK_a$ of Ni(II)-coordinated ethanol is 8.65 by as determined by a half-neutralization experiment at $[Ni(ClO_4)_2]$ = 1 mM; the second macroscopic ${}^{s}_{s}pK_a$ is 8.95. Such a steep titration profile indicates strong correlation between first and second dissociation steps, possibly due to a dimerization or oligomerization process involving M(II):($^{-}$OR) as has been previously observed for some metal ions in methanol and ethanol (reference 20).

[26] It has been previously observed that, in the case of Zn^{2+} ions, binding of the second ligand tends to be stronger than the first. For example, the sequential binding constants of chloride anions to Zn^{2+} in methanol are equal to $K_1 = 7.76 \times 10^3$ M^{-1} and $K_2 = 1.71 \times 10^4$ M^{-1}.[27] This cooperative effect is often thought to be a consequence of the change in coordination sphere as a result of binding the first ligand.

[27] Doe, H.; Kitagawa, T. K. *Inorg. Chem.* **1982**, *21*, 2272.

[28] In the low ${}^{s}_{s}$pH domain of the log(k_2) plot, the data begin to curve downward (lowest ${}^{s}_{s}$pH datum omitted) which may be indicative of weakened binding between Ni^{2+} and **4.2** due to the onset of competitive protonation of the benzimidazole nitrogens. This process, however, does not appear to affect the overall activity of the complex (k_{max}).

[29] In the case of strong interactions between the metal ion and substrate, the determination of the binding constant is inherently difficult and often only a lower limit can be defined with any certainty.

[30] IUPAC. *Compendium of Chemical Terminology*, 2nd ed. (the "Gold Book"), Compiled by A. D. McNaught and A. Wilkinson. Blackwell Scientific Publications, Oxford, U.K., 1997. XML on-line corrected version: http://goldbook.iupac.org 2006 – created by Nic, M.; Jirat, J.; Kosata, B.; updates compiled by Jenkins, A. ISBN 0967855098. DOI:10.1351/goldbook.

[31] While intermolecular and intramolecular attack of methoxide are kinetically indistinguishable processes, the latter process is most likely based on the results with the Cu(II) complex.

[32] Rabinovich, V. A.; Khavin, Z. *Concise Handbook of Chemistry*; Khimiya: Leningrad, 1977 [in Russian].

[33] Kapinos, L. E.; Sigel, H. *Inorg. Chim. Acta* **2002**, *337*, 131.

[34] Kapinos, L. E.; Song, B.; Sigel, H. *Chem. Eur. J.* **1999**, *5*, 1794.

[35] The apparent $k_2^{^{-}OR}$ rate constant for attack of alkoxide on the M(II) complex of **4.1** or **4.2** is given as $k_2 = k_{max}^{obs} \cdot ({}^{s}_{s}K_a/({}^{s}_{s}K_a + [H^+]))$[16,17]. Under conditions where $[H^+] > {}^{s}_{s}K_a$ (or ${}^{s}_{s}pH < {}^{s}_{s}pK_a$), the reaction is first order in $[^{-}OR]$ since $k_2 = k_{max}^{obs} \cdot {}^{s}_{s}K_a/[H^+] = k_{max}^{obs} \cdot ({}^{s}_{s}K_a/(K_{auto}))[^{-}OCH_3]$. Given ${}^{s}_{s}pK_a$ values of 5.79 for formation of **4.1**:Cu(II):($^{-}OCH_3$), and 8.36 for formation of **4.2**:Zn(II):($^{-}OCH_3$) and an autoprotolysis constant for methanol of $K_{auto} = 10^{-16.77}$ M^2, one computes that $k_2^{\mathbf{4.1}:Cu(II)} = 5.7 \times 10^8$ $M^{-1} \cdot s^{-1}$ while $k_2^{\mathbf{4.2}:Zn(II)}$ is 1.5×10^5 $M^{-1} \cdot s^{-1}$.

[36] (a) Bachviser, S. F; Gehlen, M. H. *J. Chem. Soc., Faraday Trans.* **1997**, *93*, 1133. (b) Zanini, G. P.; Montejano, H. A.; Previtali, C. M. *J. Chem. Soc., Faraday Trans.* **1995**,

91, 1197. (c) Marshall, D. B.; Eyring, H. M.; Strohbusch, F.; White, R. D. *J. Am. Chem. Soc.* **1980**, *102*, 7065.

[37] Schwartz, H. A.; Gill, P. S. *J. Chem. Phys.* **1977**, *81*, 22.

[38] Phan, T. B.; Mayr, H. *Can. J. Chem.* **2005**, *83*, 1554.

[39] (a) Schowen, R. L; Behn, G. C. *J. Am. Chem. Soc.* **1968***, 90,* 5839, (220 ± 100 $M^{-1}\cdot s^{-1}$, 27.2 °C). (b) Guanti, G.; Cevasco, G.; Thea, S; Dell'Erba, C; Petrillo, G. *J. Chem. Soc., Perkin Trans. 2* **1981**, 327, (107 ± 2 $M^{-1}\cdot s^{-1}$, 22 °C).

[40] Wolfenden, R. *Nature* **1969**, *223*, 704.

[41] For applications of this to phosphate cleavage and other reactions see: (a) Yatsimirsky, A. K. *Coord. Chem. Rev*. **2005**, *249*, 1997 and references therein. (b) Iranzo, O.; Kovalevsky, A. Y.; Morrow, J. R.; Richard, J. P. *J. Am. Chem. Soc.* **2003**, *125*, 1988. (c) Bunn, S. E.; Liu, C. T.; Lu, Z.-L.; Neverov, A. A.; Brown, R. S. *J. Am. Chem. Soc.* **2007**, *129*, 16239. (d) Liu, C. T.; Neverov, A. A.; Brown, R. S. *J. Am. Chem. Soc.* **2008**, *130*, 16711.

[42] While the actual reaction must proceed through the bound form of **S**:M(II):($^{-}$OR), the experimental kinetic regime did not allow us to determine the actual binding constants for this species. Hence, for the purposes of determining the energetics associated with the process described in Scheme 4-2, the third order rate constant was determined as the average of the second order rate constant for metal dependence at each $^{s}_{s}$pH divided by the [$^{-}$OR].

[43] Liu, C. T.; Maxwell, C. I.; Pipe, S. G.; Neverov, A. A.; Mosey, N. J.; Brown, R. S. *J. Am. Chem. Soc.* **2011**, *133*, 20068.

Chapter 5 – Palladacycle-promoted methanolysis of a series of tertiary thiobenzanilides: Involvement of a second catalyst facilitates leaving group departure

5.1 – Preface

The kinetic experiments and spectrophotometric titrations for this chapter were performed by Mark Raycroft. The syntheses were performed by Mark Raycroft, Ms. Stephanie Pipe, and Dr. C. Tony Liu.

5.2 – Introduction

Metalloaminopeptidases employ one or two metal ions in their active sites in order to cleave amide bonds, enabling protein modification and degradation.[1] The considerable rate accelerations of peptide bond cleavage provided by this as well as other classes of metal-containing peptidases suggest several modes of metallo-catalysis are employed in a highly-tuned, well-defined manner. In solution, on the other hand, small-molecule catalysts suffer from poor binding affinities to amide substrates and scarcely provide assistance to the departing group resulting in only modest rate accelerations for cleavage. While La^{3+} and Zn^{2+} ions have been shown to efficiently catalyze the alcoholysis of phosphate and carboxylate esters[2] as well as some highly-activated carboxamides,[3] they fare poorly in the catalysis of unactivated amide bond cleavage. Especially in cases where leaving group departure is rate-limiting, it may be critical for a Lewis or Brønsted acid to be strategically positioned in order to assist LG departure with only minor conformational changes required of the catalyst. To gain insight into the necessity for LGA, employment of a thioamide substrate may be useful given that, in the presence of a soft metal ion, the

soft-soft interaction between substrate and catalyst could drastically enhance binding and permit the investigation of the steps subsequent to binding. Compared to amides, thioamides exhibit greater double-bond character between the C and N resulting in additional hindrance to rotation (by ~5–7 kcal·mol^{-1}) about the C–N bond.[4] While the addition of a nucleophile to the C=S group is generally more rapid than to C=O,[5] thioamides tend to be more resistant to solvolytic and enzymatic cleavage (unless the enzyme is substituted with a metal ion of higher thiophilicity).[6,7] Together, these observations point to rate-limiting LG departure in the solvolysis of thioamides.

Palladacycle **5.2** was shown to efficiently cleave a series of phosphorothioate triesters with different phenolic LGs.[8] Throughout the substrate series, the departing phenoxide is sufficiently stabilized (intrinsically) to negate the requirement for assistance from the metal ion. However in the solvolysis of thiobenzanilides, LG departure is rate-limiting[6] and because the anilide LG is sufficiently unstable to depart on its own, LGA may be requisite for efficient cleavage. In such a case, the hard/soft characteristics of the metal ion as well as its azophilicity may be important considerations in catalyst design. Indeed, the abovementioned palladacycle exhibits 10^8-fold acceleration over the methoxide-promoted cleavage of *N*-methyl-*N*-(4-nitrophenyl)-thiobenzamide **5.1b** (Scheme 5-1).[9] A combination of experimental and theoretical data reveals the important features exhibited by the catalyst for promoting methanolysis are:

1. Electrophilic activation of the C=S unit.
2. Nucleophile activation and delivery.
3. Stabilization of the tetrahedral intermediate.
4. Assistance to the departure of the anilide LG.

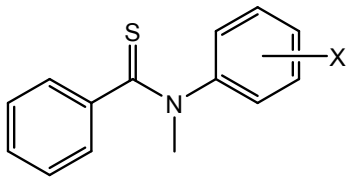

5.1a X = 3,5-diNO_2
5.1b X = 4-NO_2
5.1c X = 3-NO_2
5.1d X = 4-Cl
5.1e X = H

Scheme 5-1. Overall reaction for the palladacycle-catalyzed methanolysis of *N*-methyl-*N*-(4-nitrophenyl)thiobenzamide forming methyl thiobenzoate (MTB) and *N*-methyl-4-nitroaniline (NMA-H).

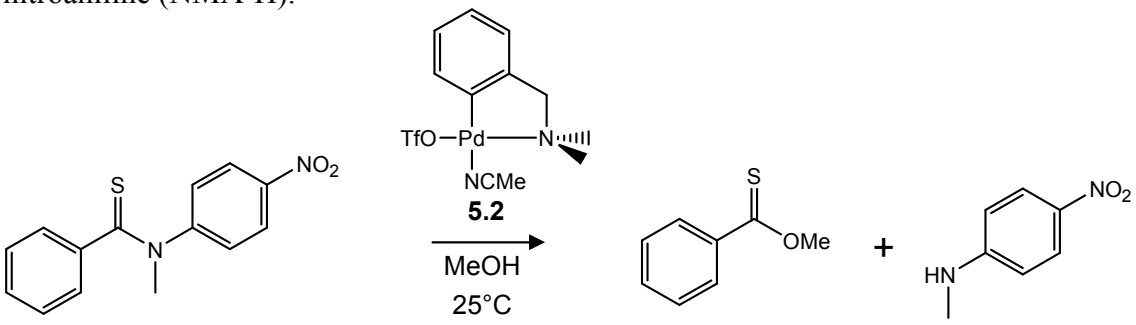

The current study expands upon the abovementioned report through the kinetic analysis of the palladacycle-promoted cleavage of thiobenzanilides **5.1a**–**e**. The dependence of the rate constants for cleavage on catalyst concentration, $^{s}_{s}$pH, and Hammett parameters clarify the cleavage mechanism and identify changes in mechanism as a function of LG structure.

5.3 – Experimental

5.3.1 – Materials

Triethylamine (99%), palladium chloride (≥99.9%), silver trifluoromethanesulfonate (≥99.9%), benzoyl chloride (≥99%), phosphorus pentasulfide (99%), *N*-methyl-4-nitroaniline (97%), 3-nitroaniline (98%), *N*-methylaniline (98%), potassium hydroxide

(≥90% flakes), iodomethane (99%), *N*-ethylmorpholine (97%), and 2,2,6,6-tetramethylpiperidine (≥99%) were obtained from Aldrich. Tetrabutylammonium hydroxide (1.0 M solution in methanol, titrated against N/2 Fisher Certified standard aqueous HCl solution and found to be 1.05 M) and trifluoromethanesulfonic acid (HOTf, ≥99%) were also acquired from Aldrich. Sodium bicarbonate (≥99.7%) was purchased from Sigma, *N*,*N*-dimethylbenzylamine (99%) was purchased from Acros Organics, and methanol-D_4 (99.8% D) was obtained from Cambridge Isotope Laboratories. 1-Methylpiperidine (99%), 3,5-dinitroaniline (≥98%), and 4-chloro-*N*-methylaniline (≥97%) were purchased from TCI America Laboratory Chemicals. Methanol (99.8%, anhydrous), acetonitrile (99.8%, anhydrous), and tetrahydrofuran (≥99.9%, anhydrous) were purchased from EMD Chemicals. Dichloromethane (≥99.5%), ethyl acetate (≥99.5%), and pentane (98%) were purchase from ACP Chemicals. Acetone (≥99.5%) and ethanol (95%) were purchased from Fisher Scientific and Commercial Alcohols, respectively.

5.3.2 – General methods

All ^{1}H NMR spectra were determined at 400 MHz and ^{13}C NMR spectra at 100.66 MHz; all chemical shift values were referenced internally to the solvent. All mass spectra were determined by EI+ TOF. $CH_3OH_2^+$ concentrations were determined potentiometrically using a combination glass Fisher Scientific Accumet electrode model no. 13-620-292 calibrated with certified standard aqueous buffers (pH 4.00 and 10.00) as described previously.[10] The $^{s}_{s}$pH values in methanol were determined by subtracting a correction constant of -2.24 from the electrode readings and the autoprotolysis constant for

methanol was taken to be $10^{-16.77}$ M^{2}.[11] The $^{s}_{s}$pH values for the kinetic experiments were measured at the end of the reactions to avoid the effect of KCl leaching from the electrode.

5.3.3 – Synthesis of materials

3.3.3.1 – Thiobenzanilides (**5.1a**–**e**)

All thiobenzanilides were prepared using several literature sources.[6,12] An exemplary procedure is described below. In the cases of **5.1b**, **5.1d**, and **5.1e**, the substituted *N*-methylanilines were commercially available, thus enabling circumvention of the methylation step.

Thiobenzanilide **5.1c** was synthesized by first mixing 3.81 g (27.6 mmol) of 3-nitroaniline with 3.53 mL (30.4 mmol) of benzoyl chloride in 50 mL dry THF. The cloudy mixture was heated to reflux for 2 hours, at which point the solution turned light brown. After the mixture cooled to room temperature, it was washed with 30 mL saturated aqueous $NaHCO_3$ solution (2×), 30 mL of 1 M aqueous HCl solution (2×), and 30 mL of DI H_2O (2×). After removing all the organic solvent, the secondary amide was recrystallized from 8:2 ethanol:water, yielding 5.8 g (23.9 mmol, 87% yield). In the next step, 1.81 g (7.48 mmol) of the secondary amide, 1.4 mL (22.4 mmol) of iodomethane, and 0.93 g (14.9 mmol) of crushed KOH were combined in 40 mL of HPLC grade acetone and refluxed for 10 minutes. After the mixture cooled to room temperature, the remaining solids were filtered off. The solvent was removed before purifying the product by flash chromatography using a 3:7 ratio of ethyl acetate and pentane. The isolated

product was further purified by recrystallization out of 6:4 ethanol:water to obtain the methylated product in 1.81 g (7.06 mmol, 94% yield). In the final step, 1.51 g (5.87 mmol) of tertiary amide and 3.13 g (7.04 mmol) of phosphorus pentasulfide were mixed in 30 mL dry THF and stirred at 35 °C for 1 hour and sonicated for 1 hour. The solid was then filtered off and the solvent was removed under vacuum. After extracting the product into dichloromethane, the concentrated solution was purified with flash chromatography using an 8:2 ratio of dichloromethane and pentane. Recrystallization out of 6:4 ethanol:water yielded 0.40 g (1.47 mmol, 25% yield) of *N*-methyl-*N*-(3-nitrophenyl)thiobenzamide **5.1c**.

Spectral data for **5.1a** and **5.1c** are listed below; those for **5.1b**, **5.1d**, **5.1e** are consistent with previous reports.[6,12]

***N*-Methyl-*N*-(3,5-dinitrophenyl)thiobenzamide (5.1a)**

^{1}H NMR (400 MHz, CD_3OD, 25 °C): δ 8.77 (t, 1H, Ar–H, J = 2.5 Hz), 8.48 (d, 2H, Ar–H, J = 1.8 Hz), 7.33 (m, 2H, Ph–H), 7.21 (m, 3H, Ph–H), 3.91 (s, 3H, CH_3); ^{13}C NMR (100.66 MHz, CD_3OD, 25 °C): δ 204.7, 149.53, 149.46, 144.0, 129.8, 128.8, 128.59, 128.56, 117.6, 45.8; HRMS(EI+ TOF): calculated for $C_{14}H_{11}N_3O_4S$: 317.0470 amu, found 317.0467 amu; λ_{max} (CH_3OH): 232 nm (ε = 24000 $M^{-1}\cdot cm^{-1}$), 290 nm (ε = 12600 $M^{-1}\cdot cm^{-1}$); melting point: 169–172 °C.

***N*-Methyl-*N*-(3-nitrophenyl)thiobenzamide (5.1c)**

^{1}H NMR (400 MHz, CD_3OD, 25 °C): δ 8.04 (m, 2H, Ph–H), 7.55 (d, 1H, Ar–H, J = 7.8 Hz), 7.48 (m, 1H, Ar–H), 7.25 (m, 2H, Ar–H), 7.14 (m, 3H, Ph–H); ^{13}C NMR (100.66

MHz, CD_3OD, 25 °C): δ 205.0, 149.8, 148.9, 144.8, 134.0, 131.4, 129.9, 129.0, 128.8, 123.1, 122.9, 46.4; HRMS(EI+ TOF): calculated for $C_{14}H_{12}N_2O_2S$: 272.0620 amu, found 272.0611 amu; λ_{max} (CH_3OH): 246 nm (ε = 17065 $M^{-1}\cdot cm^{-1}$), 280 nm (ε = 15550 $M^{-1}\cdot cm^{-1}$); melting point: 126–128 °C.

3.3.3.2 – Pd(*N*,*N*-dimethylbenzylamine)(CH_3CN)(OSO_2CF_3) (**5.2**)

The palladacycle complex, Pd(*N*,*N*-dimethylbenzylamine)(CH_3CN)(OSO_2CF_3), was synthesized and characterized as previously reported.[13]

5.3.4 – General UV-vis titrations

All spectrophotometric titration experiments were conducted using a Cary Bio 100 UV-vis spectrophotometer with the cell compartment thermostatted at 25.0 ± 0.1°C. A typical titration experiment involved preparation of a methanol solution containing triflic acid[14] (0.1 mM), **5.1** (0.04 mM), followed by 10-μL additions of **5.2** (0.004–0.08 mM) in a 1-cm path length quartz cuvette. A scan from 500 to 200 nm was recorded after each addition. Absorbance values at the λ_{max} for the **5.2**:**5.1** complex were corrected for both dilution and absorbance due to **5.2** and plotted as a function of [**5.2**]. The data were fitted to a strong binding equation[15] to yield K_b in units of M^{-1}.

5.3.5 – General UV-vis kinetics

All kinetic experiments were conducted using a Cary Bio 100 UV-vis spectrophotometer with the cell compartment thermostatted at 25.0 ± 0.1°C. The reactions were conducted in the presence of buffers composed of various ratios of amine and HOTf to maintain

the ${}^{s}_{s}$pH in methanol (*N*-ethylmorpholine ${}^{s}_{s}$pH 8.5, 9.2; *N*-methylpiperidine ${}^{s}_{s}$pH 9.6, 10.2, 10.6; *N*,*N*,*N'*,*N'*-tetramethylpiperidine ${}^{s}_{s}$pH 11.1, 11.5, 11.7). In the high-${}^{s}_{s}$pH domain, excess tetrabutylammonium methoxide (0.6 mM ${}^{s}_{s}$pH 13.5, 6 mM ${}^{s}_{s}$pH 14, 16 mM ${}^{s}_{s}$pH 14.5) was used to maintain the ${}^{s}_{s}$pH in methanol. A typical kinetic experiment for the methanolysis of **5.1** involved preparation of a methanol solution containing buffer (4 mM), **5.1** (0.04 mM), and **5.2** (0.01–0.15 mM) in a 1-cm path length quartz cuvette. The reaction was initiated by the addition of an aliquot of **5.2** to the buffered solution containing **5.1** to achieve the desired concentrations of the reaction components at a final volume of 2.5 mL. All experiments were performed in duplicate. The palladacycle-promoted methanolyses of **5.1a**, **5.1b**, and **5.1c** were monitored at 415 nm, 385 nm, and 400 nm, respectively, for the appearance of the corresponding *N*-methylaniline. Those of **5.1d** and **5.1e** were monitored at 260 nm for the appearance of the corresponding *N*-methylaniline. Due to the occurrence of product inhibition, the data were treated using the initial rates method wherein the first 5–10% of the absorbance versus time traces for the appearance of product was fitted with a linear regression to generate an initial rate in units of $Abs \cdot s^{-1}$. To obtain the k_{obs} values in units of s^{-1}, the initial rate was divided by the total absorbance change for the reaction.

5.3.6 – Product analysis

Formation of the substituted *N*-methylaniline product was confirmed by comparison of the UV-vis or ^{1}H NMR spectrum of the product mixture with those of the authentic materials.

5.4 – Results

5.4.1 – Binding constants

Binding constants were determined via spectrophotometric titration of **5.1** with **5.2** as shown in Figure 5-1. All five thiobenzanilides bind to **5.2** in a 1:1 fashion and exhibit tight binding ($K_b > 10^5$ M^{-1}); their binding profiles can be found in Supporting Information 5-1. The magnitude of the binding constants decreases with increasing electron-withdrawing ability of the substituent on the aniline group, represented in the form of a Hammett plot in Figure 5-2 and tabulated in Table 5-1.

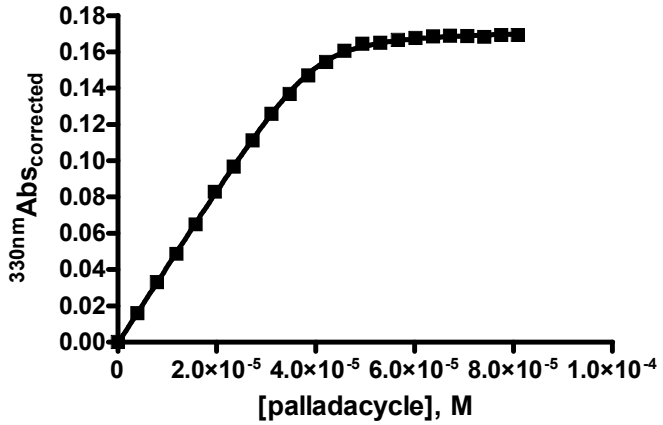

Figure 5-1. Exemplary plot of absorbance (at 330 nm, corrected for dilution as well as absorbance due to the added complex) for the **5.2**:**5.1c** complex vs [**5.2**] where [**5.1c**] = 0.04 mM and [HOTf] = 0.1 mM[14] in anhydrous methanol at 25 °C. The data are fitted to a NLLSQ relationship[15] computing $K_b = 10^{6.15\pm0.03}$ M^{-1}; $r^2 = 0.9998$.

Table 5-1. Logarithm of the binding constants for **5.2**:**5.1** at [HOTf] = 0.1 mM[14] in anhydrous methanol at 25 °C.

Substrate	$\log(K_b, M^{-1})$
5.1a	5.38 ± 0.04
5.1b	6.14 ± 0.06
5.1c	6.15 ± 0.03
5.1d	6.8 ± 0.1
5.1e	6.9 ± 0.2

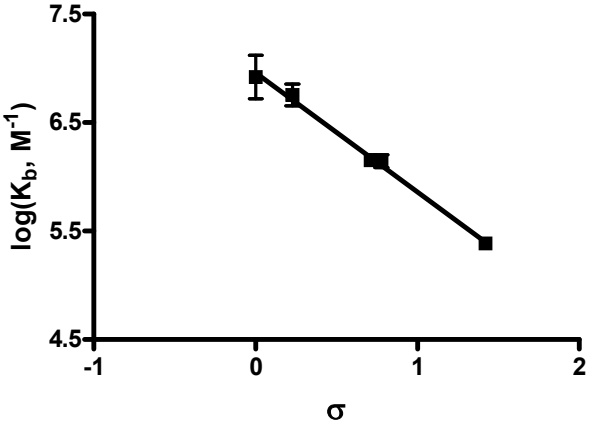

Figure 5-2. Hammett plot of $\log(K_b)$ for **5.2**:**5.1a**–**e** vs σ where [HOTf] = 0.1 mM[14] in anhydrous methanol at 25 °C. The data are fitted to a linear regression computing $\rho = -1.10 \pm 0.04$; $r^2 = 0.9960$.

5.4.2 – Catalyst concentration-k_{obs} profiles

*Catalyst concentration-k_{obs} profiles for the **5.2**-promoted methanolysis of **5.1a** and **5.1b***

The rate of the palladacycle-promoted methanolysis of **5.1a** was studied in the ${}^{s}_{s}$pH range of 7.8 to 10.0 (Figure 5-27 to Figure 5-31, Supporting Information 5-3). The dependence of the observed rate constant on [catalyst] exhibits saturation kinetics (Figure 5-3) and can therefore be modelled using a one-site universal binding equation[16] computing values for k_{max} and K_b. To maintain consistency in fitting among the different substrates, the second order rate constant was derived from the linear relationship between the first four data points. At higher concentrations of alkoxide (${}^{s}_{s}$pH $\geq$ 10), a form of inhibition becomes apparent through the downward curvature of the saturation profile and may also affect the steepness of the plots observed at lower ${}^{s}_{s}$pH. Mass spectral data support the formation of palladacycle dimers in the alkaline domain. Because **5.1a** is the weakest binding of the five substrates under investigation, it is anticipated that formation of the 1:1 catalyst-substrate complex at high ${}^{s}_{s}$pH would be most highly affected by this dimerization of the five substrates under investigation.

The palladacycle-promoted methanolysis of **5.1b** was studied in the ${}^{s}_{s}$pH range of 8.2 to 10.6 (Figure 5-32 to Figure 5-36, Supporting Information 5-3). Like **5.1a**, the dependence of the observed rate constant on [catalyst] exhibits saturation kinetics and can be modelled using a one-site universal binding equation[16] (Figure 5-3).

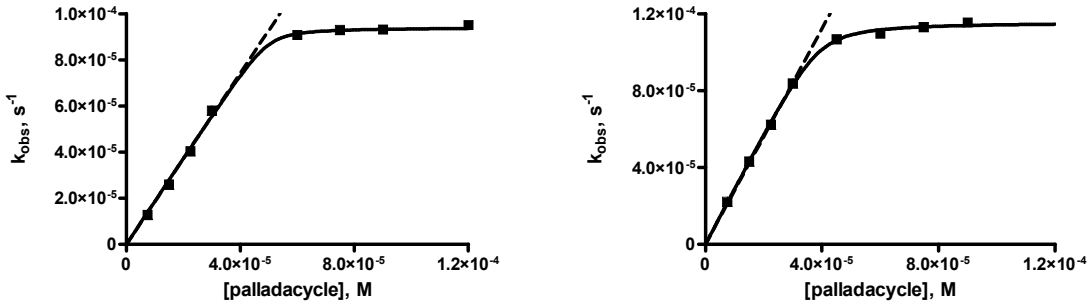

Figure 5-3. (Left) Plot of k_{obs} for the cleavage of **5.1a** (4×10^{-5} M) vs [**5.2**] buffered at ${}^{s}_{s}$pH 7.8 (4 mM *N*-ethylmorpholine, 2.5 mM HOTf) in anhydrous methanol at 25 °C. The data are fitted to a NLLSQ[16] relationship computing $k_{max} = (9.4 \pm 0.1) \times 10^{-5}$ s^{-1} and $K_b = 10^{6.5\pm6.5}$ M^{-1}; $r^2 = 0.9980$. The data in the catalyst-dependent region are fitted to a linear regression computing $k_2 = (1.86 \pm 0.05)$ $M^{-1}\cdot s^{-1}$. (Right) Plot of k_{obs} for the cleavage of **5.1b** (4×10^{-5} M) vs [**5.2**] buffered at ${}^{s}_{s}$pH 8.3 (4 mM *N*-ethylmorpholine, 2 mM HOTf) in anhydrous methanol at 25 °C. The data are fitted to a NLLSQ[16] relationship computing $k_{max} = (1.15 \pm 0.01) \times 10^{-4}$ s^{-1} and $K_b = 10^{6.2\pm5.8}$ M^{-1}; $r^2 = 0.9986$. The data in the catalyst-dependent region are fitted to a linear regression computing $k_2 = (2.80 \pm 0.02)$ $M^{-1}\cdot s^{-1}$.[17]

*Catalyst concentration-k_{obs} profiles for the **5.2**-promoted methanolysis of **5.1c-e***

The **5.2**-promoted methanolyses of **5.1c**–**e** exhibit two domains that carry different nonzero dependences on catalyst concentration (Figure 5-37 to Figure 5-54, Supporting Information 5-3). In the domain where [catalyst] < [substrate], k_{obs} is second-order in [catalyst] and can be fitted to equation 5-1. In the domain where [catalyst] > [substrate], k_{obs} is first-order in [catalyst] and can be fitted to equation 5-2. In the cases of **5.1d** and **5.1e**, backward extrapolation of the linear relationship intersects the horizontal axis at [catalyst] ≈ 4×10^{-5} M (exemplary plots shown in Figure 5-4). Conversely, in the case of **5.1c**, backward extrapolation of the linear domain intersects the vertical axis (Figure 5-5).

$$k_{obs} = k_2[\mathbf{5.2}] + k_3[\mathbf{5.2}]^2 \qquad (5\text{-}1)$$

$$k_{obs} = k_2[\mathbf{5.2}] + k_{\max} \qquad (5\text{-}2)$$

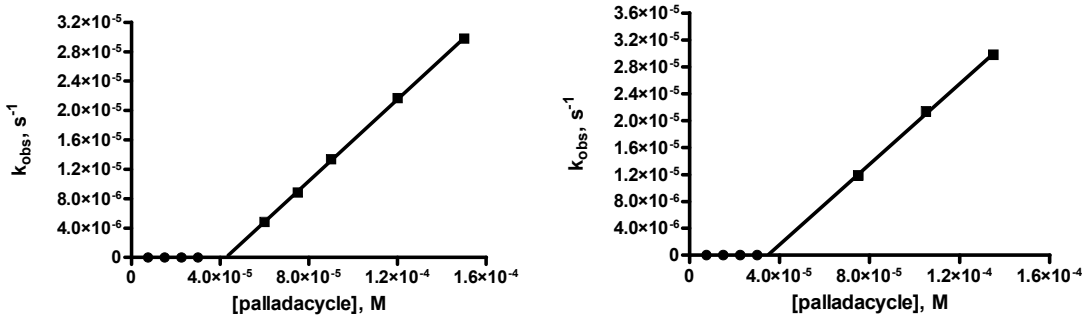

Figure 5-4. (Left) Plot of k_{obs} for the cleavage of **5.1d** (4×10^{-5} M) vs [**5.2**] buffered at ${}^{s}_{s}$pH 8.2 (4 mM *N*-ethylmorpholine, 2 mM HOTf) in anhydrous methanol at 25 °C. The ■-data are fitted to a linear regression computing $k_2 = (0.278 \pm 0.002)$ $M^{-1}{\cdot}s^{-1}$; $r^2 = 0.9998$. (Right) Plot of k_{obs} for the cleavage of **5.1e** (4×10^{-5} M) vs [**5.2**] buffered at ${}^{s}_{s}$pH 8.2 (4 mM *N*-ethylmorpholine, 2 mM HOTf) in anhydrous methanol at 25 °C. The ■-data are fitted to a linear regression computing $k_2 = (0.30 \pm 0.01)$ $M^{-1}{\cdot}s^{-1}$; $r^2 = 0.9988$. In both plots, the ●-data represent the second-order dependence of k_{obs} on [**5.2**].

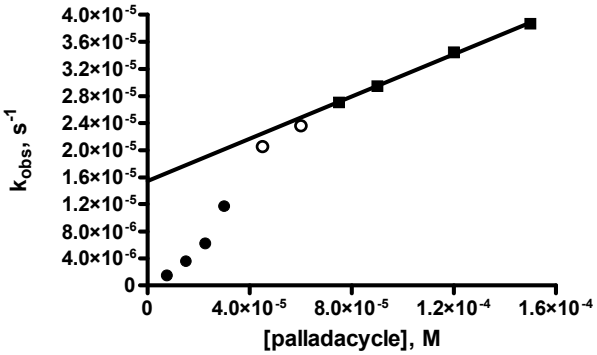

Figure 5-5. Plot of k_{obs} for the cleavage of **5.1c** (4×10^{-5} M) vs [**5.2**] buffered at ${}^{s}_{s}$pH 8.3 (4 mM *N*-ethylmorpholine, 2 mM HOTf) in anhydrous methanol at 25 °C. The ■-data are fitted to a linear regression computing $k_2 = (0.156 \pm 0.004)$ $M^{-1}{\cdot}s^{-1}$ and $k_{max} = (1.54 \pm 0.05) \times 10^{-5}$ s^{-1}; $r^2 = 0.9984$. The ●-data represent the second-order dependence of k_{obs} on [**5.2**]; the ○-data represent the transition from second-order to first-order dependence of k_{obs} on [**5.2**].

*Dependence of horizontal axis-intercept on [**5.1**]*

The concentration of **5.2** at which the transition occurs from second-order to first-order behaviour changes with corresponding changes in [**5.1**]. Catalyst concentration vs k_{obs}

plots produced with **5.1d** reveal changes in the [**5.2**]-axis intercept as shown in Figure 5-6 with the values tabulated in Table 5-2.

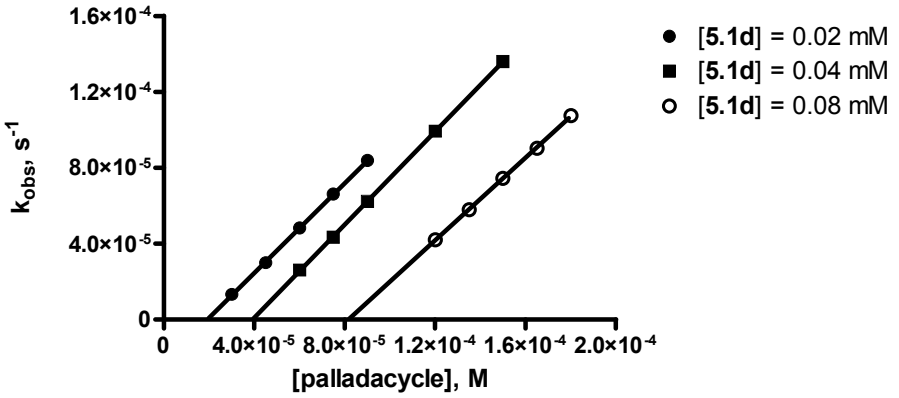

Figure 5-6. Plot of k_{obs} for the cleavage of **5.1d** vs [**5.2**] buffered at ${}^{s}_{s}$pH 9.1–9.2 (4 mM *N*-ethylmorpholine, 0.5 mM HOTf) in anhydrous methanol at 25 °C. The ●-data are fitted to a linear regression computing $k_2 = (1.18 \pm 0.01)\ M^{-1}\cdot s^{-1}$ and [**5.2**]-axis intercept = $(1.9 \pm 0.1) \times 10^{-5}$ M; $r^2 = 0.9998$. The ■-data are fitted to a linear regression computing $k_2 = (1.226 \pm 0.006)\ M^{-1}\cdot s^{-1}$ and [**5.2**]-axis intercept = $(3.9 \pm 0.1) \times 10^{-5}$ M; $r^2 = 0.9999$. The ○-data are fitted to a linear regression computing $k_2 = (1.087 \pm 0.009)\ M^{-1}\cdot s^{-1}$ and [**5.2**]-axis intercept = $(8.2 \pm 0.2) \times 10^{-5}$ M; $r^2 = 0.9998$.

Table 5-2. Second order rate constants and [**5.2**]-axis intercepts for the cleavage of **5.1d** vs [**5.2**] buffered at ${}^{s}_{s}$pH 9.1–9.2 in anhydrous methanol at 25 °C.

[**5.1d**] ($10^5 \times$ M)	[**5.2**]-axis intercept ($10^5 \times$ M)	k_2 ($M^{-1}\cdot s^{-1}$)	${}^{s}_{s}$pH
2.0	1.9 ± 0.1	1.18 ± 0.01	9.1
4.0	3.9 ± 0.1	1.226 ± 0.006	9.2
8.0	8.2 ± 0.2	1.087 ± 0.009	9.1

5.4.3 – $^{s}_{s}$pH-log(k_2) profiles for the 5.2-promoted methanolysis of 5.1a–e

The gradient of the linear domains of each catalyst concentration-k_{obs} plot represents the second order rate constants (k_2) for cleavage. The logarithms of the k_2 values for the **5.2**-promoted methanolyses of **5.1a–e** exhibit linear dependences on $^{s}_{s}$pH (Figure 5-7). All profiles have a gradient of approximately unity (Supporting Information 5-2).

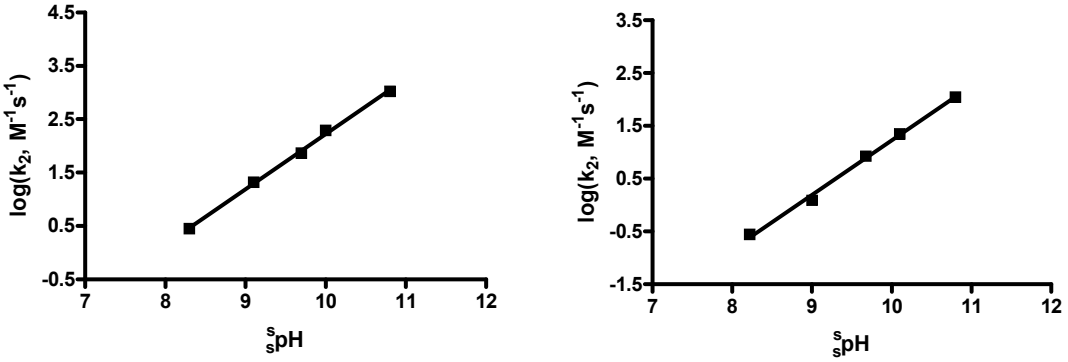

Figure 5-7. (Left) Plot of log(k_2) for the palladacycle-promoted cleavage of **5.1b** (4×10^{-5} M) vs $^{s}_{s}$pH in anhydrous methanol under buffered conditions (4 mM amine, various concentrations of HOTf) at 25 °C. The line through the data is generated from a linear regression to provide a slope of 1.03 ± 0.03; $r^2 = 0.9977$. (Right) Plot of log(k_2) for the palladacycle-promoted cleavage of **5.1d** (4×10^{-5} M) vs $^{s}_{s}$pH in anhydrous methanol under buffered conditions (4 mM amine, various concentrations of HOTf) at 25 °C. The line through the data is generated from a linear regression to provide a slope of 1.03 ± 0.04; $r^2 = 0.9963$.

5.4.4 – $^{s}_{s}$pH-log(k_3) profiles for the 5.2-promoted methanolysis of 5.1c–e

Fitting the [catalyst] < [substrate] domains of the catalyst concentration-k_{obs} plots for **5.1c–e** generates third order rate constants (k_3) for cleavage. The logarithms of the k_3 values for the **5.2**-promoted methanolyses of **5.1c–e** exhibit linear dependences on $^{s}_{s}$pH (Figure 5-8). All profiles have a gradient of approximately unity (Supporting Information 5-2).

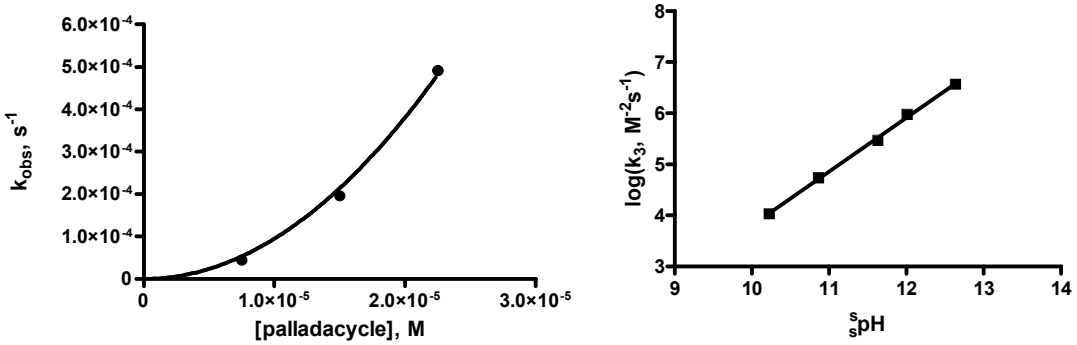

Figure 5-8. (Left) Exemplary plot of k_{obs} for the cleavage of **5.1e** in the [catalyst] < [substrate] domain vs [**5.2**] buffered at ${}^{s}_{s}$pH 10.0 (4 mM *N*,*N*,*N'*,*N'*-tetramethylpiperidine, 2 mM HOTf) in anhydrous methanol at 25 °C. The data are fitted to equation 5-1 computing $k_3 = (9.5 \pm 0.3) \times 10^5$ $M^{-2} \cdot s^{-1}$; $r^2 = 0.9950$. (Right) Plot of $\log(k_3)$ for the palladacycle-promoted cleavage of **5.1e** (4×10^{-5} M) vs ${}^{s}_{s}$pH in anhydrous methanol under buffered conditions (4 mM amine, various concentrations of HOTf) at 25 °C. The line through the data is generated from a linear regression to provide a slope of 1.05 ± 0.02; $r^2 = 0.9981$.

5.4.5 – ${}^{s}_{s}$pH-log(k_{max}) profiles for the 5.2-promoted methanolysis of 5.1a–c

The k_{max} values for the cleavage of **5.1a** and **5.1b** are determined directly from the fitting. In the case of **5.1c**, k_{max} is determined from the extrapolation of the linear dependence back to the vertical axis. The logarithms of the maximum observed rate constants for the palladacycle-promoted methanolyses of **5.1a–c** exhibit linear dependences on ${}^{s}_{s}$pH. All profiles have a slope of approximately unity (Supporting Information 5-2).

5.4.6 – Hammett plots

Hammett plot (k_2^{MeO-})

The dependence of k_{max} on [alkoxide] yields a linear relationship from which a second order rate constant can be derived (k_2^{MeO-}). The relationship between the logarithm of k_2^{MeO-} for the palladacycle-promoted methanolyses of **5.1a–c** and the substituent constant, σ^-, is linear exhibiting a ρ^- value of 1.45 (Figure 5-9).

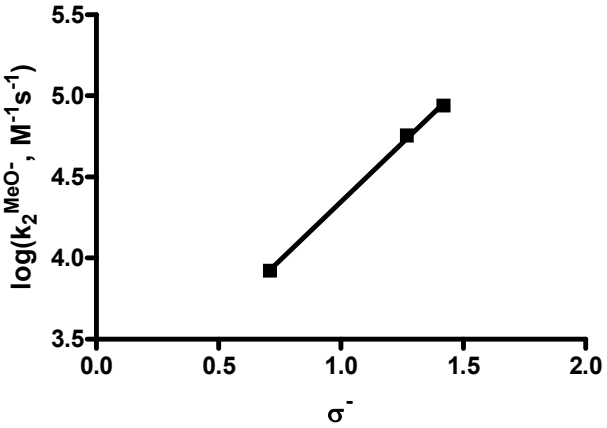

$$v = k_2^{MeO^-}[\mathbf{5.2 : 5.1}][MeO^-]$$
$$v = k_{obs}[\mathbf{5.2 : 5.1}]$$
$$k_{obs} = k_2^{MeO^-}[MeO^-]$$

Figure 5-9. Hammett plot of $\log(k_2^{MeO-})$ for the palladacycle-promoted cleavage of **5.1a–c** (4×10^{-5} M) vs σ^- in anhydrous methanol under buffered conditions (4 mM amine, various concentrations of HOTf) at 25 °C. The line through the data is generated from a linear regression computing $\rho^- = 1.45 \pm 0.04$; $r^2 = 0.9991$.

Hammett plot (k_3^{MeO-})

The dependence of k_2 on [alkoxide] yields a linear relationship from which a third order rate constant can be derived (k_3^{MeO-}). The relationship between the logarithm of k_3^{MeO-} for the palladacycle-promoted methanolyses of **5.1c–e** and the substituent constant, σ^-, is linear exhibiting a ρ^- value of ~0 (Figure 5-10).

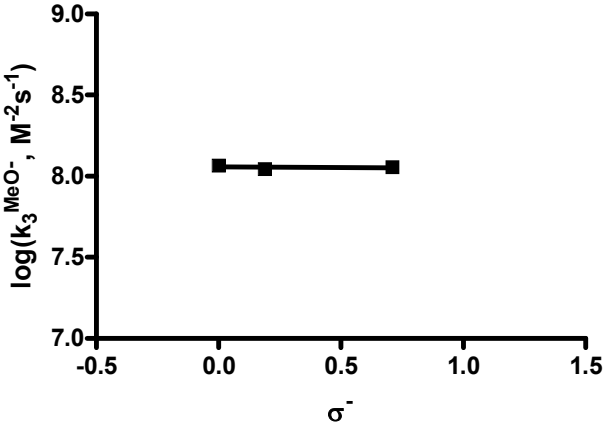

$$v = k_3^{MeO^-}[\mathbf{5.2 : 5.1}][\mathbf{5.2}][MeO^-]$$
$$v = k_2[\mathbf{5.2 : 5.1}][\mathbf{5.2}]$$
$$k_2 = k_3^{MeO^-}[MeO^-]$$

Figure 5-10. Hammett plot of $\log(k_3^{MeO-})$ for the palladacycle-promoted cleavage of **5.1c–e** (4×10^{-5} M) vs σ^- in anhydrous methanol under buffered conditions (4 mM amine, various concentrations of HOTf) at 25 °C. The line through the data is generated from a linear regression computing $\rho^- = -0.01 \pm 0.03$.

5.5 – Discussion

In the previous study,[9] the palladacycle-promoted methanolysis of **5.1b** was shown to involve the decomposition of the complex formed between **5.1b**, palladacycle, and methoxide. The computations reveal a stable tetrahedral intermediate is formed along the cleavage pathway and that metal ion-promoted LGA plays a role in stabilizing the TS for leaving group departure. Kinetic data collected as part of the current study suggest that as the departing anilide becomes more basic, the dependence of the observed rate constant on [catalyst] takes on a higher order with no changes in order with respect to either substrate or methoxide. It is anticipated that the same modes of metallo-catalysis would be operative in this mechanistic regime, however the various roles may be distributed among the two metal ions in order to capitalize on the availability of additional Lewis acidity. The following sections distinguish and examine the kinetic behaviours exhibited by the system throughout the substrate scope of this study.

5.5.1 – Palladacycle-promoted cleavage of 5.1a and 5.1b

Both the palladacycle-promoted cleavages of **5.1a** and **5.1b** exhibit saturation behaviour in their k_{obs} vs [catalyst] plots. The dependences of k_{max} and k_2 on $^{s}_{s}$pH are linear and have gradients of unity. Together, the data suggest a 1:1:1 substrate-catalyst-methoxide complex is the active form leading to methanolytic cleavage. It is of note that in some cases, the kinetically-determined binding constants appear greater than those determined by spectrophotometric titration. This may be a consequence of enhanced binding due to coordination of methoxide and/or dimerization of the palladacycle at higher [methoxide] and [palladacycle] which is most evident in Figure 5-31 (Supporting Information 5-3).

5.5.2 – Palladacycle-promoted cleavage of 5.1d and 5.1e

In the domain where [catalyst] < [substrate], the dependence of k_{obs} on [catalyst] exhibits upward curvature indicating the reaction is second order with respect to catalyst concentration. The dependence of k_3 on ${}^{s}_{s}$pH is linear with a gradient of unity, suggesting that, in this domain, the active species includes one substrate, two catalysts, and one methoxide. In the domain where [catalyst] $\geq$ [substrate], the dependence of k_{obs} on [catalyst] transitions to a linear relationship. Given the large binding constants for **5.2**:**5.1d** and **5.2**:**5.1e** (determined via spectrophotometric titration, Supporting Information 5-1), it is anticipated that one equivalent of catalyst is tightly bound to the substrate at and beyond [catalyst] = [substrate]. The transition from second to first order behaviour must therefore signal complete binding of one catalyst but not the other. The linear behaviour of the second catalyst indicates that it does not become tightly associated with the substrate. Upon backward extrapolation of the linear portion, the line intercepts the horizontal axis at [catalyst] ≈ 0.04 mM, in other words, where [catalyst] = [substrate]. This behaviour is found to be general – as the concentration of **5.1d** is changed, the linear extrapolation consistently meets the horizontal axis where [catalyst] = [substrate]. The data thus indicate the 1:1:1 substrate-catalyst-methoxide complex has little or no activity toward cleavage, the however participation of a second catalyst promotes methanolysis.

5.5.3 – Palladacycle-promoted cleavage of 5.1c

The dependence of k_{obs} on [catalyst] for **5.1c** bears resemblance to that of **5.1d** and **5.1e** with the exception of the nature of the extrapolated intercept. Upon backward extrapolation of the linear region for **5.1c**, the line meets the vertical axis when

[catalyst] = 0 M. The k_{obs} at which this line intersects the vertical axis is thought to represent the maximum achievable rate constant for cleavage of the 1:1:1 substrate-catalyst-methoxide complex. Given the dependence of k_{obs} on two catalysts as well as the activity of the 1:1:1 complex, the rate-limiting TSs for these two pathways must be similar in energy, thereby permitting this substrate to undergo cleavage via two different mechanistic pathways.

5.5.4 – Mechanistic considerations

The previous study[9] involving **5.2** and **5.1b** revealed that the solvolysis reaction elicits a trifunctional role for the metal ion involving its pre-equilibrium coordination to and activation of the C=S unit, subsequent intramolecular attack of a Pd(II)-coordinated methoxide, and Pd(II)-assisted C–N cleavage. The catalyst concentration vs k_{obs} and ${}^{s}_{s}$pH-log(k_{max}) profiles reveal one catalyst, one substrate, and one methoxide are involved in the rate-limiting transition state for cleavage.

The current study reveals thiobenzanilides **5.1a** and **5.1b** undergo methanolysis as described in the previous study, requiring one catalyst and one methoxide to accomplish cleavage (Scheme 5-2: Path A). In contrast, **5.1d** and **5.1e** exhibit a higher-order dependence on [palladacycle] in their catalyst concentration-k_{obs} profiles, pointing to the requirement for two catalysts. Both the ${}^{s}_{s}$pH-log(k_2) and ${}^{s}_{s}$pH-log(k_3) profiles have unit gradients, implying only one methoxide is required to promote methanolysis (Scheme 5-2: Path B or C). Substrate **5.1c** appears to straddle the transition point between the two mechanisms as both pathways appear operative in its cleavage reaction.

At ${}^{s}_{s}$pH values higher than those reported here, the [catalyst]-k_{obs} plots for **5.1c**–**e** exhibit downward curvature and appear square-root in nature. It is therefore neither possible to accurately define the anticipated kinetic ${}^{s}_{s}pK_a$ nor to determine the domain where the system attains saturation with respect to the concentration of the second catalyst. The square-root nature of the curvature indicates that one species must dissociate into two in order to produce the catalytically active form. In this context, it could reflect either the dissociation of a palladacycle dimer (producing two MeO^-:**5.2** species) or the dissociation of MeO^-:**5.2** to produce a free catalyst and methoxide, or possibly both if the dependence is more complicated than a simple square-root. Defining reliable kinetic parameters from a square-root relationship can be sufficiently challenging without the added complication arising from a transition in kinetic order from a square to a square root. For this reason, data were only collected and analyzed in the domains where the relationship between k_{obs} and [**5.2**] is linear.

The [catalyst]-k_{obs} profiles highlight a change in order in [catalyst] from **5.1a** through to **5.1e**, signaling a change in mechanism. The involvement of a second metal ion coincides with a drastic reduction in the dependence of rate on the substituent (ρ^- = 1.45 to -0.01) and therefore in the charge on the leaving group in the rate-limiting transition state. Together, these can be interpreted as one of the two metal ions providing significant stabilization to the developing charge on the LG concurrent with its departure. In the case of substituents with less electron-withdrawing character, a greater degree of negative charge is expected to accumulate on the departing N and the LG would require a greater degree of stabilization by the metal ion in order to depart. A small ρ^- value like -0.01

suggests substantial involvement of a second metal ion such that the accumulation of electron density on the departing N is very small. In this domain, two kinetically indistinguishable pathways may be operating and are represented as B and C in Scheme 5-2. Path C describes a mechanism wherein one catalyst binds tightly to the substrate followed by intermolecular nucleophilic attack by an externally-derived Pd(II)-bound methoxide. Subsequent to delivering the nucleophile, the second catalyst may then become associated with the N of the LG. In Path B, one catalyst binds tightly to the substrate as well as a methoxide and intramolecularly delivers the nucleophile to the C=S unit. Subsequent to formation of the tetrahedral intermediate, a second catalyst becomes transiently coordinated to the lone pair on the N of the LG and stabilizes its departure. A near-zero value for ρ^- could also arise from compensatory effects of the substituent on steps leading up to and including the rate-limiting step. Path B is shown in greater detail in Scheme 5-3 where it becomes clear that ρ^- is a composite of several equilibria and chemical steps leading to cleavage.

Studies by Broxton, Deady, and Rowe indicate the methoxide-catalyzed cleavage of **5.3a**–**g** shows a consistent mechanism throughout the substrate range where leaving group departure is the rate-limiting step and $\rho^- = 2.16$.[6] The magnitude of ρ^- in the methoxide-promoted reaction is larger than that of the palladacycle-promoted reactions, substantiating the idea that the Pd ion(s) stabilizes charge development in the steps up to

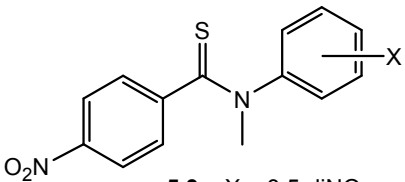

5.3a X = 3,5-diNO_2
5.3b X = 4-NO_2
5.3c X = 3-NO_2
5.3d X = 3-Cl
5.3e X = 4-Br
5.3f X = H
5.3g X = 4-CH_3

and including the rate-limiting step. The reduction in the dependence of k_{obs} on the nature of the LG due to metal ion-promoted LGA has been previously documented in cases involving phosphate esters.[18,19]

Scheme 5-2. Proposed reaction scheme for the palladacycle-promoted methanolysis of **5.1**.

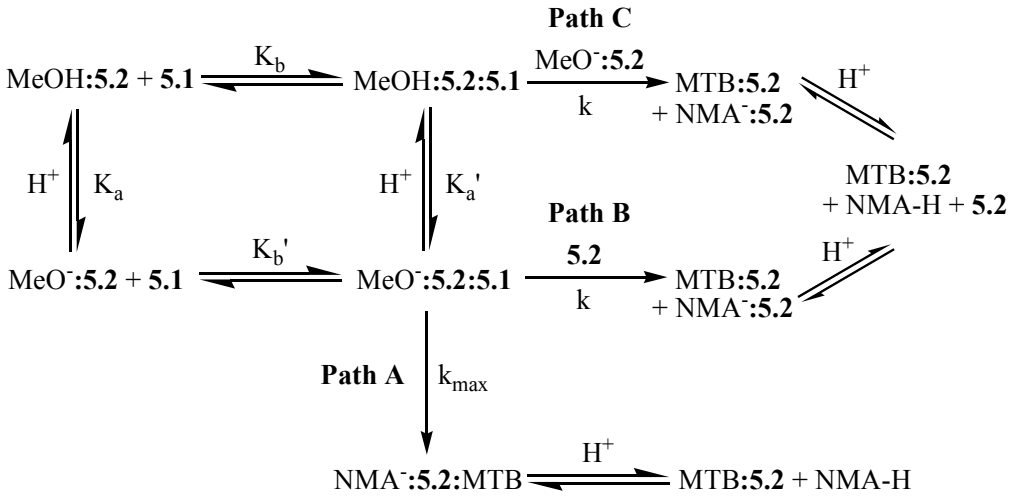

Scheme 5-3. Detailed representation of Path B illustrating the interaction of **5.2** with the tetrahedral intermediate (T_S-) on the pathway to methanolysis.

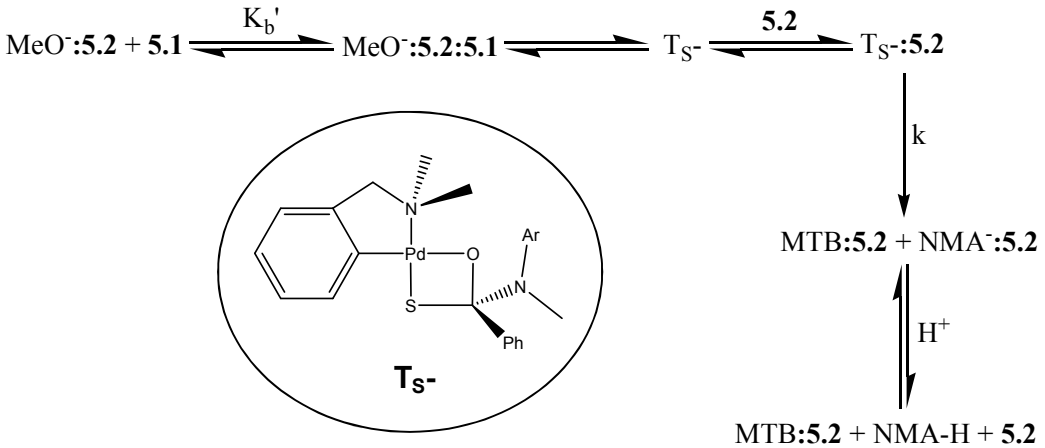

5.6 – Conclusions

Within the range of thiobenzanilides under investigation, the kinetic data suggest a change in mechanism occurs from a domain where one catalyst and one methoxide are necessary to promote methanolysis of the substrate, to a second domain where two catalysts and one methoxide are required. Such kinetic studies provide evidence for the stoichiometry of the rate-limiting transition state, but cannot distinguish between different pathways involving the same stoichiometry. It appears that when the LG is sufficiently basic, a second pathway becomes energetically available in which the roles of the catalyst are redistributed over two metal ions (catalysts). With the additional positive charge available for stabilization of the departing LG, the overall dependence of the reaction rate on the nature of the LG becomes negligibly small.

Several experiments could be performed to further substantiate the existence of a complex composed of one substrate, two catalysts, and one methoxide. Mass spectrometric measurements could be carried out under conditions of excess catalyst; both the mass and distinct isotopic pattern would provide definitive evidence for this species. In order to distinguish this complex from a tetrahedral intermediate with a second catalyst bound to it, MS-MS may also be employed. Evidence could also be derived from a dinuclear catalyst that exhibits enhanced activity toward the methanolysis of **5.1c–e** relative to the mononuclear case by reducing the entropic component for bringing two catalysts and a substrate together in solution. Finally, a set of experiments could be performed in which a 1:1:1 mixture of palladacycle, substrate, and methoxide are subjected to different concentrations of a second, different, metal ion. If these metal

ions are also able to promote cleavage, this would provide evidence for a relatively inactive MeO^-:**5.2**:**5.1** complex that requires assistance from an external Lewis acid. Any trends with respect to the identity of the metal ion may also be useful for assessing the ability of particular metal ions to assist in the departure of nitrogen-based leaving groups.

Lastly, product analysis using ^1H NMR has provided evidence for some formation of the C=O analogue of the thionester product. This observation suggests that the palladacycle catalyst may promote desulfurization of the thionester subsequent to thiobenzanilide methanolysis. A full kinetic study of this adventitious reaction would be necessary to ascertain whether it interferes in any way with the kinetic analysis of the reaction of interest.

5.7 – Supporting Information

5.7.1 – Supporting Information 5-1: Spectrophotometric titrations

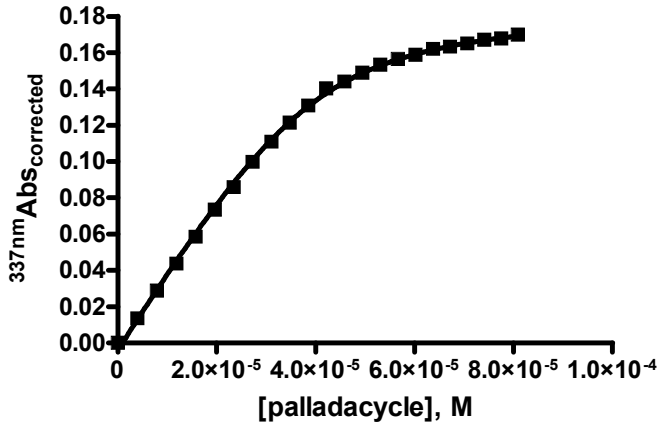

Figure 5-11. Plot of absorbance (at 337 nm, corrected for dilution as well as absorbance due to the added complex) for the **5.2**:**5.1a** complex vs [**5.2**] where [**5.1a**] = 0.04 mM and [HOTf] = 0.1 mM[14] in anhydrous methanol at 25 °C. The data are fitted to a NLLSQ relationship[15] computing $K_b = 10^{5.38\pm0.04}$ M^{-1}; $r^2 = 0.9994$.

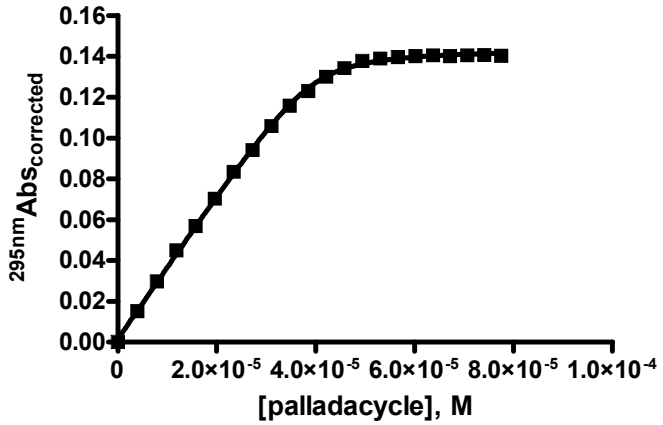

Figure 5-12. Plot of absorbance (at 295 nm, corrected for dilution as well as absorbance due to the added complex) for the **5.2**:**5.1b** complex vs [**5.2**] where [**5.1b**] = 0.04 mM and [HOTf] = 0.1 mM[14] in anhydrous methanol at 25 °C. The data are fitted to a NLLSQ relationship[15] computing $K_b = 10^{6.14\pm0.06}$ M^{-1}; $r^2 = 0.9996$.

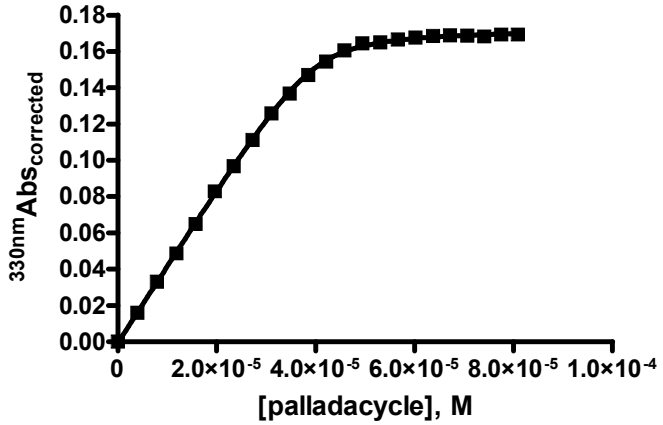

Figure 5-13. Plot of absorbance (at 330 nm, corrected for dilution as well as absorbance due to the added complex) for the **5.2**:**5.1c** complex vs [**5.2**] where [**5.1c**] = 0.04 mM and [HOTf] = 0.1 mM[14] in anhydrous methanol at 25 °C. The data are fitted to a NLLSQ relationship[15] computing $K_b = 10^{6.15\pm0.03}$ M^{-1}; $r^2 = 0.9998$.

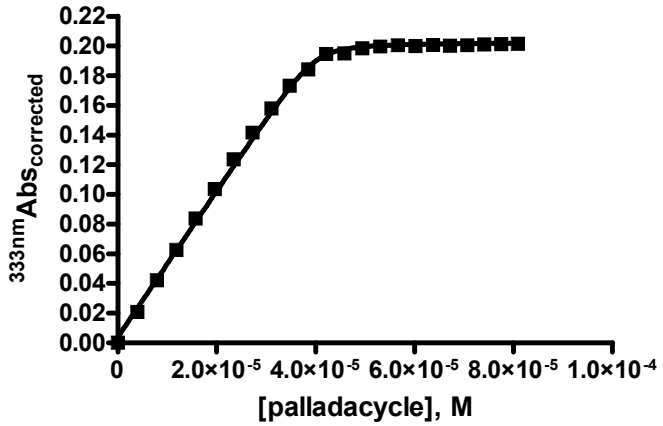

Figure 5-14. Plot of absorbance (at 333 nm, corrected for dilution as well as absorbance due to the added complex) for the **5.2**:**5.1d** complex vs [**5.2**] where [**5.1d**] = 0.04 mM and [HOTf] = 0.1 mM[14] in anhydrous methanol at 25 °C. The data are fitted to a NLLSQ relationship[15] computing $K_b = 10^{6.8\pm0.1}$ M^{-1}; $r^2 = 0.9990$.

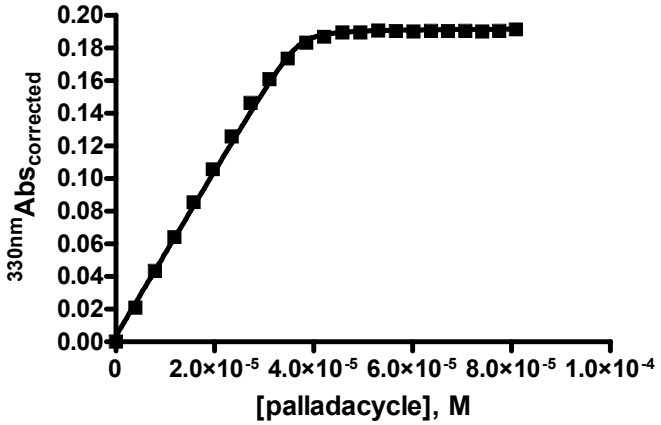

Figure 5-15. Plot of absorbance (at 330 nm, corrected for dilution as well as absorbance due to the added complex) for the **5.2**:**5.1e** complex vs [**5.2**] where [**5.1e**] = 0.04 mM and [HOTf] = 0.1 mM[14] in anhydrous methanol at 25 °C. The data are fitted to a NLLSQ relationship[15] computing $K_b = 10^{6.9\pm0.2}$ M^{-1}; $r^2 = 0.9988$.

5.7.2 – Supporting Information 5-2: Plots of log(k) vs $^{s}_{s}$pH

Plots of log(k_2) vs $^{s}_{s}$pH

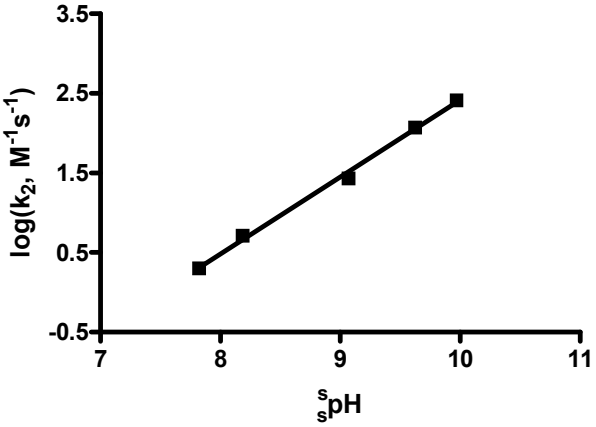

Figure 5-16. Plot of log(k_2) for the palladacycle-promoted cleavage of **5.1a** (4×10^{-5} M) vs $^{s}_{s}$pH in anhydrous methanol under buffered conditions (4 mM amine, various concentrations of HOTf) at 25 °C. The line through the data is generated from a linear regression to provide a slope of 0.97 ± 0.03; $r^2 = 0.9965$.

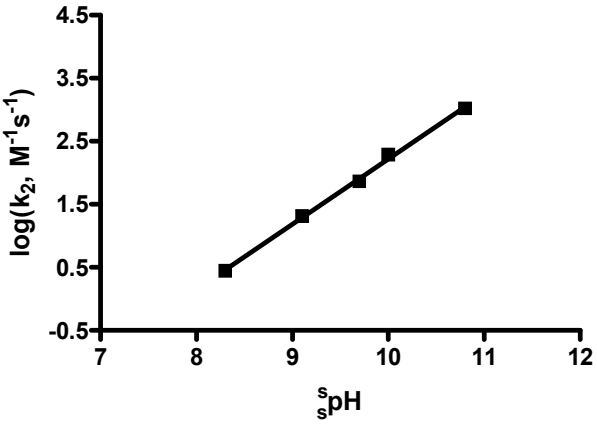

Figure 5-17. Plot of $\log(k_2)$ for the palladacycle-promoted cleavage of **5.1b** (4×10^{-5} M) vs ${}^{s}_{s}$pH in anhydrous methanol under buffered conditions (4 mM amine, various concentrations of HOTf) at 25 °C. The line through the data is generated from a linear regression to provide a slope of 1.03 ± 0.03; $r^2 = 0.9977$.

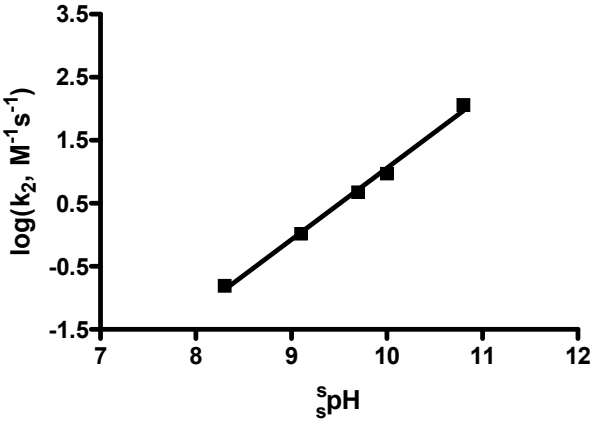

Figure 5-18. Plot of $\log(k_2)$ for the palladacycle-promoted cleavage of **5.1c** (4×10^{-5} M) vs ${}^{s}_{s}$pH in anhydrous methanol under buffered conditions (4 mM amine, various concentrations of HOTf) at 25 °C. The line through the data is generated from a linear regression to provide a slope of 1.14 ± 0.05; $r^2 = 0.9951$.

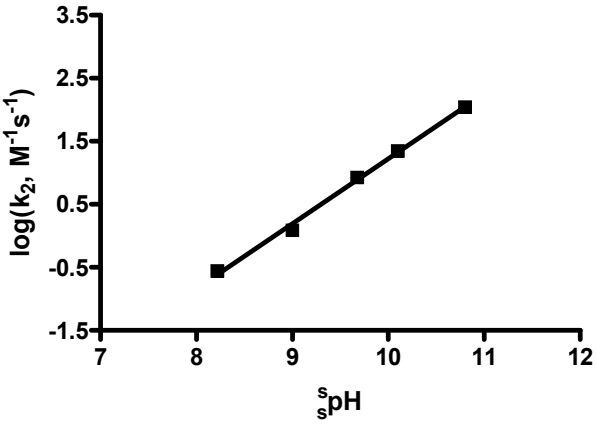

Figure 5-19. Plot of $\log(k_2)$ for the palladacycle-promoted cleavage of **5.1d** (4×10^{-5} M) vs ${}^{s}_{s}$pH in anhydrous methanol under buffered conditions (4 mM amine, various concentrations of HOTf) at 25 °C. The line through the data is generated from a linear regression to provide a slope of 1.03 ± 0.04; $r^2 = 0.9963$.

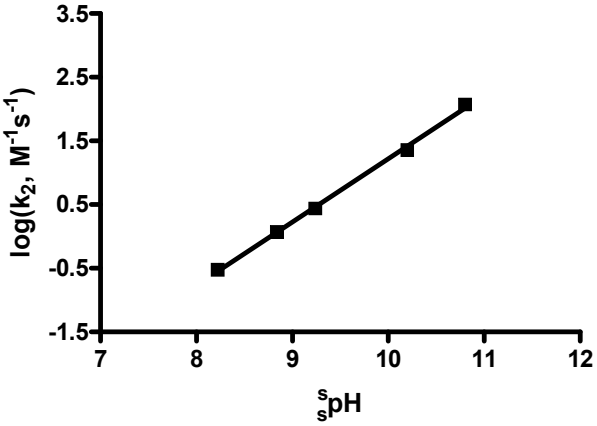

Figure 5-20. Plot of $\log(k_2)$ for the palladacycle-promoted cleavage of **5.1e** (4×10^{-5} M) vs ${}^{s}_{s}$pH in anhydrous methanol under buffered conditions (4 mM amine, various concentrations of HOTf) at 25 °C. The line through the data is generated from a linear regression to provide a slope of 1.00 ± 0.02; $r^2 = 0.9981$.

Plots of log(k_{max}) vs ${}^{s}_{s}pH$

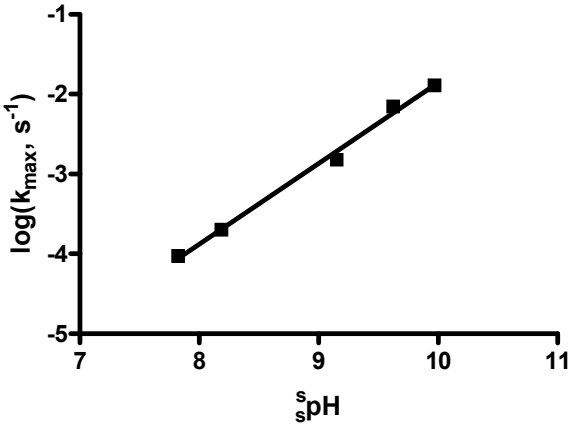

Figure 5-21. Plot of log(k_{max}) for the palladacycle-promoted cleavage of **5.1a** (4×10^{-5} M) vs ${}^{s}_{s}pH$ in anhydrous methanol under buffered conditions (4 mM amine, various concentrations of HOTf) at 25 °C. The line through the data is generated from a linear regression to provide a slope of 1.01 ± 0.04; $r^2 = 0.9943$.

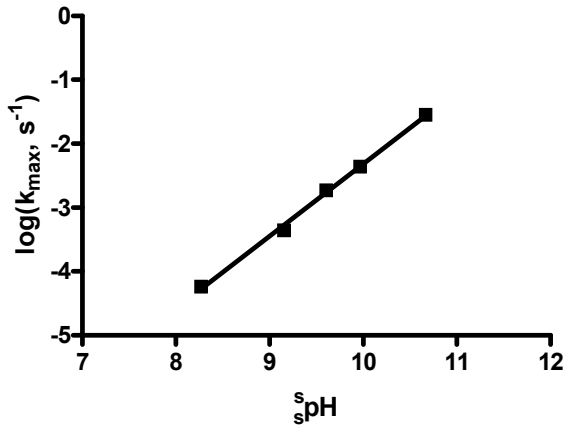

Figure 5-22. Plot of log(k_{max}) for the palladacycle-promoted cleavage of **5.1b** (4×10^{-5} M) vs ${}^{s}_{s}pH$ in anhydrous methanol under buffered conditions (4 mM amine, various concentrations of HOTf) at 25 °C. The line through the data is generated from a linear regression to provide a slope of 1.13 ± 0.03; $r^2 = 0.9978$.

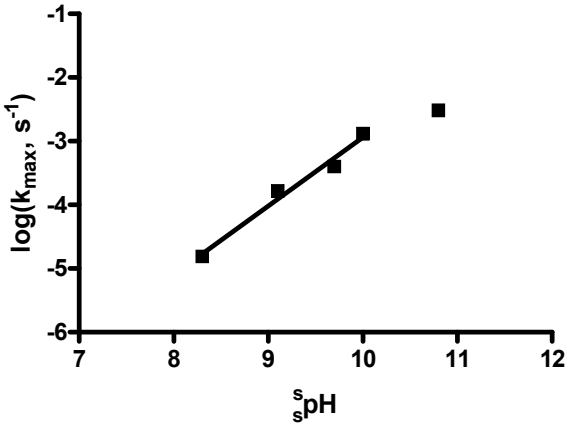

Figure 5-23. Plot of $\log(k_{max})$ for the palladacycle-promoted cleavage of **5.1c** (4×10^{-5} M) vs ${}^{s}_{s}$pH in anhydrous methanol under buffered conditions (4 mM amine, various concentrations of HOTf) at 25 °C. The line through the data is generated from a linear regression to provide a slope of 1.1 ± 0.1; $r^2 = 0.9804$.

Plots of log(k_3) vs ${}^{s}_{s}$pH

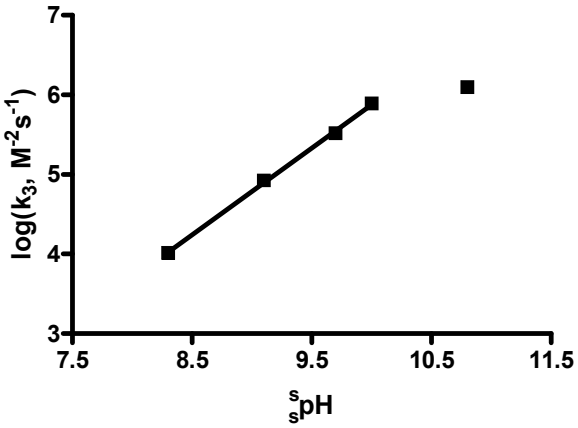

Figure 5-24. Plot of $\log(k_3)$ for the palladacycle-promoted cleavage of **5.1c** (4×10^{-5} M) vs ${}^{s}_{s}$pH in anhydrous methanol under buffered conditions (4 mM amine, various concentrations of HOTf) at 25 °C. The line through the data is generated from a linear regression to provide a slope of 1.09 ± 0.02; $r^2 = 0.9990$.

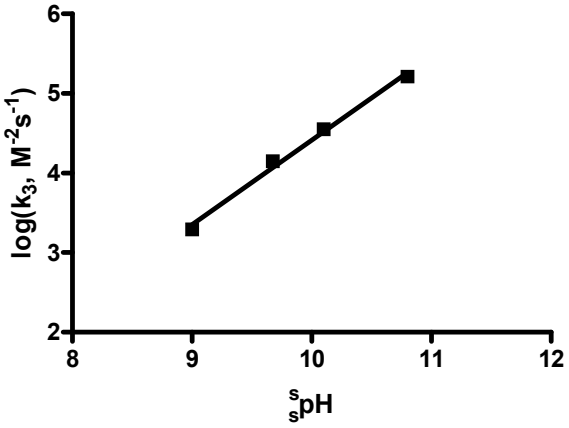

Figure 5-25. Plot of log(k_3) for the palladacycle-promoted cleavage of **5.1d** (4×10^{-5} M) vs $^{s}_{s}$pH in anhydrous methanol under buffered conditions (4 mM amine, various concentrations of HOTf) at 25 °C. The line through the data is generated from a linear regression to provide a slope of 1.06 ± 0.06; $r^2 = 0.9930$.

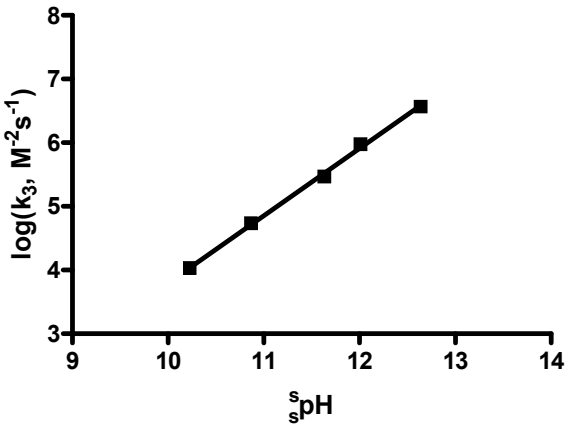

Figure 5-26. Plot of log(k_3) for the palladacycle-promoted cleavage of **5.1e** (4×10^{-5} M) vs $^{s}_{s}$pH in anhydrous methanol under buffered conditions (4 mM amine, various concentrations of HOTf) at 25 °C. The line through the data is generated from a linear regression to provide a slope of 1.05 ± 0.02; $r^2 = 0.9981$.

5.7.3 – Supporting Information 5-3: Plots of k_{obs} vs [catalyst]

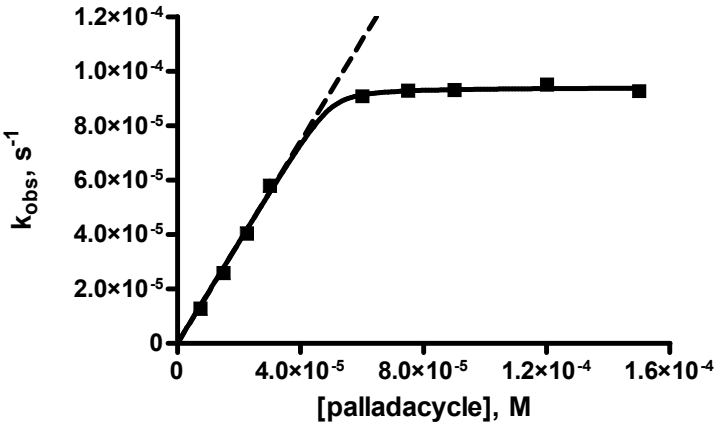

Figure 5-27. Plot of k_{obs} for the cleavage of **5.1a** (4×10^{-5} M) vs [**5.2**] buffered at ${}^{s}_{s}$pH 7.8 (4 mM *N*-ethylmorpholine, 2.5 mM HOTf) in anhydrous methanol at 25 °C. The data in the catalyst-dependent region are fitted to a linear regression computing $k_2 = (1.86 \pm 0.05)\ M^{-1} \cdot s^{-1}$.

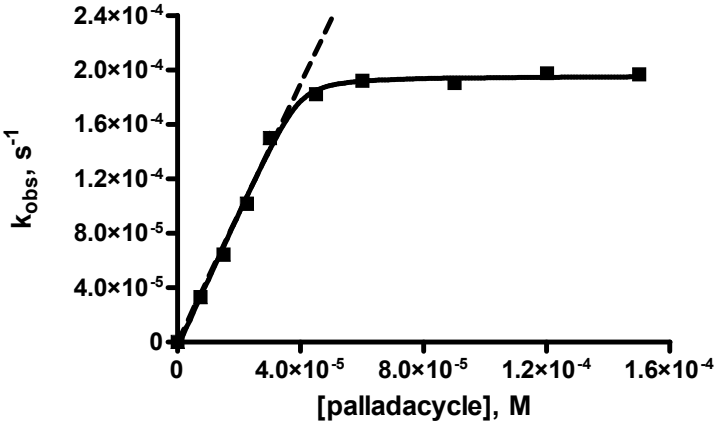

Figure 5-28. Plot of k_{obs} for the cleavage of **5.1a** (4×10^{-5} M) vs [**5.2**] buffered at ${}^{s}_{s}$pH 8.2 (4 mM *N*-ethylmorpholine, 2 mM HOTf) in anhydrous methanol at 25 °C. The data in the catalyst-dependent region are fitted to a linear regression computing $k_2 = (4.7 \pm 0.1)\ M^{-1} \cdot s^{-1}$.

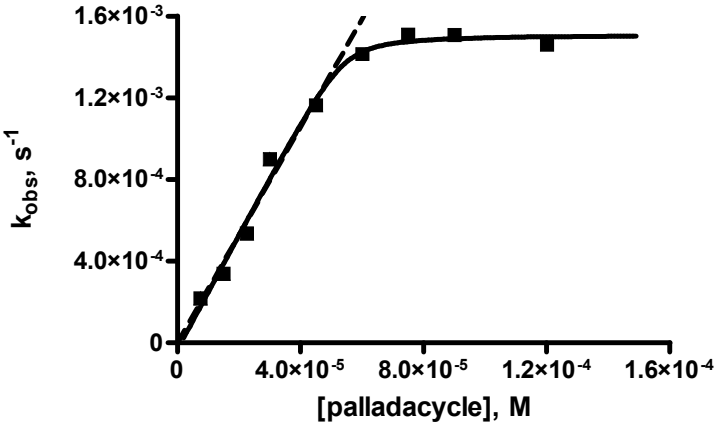

Figure 5-29. Plot of k_{obs} for the cleavage of **5.1a** (4×10^{-5} M) vs [**5.2**] buffered at $^{s}_{s}$pH 9.2 (4 mM *N*-ethylmorpholine, 0.5 mM HOTf) in anhydrous methanol at 25 °C. The data in the catalyst-dependent region are fitted to a linear regression computing $k_2 = (27 \pm 1)$ $M^{-1} \cdot s^{-1}$.

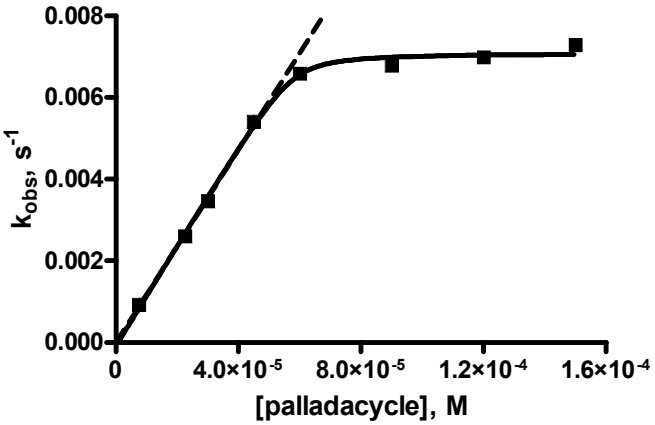

Figure 5-30. Plot of k_{obs} for the cleavage of **5.1a** (4×10^{-5} M) vs [**5.2**] buffered at $^{s}_{s}$pH 9.6 (4 mM *N*-methylpiperidine, 2.8 mM HOTf) in anhydrous methanol at 25 °C. The data in the catalyst-dependent region are fitted to a linear regression computing $k_2 = (118 \pm 1)$ $M^{-1} \cdot s^{-1}$.

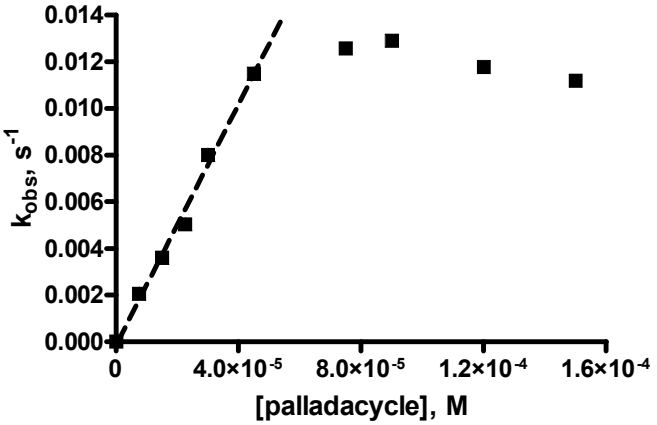

Figure 5-31. Plot of k_{obs} for the cleavage of **5.1a** (4×10^{-5} M) vs [**5.2**] buffered at $^{s}_{s}$pH 10.0 (4 mM *N*-methylpiperidine, 2 mM HOTf) in anhydrous methanol at 25 °C. The data in the catalyst-dependent region are fitted to a linear regression computing $k_2 = (260 \pm 16)$ $M^{-1} \cdot s^{-1}$.

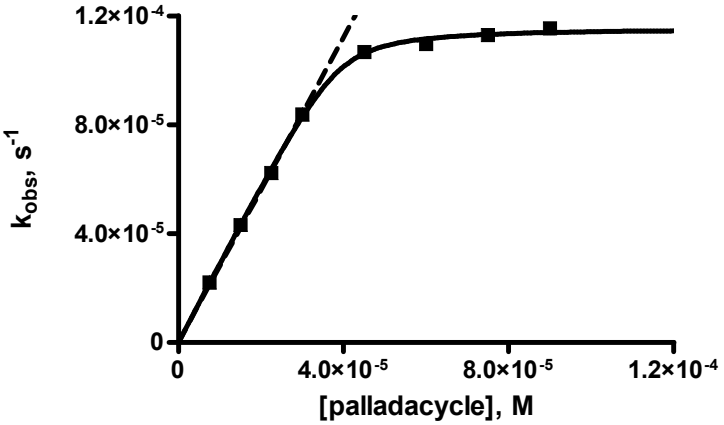

Figure 5-32. Plot of k_{obs} for the cleavage of **5.1b** (4×10^{-5} M) vs [**5.2**] buffered at $^{s}_{s}$pH 8.3 (4 mM *N*-ethylmorpholine, 2 mM HOTf) in anhydrous methanol at 25 °C. The data in the catalyst-dependent region are fitted to a linear regression computing $k_2 = (2.80 \pm 0.02)$ $M^{-1} \cdot s^{-1}$.

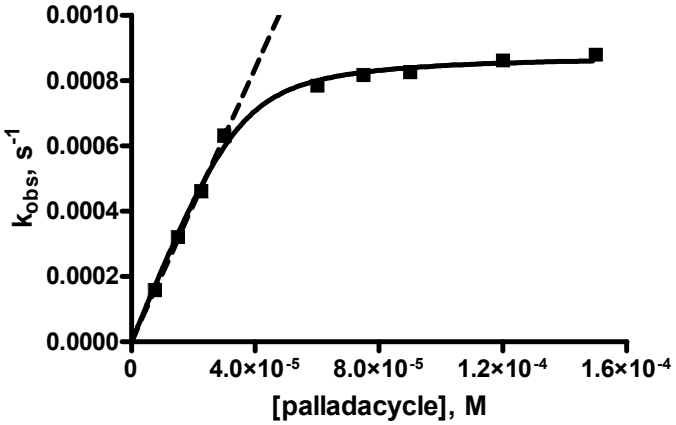

Figure 5-33. Plot of k_{obs} for the cleavage of **5.1b** (4×10^{-5} M) vs [**5.2**] buffered at ${}^{s}_{s}$pH 9.2 (4 mM *N*-ethylmorpholine, 0.5 mM HOTf) in anhydrous methanol at 25 °C. The data in the catalyst-dependent region are fitted to a linear regression computing $k_2 = (20.9 \pm 0.2)$ $M^{-1} \cdot s^{-1}$.

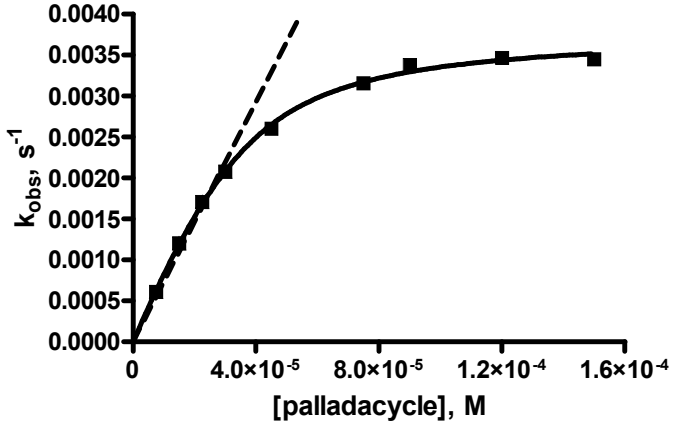

Figure 5-34. Plot of k_{obs} for the cleavage of **5.1b** (4×10^{-5} M) vs [**5.2**] buffered at ${}^{s}_{s}$pH 9.6 (4 mM *N*-methylpiperidine, 2.8 mM HOTf) in anhydrous methanol at 25 °C. The data in the catalyst-dependent region are fitted to a linear regression computing $k_2 = (73 \pm 3)$ $M^{-1} \cdot s^{-1}$.

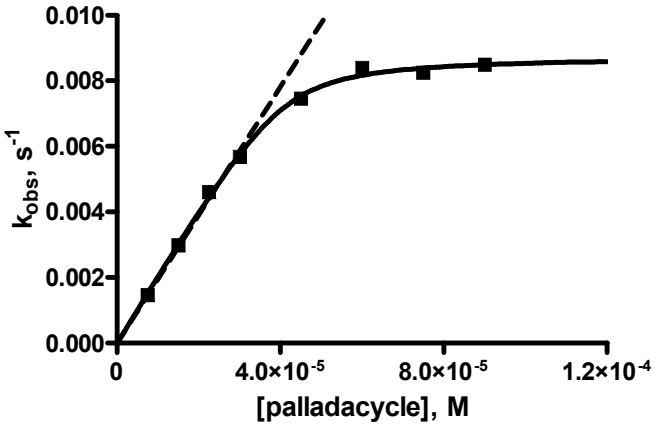

Figure 5-35. Plot of k_{obs} for the cleavage of **5.1b** (4×10^{-5} M) vs [**5.2**] buffered at $^{s}_{s}$pH 10.0 (4 mM *N*-methylpiperidine, 2 mM HOTf) in anhydrous methanol at 25 °C. The data in the catalyst-dependent region are fitted to a linear regression computing $k_2 = (195 \pm 4)$ $M^{-1} \cdot s^{-1}$.

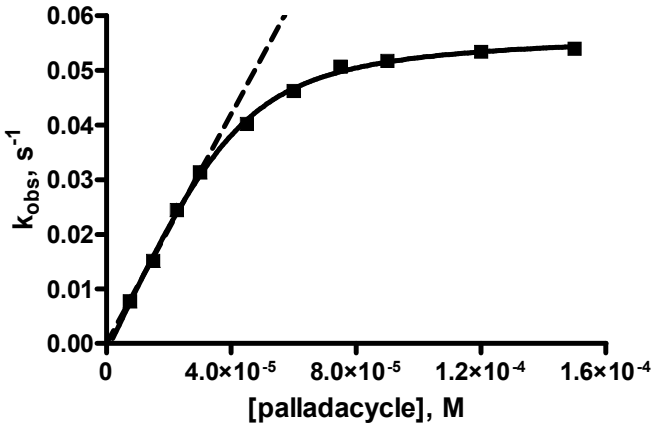

Figure 5-36. Plot of k_{obs} for the cleavage of **5.1b** (4×10^{-5} M) vs [**5.2**] buffered at $^{s}_{s}$pH 10.7 (4 mM *N*-methylpiperidine, 0.5 mM HOTf) in anhydrous methanol at 25 °C. The data in the catalyst-dependent region are fitted to a linear regression computing $k_2 = (1050 \pm 10)$ $M^{-1} \cdot s^{-1}$.

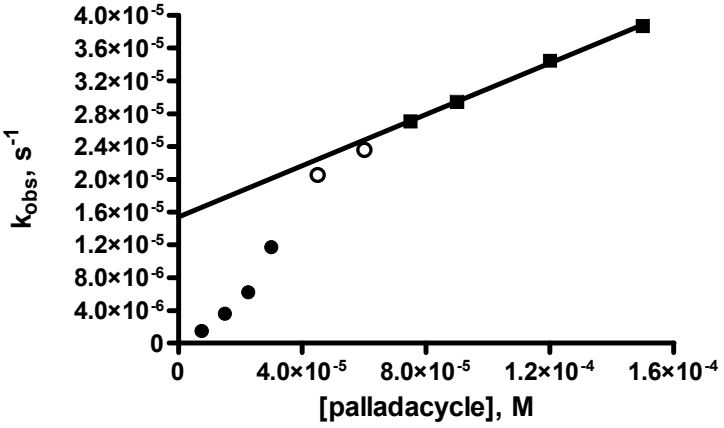

Figure 5-37. Plot of k_{obs} for the cleavage of **5.1c** (4×10^{-5} M) vs [**5.2**] buffered at ${}^{s}_{s}$pH 8.3 (4 mM *N*-ethylmorpholine, 2 mM HOTf) in anhydrous methanol at 25 °C. The ■-data are fitted to a linear regression computing $k_2 = (0.156 \pm 0.004)$ $M^{-1} \cdot s^{-1}$ and $k_{max} = (1.54 \pm 0.05) \times 10^{-5}$ s^{-1}. The ●-data represent the second-order dependence of k_{obs} on [**5.2**]; the ○-data represent the transition from second-order to first-order dependence of k_{obs} on [**5.2**].

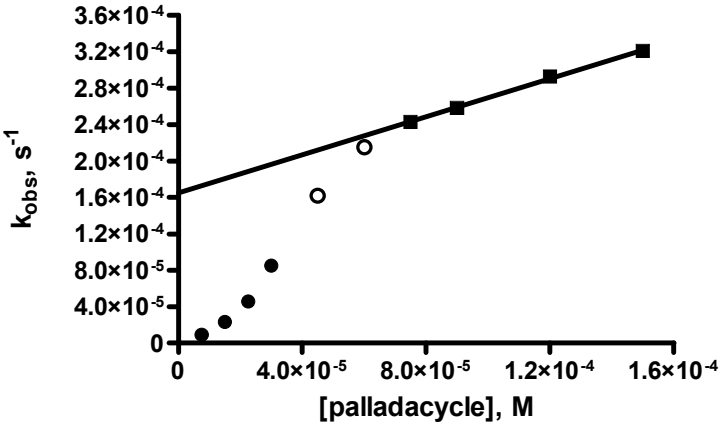

Figure 5-38. Plot of k_{obs} for the cleavage of **5.1c** (4×10^{-5} M) vs [**5.2**] buffered at ${}^{s}_{s}$pH 9.1 (4 mM *N*-ethylmorpholine, 0.5 mM HOTf) in anhydrous methanol at 25 °C. The ■-data are fitted to a linear regression computing $k_2 = (1.05 \pm 0.03)$ $M^{-1} \cdot s^{-1}$ and $k_{max} = (1.65 \pm 0.03) \times 10^{-4}$ s^{-1}. The ●-data represent the second-order dependence of k_{obs} on [**5.2**]; the ○-data represent the transition from second-order to first-order dependence of k_{obs} on [**5.2**].

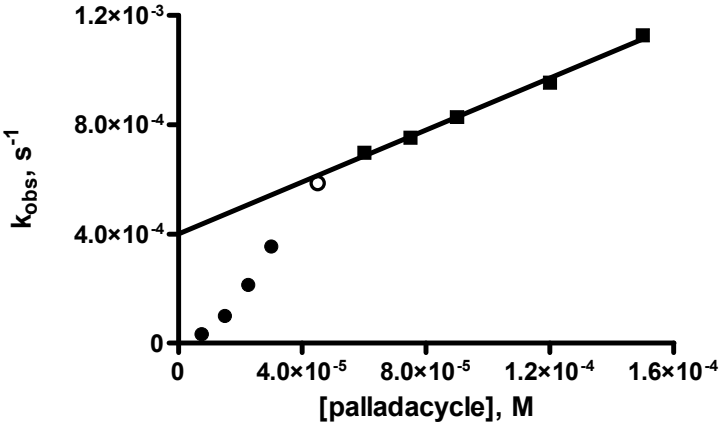

Figure 5-39. Plot of k_{obs} for the cleavage of **5.1c** (4×10^{-5} M) vs [**5.2**] buffered at $^{s}_{s}$pH 9.7 (4 mM *N*-methylpiperidine, 2.8 mM HOTf) in anhydrous methanol at 25 °C. The ■-data are fitted to a linear regression computing $k_2 = (4.8 \pm 0.2)\ M^{-1}\cdot s^{-1}$ and $k_{max} = (4.0 \pm 0.2) \times 10^{-4}\ s^{-1}$. The ●-data represent the second-order dependence of k_{obs} on [**5.2**]; the ○-data represent the transition from second-order to first-order dependence of k_{obs} on [**5.2**].

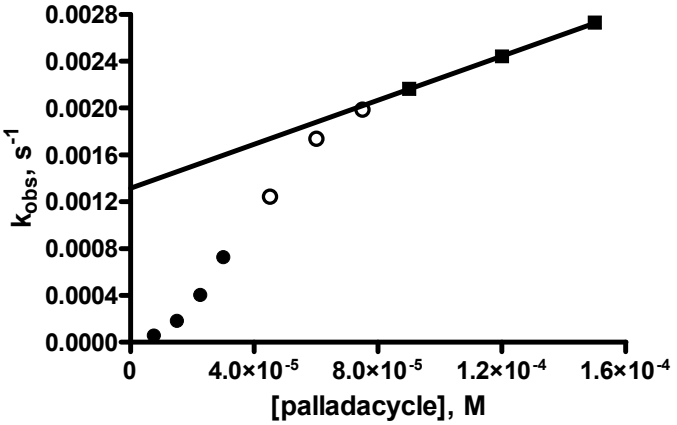

Figure 5-40. Plot of k_{obs} for the cleavage of **5.1c** (4×10^{-5} M) vs [**5.2**] buffered at $^{s}_{s}$pH 10.0 (4 mM *N*-methylpiperidine, 2 mM HOTf) in anhydrous methanol at 25 °C. The ■-data are fitted to a linear regression computing $k_2 = (9.4 \pm 0.1)\ M^{-1}\cdot s^{-1}$ and $k_{max} = (1.32 \pm 0.01) \times 10^{-3}\ s^{-1}$. The ●-data represent the second-order dependence of k_{obs} on [**5.2**]; the ○-data represent the transition from second-order to first-order dependence of k_{obs} on [**5.2**].

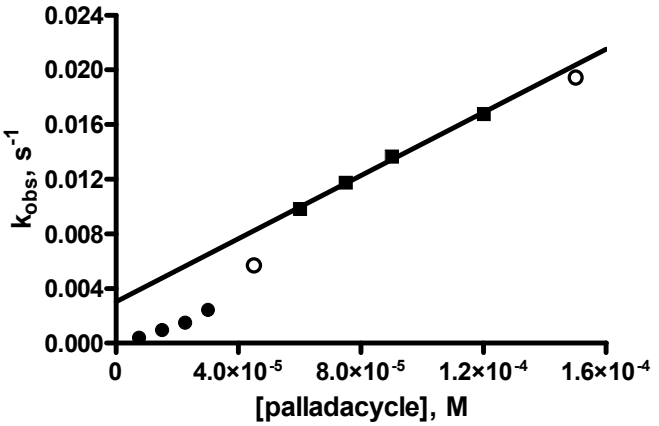

Figure 5-41. Plot of k_{obs} for the cleavage of **5.1c** (4×10^{-5} M) vs [**5.2**] buffered at $^{s}_{s}$pH 10.8 (4 mM *N*-methylpiperidine, 0.5 mM HOTf) in anhydrous methanol at 25 °C. The ■-data are fitted to a linear regression computing $k_2 = (115 \pm 5)\ M^{-1}\cdot s^{-1}$ and $k_{max} = (3.1 \pm 0.4) \times 10^{-3}\ s^{-1}$. The ●-data represent the second-order dependence of k_{obs} on [**5.2**]; the ○-data signal changes in order of [**5.2**].

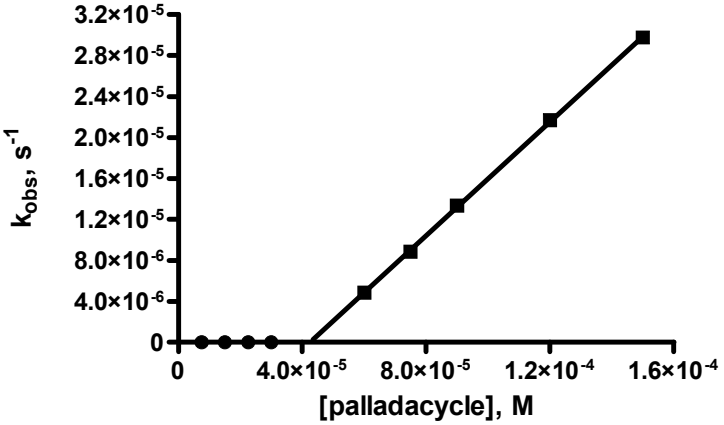

Figure 5-42. Plot of k_{obs} for the cleavage of **5.1d** (4×10^{-5} M) vs [**5.2**] buffered at $^{s}_{s}$pH 8.2 (4 mM *N*-ethylmorpholine, 2 mM HOTf) in anhydrous methanol at 25 °C. The ■-data are fitted to a linear regression computing $k_2 = (0.278 \pm 0.002)\ M^{-1}\cdot s^{-1}$. The ●-data represent the second-order dependence of k_{obs} on [**5.2**].

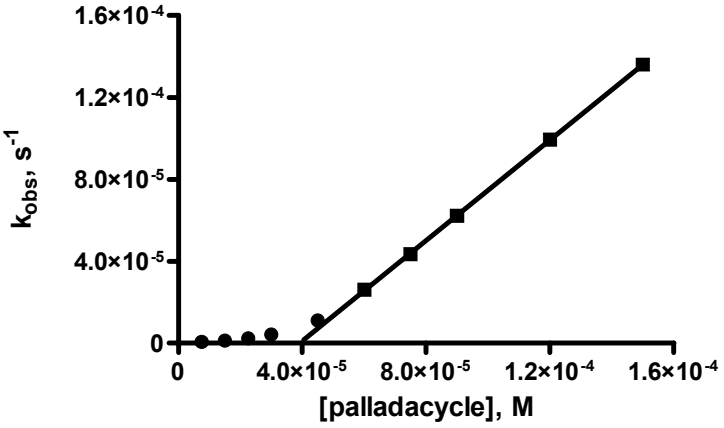

Figure 5-43. Plot of k_{obs} for the cleavage of **5.1d** (4×10^{-5} M) vs [**5.2**] buffered at ${}^{s}_{s}$pH 9.0 (4 mM *N*-ethylmorpholine, 0.5 mM HOTf) in anhydrous methanol at 25 °C. The ■-data are fitted to a linear regression computing $k_2 = (1.226 \pm 0.006)\ M^{-1}\cdot s^{-1}$. The ●-data represent the second-order dependence of k_{obs} on [**5.2**].

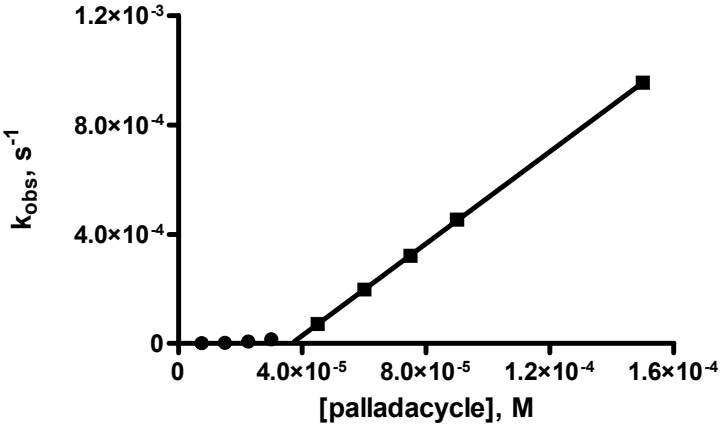

Figure 5-44. Plot of k_{obs} for the cleavage of **5.1d** (4×10^{-5} M) vs [**5.2**] buffered at ${}^{s}_{s}$pH 9.7 (4 mM *N*-methylpiperidine, 2.8 mM HOTf) in anhydrous methanol at 25 °C. The ■-data are fitted to a linear regression computing $k_2 = (8.42 \pm 0.03)\ M^{-1}\cdot s^{-1}$. The ●-data represent the second-order dependence of k_{obs} on [**5.2**].

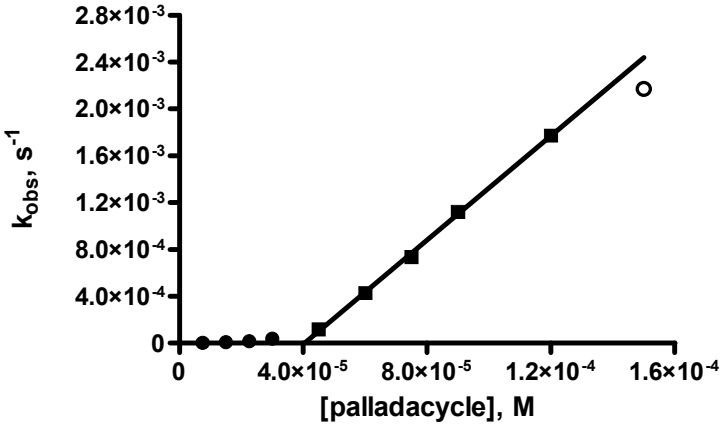

Figure 5-45. Plot of k_{obs} for the cleavage of **5.1d** (4×10^{-5} M) vs [**5.2**] buffered at ${}^{s}_{s}$pH 10.1 (4 mM *N*-methylpiperidine, 2 mM HOTf) in anhydrous methanol at 25 °C. The ■-data are fitted to a linear regression computing $k_2 = (22.3 \pm 0.4)\ M^{-1}\cdot s^{-1}$. The ●-data represent the second-order dependence of k_{obs} on [**5.2**]; the ○-data signal a change in order of [**5.2**].

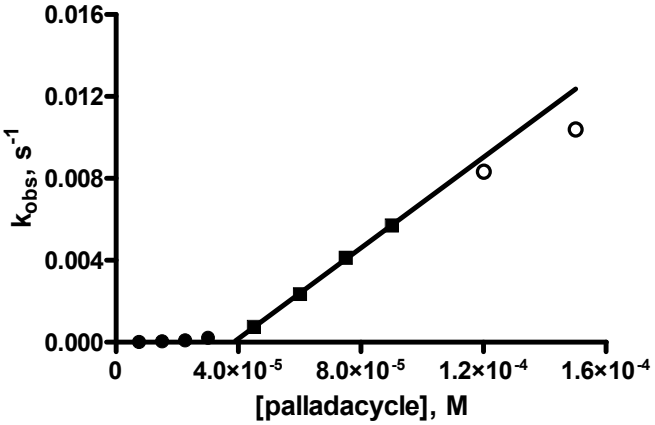

Figure 5-46. Plot of k_{obs} for the cleavage of **5.1d** (4×10^{-5} M) vs [**5.2**] buffered at ${}^{s}_{s}$pH 10.8 (4 mM *N*-methylpiperidine, 0.5 mM HOTf) in anhydrous methanol at 25 °C. The ■-data are fitted to a linear regression computing $k_2 = (111 \pm 2)\ M^{-1}\cdot s^{-1}$. The ●-data represent the second-order dependence of k_{obs} on [**5.2**]; the ○-data signal a change in order of [**5.2**].

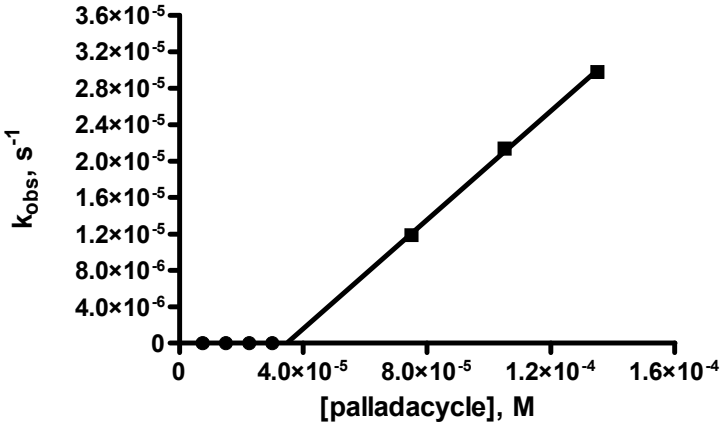

Figure 5-47. Plot of k_{obs} for the cleavage of **5.1e** (4×10^{-5} M) vs [**5.2**] buffered at ${}^{s}_{s}$pH 8.2 (4 mM *N*-ethylmorpholine, 2 mM HOTf) in anhydrous methanol at 25 °C. The ■-data are fitted to a linear regression computing $k_2 = (0.30 \pm 0.01)\ M^{-1}\cdot s^{-1}$. The ●-data represent the second-order dependence of k_{obs} on [**5.2**].

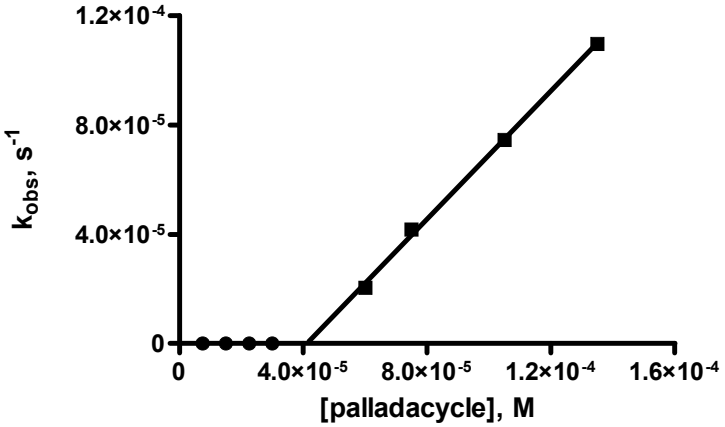

Figure 5-48. Plot of k_{obs} for the cleavage of **5.1e** (4×10^{-5} M) vs [**5.2**] buffered at ${}^{s}_{s}$pH 8.8 (4 mM *N*-ethylmorpholine, 0.8 mM HOTf) in anhydrous methanol at 25 °C. The ■-data are fitted to a linear regression computing $k_2 = (1.17 \pm 0.03)\ M^{-1}\cdot s^{-1}$. The ●-data represent the second-order dependence of k_{obs} on [**5.2**].

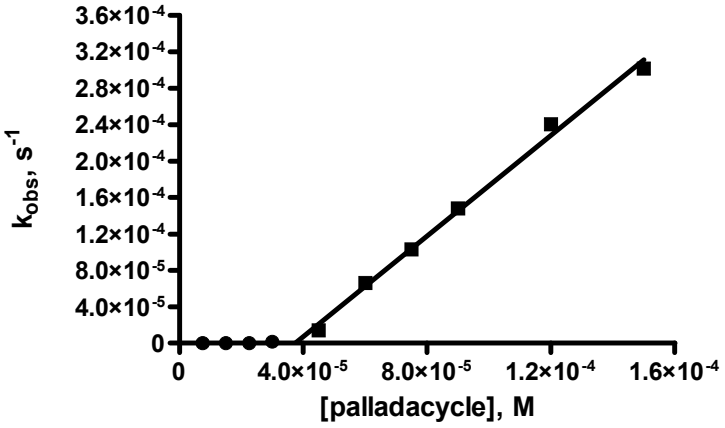

Figure 5-49. Plot of k_{obs} for the cleavage of **5.1e** (4×10^{-5} M) vs [**5.2**] buffered at ${}^{s}_{s}$pH 9.2 (4 mM *N*-methylpiperidine, 3.5 mM HOTf) in anhydrous methanol at 25 °C. The ■-data are fitted to a linear regression computing $k_2 = (2.8 \pm 0.1)\ M^{-1}{\cdot}s^{-1}$. The ●-data represent the second-order dependence of k_{obs} on [**5.2**].

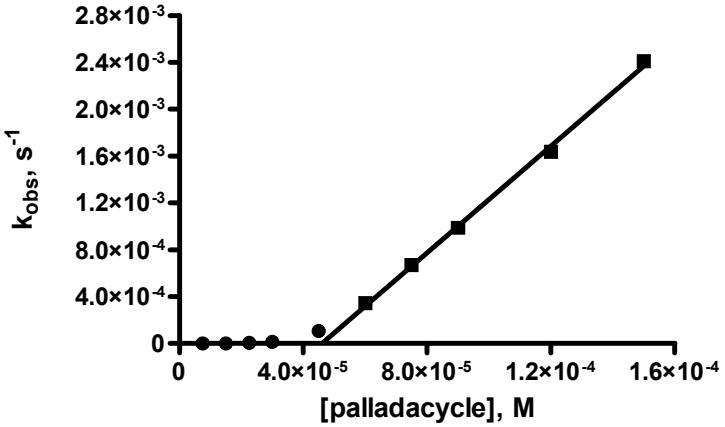

Figure 5-50. Plot of k_{obs} for the cleavage of **5.1e** (4×10^{-5} M) vs [**5.2**] buffered at ${}^{s}_{s}$pH 10.2 (4 mM *N*-methylpiperidine, 2 mM HOTf) in anhydrous methanol at 25 °C. The ■-data are fitted to a linear regression computing $k_2 = (22.8 \pm 0.6)\ M^{-1}{\cdot}s^{-1}$. The ●-data represent the second-order dependence of k_{obs} on [**5.2**].

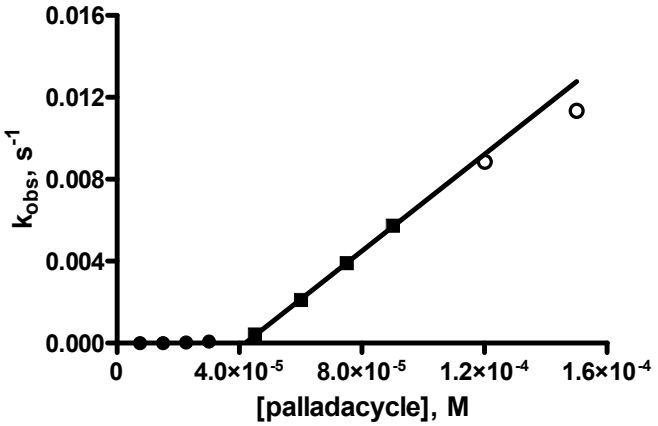

Figure 5-51. Plot of k_{obs} for the cleavage of **5.1e** (4×10^{-5} M) vs [**5.2**] buffered at $^{s}_{s}$pH 10.8 (4 mM *N*-methylpiperidine, 2 mM HOTf) in anhydrous methanol at 25 °C. The ■-data are fitted to a linear regression computing $k_2 = (118 \pm 2)$ $M^{-1} \cdot s^{-1}$. The ●-data represent the second-order dependence of k_{obs} on [**5.2**]; the ○-data signal a change in order of [**5.2**].

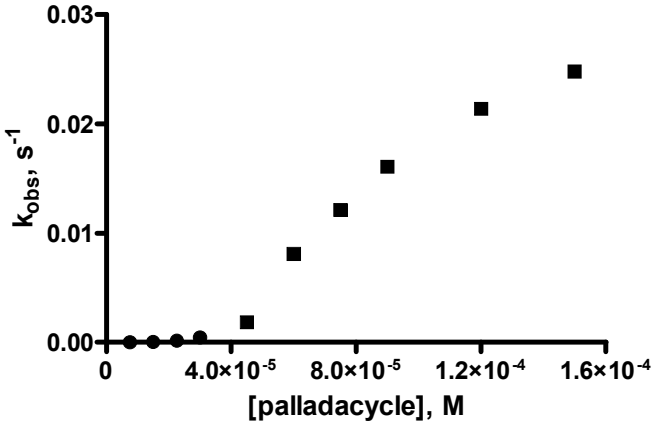

Figure 5-52. Plot of k_{obs} for the cleavage of **5.1e** (4×10^{-5} M) vs [**5.2**] buffered at $^{s}_{s}$pH 11.6 (4 mM *N,N,N',N'*-tetramethylpiperidine, 3.5 mM HOTf) in anhydrous methanol at 25 °C. The ●-data represent the second-order dependence of k_{obs} on [**5.2**]; the ■-data represent a nonlinear dependence of k_{obs} on [**5.2**].

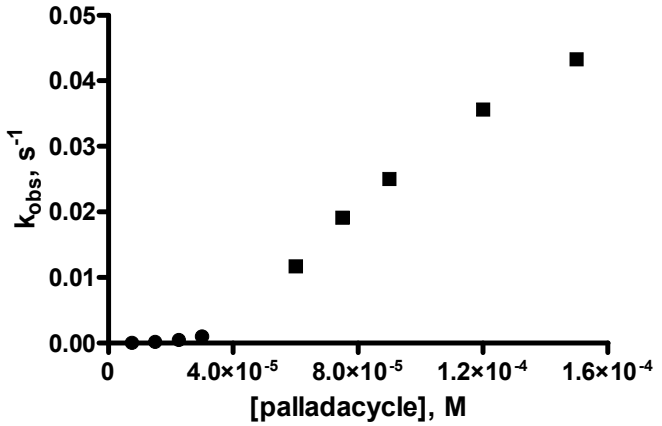

Figure 5-53. Plot of k_{obs} for the cleavage of **5.1e** (4×10^{-5} M) vs [**5.2**] buffered at $^{s}_{s}$pH 12.0 (4 mM *N*,*N*,*N'*,*N'*-tetramethylpiperidine, 2 mM HOTf) in anhydrous methanol at 25 °C. The ●-data represent the second-order dependence of k_{obs} on [**5.2**]; the ■-data represent a nonlinear dependence of k_{obs} on [**5.2**].

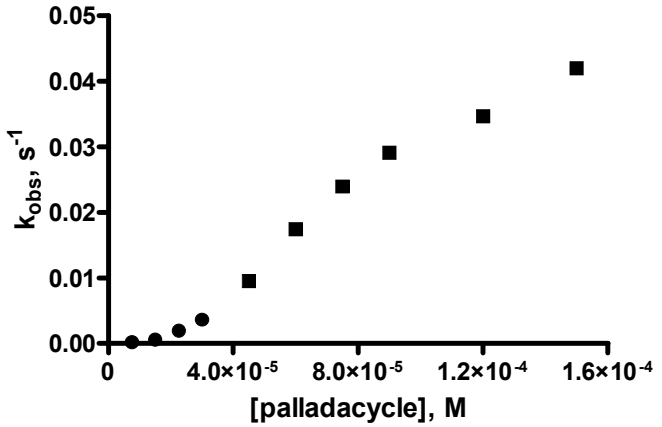

Figure 5-54. Plot of k_{obs} for the cleavage of **5.1e** (4×10^{-5} M) vs [**5.2**] buffered at $^{s}_{s}$pH 12.6 (4 mM *N*,*N*,*N'*,*N'*-tetramethylpiperidine, 0.5 mM HOTf) in anhydrous methanol at 25 °C. The ●-data represent the second-order dependence of k_{obs} on [**5.2**]; the ■-data represent a nonlinear dependence of k_{obs} on [**5.2**].

5.7.4 – Supporting Information 5-4: Hammett plots

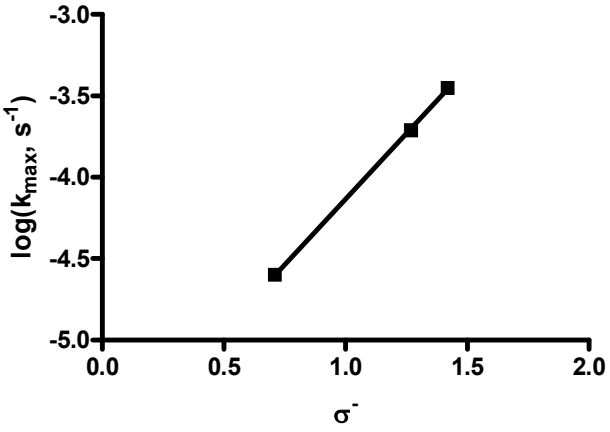

Figure 5-55. Hammett plot of log(k_{max}) for the palladacycle-promoted cleavage of **5.1a**–**c** (4×10^{-5} M) vs σ^- in anhydrous methanol under buffered conditions (4 mM amine, various concentrations of HOTf) at $^{s}_{s}$pH 8.4 and 25 °C. These k_{max} values are interpolated from overlaid $^{s}_{s}$pH-log(k_{max}) profiles for **5.1a**–**c**. The line through the data is generated from a linear regression computing $\rho^- = 1.61 \pm 0.02$; $r^2 = 0.9998$.

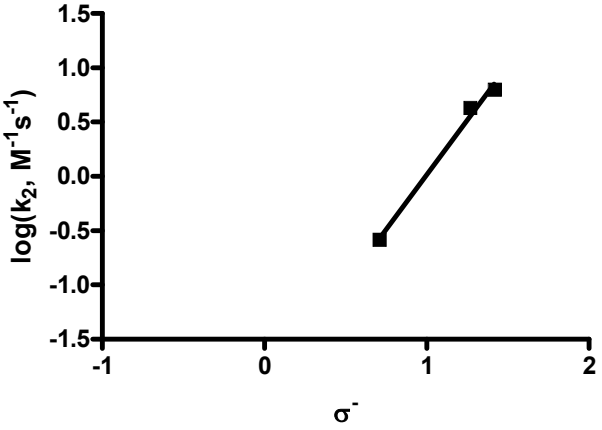

Figure 5-56. Hammett plot of log(k_2) for the palladacycle-promoted cleavage of **5.1a**–**c** (4×10^{-5} M) vs σ^- in anhydrous methanol under buffered conditions (4 mM amine, various concentrations of HOTf) at $^{s}_{s}$pH 8.4 and 25 °C. These k_2 values are interpolated from overlaid $^{s}_{s}$pH-log(k_2) profiles for **5.1a**–**c**. The line through the data is generated from a linear regression computing $\rho^- = 2.0 \pm 0.2$; $r^2 = 0.9920$.

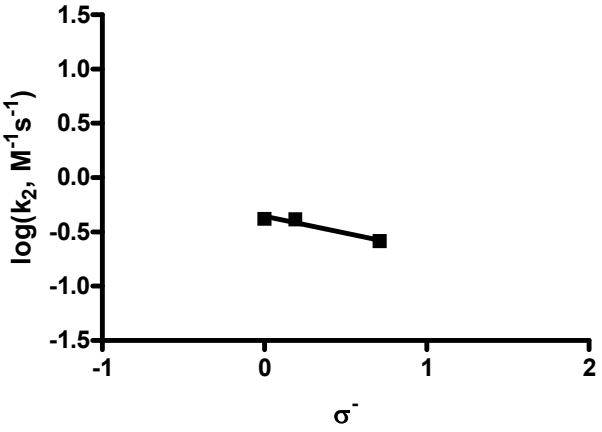

Figure 5-57. Hammett plot of log(k_2) for the palladacycle-promoted cleavage of **5.1c**–**e** (4×10^{-5} M) vs σ^- in anhydrous methanol under buffered conditions (4 mM amine, various concentrations of HOTf) at $^{s}_{s}$pH 8.4 and 25 °C. These k_2 values are interpolated from overlaid $^{s}_{s}$pH-log(k_2) profiles for **5.1c**–**e**. The line through the data is generated from a linear regression computing $\rho^- = -0.31 \pm 0.07$; $r^2 = 0.9474$.

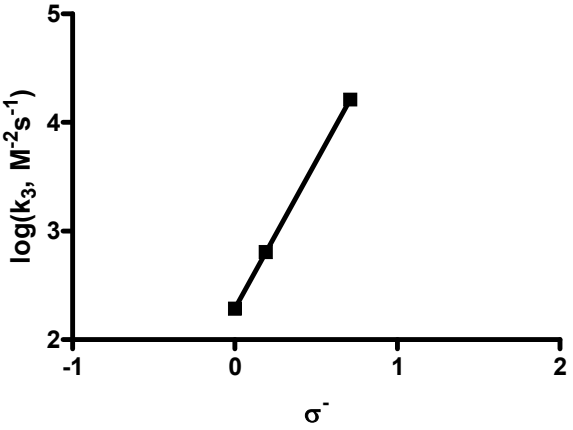

Figure 5-58. Hammett plot of log(k_3) for the palladacycle-promoted cleavage of **5.1c**–**e** (4×10^{-5} M) vs σ^- in anhydrous methanol under buffered conditions (4 mM amine, various concentrations of HOTf) at $^{s}_{s}$pH 8.4 and 25 °C. These k_3 values are extrapolated from overlaid $^{s}_{s}$pH-log(k_3) profiles for **5.1c**–**e**.The line through the data is generated from a linear regression computing $\rho^- = 2.71 \pm 0.01$; $r^2 = 1.000$.

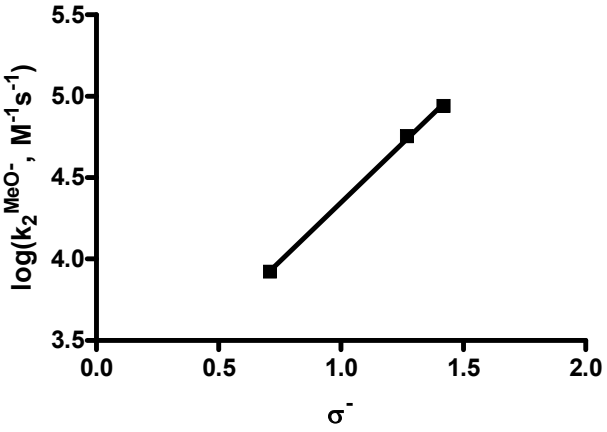

Figure 5-59. Hammett plot of $\log(k_2^{MeO^-})$ for the palladacycle-promoted cleavage of **5.1a–c** (4×10^{-5} M) vs σ^- in anhydrous methanol under buffered conditions (4 mM amine, various concentrations of HOTf) at 25 °C. The line through the data is generated from a linear regression computing $\rho^- = 1.45 \pm 0.04$; $r^2 = 0.9991$.

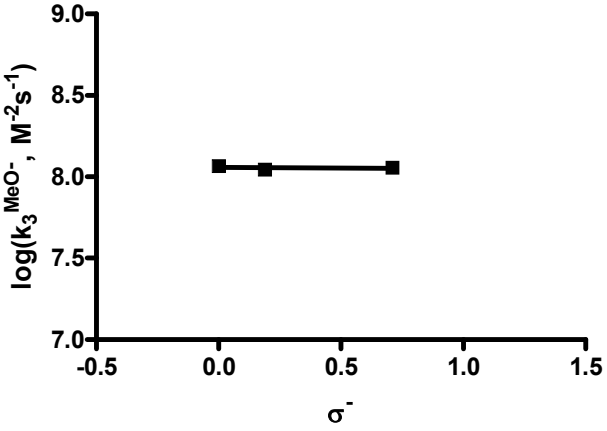

Figure 5-60. Hammett plot of $\log(k_3^{MeO^-})$ for the palladacycle-promoted cleavage of **5.1c–e** (4×10^{-5} M) vs σ^- in anhydrous methanol under buffered conditions (4 mM amine, various concentrations of HOTf) at 25 °C. The line through the data is generated from a linear regression computing $\rho^- = -0.01 \pm 0.03$.

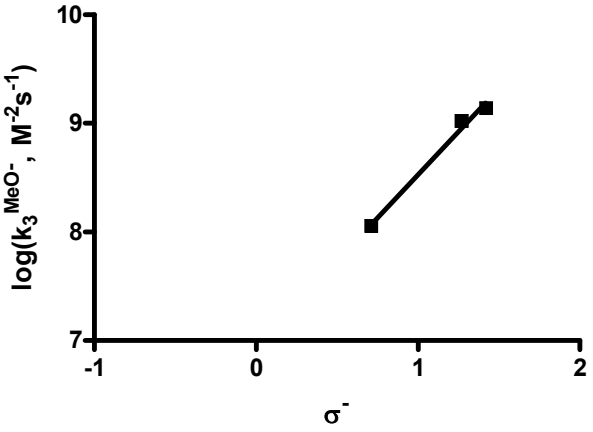

Figure 5-61. Hammett plot of $\log(k_3^{MeO-})$ for the palladacycle-promoted cleavage of **5.1a–e** (4×10^{-5} M) vs σ^- in anhydrous methanol under buffered conditions (4 mM amine, various concentrations of HOTf) at 25 °C. The line through the data is generated from a linear regression computing $\rho^- = 1.6 \pm 0.2$; $r^2 = 0.9894$.

5.8 – References and notes

[1] Wilcox, D. E. *Chem. Rev.* **1996**, *96*, 2435. Weston, J. *Chem. Rev.* **2005**, *105*, 2151.

[2] Brown, R. S.; Neverov, A. A. *Adv. Phys. Org. Chem.* **2008**, *42*, 271.

[3] (a) Neverov, A. A.; Brown, R. S. *Org. Biomol. Chem.* **2004**, *2*, 2245. (b) Brown, R. S.; Neverov, A. A.; Tsang, J. S. W.; Gibson, G. T. T.; Montoya-Pelaez, P. J. *Can. J. Chem.* **2004**, *82*, 1791.

[4] (a) Neuman, R. C., Jr.; Roark, D. N.; Jonas, V. *J. Am. Chem. Soc.* **1967**, *89*, 3412. (b) Ramiah, K. V.; Chalapathi, V. V. *Curr. Sci. India* **1971**, *14*, 363. (c) Leopardi, C. P.; Fabre, O.; Zimmerman, D.; Reisse, J.; Cornea, F.; Fulea, C. *Can. J. Chem.* **1977**, *55*, 2649. (d) Wiberg, K. B. *Acc. Chem. Res.* **1999**, *32*, 922. (e) Wiberg, K. B.; Rush, D. J. *J. Am. Chem. Soc.* **2001**, *123*, 2038.

[5] (a) Smith, S. G.; O'Leary, M. J. *Org. Chem.* **1963**, *28*, 2825. (b) Powers, J. C.; Westheimer, F. H. *J. Am. Chem. Soc,* **1960**, *82*, 5431.

[6] Broxton, T. J.; Deady, L. W.; Rowe, J. E. *Aust. J. Chem.* **1978**, *31*, 1731.

[7] (a) Campbell, P.; Nashed, N. T. *J. Am. Chem. Soc.* **1982**, *104*, 5221. (b) Bartlett, P. A.; Spear,K. L.; Jacobsen,N. E. *Biochemistry* **1982**, *21*, 1608. (c) Mock, W. L.; Chen, J.-T.; Tsang, J. W. *Biochem. Biophys. Res. Commun.* **1981**, *102*, 389. (d) Bond, M. D.; Holmquist, B.; Vallee, B. L. *J. Inorg. Biochem.* **1986**, *28*, 97.

[8] (a) Liu, C. T.; Maxwell, C. I.; Edwards, D. R.; Neverov, A. A.; Mosey, N. J.; Brown, R. S. *J. Am. Chem. Soc.* **2010**, *132*, 16599. (b) Liu, C. T.; Neverov, A. A.; Brown, R. S. *Inorg. Chem.* **2011**, *50*, 7852.

[9] Liu, C. T.; Maxwell, C. I.; Pipe, S. G.; Neverov, A. A.; Mosey, N. J.; Brown, R. S. *J. Am. Chem. Soc.* **2011**, *133*, 20068.

[10] Gibson, G.; Neverov, A. A.; Brown, R. S. *Can. J. Chem.* **2004**, *81*, 495.

[11] For the designation of pH in non-aqueous solvents we use the nomenclature recommended by the IUPAC, *Compendium of Analytical Nomenclature. Definitive Rules 1997* 3rd ed., Blackwell, Oxford, U.K. 1998. The pH meter reading for an aqueous solution determined with an electrode calibrated with aqueous buffers is designated as ${}^{w}_{w}$pH; if the electrode is calibrated in water and the 'pH' of the neat buffered methanol solution then measured, the term ${}^{s}_{w}$pH is used; and if the electrode is calibrated in the same solvent and the 'pH' reading is made, then the term ${}^{s}_{s}$pH is used. In methanol, ${}^{s}_{w}$pH – (-2.24) = ${}^{s}_{s}$pH and since the autoprotolysis constant of methanol is $10^{-16.77}$, neutral ${}^{s}_{s}$pH is 8.4.

[12] (a) Walter, W.; Bauer, O. H. *Liebigs Ann. Chem*. **1979**, 248. (b) Ma, J. C. N.; Warnhoff, E. W.; *Can. J. Chem*. **1965**, *43*, 1849.

[13] Liu, C. T.; Neverov, A. A.; Brown, R. S. *Inorg. Chem*. **2011**, *50*, 7852.

[14] Triflic acid was used in order to suppress the base-promoted solvolytic reaction during the course of the titration.

[15] $Abs^{corrected} = Abs^{initial}+Abs^{final}\times(1+10^{Kb}\times[\mathbf{5.1}]+([\mathbf{5.2}]-A)\times10^{Kb}-(1+2\times10^{Kb}\times[\mathbf{5.1}]+2\times([\mathbf{5.2}]-A)\times10^{Kb}+(10^{Kb})^2\times[\mathbf{5.1}]^2-2\times(10^{Kb})^2\times([\mathbf{5.2}]-A)\times[\mathbf{5.1}]+([\mathbf{5.2}]-A)^2\times(10^{Kb})^2)^{0.5})/(2\times10^{Kb})/[\mathbf{5.1}]$

[16] $k_{obs} = k_{max}(1+K_B[\mathbf{5.1}]+[\mathbf{5.2}]K_B-X)/(2K_B)/[\mathbf{5.1}]$ where

$X = (1+2K_B[\mathbf{5.1}]+2[\mathbf{5.2}]K_B+K_B^2[\mathbf{5.1}]^2-2K_B^2[\mathbf{5.2}][\mathbf{5.1}]+[\mathbf{5.2}]2K_B^2)^{0.5}$

This universal binding equation was obtained from the equations for equilibrium binding and for conservation of mass by using the commercially available MAPLE software:

Maple 9.00, June 13, *2003*, Build ID 13164; Maplesoft, a division of Waterloo Maple Inc.: Waterloo, Ontario, Canada, 1981–2003.

[17] The second-order rate constants (k_2) were determined by linear regression of the first four data points rather than computing $k_{max} \cdot K_b$ due to the large uncertainties in the binding constants (K_b) which stem from strong interactions between the metal ion and the substrate. In the case of strong interactions between the metal ion and substrate, the determination of the binding constant is inherently difficult and often only a lower limit can be defined with any certainty.

[18] Edwards, D. R.; Liu, C. T.; Garrett, G. E.; Neverov, A. A.; Brown, R. S. *J. Am. Chem. Soc.* **2009**, *131*, 13738.

[19] Brown, R. S. *Pure Appl. Chem.* **2015**, *87*, 601.

Chapter 6 – Summary and conclusions

Despite sustained effort by the research community, few accounts in the literature describe catalysts exhibiting enzyme-like rate enhancements for phosphoryl- or acyl-transfer reactions. In particular, those conducted in aqueous media have yielded only modest acceleratory effects and most disappointingly, they rarely exceed the catalysis provided by free hydroxide. The failure to produce mimics that rival natural systems points out there are several missing pieces yet to be discovered. The inspiration for conducting this body of work came from a desire to investigate the catalytic features that may help bridge the acceleratory gap between enzymes and small-molecule catalysts. Three significant barriers that cannot easily be overcome through minor modifications of existing systems have to do with binding of the substrate to the catalyst, the microscopic environment of the enzyme active site, and the orientation of catalytically-relevant groups. Through their tertiary structure, enzymes are able to adopt a highly-tuned conformation enabling many key interactions that recognize and bind their natural substrates such that a bi- or trimolecular process occurs by an essentially unimolecular one. The interior of the active site does not resemble bulk water and exhibits a much lower effective dielectric constant, one that is closer to that of organic solvents. This microenvironment greatly enhances interactions between oppositely-charged species leading to considerable stabilization of TSs and intermediates along reaction pathways. The tertiary structure also enables enzymes to finely-tune the positions of critical catalytic groups, such as metal ions, so that the substrate may be escorted along the reaction coordinate, having the necessary residues in the appropriate place at the

appropriate time. By carrying out these investigations using highly-contrived systems in low-dielectric media, it has been possible to employ several of these strategies to exemplify their utility in achieving enzyme-like rate enhancements. In particular, systems where the metal ion is placed in close proximity to the LG, and especially when that metal ion is also capable of carrying out other modes of catalysis in conjunction with LGA, consistently produce large effects that translate into accelerations on par with enzymes.

Chapter 2 describes the mechanistic investigation into the solvolysis of a homologous set of phosphate mono-, di-, and triesters designed to anchor a Cu(II) ion in close proximity to the departing phenoxide oxygen. In order to determine the mechanism by which these complexes decompose and how this process is influenced by the medium, a series of pH/rate profiles, solvent deuterium kinetic isotope effects, and activation parameters were collected in water and ethanol and discussed in light of data obtained in methanol. The pH/rate profile for each ester in a given solvent exhibits an extended plateau due to solvent attack on the active form of the complex. The solvent DKIE values measured in the plateau regions are slightly inverse for the monoester, near-unit for the diester, and normal for the triester in all three solvents. Such values reflect a spectrum of TSs, from loose in the case of the monoester to tight in the case of the triester, with the diester falling somewhere in between. Notably, the large primary DKIE for cleavage of the triester points to solvent-assisted delivery of ROH through a highly associative mechanism. This outcome is of importance as it demonstrates that with adequate assistance for the LG, the TSs for cleavage become sufficiently loose that the weakest

nucleophile in solution is potent enough to induce solvolysis. Comparison of activation parameters for each substrate in the solvents indicate that the transition from methanol to ethanol for each substrate involves a near cancellation of the $\Delta\Delta H^{\ddagger}$ and $-T\Delta\Delta S^{\ddagger}$ values at 25 °C, translating into similar rate constants. The transition from alcohol to water produces variable effects, with $\Delta\Delta H^{\ddagger}$ and $-T\Delta\Delta S^{\ddagger}$ values canceling for cleavage of the triester and being additive for the mono- and diesters, giving rise to a 100−500 rate reduction in passing from methanol to water. While the trends are not straightforward, it is clear that the acceleratory effects of the Cu(II)-promoted leaving group assistance in all three solvents are substantial and estimated at 10^{12} to 10^{15} for the monoester, 10^{12} to 10^{14} for the diester, and 10^{5} for the triester relative to their background reactions. These results suggest that with the appropriate positioning of a strong Lewis acid, large accelerations can be accomplished in the solvolysis of phosphate esters under mild conditions and in a variety of hydroxylic media.

Chapter 3 describes a similar phenomenon in the methanolytic decomposition of the Cu(II) complexes of *N*,*N*-bis(2-picolyl)benzamides. This series of benzamides, bearing different substituents on the acid ring, are able to bind a Cu(II) in a tridentate fashion, thereby enforcing a metal-N_{amide} interaction that decouples its conjugation with the adjacent C=O. A Hammett plot of the unimolecular decomposition of the alkoxide complexes was determined experimentally and computationally, exhibiting ρ values of 0.80 and 0.84, respectively. Solvent DKIE values of 1.12 and 1.20 as well as $\Delta S^{\ddagger}$ values of -5.1 and -2 cal K^{-1} mol^{-1} were determined for decomposition of the Cu(II) complexes of the 4-nitro and 4-methoxy derivatives in the plateau region of the their $^{s}_{s}pH/\log(k_x)$

profiles. The experimental and computational data support a mechanism where the metal ion, coordinated to the *N*,*N*-bis(2-picolyl)amide unit, delivers a Cu(II)-coordinated methoxide to the C=O in the rate-limiting transition state of the reaction. The computations reveal a tetrahedral intermediate occupies a shallow minimum on the free energy surface with the Cu(II) coordinated to both the methoxide and the amidic N. Near-barrierless breakdown involves Cu(II)-assisted departure of the bis(2-picolyl)amide anion. The metal ion appears to fulfill a trifunctional role where it activates the substrate through coordination to the amide nitrogen, activates and delivers the nucleophile, and subsequently assists leaving group departure in the second step. Comparing the rate constant for the attack of methoxide on the 4-nitro derivative to its Cu(II)-complex reveals an acceleration attributable to Cu(II)-coordination exceeding 10^{16}. This system provides a small-molecule example of how an enzyme may couple highly endergonic processes (in this case, C–N cleavage) with exergonic ones (such as LG binding) in order to rapidly modify kinetically-inert substrates.

Chapter 4 expands upon the findings from Chapter 3 by addressing the methanolysis and ethanolysis of the Ni(II), Zn(II), and Cu(II) complexes of *N*,*N*-bis(2-picolyl)-*p*-nitrobenzamide and *N*,*N*-bis((1*H*-benzimidazol-2-yl)methyl)-*p*-nitrobenzamide. The k_{obs} values for the reaction under pseudo first order conditions as a function of $[M^{2+}]$ give saturation kinetics for the Cu(II)-promoted reactions of **4.1** and **4.2** in both solvents, the Zn(II)-promoted reaction of **4.1** in methanol, and the Zn(II)- and Ni(II)-promoted reactions of **4.2** in methanol and ethanol. Due to limitations imposed by metal ion-alkoxide oligomerization, the kinetic pK_a values, as determined from that log of the

maximal observed rate constants plotted versus $^{s}_{s}$pH, and the subsequent plateau regions were only accessible for the Cu(II) complexes of **4.1** and **4.2** in both solvents and the Zn(II) complex of **4.1** in methanol. Despite differences in the metal-binding abilities and pK_a values for formation of the active form, all systems appear to follow the mechanism described in Chapter 2. Comparing the rate constant for the attack of methoxide or ethoxide on the M(II)-complexed 4-nitro-substituted benzamides to the uncomplexed form reveals accelerations ranging from 10^{14} to 10^{19}, attributable to the multifunctional role of the metal ion.

Chapter 5 describes the kinetic study of the methanolysis of a set of tertiary thiobenzanilides by a simple palladacycle catalyst which appears to employ metal ion-promoted LGA in conjunction with other modes of metallo-catalysis. In general, metal ion-catalyzed solvolysis of carboxamides suffers from weak interactions between the metal ion and either the acyl oxygen or the leaving group nitrogen, precluding significant stabilization of the transition states leading to cleavage. Previous work in this laboratory has shown that a palladacycle complex interacts strongly with *N*-methyl-*N*-(4-nitrophenyl)thiobenzamide in methanol, capitalizing on soft-soft interactions between the substrate and catalyst as well as the lower dielectric constant of methanol (relative to water), and in turn accelerates cleavage of the amide bond by 10^8 relative to the alkoxide-promoted reaction. The DFT-computed pathway demonstrates that leaving group assistance by the metal ion is an important component in stabilizing the rate-limiting transition state. Overall, the metal ion enacts a trifunctional role involving its pre-equilibrium coordination to and activation of the C=S unit, subsequent intramolecular

attack of a Pd(II)-coordinated methoxide, and Pd(II)-assisted C–N cleavage. The catalyst concentration-k_{obs} and ${}^{s}_{s}$pH-log(k_{max}) profiles reveal one catalyst, one substrate, and one methoxide are involved in the rate-limiting transition state for cleavage. By changing the nature of the anilinyl LG, two mechanistic regimes are illuminated: a mechanism that employs one equivalent of catalyst and another that recruits two. The [catalyst]-k_{obs} profiles in the latter regime highlight a change in order in [catalyst], signaling a change in mechanism. The involvement of a second metal ion coincides with a drastic reduction in the dependence of rate on the substituent (ρ^{-} = 1.45 to -0.01) and therefore in the charge on the leaving group in the rate-limiting transition state. It follows that one of the two metal ions provides significant stabilization to the developing charge on the LG in the rate-limiting TS. A two-step mechanism consistent with these data involves one catalyst that binds tightly to the substrate as well as a methoxide and facilitates intramolecular nucleophilic attack leading to a stabilized tetrahedral intermediate. Subsequently, a second catalyst becomes transiently coordinated to the lone pair on the N of the LG and stabilizes its departure during the rate-limiting step. In either mechanistic regime, it appears as though the rate-limiting step is departure of the LG. This study suggests that when Nature must cope with the departure of a reluctant LG, it may alter the cleavage mechanism in order to employ available metal ions to facilitate leaving group departure.

Given the poor nucleofugality of LGs in natural substrates, it seems critical that such groups be stabilized by some form of Lewis or Brønsted acid. The ubiquity of metal ions in the active sites of enzymes responsible for cleaving kinetically inert substrates points to a metal ion-promoted means of LG stabilization. The impressive effects brought on by

this mode of catalysis in highly-contrived systems suggest enzymes would have little difficulty capitalizing on such an effect given access to a highly-tunable tertiary structure. The aforementioned studies have provided further insight into the mechanism and magnitude of metal ion-promoted LGA. Moving forward, the next generation of enzyme mimics as well as catalysts in general may benefit from the incorporation of metal ion-promoted LGA in combination with the other modes of metallo-catalysis and a low-dielectric medium.